Homogeneous and heterogeneous CuAAC-systems for self-healing and stress-sensing applications

Dissertation

zur Erlangung des
Doktorgrades der Naturwissenschaften (Dr. rer. nat.)

der

Naturwissenschaftlichen Fakultät II
Chemie, Physik und Mathematik

der Martin-Luther-Universität
Halle-Wittenberg

vorgelegt

von Herrn Steve Neumann
geb. am 22.11.1988 in Berlin

Gutachter

1. Prof. Dr. Wolfgang H. Binder

2. Prof. Dr. Morten Meldal

Verteidigung: 26.03.2019   Halle (Saale), 28.11.2018

Abstract

Multivalent components, equipped with the newest generation of "click" type moiety, suitable for the chelation-assisted copper(I)-alkyne/azide cycloaddition (ca-CuAAC), were investigated in respect to their crosslinking efficiency, addressing autonomous self-healing (SH) of growing microcracks at low temperatures (< 20 °C) via fast network formation reactions.

Two different regioisomers of picolyl azides (**4**, **7**) were successfully synthesized and further tested upon efficiency in solution via NMR spectroscopy. The model reaction of picolyl azide **3** and phenylacetylene was completed within five minutes at room temperature (RT), using CuBr as a catalyst and DIPEA as a base. The crosslinking efficiency of low molecular weight and trivalent picolyl azide (**18**) in the ca-CuAAC was studied via DSC-measurements, using homogeneous and heterogeneous Cu(I)-catalysts. The begin of the ca-CuAAC crosslinking at 4 °C was verifying the essential low temperature activity of **18** and a trivalent alkyne (**20**). A high molecular weight crosslinking approach was designed by attaching picolyl azides **4** or **7** to star-shaped poly(isobutylenes) (PIBs) (**34a**, **34b**) (M_n ~ 6 000 g/mol), synthesized via living carbocationic polymerization (LCCP) technique. The network-formation of **34a** (or **34b**) and star-shaped alkyne-PIB (**35**) in rheology experiments was completed within 15 minutes at 20 °C and within 71 minutes at 10 °C, proving the concept of low temperature crosslinking in the melt. Star-shaped picolyl azido telechelic PIB (**34b**), [CuBr(PPh$_3$)$_3$], coumarin azide (**36**) as sensing precursor and the trivalent alkyne (**20**), encapsulated in an urea-formaldehyde (UF)-shell, were compounded to a scaffolding PIB-matrix. Notching the specimen with a razor blade led to the rupture of the embedded capsules and thus the release of the liquid alkyne component, which upon contact with the Cu(I)-catalyst and the azides triggered the autonomous SH and fluorescent network formation.

A second approach aimed for the optimization of a Cu(I)-mechanocatalyst, being employed in an autonomous sensing material, triggering the fluorogenic CuAAC by mechanical impact. A new chain transfer agent (CTA) (**40**) bearing an imidazolium group was designed, enabling the synthesis of long polymer handles (poly(styrene) (PS) (**49**) or poly(*n*-butyl acrylate) (P-*n*BuA) (**51**)) via reversible addition fragmentation transfer (RAFT) polymerization. Thus, a direct attachment of the *N*-heterocyclic carbene (NHC) ligand to the polymer chain was ensured, preventing the otherwise required and often inefficient post-polymerization functionalization. The bis(polymer-NHC)-Cu(I)-mechanocatalyst (**52**), coumarin azide (**36**) and phenylacetylene were embedded into a pTHF-matrix, which was formed to a pellet. The scission of the otherwise inactive catalyst into the active Cu(I)-monocarbene species was triggered upon compression, leading to an increase in fluorescence emission by formation up to 22% of the „click"-product, demonstrating the ability of the concept to act as an autonomous sensing tool.

Kurzdarstellung

Multivalente Verbindungen wurden mit der neuesten „Click" Generation ausgestattet und hinsichtlich ihrer Vernetzungseffizienz in der ca-CuAAC untersucht. Eine sehr schnelle und effiziente Netzwerkbildung in autonomen Selbstheilungs- (SH)-Systemen sollte somit auch bei niedrigen Temperaturen (< 20 °C) die Ausbreitung von Mikrorissen durch Versiegelung verhindern können.

Zwei Regioisomere des Picolylazides (**4**, **7**) wurden erfolgreich synthetisiert und anschließend in Lösung mittels NMR Spektroskopie hinsichtlich ihrer Effektivität in der ca-CuAAC untersucht. Picolylazid **3** und Phenylacetylen zeigten bei RT innerhalb von 5 Minuten in Gegenwart von CuBr als Katalysator und DIPEA als Base einen vollständigen Produktumsatz. Die Vernetzungseffizienz des trivalenten Picolylazides (**18**) von niedrigem Molekulargewicht wurde sowohl in Gegenwart von homogenen als auch heterogenen Cu(I)-Katalysatoren mittels DSC-Messungen untersucht. Der Vernetzungsprozess zwischen **18** und einem trivalentem Alkin (**20**) begann bei 4 °C und bestätigte somit die entscheidende Niedrigtemperatur-Aktivität der multivalenten Verbindungen. Sternenförmige PIBs (**34a**, **34b**) von hohem Molekulargewicht (M_n ~ 6 000 g/mol) wurden mittels lebender carbokationischer Polymerisation synthetisiert und anschließend durch Endgruppenmodifikation mit Picolylaziden (**4** oder **7**) funktionalisiert. Schmelzrheologische Experimente von **34a** (oder **34b**) und sternenförmigen PIB-Alkin (**35**) zeigten die Ausbildung eines vollständigen Netzwerkes innerhalb von 15 Minuten bei 20 °C sowie innerhalb von 71 Minuten bei 10 °C und belegten somit die Niedrigtemperatur-Vernetzung des ca-CuAAC Konzepts in der Schmelze. Sternenförmiges Picolylazid-PIB (**34b**), [CuBr(PPh$_3$)$_3$], Coumarinazid (**36**) als Sensorvorstufe und das trivalente Alkin (**20**), eingekapselt in einer Harnstoff-Formaldehyd Schale, wurden in eine PIB-Matrix eingebracht. Das Schneiden des Probekörpers mit einer Rasierklinge führte zum Bruch der eingebetteten Kapseln und der Freisetzung des flüssigen Alkins, welches bei Kontakt mit dem Cu(I)-Katalysator die selbstheilende und fluoreszierende Netzwerkbildung mit den Aziden bewirkte.

Eine weitere Anwendung zielte auf die Optimierung eines Cu(I)-Mechanokatalysators ab, der in einem autonomen Sensormaterial durch mechanische Beanspruchung aktiviert wird. Dazu wurde ein CTA (**40**) mit einer Imidazolium-Endgruppe entwickelt, der die Synthese von langen Polymerhanteln (bestehend aus PS (**49**) oder P-*n*BuA (**51**) mit M_n > 25 kg/mol) mittels der RAFT Polymerisation ermöglichte. Dadurch konnten die NHC-Liganden direkt an das Ende der Polymerkette angebracht werden, was eine Alternative zur ansonsten benötigten und häufig limitierten post-Funktionalisierung des Polymers darstellt. Der bis(Polymer-NHC)-Cu(I)-Mechanokatalysator (**52**) wurde zusammen mit Coumarinazid (**36**) und Phenylacetylen in eine hoch molekulare pTHF-Matrix eingebracht und anschließend zu einer Tablette gepresst. Die Spaltung des ansonsten inaktiven Katalysators in die aktive Cu(I)-Monocarbenspezies wurde durch Kompression der Tablette ausgelöst. Dies bewirkte einen Anstieg der Fluoreszenz-Emission in Folge der Bildung von bis zu 22% des „Klick"-Produktes und zeigte somit die potentielle Anwendbarkeit des Konzeptes als autonomen Schadenssensor.

Table of Contents

List of abbreviations

AAC	alkyne/azide cycloaddition
AIBN	2,2′-azobis(2-methylpropionitrile)
ATMS	allyltrimethylsilane
ATRP	atom transfer radical polymerization
9-BBN	9-borabicyclo[3.3.1]nonane
BimH	benzimidazolylmethyl with substituent H
BINAP	(R)-(+)-(1,1′-binaphthalene-2,2′-diyl)bis(diphenylphosphine)
BPS	sodium 4,4'-(1,10-phenanthroline-4,7-diyl)dibenzenesulphonate
BTTAA	2-[4-(bis[(1-$tert$-butyl-1H-1,2,3-triazol-4-yl)methyl]amino)methyl -1H-1,2,3-triazol-1-yl]acetic acid
BTTE	2-[4-(bis[(1-$tert$-butyl-1H-1,2,3-triazol-4-yl)methyl]amino)methyl-1H-1,2,3-triazol-1-yl]ethyl
BTTES	2-[4-(bis[(1-$tert$-butyl-1H-1,2,3-triazol-4-yl)methyl]amino)methyl-1H-1,2,3-triazol-1-yl]ethyl hydrogen sulfate
BTTP	3-[4-(bis[(1-$tert$-butyl-1H-1,2,3-triazol-4-yl)methyl]amino)methyl-1H-1,2,3-triazol-1-yl]propyl
BTTPS	3-[4-(bis[(1-$tert$-butyl-1H-1,2,3-triazol-4-yl)methyl]amino)methyl-1H-1,2,3-triazol-1-yl]propyl hydrogen sulfate
ca-CuAAC	chelation-assisted copper(I)-alkyne/azide cycloaddition
CNT	carbon nanotube
CTA	chain transfer agent
CuAAC	copper(I)-alkyne/azide cycloaddition
CVD	chemical vapor deposition
C18$_6$tren	tris(2-dioctadecylaminoethyl)amine
DA	Diels-Alder cycloaddition reaction
DBN	1,5-diazabicyclo[4.3.0]non-5-ene
DBTL	dibutyltin dilaurate
DBU	1,8-diazabicyclo[5.4.0]undec-7-ene
DCC	N,N'-dicyclohexylcarbodiimide
DCCl	5-$tert$-butyl-1,3-bis(1-chloro-1-methylethyl)-benzene
DCM	dichloromethane
DCPD	dicyclopentadiene
DCTB	$trans$-2-[3-(4-$tert$-butylphenyl)-2-methyl-2-propenylidene] malononitrile
DCU	1,3-dicyclohexylurea
DIPEA	N,N-diisopropylethylamine
Dithranol	1,8-dihydroxy-9,10-dihydroanthracen-9-one
DMA	N,N-dimethylacetamide
DMAP	N,N-dimethylpyridin-4-amine
DMF	dimethylformamide
DMSO	dimethyl sulfoxide
dppe	ethane-1,2-diylbis(diphenylphosphane)
DSC	different-scanning-calorimetry
DtBP	2,6-di-$tert$-butylpyridine
EDC	3-(ethyliminomethyleneamino)-N,N-dimethylpropan-1-amine
EDU	1-ethyl-3-(3-dimethylaminopropyl)urea

ESI		electron-spray-ionization
FAAS		flame atomic absorbtion spectroscopy
FTIR		fourier-transform infrared spectroscopy
GO		graphene oxide
GPC		gel permeation chromatography
HAP		hydroxyapatite
HPLC		high-performance liquid chromatography
IB		isobutylene
IL		ionic liquid
IMes		1,3-bis(2,4,6-trimethylphenyl)imidazol-2-ylidene
IR		infrared
	s	strong
	m	middle
	w	weak
IPr		1,3-bis(2,6-diisopropylphenyl)imidazol-2-ylidene
KHMDS		potassium 1,1,1-trimethyl-*N*-(trimethylsilyl)silanaminide
LCCP		living carbocationic polymerization
LMCT		ligand-metal charge-transfer
MALDI		matrix-assisted-laser-desorption-ionization
MC		merocyanine
m-CPBA		3-chlorobenzene-1-carboperoxoic acid
MOF		metal-organic framework
MW		multi walled
NaAsc		sodium ascorbate
NMP		nitroxide-mediated radical polymerization
NMR		nuclear magnetic resonance
	bs	broad singlet
	d	duplet
	dd	double duplet
	dt	double triplet
	m	multiplet
	q	quartet
	quint	quintet
	s	singlet
	sep	septet
	sext	sextet
	t	triplet
NHC		*N*-heterocyclic carbene
NP		nano particle
NSHC		*N,S*-heterocyclic carbene
PBMA		poly(butyl methacrylate)
PIB		poly(isobutylene)
PDI		polydispersity index (dispersity)
PDMS		poly(dimethylsiloxane)
phen		1,10-phenanthroline
pK$_A$		negative common logarithm of acid dissociation constant, K_a
pK$_B$		negative common logarithm of base dissociation constant, K_b

PMDETA	*N,N,N',N'',N''*-pentamethyldiethylenetriamine
P-*n*BuA	poly(*n*-butyl acrylate)
POM	poly(oxometalate)
PS	poly(styrene)
pTHF	poly(tetrahydrofuran)
Py	pyridine
R$_f$	retardation factor
RAFT	reversible addition-fragmentation chain transfer
ROMP	ring-opening metathesis polymerization
ROS	reactive oxygen species
RT	room temperature
SH	self-healing
SIMes	1,3-dimesityl-4,5-dihydroimidazol-2-ylidene
SIPr	1,3-bis(2,6-di-*i*-propylphenyl)imidazolidin-2-ylidene
SP	spiropyran
SPAAC	strain-promoted alkyne/azide cycloaddition
STP	spirothiopyran
SW	single walled
TABTA	3-[4-(bis[(1-*tert*-butyl-1*H*-1,2,3-triazol-4-yl)methyl]aminomethyl) 1*H*-1,2,3-triazol-1-yl]propyltrimethylammonium trifluoroacetate
TBTA	tris[(1-benzyl-1*H*-1,2,3-triazol-4-yl)methyl]amine
TEM	transmission electron microscopy
THF	tetrahydrofuran
THPTA	tris[(1-hydroxypropyl-1*H*-1,2,3-triazol-4-yl)methyl]amine
TLC	thin layer chromatography
TMC	thiomerocyanine
TMPCl	2-chloro-2,4,4-trimethyl-pentane
TREGO	thermally reduced exfoliated graphene oxide
TRGO	thermally reduced graphene oxide
TriCuOMe	1,3,5-tris(2-methoxyisopropyl)benzene, (tricumyl methoxy)
Trz	triazole
TTTA	tris[(1-*tert*-butyl-1*H*-1,2,3-triazol-4-yl)methyl]amine
UF	urea-formaldehyde
US	ultra sonication
USY	ultrastable Y
UV	ultraviolet
XRD	X-ray diffraction

Parts of the results and discussion as well of the experimental part were already published in *"Chelation-assisted CuAAC in star-shaped polymers enables fast self-healing at low temperatures"* (Neumann, S.; Döhler, D.; Ströhl, D., Binder, W.H. *Polym. Chem.* **2016**, *7*, 2342. DOI: 10.1039/c5py01818h) - Published by The Royal Society of Chemistry and were in parts adapted with permission from The Royal Society of Chemistry (Copyright 2016).

1 Introduction

1.1 Copper(I)-alkyne/azide cycloaddition (CuAAC)

The pursuit for reactions that are easily capable of building complex macromolecular structures as defined by quantitative carbon-X-carbon formation culminated in the development of "click" reactions. These were first defined by Sharpless *et al.* 2001: „*The reaction must be modular, wide in scope, give very high yields, generate only inoffensive byproducts [...], and be stereospecific. The required process characteristics include simple reaction conditions (ideally, the process should be insensitive to oxygen and water), readily available starting materials and reagents, the use of no solvent or a solvent that is benign (such as water) or easily removed, and simple product isolation.*"[1] These conditions are transferred to polymeric systems[2] and can still be described as reactions, which are characterized by a thermodynamic gain of at least 20 kcal/mol.[1, 3-4] „Click" chemistries (see Figure 1) such as the metal-catalyzed 1,3-dipolar cycloadditions[3-9] (A) and the metal-free surrogates (B-H) such as the strain-promoted alkyne/azide cycloaddition (SPAAC)[10-13] (B), the thiol-ene/yne[14-16] (C-D), the thiol-bromo[14, 17] (E), the oxime formation[18-19] (F), the Diels-Alder cycloaddition[20-22] (DA) (G) and tetrazole-alkene[23-24] (H) reaction are most frequently applied, when rapid (within hours, $T < 25$ °C) and complete conversion in macromolecular synthesis is required. This pool of "click" chemistries is completed by the mild conjugation approaches such as the Michael-addition[25-26] (I), the thiol-isocyanate reaction[27-28] (J) and the nitrile-oxide cycloaddition[29-30] (K). These approaches provide similar results in reaction rates, but lack the required orthogonality to be called "click" chemistries, limiting their application range[2, 31].
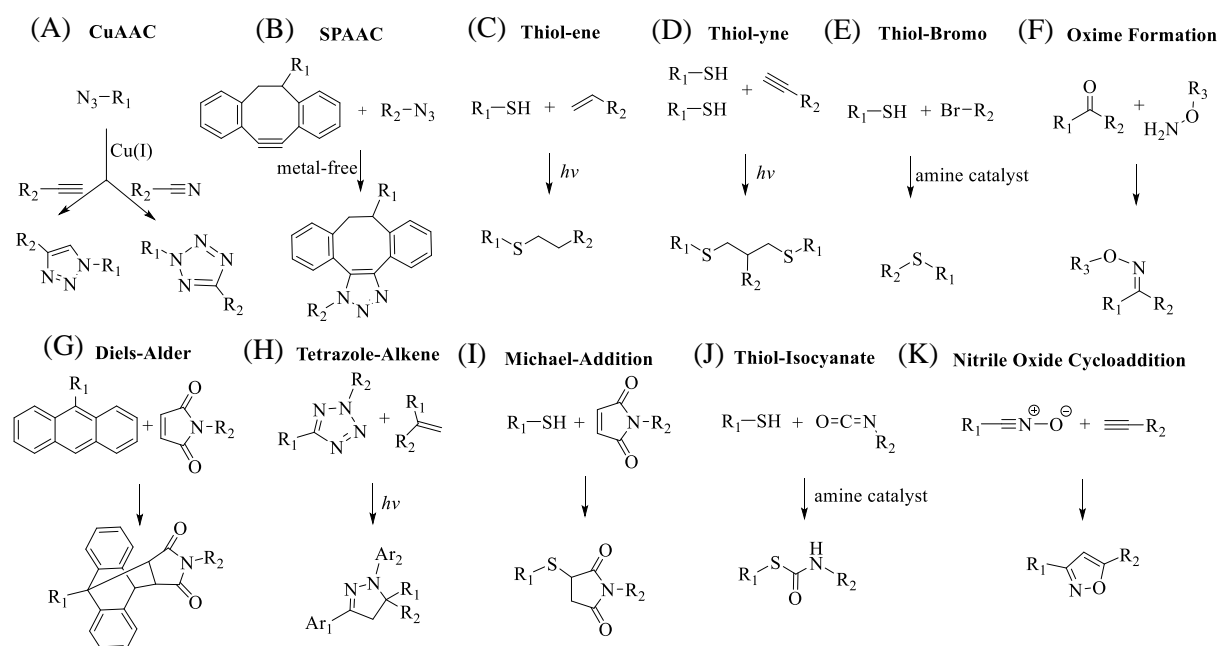
Figure 1. Overview of rapid converting chemistries ($T \leq 25$ °C, $t \leq 2$ h), subdivided in "click" based (A-H) and mild conjugation (I-K) chemistries.

In terms of ease, expanded application range, solvent- and substrate- insensitivity the copper(I)-alkyne/azide cycloaddition (CuAAC) is one of the most used "click" reaction[3-9, 13, 32-54], making it the method of choice to efficiently link two molecules under ambient conditions. The uncatalyzed Huisgen reaction[55-56] is the pure thermal conversion of azides and terminal alkynes leading to a mixture consisting of 1,4- and 1,5-regioisomers of 1,2,3-triazole products (see Figure 2a). The excellent characteristics of a "click"-reaction are gained by the addition of copper(I), that is initially described by Meldal and Sharpless in 2001/2002 independently (see Figure 2b).[57-59] The copper(I) catalysis

introduces the regioselective formation of the 1,4-regioisomer, the feasibility of the reaction at organic solvents, water or ionic-liquids[60] and an increased reaction rate of up to seven orders of magnitude[36, 61-62] and thus pushes the CuAAC to completeness within minutes at room temperature. Besides the copper(I) catalyzed Huisgen reaction, other metals such as Ni(II)[63], Pd(II)[63-64] and Pt(II)[63] (see Figure 2c) are applied to conduct the regioselective conversion of azides and terminal alkynes or internal thio-alkynes in case of iridium(I)-catalyzed intermolecular AAC[65] (see Figure 2d). In dependence of the alkyne structure and the Ru(II)-catalyst composition, 1,2,3-triazoles of either exclusive 1,4- or 1,5-regioisomers or mixtures of both can be provided in the ruthenium(II)-alkyne/azide cycloaddition (RuAAC)[66]. RuAAC is most frequently conducted at ambient to elevated temperatures (25 – 110 °C) and leads to moderate yields (see Figure 2e)[9, 67]. Furthermore, the CuAAC of internal unstrained metal-alkynes is performed under mild conditions applying either Au(I)-[68-70] or Te(I)-[71] acetylene complexes (see Figure 2f). However, with regard to efficiency (yield, time, temperature), scope of application and ease in feasibility none of them can compete with the potential benefits obtained by the copper(I) catalysis.
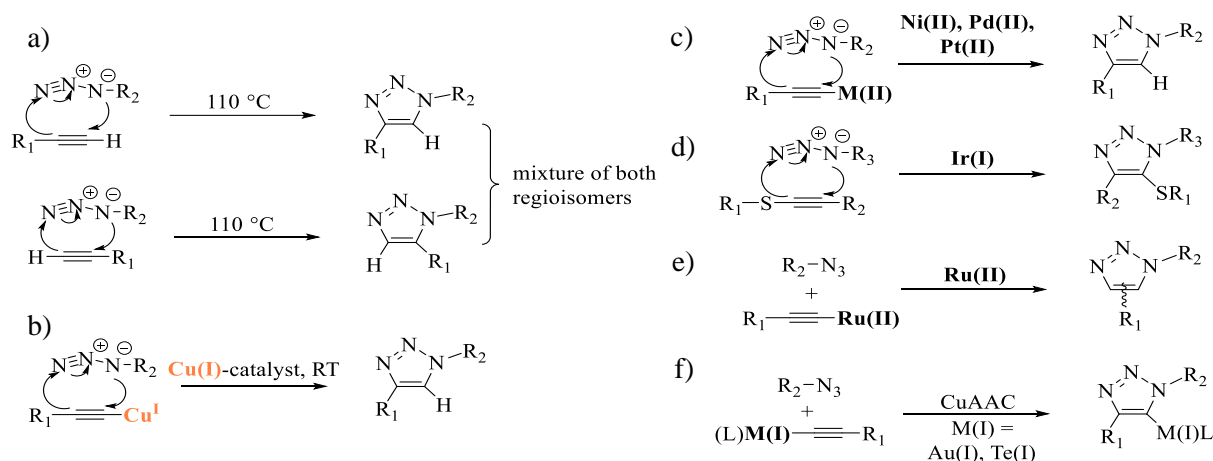
Figure 2. a) Thermal Huisgen reaction; b) CuAAC; c) other metal(II) catalyzed AAC; d) Ir(I)-catalyzed AAC; e) RuAAC; f) CuAAC of Au(I)- or Te(I)- internal unstrained alkynes.

Exploiting the CuAAC tool opens access to defined and complex architectures in polymer science[3-4, 8, 72] such as star-[73-75], block-[76-77], graft-[78-79] polymers and dendrimers (see Figure 3)[80-81], which is otherwise often impossible due to incomplete conversions or a difficult work-up.
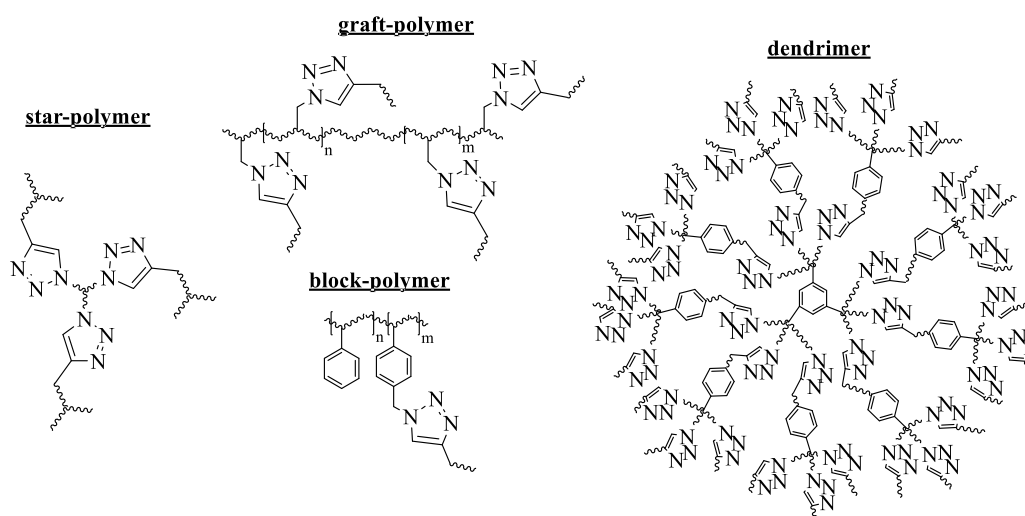
Figure 3. Specific examples of complex architectures obtained by CuAAC „click"-chemistry. Here shown for star-, graft-, block- polymers and dendrimers.

The beneficial outcome of copper(I) catalyzing the thermal Huisgen reaction is mainly attributed to the change of mechanism and thus the overcoming of the kinetic barrier in formation of the desired triazole-ring. Computational and experimental studies led to a change of mechanistic proposals from mononuclear[58] to at least dinuclear and the currently accepted mechanism for the CuAAC (see Figure 4).[4, 6-9, 46, 82-84] Initially a π-complex of the copper(I)- and the alkyne- substrate is formed (**I**), lowering the pk_A-value of the acetylide to 9.8[85] and thus facilitating the generation of the copper(I)-acetylide (**II**) even in absence of a base. In the next step, the formation of the dinuclear complex (**III**) with the coordinated azide group leads to a pre-orientation of the reactive functional groups, which in return leads to the formation of a six-membered ring, introducing the first covalent C-N-bond (**IV**). The desired 1,2,3-triazole-product (**V**) is provided with formation of the second C-N-bond, which is generating the exclusive 1,4-regioisomer (**VI**) after final protonation.
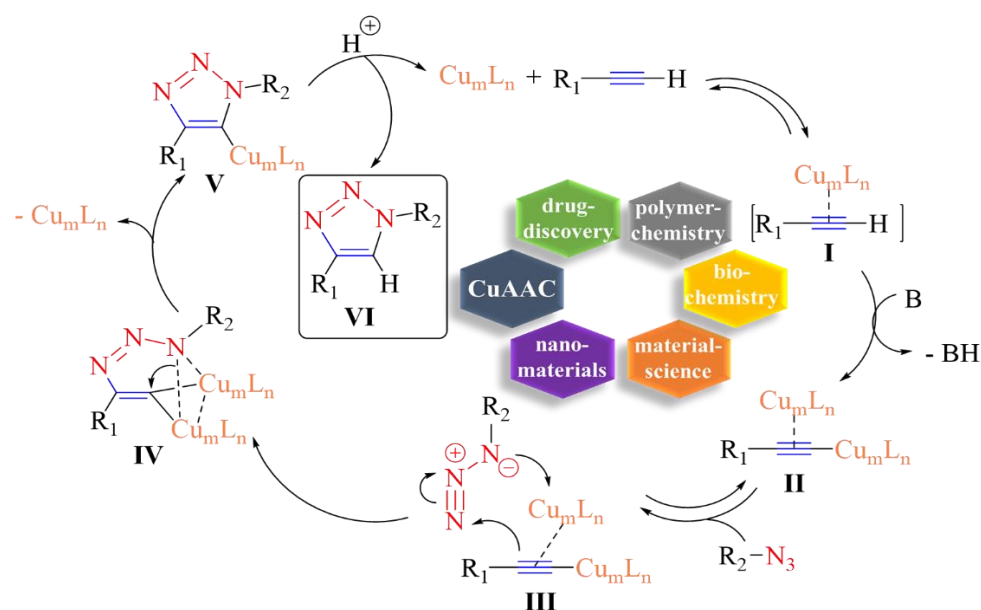
Figure 4. Mechanistic details of the CuAAC, including the areas of application.

Plenty applications of the CuAAC in the fields of drug discovery[8, 86-87], polymer chemistry[3-8, 34-35], biochemistry[8, 13, 37, 41, 54, 88-90], material science[91] and nanomaterials[92] followed-up as a consequence of its outstanding advantages. The potential application field of the CuAAC is widely distributed due to its numerous benefits and its low tendency to undergo disturbing side reactions. Nonetheless, a few of them are existing such as the alkyne-coupling, the triazole-coupling and the Staudinger reduction with phosphines (see Figure 5a-d). Alkyne-coupling can appear by oxidative conditions in form of Glaser coupling (homocoupling) (see Figure 5a) or by Cadiot - Chodkiewicz heterocoupling conditions in presence of a catalytical amount of copper(I)salts and unhindered amines, such as TMEDA or pyridine (see Figure 5b), which are frequently used to accelerate the kinetic behavior in the CuAAC.[83, 93-95] The exchange of amine-protons with bulky substituents is forming sterically hindered bases, which reduce the ligand donor properties of the base and thus the stabilization of the intermediate to form coupled alkynes. These kind of external ligands (for more details see chapter 1.1.3) are further capable to protect copper(I) from oxidation to copper(II), which otherwise would lead to the termination of the CuAAC and is therefore the most prominent side-reaction within this "click"-tool.[3-4, 63] Especially in the presence of potassium carbonate the formation of bis(triazoles) as a major product is observed, when conducting the CuAAC at basic conditions (see Figure 5c)[96]. A few functional groups can interfere with the CuAAC, e.g. free accessible thiols and triphenylphosphanes are able to reduce the azides to primary amines via a Staudinger reaction (see Figure 5d)[97]. Further interfering groups are made of

strongly activated cyanides (see Figure 5e)[32] and strained or electronically activated alkenes (see Figure 5f)[55].
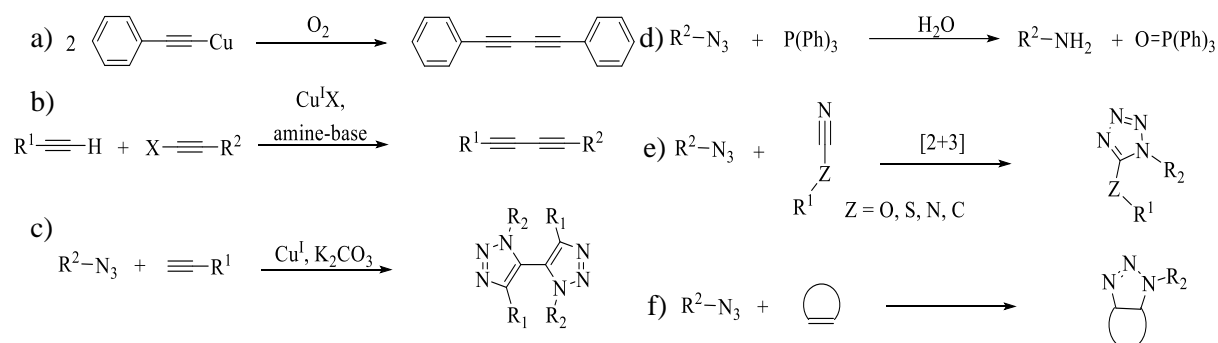
Figure 5. Side reactions and groups the CuAAC can interfere with: a) Glaser coupling; b) Cadiot - Chodkiewicz heterocoupling; c) triazole-coupling; d) Staudinger reduction with triphenylphosphane; e) tetrazole-formation with electron-deficient cyanides; f) cyclic alkenes.

Further improvement of the CuAAC included the investigation of the homogeneous (see chapter 1.1.1), the heterogeneous (see chapter 1.1.2) and the ligand-accelerated CuAAC (see chapter 1.1.3).

1.1.1 Homogeneous CuAAC

The potential application field of the CuAAC can be distinguished in the various ways copper(I) is introduced to the system. In case of homogeneous catalysis, the educts and the catalyst are in the same phase, which is in general afforded by the addition of a solvent as the liquid phase.[98] The catalytical active copper(I) species is generated either by *in situ* reduction of copper(II) salts in presence of a reductive environment (A), by the direct addition of a copper(I) salt (B) or even in absence of copper under specific conditions (C).

A) Copper(II)-salts

The most frequently used system consists of $Cu(II)SO_4 \cdot 5H_2O$, which is reduced by sodium ascorbate in aqueous or alcoholic solutions (see Figure 6a)[58, 82-83, 99]. The choice of such polar solvent requires the usage of hydrophilic azides and alkynes. As an alternative the water-soluble tris(2-carboxyethyl)phosphine (TCEP)[90, 100-106] is used as a reducing agent for Cu(II)-salts, although it can form inhibitory complexes with Cu(I) and can interfere with aliphatic azides via Staudinger reduction, if applied in excess[107]. Thus, it opens access to biorthogonal ligation of living cells, which is often supported by the addition of external agents to prevent the formation of the toxic reactive-oxygen-species (ROS), which is generated by interaction of copper(I/II) and oxygen (for more detailed discussion see chapter 1.1.3). Furthermore, $Cu(II)(OAc)_2$ gets along without any reducing agent (see Figure 6b)[99, 108]. Subsequently copper(I) is generated by alcohol-oxidation making use of corresponding solvents or the oxidative homocoupling of terminal alkynes (see Figure 6c)[109]. Besides the chemical reduction method, the photochemical reduction (see Figure 6d-e) is also applied. For instance, leads the continuous exposure of Cu(II)/PMDETA in presence of benzyl azide and terminal alkynes to UV-irradiation to high yields in the CuAAC conversion (see Figure 6d)[110]. In depth, the tertiary amine is acting as an electron-donor via a ligand-metal charge-transfer (LMCT) complex and further stabilizes the resulting oxidation state of copper(I) by complexation. Additionally, photoinitiators can be introduced to the system, to evoke the reduction of Cu(II) by radiation (see Figure 6e)[111].
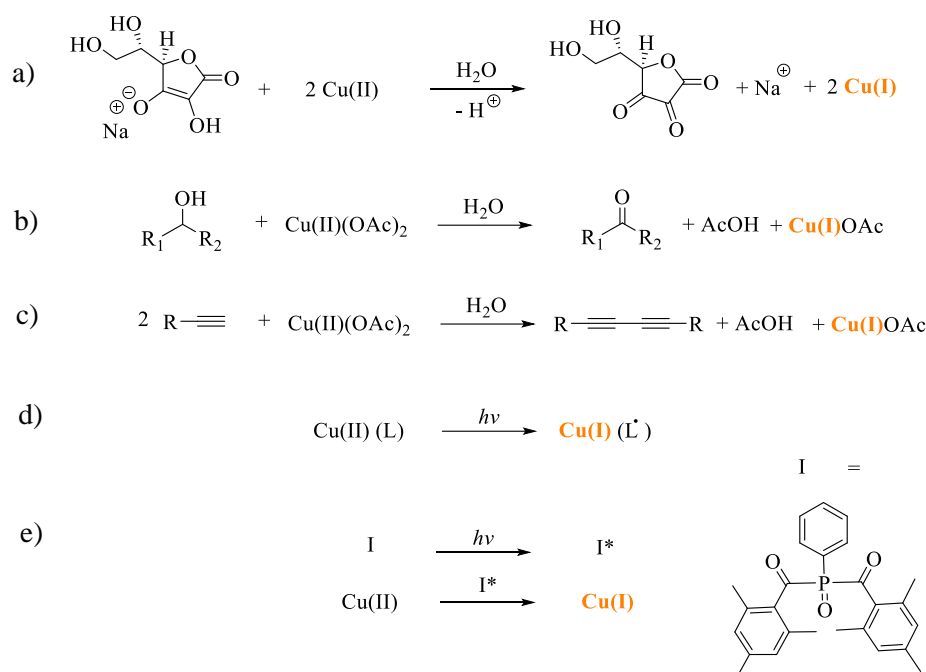
Figure 6. Chemical (a-c) and photochemical (d-e) strategies to *in situ* generate copper(I) from copper(II) by reduction. a) By adding the reducing agent sodium ascorbate; b) by alcohol-oxidation in corresponding solvents; c) by oxidative homocoupling of alkynes; d) by LMCT under UV-irradiation; e) by radical generating photoinitiator under UV-irradiation.

B) Copper(I)-salts

Exploiting of copper(I) salts offers the potential to exclude reducing agents, instead copper(I) needs to be stabilized against aqueous moisture, otherwise the appearing disproportionation to copper(0) and copper(II) would disturb the CuAAC immediately (for a more detailed discussion see chapter 1.1.3). Thus, the reaction has to be conducted at inert conditions or bulky organic substituents are required to stabilize the copper(I) complex. Therefore, $[CuBr(PPh_3)_3]$, $CuI \cdot P(OEt)_3$, $[CuF(PPh_3)_3]$ and $[Cu(MeCN)_4]PF_6$ are appropriate catalysts (see Figure 7a-c), possessing additionally a good solubility in organic solvents[40, 42]. Even better protection and further increased reaction rates are observed in presence of amine-bases as a consequence of accelerated copper(I)-acetylide formation[58, 63]. Depending on the structure of the applied catalysts the CuAAC can be exploited in water or in organic solvents and can be further promoted by microwave radiation[60].

Taking advantage of pre-catalysts is another way to address the oxidation-instability of copper(I). Utilization of NHC-ligands (for a more detailed discussion see chapter 1.1.3.3) that are able to build a copper(I)-carbene-bond and thus enable the implementation of bulky substituents to copper(I) leading to a better protection of the catalyst against moisture and air (see Figure 7d-g). The hydrophilic catalysts are mainly applied in aqueous media to conduct the CuAAC. For instance, the dinuclear NHC-complex (see Figure 7d)[112], the water-soluble 1,3-bis(2,6-di-*iso*-propylphenyl)imidazolidin-2-ylidene (SIPr) copper(I) complex (see Figure 7e)[113] and 1,3-bis(2,6-di-methylphenyl)imidazolidin-2-ylidene (SIMes) copper(I)iodide complex (see Figure 7f)[114] can provide quantitative conversions in the CuAAC in absence of sacrificial reducing agents. Similar results are obtained by applying (2-bis-*N*-crotyl)benzothiazolin-2-ylidene (NSHC)$_2$ copper(I) bromide complex (see Figure 7g)[115], when one N-donor atom of the NHC complex is exchanged versus one sulfur-atom.

Furthermore, homogeneous Cu(I) catalysts anchored to polymeric substrates are developed (see Figure 7h-i). For instance, a PIB-supported Cu(I) catalyst is designed, that is able to efficiently conduct the CuAAC in ethanol/heptane- mixtures at 90 °C (see Figure 7h)[116]. Additionally, this kind of catalyst is reusable by gravity-based separation of the catalyst from the product in subsequent reactions. Applying dendrimers as support material for Cu(I)- nanoparticles (NPs) leads to the simple removal of the

products by extracting the aqueous reaction-media with an organic solvent (liquid-liquid extraction) and thus allows for multiple uses of the same catalyst (see Figure 7i)[117]. Treating the triazole containing dendrimer with copper(II)sulfate and with sodium-ascorbate affords a polymeric copper(I) catalyst, which promotes the CuAAC very efficiently at 25 °C and up to 10 times in a row without a significant loss in yields.
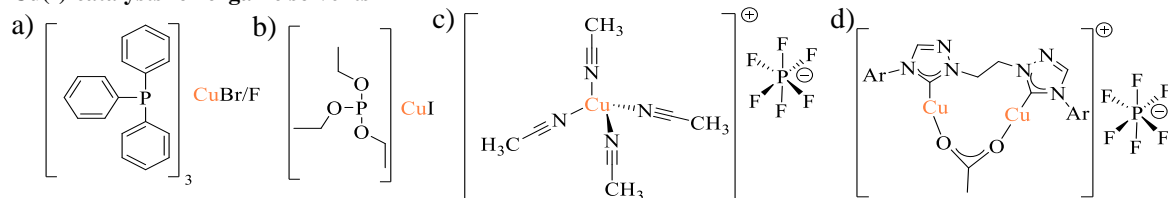
Figure 7. Structures of copper(I) catalysts suitable for the CuAAC at organic or aqueous conditions. a) Bromo/Fluorotris(triphenylphosphine)copper(I); b) iodocopper(I)-triethyl phosphite; c) tetrakis(acetonitrile)copper(I) hexafluorophosphate; d) dinuclear bis-triazolylidene copper(I) acetate hexafluorophosphate; e) (1,3-bis(2,6-diisopropyl-4-((tributylammonio)methyl)phenyl)imidazolidin-2-yl)copper(I) bromide dichloride; f) 1,3-bis(2,6-trimethylphenyl-4-triazolyl-choline)imidazolin-2-ylidene copper(I) iodide; g) (2-bis-*N*-crotyl)benzothiazolin-2-ylidene copper(I) bromide; h) (PIB)-supported Cu(I) catalyst; i) Cu(I)-NPs anchored on dendrimer support.

C) Copper-free CuAAC

Homogeneous conducted CuAAC includes the copper-free "click" chemistry, since reactive components are in the same phase. The elimination of copper(I/II) is of major importance to prevent the formation of toxic copper-ROS and is thus most frequently applied to label living cells or proteins in water[118]. To maintain the good reactivity even in absence of copper(I) another driving force is required. The SPAAC is using the release of the high ring strain of cyclooctynes when converted with azides (see Figure 8a)[10-13]. Accordingly, SPAAC is most frequently utilized for bio-orthogonal labeling due to its insensitivity towards water, its high tolerance to amines and thiols (which are present in living cells) and its stability to redox-processes. It further offers good conversions, even without external pressure, heating or high concentrations of reactants. The efficiency can be increased by modification of the ring-

strain, e.g. by attachment of substituents[119] or electron-deficient moieties as fluor-atoms[10] adjacent to the internal alkyne. However, even the fastest of the strained alkynes ((aza)dibenzocyclooctyne) – achieving a reaction rate of 0.96 $M^{-1} s^{-1}$, which is 450 times higher compared to unactivated cyclooctyne[12] – cannot compete with common rates received by the ligand-accelerated CuAAC (k_{obs} = 10 – 100 $M^{-1} s^{-1}$ per 10 – 100 µM Cu(I)/Cu(II))[120] (for a more detailed discussion see chapter 1.1.3). The pressure-accelerated AAC represents the second copper free "click" version besides SPAAC (see Figure 8b)[121]. Azides and terminal alkynes are pre-organized by supramolecular interactions and AAC is induced by treatment in a hydraulic press, leading to a pressure-accelerated copper-free AAC at room temperature with exclusive formation of the 1,4-triazole-isomer.
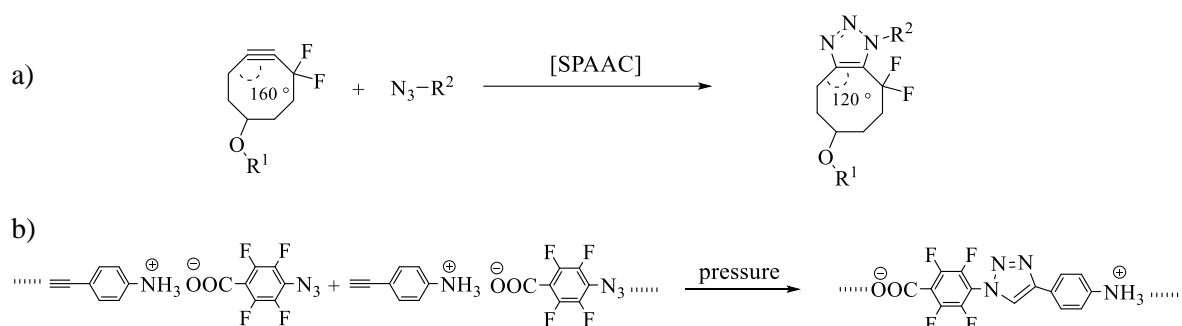
Figure 8. Possibilities for a copper-free „click"-chemistry. a) The release of the ring-strain in SPAAC of highly activated cyclooctyne and azide leads to a copper-free triazole formation. b) Pressure-accelerated cycloaddition of azides and alkynes.

1.1.2 Heterogeneous CuAAC

Heterogeneous catalysis is present, when reactants and catalyst are of different phases and can thus be separated easily from each other.[98] This concept is accessible by the implementation of the active catalytical species to support-materials, which are commonly inert to their environment. The ease in separation of the product and the catalyst is the biggest advantage, when compared to homogeneous catalysis. Thus, the catalyst can be recycled and reused by simple filtration in contrast to the often required chromatographic purification methods in the homogeneous CuAAC. Residual catalyst in products can be neglected, as the amount is lowered tremendously or not present at all in comparison to the homogeneous version. Consequently, heterogeneous catalysis delivers heavy metal free products, thus coming close to be considered as „green-chemistry". It is estimated that 90% of the industrial processes are catalyzed and most of them belong to the heterogeneous catalyzed reactions due to its beneficial characteristics.[122] In case of the heterogeneous CuAAC, the copper(I) is anchored to different support materials, introducing the desired property of insolubility in aqueous or organic solvents. The support materials are composed of various classes such as polymeric substrates, carbon materials, inorganic solids and metallic copper, differing in their complex architectures (see Table 1)[123].

Table 1. Overview of supporter materials applied in the heterogeneous CuAAC.

	kind of supporter material	structure	copper-salt	conditions for the CuAAC	recycle-times
A)	**polymeric substrates**				
1	polymer-networks	1A / 1B	CuI	in MeCN and DCM at RT: > 90 % yields	4 times [124]
			CuI	in t-BuOH:H₂O at RT: 99 % yields	10 times [125]
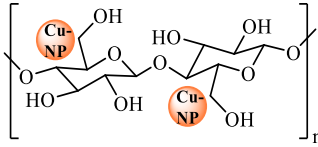
2	biopolymers	OH, HO, OH, Cu-NP, HO, OH, Cu-NP, OH $[\ ]_n$	CuI	in H$_2$O at 70 °C: 96 % yield	5 times [126]

B)	**carbon materials**				
3	charcoal	Cu-NP, Cu-NP, Cu-NP, **charcoal**	Cu(NO$_3$)$_2$	in dioxane at 60 °C: 99 % yield	3 times [127]
4	CNT	Cu-NP, Cu-NP, Cu-NP, Cu-NP, Cu-NP, Cu-NP = (Cu^I porphyrin with Cl substituents)		in H$_2$O at RT: 95 % yield	10 times [128]
5	graphene	Cu$_2$O, Cu$_2$O (on graphene)	Cu(OAc)$_2$	in THF at 40 °C: 99 % yield	10 times [45]
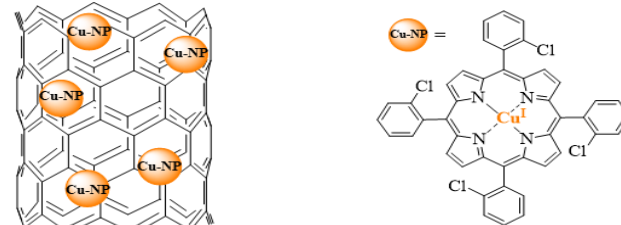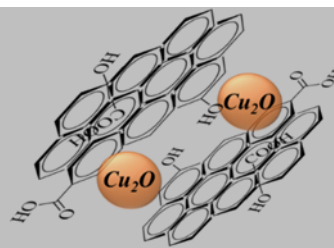
C)	**inorganic solids**				
6	Si	SiO$_2$, ICu, N, R	CuI	no solvent, at RT: 93 % yield	10 times [129]
7	Al	*milling*, **CuSO$_4$/Al$_2$O$_3$**	CuSO$_4$·5 H$_2$O	no solvent, ball-milling required, at RT: 92 % yield	8 times [130]
8	Ti	**Cu(OH)$_x$/TiO$_2$**	CuCl$_2$·2 H$_2$O + NaOH	in toluene, at 60 °C: 99 % yield	3 times [131]
9	mesoporous Si	Si, **SBA-15**, AcO–Cu–OAc, N	Cu(OAc)$_2$	in H$_2$O:HCl at RT: 98 % yield	3 times [132]
10	microporous zeolite	USY-cage type: (Cu$^+$)$_x$[(AlO$_2$)$_x$(SiO$_2$)$_y$]$^{x-}$	CuCl	in toluene at RT: 92 % yield	4 times [133]
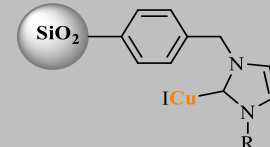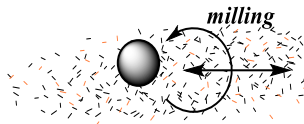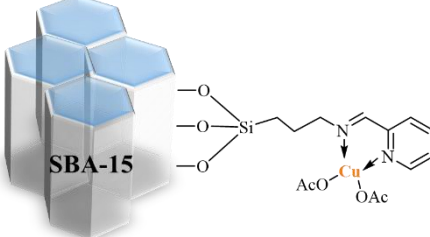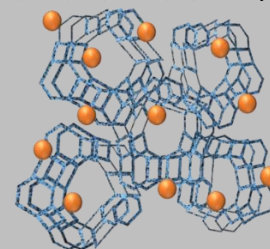
11	microporous metal organic frameworks (MOFs)		Cu(OAc)$_2$	neat at 50 °C: 94 % yield	5 times [134]
12	layered hydrotalites	brucite-like layer $[M^{2+}_{1-x}M^{3+}_x(OH)_2]^{x+}$ $M^{2+} = Cu^{2+} // M^{3+} = Al^{3+}$ interlayer anions / water-molecules $[(A^{n-})_{x/n} \cdot m(H_2O)]^{x-}$ $A^{n-} = NO_3^-, [CO_3]^{2-}$	Cu(NO$_3$)$_2$	in H$_2$O at RT: 93 % yield	5 times [135]
13	layered clays	$(M^+_x)[(Si)_8(M^{3+}_{4-x}\text{-}M^{2+}_x)O_{20}(OH)_4]^{x-}$ Wyoming·CuI	CuI	in DCM at RT: 99 % yield	5 times [136]
14	non-porous poly-(oxometalate) (POM)	$[(n\text{-}C_4H_9)_4N]_4[\gamma\text{-}H_2SiW_{10}O_{36}Cu_2(N_3)_2]$	CuCl$_2$	in MeCN, at 60 °C: 98 % yield	3 times [137]
15	non-porous spinels	CuFe$_2$O$_4$-NP	CuFe$_2$O$_4$	in H$_2$O at 70 °C: 93 % yield	4 times [138]
16	non-porous hydroxyapatite	$[Ca_{10-n}Cu_n(PO_4)_6(OH)_2]$	Cu(NO$_3$)$_2$	in H$_2$O at 70 °C: 95 % yield	8 times [139]
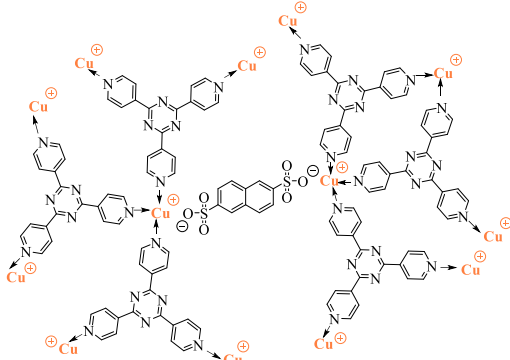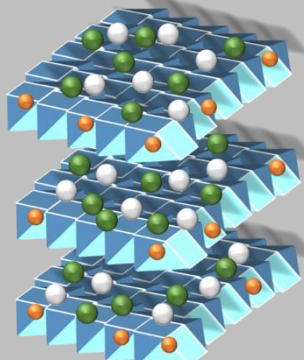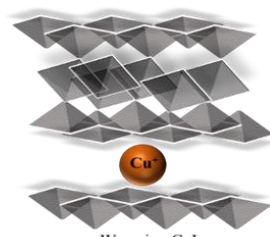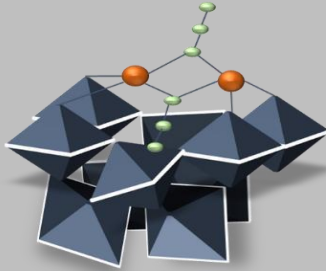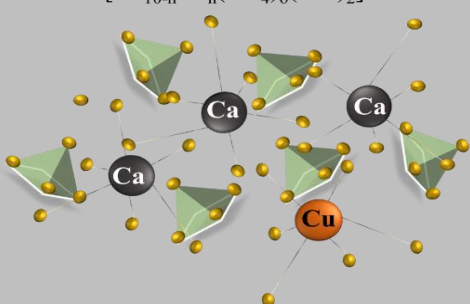
	D)	metallic copper				
17	nanoparticles		$CuSO_4 \cdot 5 H_2O$ + $N_2H_4 \cdot H_2O$	in MeOH at RT: 93 % yield	3 times [140]
18	nanoporous copper	electrochemically de-alloyed $Cu_{30}Mn_{70}$	$Cu(0)$ + $Mn(0)$	in toluene at 70 °C: 99 % yield	10 times [141]
19	copper metals	copper-vial copper-milling ball	$Cu(0)$	milling at RT: > 95 % yield	100 times [142]
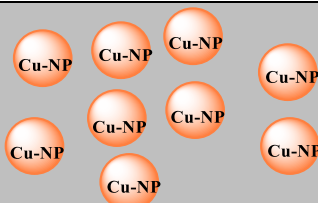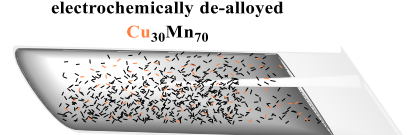
A) polymeric substrates

In the heterogeneous CuAAC polymers are used as substrates for the first time in 2006 in the form of copper(I)iodide modified Amberlyst-A21 (= weak base tertiary amine resin derived from the reaction of a secondary amine with a chloromethylated styrene-divinylbenzene copolymer)[143] (see Table 1, entry 1A)[124]. This poly(styrene) based material is decorated with dimethylaminomethyl, that is able to act as a ligand and a base at the same time, which is known to promote the CuAAC[144-145]. Subsequently, a lot of other polymer-copper(I)-substrates are designed to improve the catalytic efficiency and to increase the number of recycling cycles with less leaching of copper and thus lead to a better sustainability. Therefore, nitrogen ligand grafted polymers are commonly reacted with copper(I) salts. In turn, a catalyst with ionic-liquid group, as is present in ammonium structures, yields 99% in conversion considering a pool of azides and alkynes in water at room temperature, while no lack in activity is observed, when reusing the same catalyst up to 10 times (see Table 1, entry 1B)[125]. The search for more green chemistry and the conservation of resources by closure of material-cycles increase the interest of applying biopolymers as support-materials in the heterogeneous catalysis[123]. Accordingly, copper(I) functionalized substrates based on polysaccharides such as chitosan[146-149], alginate[150] or cellulose[126] (see Table 1, entry 2) provide almost quantitative yields in the CuAAC, requiring elevated temperatures equal to or more than 70 °C though.

B) carbon materials

Activated carbon-based materials are characterized by a good stability, inert behavior against organic molecules and a high surface area caused by porosity[151]. These beneficial properties in addition to the generally required simple and highly efficient separation issue led to their use as support materials in the heterogeneous CuAAC. Functionalization of the surface of the carbons with hydroxy- and carboxyl groups by oxidation processes enables the introduction of transition-metals forming hybrid-materials, which can be applied in heterogeneous catalysis. Especially Cu/charcoal, Cu-CNTs (carbon nanotubes) and Cu-TRGO (thermal reduced graphene oxide) demonstrate to have excellent catalytical activity in the heterogeneous CuAAC[123, 152].

Activated wood charcoal suspended in an aqueous $Cu(NO_3)_2$-solution treated by ultra-sonication leads to the impregnation of the surface with CuO and Cu_2O particles[127]. Several alkynes and benzyl azide are converted nearly quantitatively by applying the aforementioned catalyst dispersed in dioxane at 60 °C in short time scales in the presence of Et_3N (see Table 1, entry 3). This catalyst is reusable up to three times until a loss of activity is observed. A Cu/charcoal catalyst is used under continuous flow

conditions in the CuAAC, albeit the reaction is conducted at 170 °C and 20 bar pressure in acetone[153]. These high temperatures are required as Cu/charcoal systems tend to provide lower activities in comparison to other carbon support materials such as CNT or TRGO.

The change in architecture and morphology of the catalyst leads to a tremendous increase in catalytic activity. Thus, applying CNTs, activated by chemical vapor deposition (CVD) followed by the impregnation with copper(I)-porphyrin, provide up to 95% yield in the CuAAC conducted in water at room temperature (see Table 1, entry 4)[128, 154]. Significant discrepancy in the surface area of multi walled (MW-CNT) and single walled CNT (SW-CNT) lead to priority usage of the MW-CNT with larger surface area and thus better catalytic efficiency. Its cylindrical shape combined with a sufficient size of pores enable the effective dispersion of the Cu-NPs and in turn prevent their agglomeration. This improved behavior in catalysis is mainly based on the efficient anchoring of copper(I) particles on the surface of the CNT[155-156]. However, the dependency of the catalytic efficiency on the diameter of the CNT and the high costs in synthesis[157] limit the application area of these catalysts.

Graphene is obtained by separating a single carbon-layer from graphite and is characterized by remarkable thermal, electronic, mechanical and chemical properties[158]. The conventional mechanical exfoliation method provides low amounts of graphene layers. In contrast to that large amounts of graphene-oxide (GO) are obtained rapidly by the chemical approach using different oxidation routes of graphite[159]. Even though the introduced defects and the additional composition of ~ 5 layers (instead of originally one) diminish some of the beneficial properties of single layered graphene, catalysis in the CuAAC for hybrid materials, consisting of GO and metal-particles is still observed[160-162]. The honeycomb-like structure of GO serves - similar to CNTs - as a scaffold with an optimal surface area for anchoring metal ions and thus prevents the agglomeration of the nanosized particles[163]. GO is produced by chemical oxidation using the Hummers method[164] and is impregnated with $Cu(OAc)_2$. Subsequently, chemical or thermal reduction affords the finely dispersed Cu^I-nanoparticles on graphene-oxide[45]. The obtained catalyst demonstrates good performance in solution and in the melt-state. High conversions in THF at 40 °C of low molecular weight azides and alkynes are detected up to three times in a row, while excellent catalytic activity is observed for the CuAAC of star-shaped azido and alkyne telechelic polymers in the melt at room temperature (see Table 1, entry 5).

C) inorganic solids

Inorganic amorphous materials are easily accessible in large scales and are applied as heterogeneous supports simply by mixing with copper-salts. Insufficient binding of Cu-NPs to the surface of the amorphous solids leads to a significant copper-leaching[123]. In order to reduce the copper-leaching copper(I) can be covalently attached to silica supported catalysts by implementing ligands, such as nitrogen-[129] or phosphorous- moieties to the surface-area[165]. In addition to the effective prevention of copper-leaching the stabilization of the copper(I)-oxidation state is ensured (for more details see chapter 1.1.3). In case of alumina-[130] or titania-[131] supports heterogeneous catalysts are afforded by mixing Cu(II)-salts and the corresponding oxides of metals. Reduction of Cu(II) to Cu(I) in absence of reducing agents is mainly attributed to the *in situ* alkyne homocoupling. The reaction conditions are adapted to ensure an oxygen-free environment, in consequence of missing ligands, able to protect copper(I) from oxidation. Subsequently, additional acceleration by elevated temperatures or mechanical impact is indispensable. However, all of these amorphous catalysts demonstrate activity (> 90% yield) in the CuAAC and are reusable up to 10 times without a significant loss in activity or a detectable leaching of copper (see Table 1, entry 6-8).

Structured inorganic solids can be either of natural or of artificial birth and are most-likely characterized by a very defined morphology of edge-, border- and surface- attached tetrahedrons or octahedrons, often enabling the attachment of transition metals by cation-exchange. In accordance to their structure, pores of different sizes can be created and materials can be further distinguished in meso- ($d = 2 - 50$ nm) and

microporous (d = 1 - 20 Å) ones.[123] In both cases, the increasing surface area makes these support materials very interesting for heterogeneous catalysis, including the CuAAC. For instance, mesoporous silica is generally composed of spherical, cylindrical or hexagonal micelles, consisting of silica walls surrounding the former shaped organic polymers. Grafting of Cu(II)(OAc)$_2$ to the pyridine-imine functionalized surface area leads to a heterogeneous catalyst with high performance in synthesis of 1,4-disubstituted 1,2,3-triazoles at 0 °C to RT[132]. Naturally occurring zeolites inherently provide a microporous morphology and are composed of the general formula: $(M^{n+})_{x/m}[(AlO_2)_x(SiO_2)_y] \cdot wH_2O$. The cations can be exchanged with copper(I)-ions, enabling the usage of zeolites as heterogeneous supports for the CuAAC[133]. The synthetic analogon is made of metal organic frameworks (MOFs), using organic linkers between the M^+-nodes and leading to high conversions in the CuAAC (> 90%) under solvent free conditions up to five times in a row[134] (see Table 1, entry 9-11).

The usage of copper-modified layered hydrotalites[135] or clays[136] in the heterogeneous CuAAC leads to a good catalytic performance (> 90% yield) at room temperature for the regioselective organic synthesis in water or organic solvents, respectively (see Table 1, entry 12-13).

Another setup consists of inorganic amorphous and non-porous supports such as magnetic cuprospinel[138], copper(I) modified poly(oxometalates) (POMs)[137] or hydroxyapatites (HAP)[139], affording high conversions (> 90%) in the CuAAC at elevated temperatures (see Table 1, entry 14-16).

D) metallic copper

Metallic copper is able to provide the required Cu(I) for efficient CuAAC by oxidation of the metallic surface in presence of an oxygen-environment or by comproportionation of Cu(0) and residual copper(II). This process is often promoted further by impact of ultra-sonication and microwave radiation[62, 166]. The CuAAC „click"-reactions between alkynes and azides are also promoted by Cu-NPs even in absence of any support-material in methanol (see Table 1, entry 17)[140]. However, separation issues and the growing agglomeration of NPs are the main drawback of these unsupported NPs in contrast to their supported analogues[167].

Besides these neat NPs, nanoporous copper in the form of CuNPore is applied to conduct the heterogeneous CuAAC[141, 168]. Electrochemical decomposing of the Cu$_{30}$Mn$_{70}$-alloy leads to the catalyst, providing quantitative yields in the CuAAC in toluene at 70 °C (see Table 1, entry 18).

Applying metallic copper in the form of tubings[169], wires[170] and powder[171] leads to the regioselective formation of 1,4-triazoles. The concentration of residual copper in the final "click" product is very low (e.g., 4 – 9 µg/g[171]), since the solid catalyst can be removed with simple work-up techniques. Very high temperatures (100 – 150 °C) are required as a consequence of the low activity of the catalysts and the need to produce copper(I), which in turn leads to reaction conditions similar to the thermal Huisgen reaction, with the only exception of being regioselective. Large amounts of the desired triazole-products are accessible by reacting azides and alkynes especially under flow-reactor conditions combined with a good long-time stability of the applied catalyst[172]. Various alkynes and benzyl halides in presence of sodium azide are converted in a copper vial with a copper milling ball, providing high yields already at room temperature (see Table 1, entry 19)[142]. The vial is reused over 100 times without any loss in yields or reaction rate.

1.1.3 Ligand-accelerated CuAAC

The need to avoid the formation of the highly toxic ROS-species[118] when copper(I/II) encounters oxygen caused the development of new approaches, especially in the field of bioconjugation for the CuAAC. One way to address this issue is the copper free SPAAC, which however leads to tremendous reduction of the reaction-rate (10 – 100 times)[43]. In order to maintain the beneficial kinetics of copper(I) catalyzed cycloaddition another method is found: By addition of external ligands, able to form a complex with copper(I), a better control of the active species within the reaction media is gained and the formation

of the toxic ROS species is prevented by stabilization of the oxidation level (+I) and thus the required amount of the catalyst is reduced to a negligible ppm-level (see Figure 9)[7-8]. Subsequently, ligands can enhance the solubility of copper(I) in the desired media and improve the activity of the catalysts and facilitate the application range of the CuAAC in science[120, 173-175]. More precisely, ligands have to fulfill three different tasks, depending on the applied solvent: 1st, Ligands can protect copper(I) from oxidation by complexation and thus modulate the redox-potential of Cu(II)/Cu(I) pair (standard potential = 159 mV from Cu^{2+}/Cu^+ and 520 mV from Cu^+/Cu^0 (measured *vs* SHE))[176]. This low reduction potential is giving one explanation for the least thermodynamic stability of Cu(I) in solution, compared to the most common oxidation states of copper (0, +I, +II)[36]. The reduction potential is strongly depending on the solvent applied and can be shifted by the addition of ligands[84, 174]. 2nd, the ligands also influence the solvation energy of the corresponding copper-ions[177]. The smaller copper(II) ions in combination with twice the charge of copper(I) interact more strongly with their environment, triggered by their heats of hydration of – 2100 kJ/mol (copper(II)$_{aqua}$) and – 580 kJ/mol (copper(I)$_{aqua}$)[178], resulting in a very short survivability (less than one second)[179] of copper(I)-aqua complexes in solution.[177] Either weaker complexing solvents such as acetonitrile[180] or the addition of nitrogen donors, e.g. amines, pyridine and TEA[181] can counterbalance this otherwise strong disproportionation of copper(I)[182] in solution. 3rd, ligands can act as a base to promote the copper(I)-acetylide formation, thus accelerating the CuAAC[120], if applied in aqueous media. For the purpose of optimizing the conditions for each application field of the CuAAC, a huge ligand screening is performed[63, 174-175, 183-185]. Classification of these ligands is most likely done by their composition. In principal, hetero-atoms are capable of ligand-transition-metal interactions, thus nitrogen, sulfur, phosphor, oxygen and activated carbons such as NHCs are employed in the different types of ligand-classes.
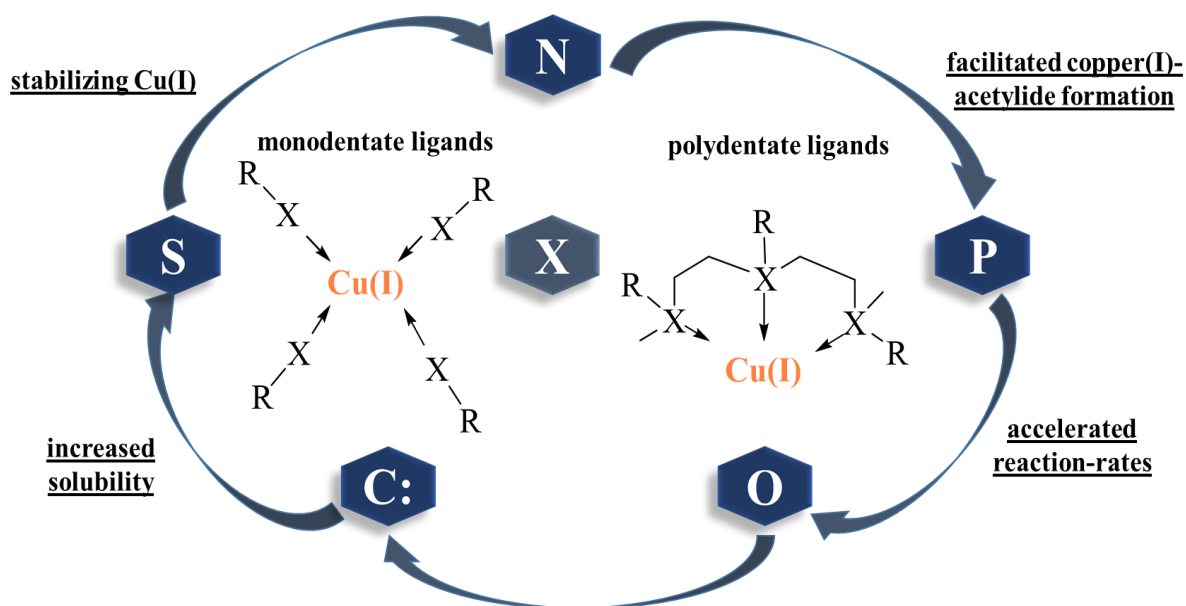
Figure 9. Schematic representation of composition, function and benefits obtained by applying external ligands in the CuAAC.

1.1.3.1 Nitrogen-ligands in the CuAAC

Nitrogen-ligands represent the broadest quantity of ligands (see Figure 10), beginning with the low-molecular sp^3-hybridized supplements such as triethyl-amine[186-187], propyl-amine[188], DIPEA[59, 89] and tributyl-amines[189], which are mainly added to promote the copper(I)-acetylide formation in aqueous media. A precise investigation of the acceleration-effect, emerging from polydentate ligands in the CuAAC of diazido-terminated poly(styrene), propargylether (ratio 1:1) and CuBr (50 mM) as catalyst in DMF at 25 °C, led to the following order[63]: PMDETA (230) > HMTETA (55) > Me$_6$TREN (50) > tpy (8.6) > TPMA (1.7) > bipyridine (0.4) > ligand-free CuAAC (1). The addition of aliphatic amines

(acceleration of 50 – 230) afforded a higher boost in reaction rate in comparison to pyridine-ligands (acceleration of 0.4 – 8.6). This is mainly attributed in the accelerated formation of the π-complex, related to a higher basicity and a higher electron-donating property of amines compared to pyridines. Tripodal PMDETA (230) is more than four times faster than the tetrapodal HMTETA (50), since the latter is coordinatively saturating the copper(I)-catalyst, thus blocking the required alkyne attachment. Applying the tripodal polytriazole-based (Trz)₃[107, 183] or tripodal benzimidazole-based (BimY)₃[174-175] ligands in the CuAAC accomplishes an even superior performance in terms of stabilized copper(I) and an increased reaction rate in different media. Utilization of the first generation ligands composed of tris-(triazolylmethyl)amine skeletons such as TBTA[183] and THPTA[190-191] in the CuAAC showed an improved stability of the desired oxidation state (+I), increasing the redox-potential of Cu(I)/Cu(II) by almost 300 mV[183]. The partial or complete exchange of linear alkyl or benzyl ligands with bulky *tert*-butyl groups as occurring in TTTA[36], BTTAA[192], TABTA[193], BTTE[185] and BTTP[194] prevents undesired alkyne-coupling (see Figure 10). Despite minor differences in acceleration-efficiency a better control in the current application task is established, e.g. better solubility in aqueous media by attachment of ionic structures such as ammonium moiety within the sidechain of the ligand.

Figure 10. Structure of common N-donor-ligands applied to accelerate the CuAAC. Acceleration factors (framed ligands) are adapted from[63] for the CuAAC in DMF at 25 °C, applying CuBr/L ratios of 1:1, except for bpy it is 1:2.
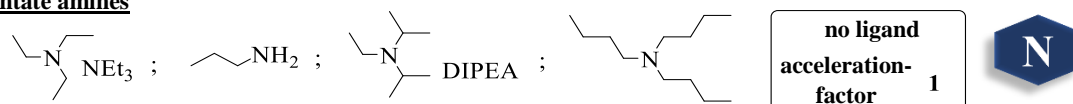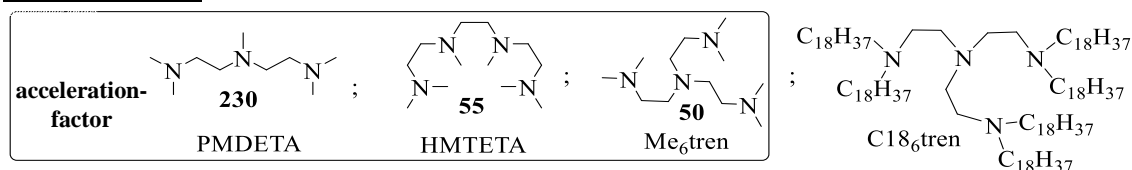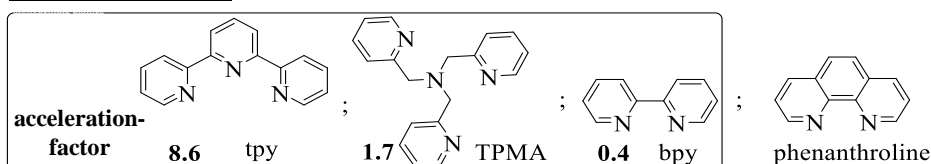
Fast reaction rates (k_{obs} = 48 – 38 455 M^{-1} s^{-1} per M Cu) for the CuAAC in DMSO:H_2O, 80:20 (Cu:L, 1:2) or in DMSO:H_2O, 10:90 (k_{obs} = 5601 – 151 879 M^{-1} s^{-1} per M Cu) (Cu:L, 2:1) are provided by tris-(heterocyclemethyl)amines, further allowing a decrease of the initial Cu concentration to 10 – 100 µM, while a significant ligand-acceleration is still ensured[120]. The ligand-accelerated CuAAC can be up to thousandfold faster in kinetics compared to the ligand-free CuAAC[183, 195]. This significant acceleration is mainly attributed to the improved solubility of the catalyst and further supported by the facilitated formation of the strained metallacycle[33, 36].

The benefit of the ligand-accelerated CuAAC is caused by a change of the mechanism[120, 173, 196], while the effect is strongly dependent on the donor-strength of the chosen ligand and the applied solvent[120] (see Figure 11). The CuAAC is accelerated most efficiently by a dinuclear copper(I) complex, which is preferably facilitated by tripodal ligands, allowing the assemble of both copper(I)-centers with free accessible coordination sites for reactants. During the catalysis-cycle a threefold competition of the free coordination sites at copper(I)-centers arises (1st: azide-reactant, 2nd: ligands, 3rd: solvent-molecules), while the donor-strength of the azide-reactant is inherently weak. The strength of the remaining two competitors can be adjusted by proper tuning of the external ligand and the solvent used for the reaction. The donor strength of solvents differentiate over a broad range, while in the current approach water belongs to the weaker donor solvents compared to DMSO, DMF and 1-methylpyrrolidin-2-one, which are referred to as the strong donor solvents in the following.

The tripodal external agents are in general composed of three different units attached to the central amine and can be subdivided into three classes (see Figure 11a). In dependence on the binding affinity of the ligands to copper(I) the following classes can be distinguished[120]: *Class I* ligands are characterized by weak donor-abilities, which are often based on (triazolylmethyl)amine (Trz) skeletons. For ligands categorized in *class II* two side-arms are exchanged either by benzimidazole (BimH) or pyridine (Py) units, which tend to bind much stronger compared to the Trz ligands of *class I*. Also replacing the third arm against BimH or Py completely inhibits the catalyst as a consequence of the very strong binding affinity and thus represents the distinctive feature of *class III* ligands. Accordingly, only ligands belonging to *class I* and *II* can be used to afford the efficient ligand-accelerated CuAAC. The proposed mechanism of the ligand-accelerated CuAAC by Finn *et al.*[120] and further adapted by Straub *et al.*[173] is giving the explanation for the different kinetics observed, when either varying the amount of ligand, its chemical composition or the donor-strength of the ligand-solvent sphere (see Figure 11b): Inhibitory complexes **A** and **B** tend to attenuate the CuAAC (see Figure 11b, right top). Complex **A** lacks the opportunity to coordinate a second copper center, which is required to facilitate the C-N bond forming step. In the dimerized complex (**B**) all coordination sites of copper are blocked by the ligand. The weaker donor-abilities of the reactants cannot compete with this ligand-sphere, thus suppressing the catalytic activity. Inhibitory complex formation is most frequently observed when *class II* ligands are applied in excess, especially when conducted in aqueous media with its weak coordination-ability. In contrast, *class I* ligands in combination with water as solvent provide excellent acceleration in kinetics even though the ligands are used in excess (up to 4:1, ligand:Cu), but can lose their potential action in a competing strong-donor-environment such as DMSO. Both, *class I* (in aqueous media) and *class II* ligands (in strong donating solvents) permit access for solvent-molecules to binding sites of copper and in turn the catalysis cycle can start by the formation of complex **C** (see Figure 11b, framed catalytic cycle). Its halide and solvent ligands can be exchanged to form the acetylide-complex (**D**), which further coordinates the second reactant (**E**), allowing for a fast ring-closure in the next step (**F**). The efficiency of ligand-acceleration is now dependent on how the desired triazole-product is released, which can follow two different routes (**path I** and **II**). In weak donor solvents (**path I**) the dinuclear copper complex persists in the inner cycle until the triazole-product is released, ready to conduct the next "click"-reaction and is thus facilitating the process. In strong donor solvents (**path II**) the dinuclear

copper complex **F**, which is required for efficient catalysis breaks up in the mononuclear copper-complex (**A**) and the solvated copper-triazole-complex (**G**) (see Figure 11b, left bottom). Even though triazole-products are produced, in the next step the copper catalyst is trapped again in the equilibrium of the inhibitory complexes **A** and **B**, which is giving the explanation for the different kinetics observed for the numerous combinatorial possibilities of external ligands and solvent media. It can be generalized that *class I* ligands are favored in aqueous media, due to their weaker binding affinity to copper,
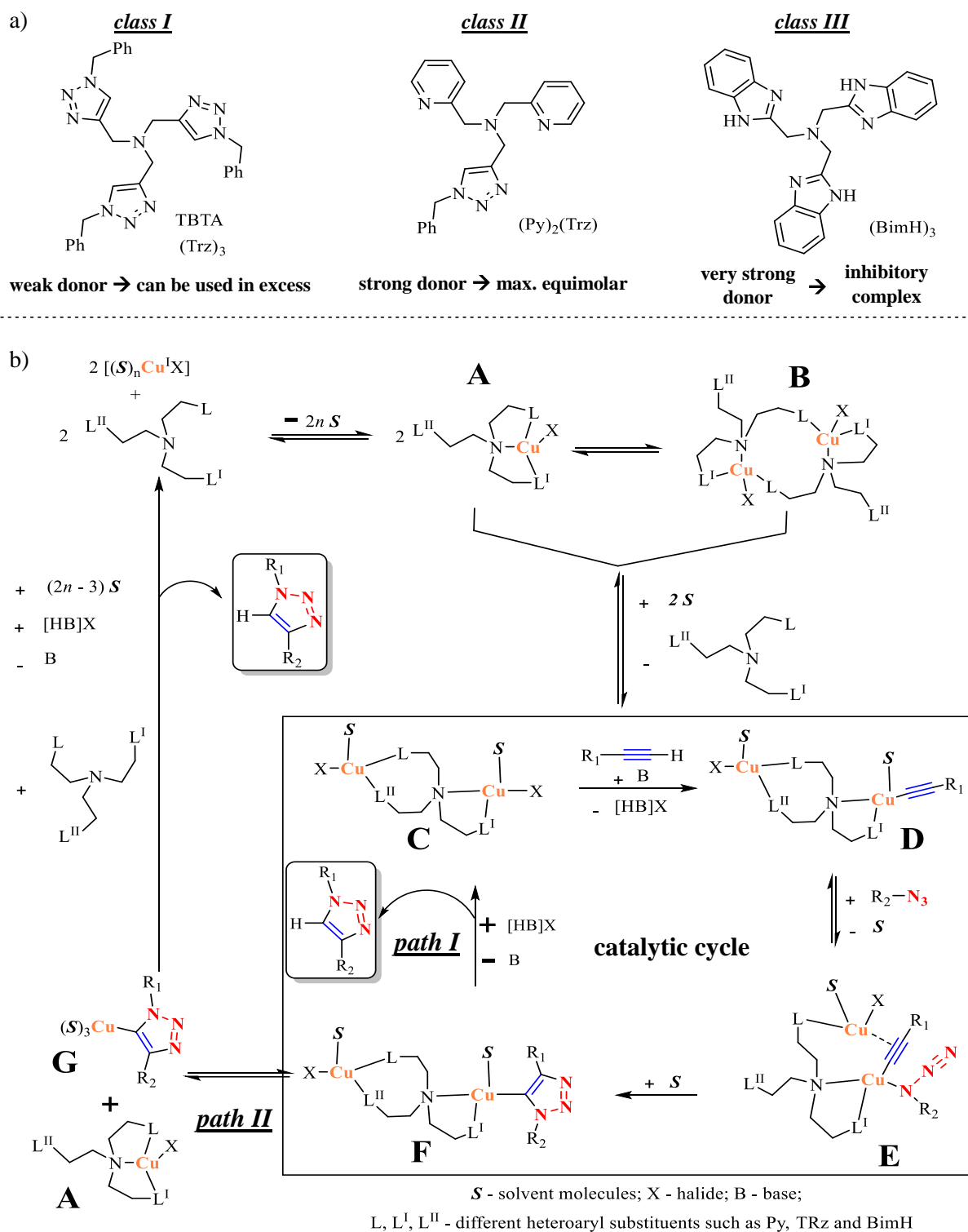
Figure 11. a) Different classes of external ligands subdivided by their ability to coordinate to copper(I) for the ligand-accelerated CuAAC. b) Proposed mechanism of the ligand-accelerated CuAAC adapted from [120, 173].

preventing the formation of inhibitory complexes (**A**) and (**B**). For the same reason *class I* ligands can be used in excess up to 4:1, while the best ligand to copper ratio is found to be 1:1 up to 2:1. In a competing environment such as strong-donor-solvents application of *class I* ligands leads to tremendous drop in kinetics of the CuAAC, whereas *class II* ligands offer their full potential. In this case the optimal copper to ligand ratio is found to be 0.5:1 to 1:1, while excess of *class II* ligands leads to a limited access of copper(I) for reactants and in turn to stagnation in catalysis.

1.1.3.2 Phosphorus-, oxygen- and sulfur-ligands in the CuAAC

Phosphane ligands are introduced to increase the solubility of copper(I) sources in organic solvents such as toluene and DCM in the following order: $(PPh_3)_3 > PCy_3 > BINAP > dppe$[197]. Several copper(I)-salts are stabilized against oxidation by attachment of phosphorus ligands as occurring in $(EtO)_3P\cdot CuI$ and $[CuBr(PPh_3)_3]$[198], which is further extended by the utilization of phosphoramidites[199] to accelerate the CuAAC (see Figure 12a). However, the reaction rates are not as fast as in the case of nitrogen-based ligand acceleration, for which further supply with DIPEA or DBU and microwave radiation is required. Oxygen containing ligands are used least in the CuAAC and are implemented in the form of L-histidine (see Figure 12b), providing similar acceleration compared to TEA and DIPEA[200]. The attachment of the amino-acid to the imidazole is essential, since neat imidazole is not providing any catalytic activity at all. L-Histidine is affecting a similar acceleration as is originated by TBTA, BPS and THPTA ligand addition, while advantageously less toxicity is observed[201]. However, L-histidine seems to be the unique representative for this purpose, since acceleration emerging from O-N-O macroligands, producing interlocked [2]rotaxanes[202], are less efficient compared to the ligand-free CuAAC. Also the hydroxylamine ligands remain inactive[203], while the sulfonated ligands (see Figure 12c) such as low-molecular thioanisoles provide good performance in water at room temperature, yielding the desired triazole-product within minutes[204]. However, in complex fields of application such as bioconjugation
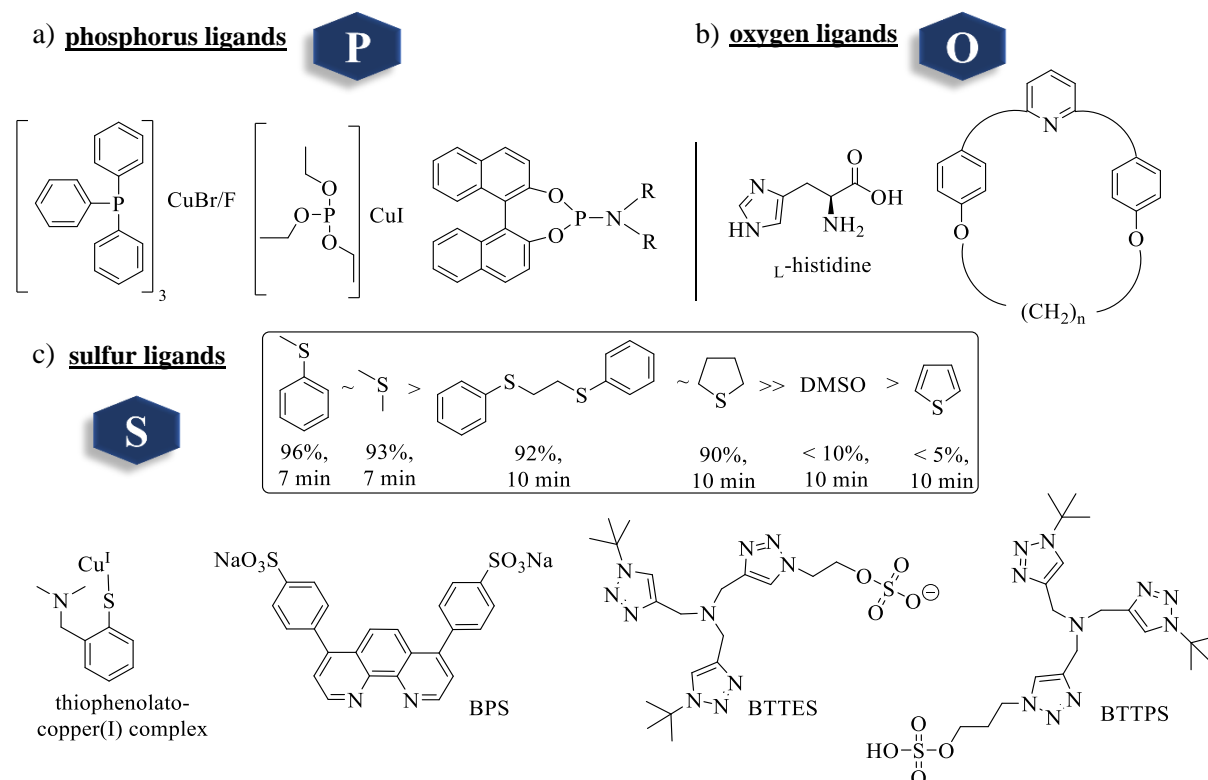
Figure 12. Structure of external ligands to accelerate the CuAAC based on a) phosphorus-, b) oxygen- and c) sulfur-ligands. Conversions of benzyl azide (0.5 mmol) and phenylacetylene (0.6 mmol) in H_2O at RT for various CuBr (5 mol%)/L (30 mol%) combinations (framed sulfur ligands) are adapted from[204].

with the aid of the CuAAC polytriazolyl-based ligands are once again the preferred choice. For instance, an increased solubility and a reduced toxicity are achieved by introducing sulfonated moieties as occurring in sulfonated bathophenanthroline (BPS)[195, 205], BTTES[206] and BTTPS[207], providing as similar efficiencies as their non-sulfonated analogues[207]. The thiophenolato-copper(I)-complex achieves good yields (> 90%) in the CuAAC in DCM and is also found to be useful for decoration of dendrimeric structures and thus is a good alternative to other Cu(I)-catalysts[208].

1.1.3.3 Carbene-ligands in the CuAAC

The NHC-based ligands (see Figure 13) evolve their protection effect by the formation of a carbene bond between the metal applied and the carbon localized in the center of two nitrogen-atoms (see also chapter 1.3) and has proven to be highly efficient in organocatalysis[209-210]. The NHC-based ligands are characterized by a remarkable stability towards moisture, heat and oxygen, allowing their application in the CuAAC in absence of any other supplements[184]. General conclusions of the catalytic performance of the NHC-Cu(I) complexes (NHC = SIMes, 1,3-bis(2,6-di-methylphenyl)imidazol-2-ylidene (IMes), SIPr, 1,3-bis(2,6-diisopropylphenyl)imidazol-2-ylidene]copper(I) (IPr), 1,3-bis(cyclohexyl)imidazol-2-ylidene]copper(I) (Icy), 1,3-bis(adamantyl)imidazol-2-ylidene]copper(I) (IAd) and 1,3-bis(*tert*-butyl)imidazol-2-ylidene]copper(I) (I*t*Bu)) in the CuAAC derived from a detailed investigation: 1st, in case of the neutral complexes of the general formula [(NHC)CuX] the saturated SIMes provide faster conversions than the unsaturated IMEs/IPr analogues[211-212]. 2nd, the respective anion of the neutral complexes also influences the reaction- acceleration of the CuAAC in the following order: iodine > bromine > chlorine for most of the NHC ligands[184, 212-217]. Applying [(IAd)CuI] in the neat CuAAC completes quantitative conversion within 10 minutes and thus is representing the most efficient catalyst amongst the neutral NHC-Cu(I) catalysts[216]. 3rd, the reaction- acceleration is strongly dependent on the applied solvent, e.g. [(SIPr)CuCl] accelerates the CuAAC most in THF > *i*-PrOH > H$_2$O > DMF > H$_2$O:*t*-BuOH, 1:1 > acetone ~ DMSO[213]. The other NHC ligands provide poor conversions in organic

NHC ligands (neutral)

SIPr   SIMes   ICy   I*t*Bu

IPr   IMes   IAd
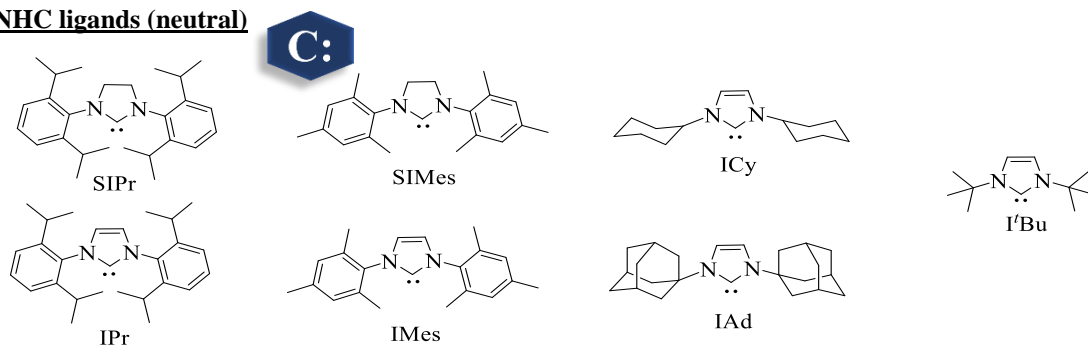
as **[(NHC)CuX]**, X = I > Br > Cl **a)**   **SIMes > IMes > SIPr > IPr b)**

NHC ligands (cationic)

as **[(NHC)$_2$Cu]X**, X = BF$_4^{\ominus}$ or PF$_6^{\ominus}$; NHC = SIPr, IPr, SIMes, IMes, ICy, IAd, I*t*Bu

[(SIMes)$_2$Cu]BF$_4$ [(IAd)$_2$Cu]BF$_4$ [(ICy)$_2$Cu]PF$_6$
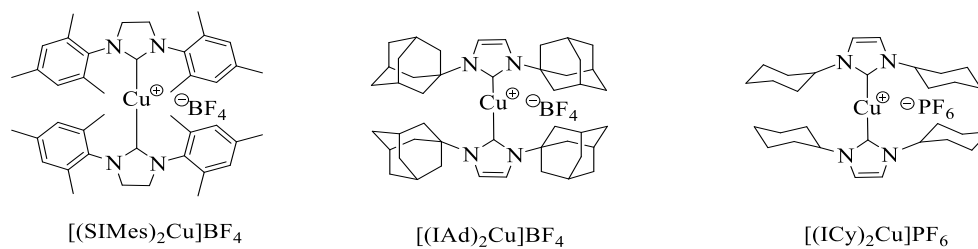
Figure 13. NHC-based Cu(I)-catalysts employed in the CuAAC, subdivided in neutral complexes of the general formula [(NHC)CuX] and cationic complexes of the general formula [(NHC)$_2$Cu]X. a) Row of the reactivity (blue) observed for neutral NHC-complexes in conducting the CuAAC of benzyl azide and phenylacetylene under neat conditions at RT[216] or b) in aqueous *t*-BuOH mixture at RT[212].

solvents such as THF, DCM and *t*-BuOH, but an improved efficiency when applied in water or under neat conditions[212, 216]. 4th, *N*-alkyl substitution seems to accelerate the CuAAC more efficiently, than *N*-aryl modified NHC-Cu(I)-complexes (IAd ~ ICy > SIPr > IPr). 5th, it is assumed that the efficiency in catalysis is strongly dependent on the binding affinity of the ligands to Cu(I), which is influenced by the bulkiness of the ligands and their electron donating properties.

The cationic derivatives of the general formula [(NHC)$_2$Cu]X, X = PF$_6^-$, BF$_4^-$ are also investigated[218]. Their catalytic performance in the CuAAC is similar to their neutral analogues, while no general trend can be observed. For instance, the cationic [(SIMes)$_2$Cu]X is the most inefficient ligand combination, in contrast to its neutral analogue [(SIMes)CuX][212], which is more efficient than IMes > IPr ligands in accelerating the CuAAC. The most efficient catalyst amongst the cationic bis(NHC)-Cu(I) complexes employed in the CuAAC of various azides and alkynes is the [(ICy)$_2$Cu]PF$_6$, leading to a noteworthy turnover number (TON) of 16 000 at low copper(I) loadings (50 ppm) for reactions conducted in water at room temperature[218].

Progressing research included the design of specific (NHC)-Cu(I) catalysts, e.g. different combinations of IPr-ligand with other NHC- or phosphorus- ligands[211, 219] (see Figure 14a-b). Furthermore, [(SIMes)CuCl] encountered by nitrogen- ligands[184, 215] (see Figure 14c) and recently abnormal NHCs-(aNHCs) Cu(I) catalysts[220-222] (transition metal is bond via C-4 carbon atom, instead of metal bonding to C-2 carbon atom in normal NHC-metal complexes) are developed (see Figure 14d). Altogether, the outcome to the CuAAC (e.g., TON of **I** = 19 800 for 0.005 mol% catalyst loading in the CuAAC of benzyl azide and phenylacetylene at 25 °C under neat conditions) is comparable to the efficiency obtained by the normal NHC-Cu(I)-catalysts, developed previously by Nolan *et al.*[209-210, 212-213, 216, 218, 223-224]. However, in the various composition of ligands a conspicuous integration of nitrogen containing moieties seems to be favored, indicating that nitrogen-based ligands facilitate the CuAAC the most.
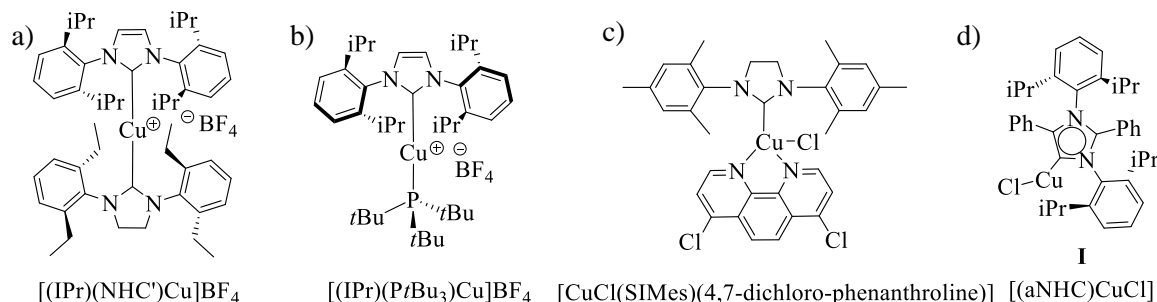
Figure 14. Development of specific NHC-Cu(I) complexes for the CuAAC included the design of a) IPr-NHC-Cu(I) combinations; b) IPr-phosphorus ligand combination; c) SIMes- nitrogen ligand combination; d) aNHC-Cu(I) catalysts.

1.1.3.4 Chelation-assisted (ca) CuAAC

Briefly after discovering the CuAAC auto-acceleration of the reaction has been observed. This is attributed to the increasing concentration of triazole-rings and referred to their ability to act as ligands to promote the reaction further (see Figure 15)[82, 107, 183]. The acceleration is mainly based on the formation of 1,2,3-triazole-rings, containing three N-donor-atoms, which are able to act as internal donors and thus forming a temporary complex with copper(I)[6, 40, 82]. As a consequence, the copper(I)-acetylide can be pre-organized, leading to a close proximity between the active centers – the copper(I)-acetylide and the next azide-group. The growing concentration of triazole-rings acting as internal ligands, leads to an increase of the reaction-rate with proceeding time, as detected for multivalent polymers (poly(acrylates) and PIBs) in the CuAAC. In turn of this auto-catalytic effect the reaction of multivalent PIBs with poly(propargyl acrylate-*co-ran-n*-butyl acrylate)s is accelerating itself by a factor of up to 4.3.[40]
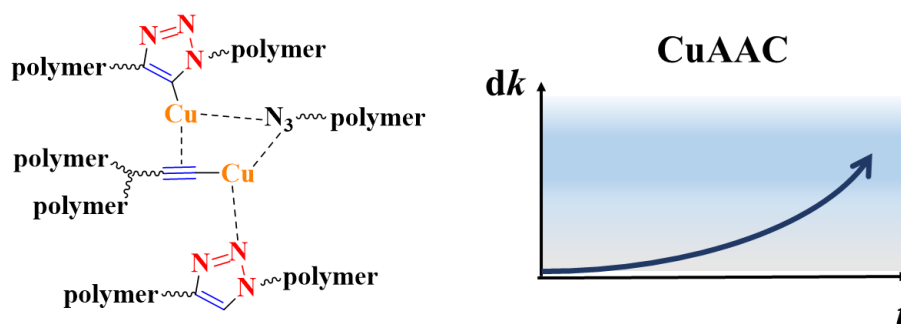
Figure 15. Autocatalytic-effect observed in the CuAAC, resulting in increasing reaction-rates with proceeding time, in turn of increasing triazole concentration, able to act as internal ligands, pre-organizing the next copper(I)-acetylide close to the next azide group.

Based on this rate acceleration by pre-organization of the reactants, the utilization of internal ligands capable of the chelation-assisted CuAAC can provide superior acceleration compared to the external nitrogen-ligands (see Figure 16). Besides the supply of external ligands and the changed structure of the alkyne-moiety as occurring in SPAAC, the direct change of composition adjacent to the azide leads to tremendous effects in kinetics. Even though picolyl azides have previously been applied as reactants in the CuAAC[225-226], their beneficial outcome in reaction-rate is described for $Cu(II)(OAc)_2$ mediated the CuAAC in alcoholic media for the first time[109]. Full conversion of „click"-reactions is observed within 120 seconds under optimal conditions at room temperature, which is addressed to the electronically and sterically facilitating property of the nitrogen-atom close to the actual active azide-moiety. Further investigations hypothesizes that the nitrogen-atom inside the pyridine-ring close to the azide group enhances its electrophilicity by chelating the catalytic copper(I)-center in close proximity to the alkylated N_α of the azide group[227]. Thus, the kinetic barrier for the rate-determining formation of the metallacycle is lowered upon nucleophilic attack of the copper(I)-acetylide.
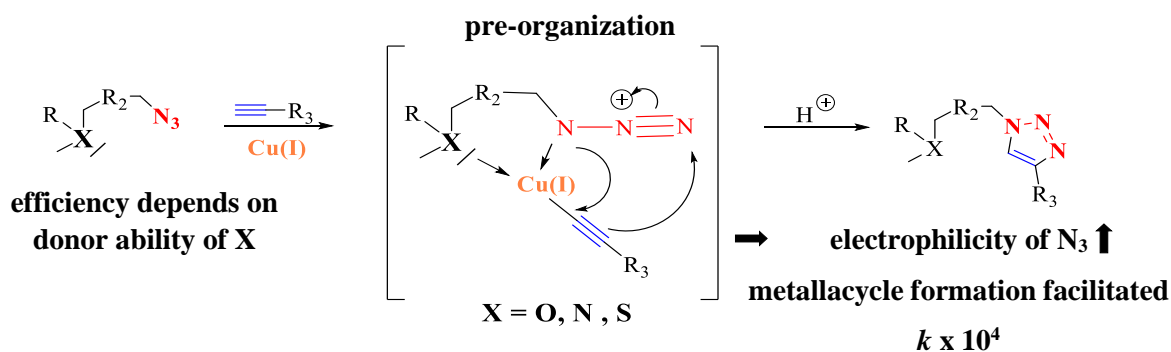
Figure 16. Mode of action of the internal chelation-assisted CuAAC.

Ligand-screening[227] for the CuAAC, exploiting $Cu(II)(OAc)_2$ as a catalyst without a reducing agent conducted in *t*-BuOH revealed that acceleration-effect of nitrogen-chelation is superior to other hetero-atoms such as sulfur and oxygen (see Figure 17a-b), which is consistent with the findings obtained by previous researches, regarding the usage of external ligands (compare with chapter 1.1.3.1 – 1.1.3.3). In depth, employing ether- and sulfur- bridged auxiliary ligands in the CuAAC provides only low to moderate yields (6 – 53%) within extended reaction times (16 – 24 hours, see Figure 17a), while most of the amine/pyridyl ligands achieve 86 – 99% triazole-yield within three hours (see Figure 17b). A detailed kinetic report of a library of azides capable of chelation-assistance subjected to the CuAAC, applying the common $CuSO_4$/NaAsc system, clearly states the superior performance by increased reaction rates of up to $4 \cdot 10^4$ times compared to standard azides without chelation-assistance (see Figure 17c)[185].
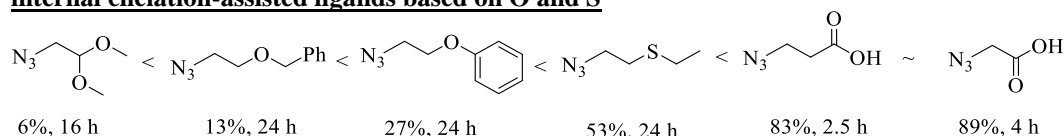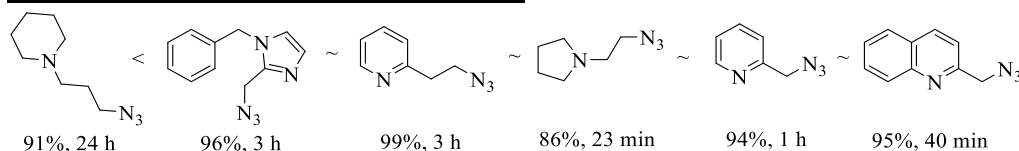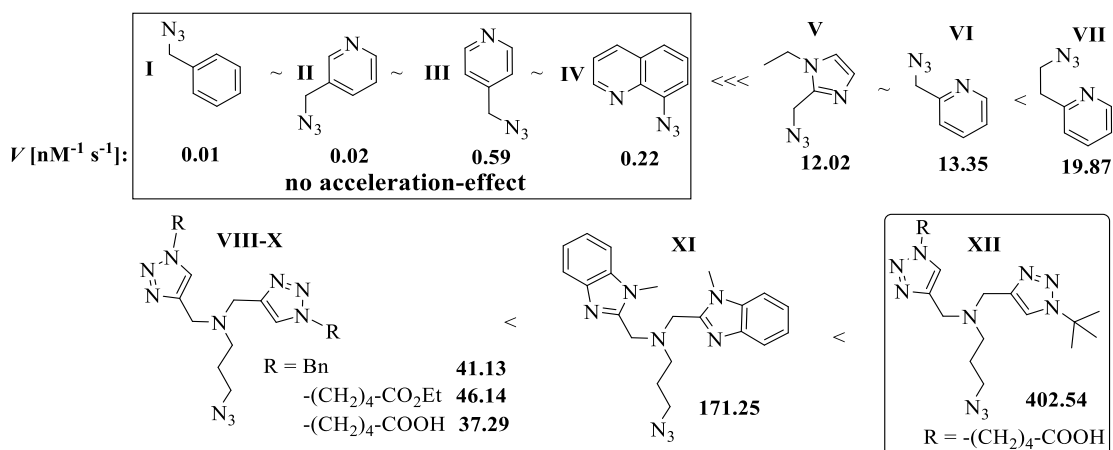
Figure 17. Design of azide-reactants, capable of chelation-assistance. a) Sulfur and oxygen based donor-ligands. Efficiency is tested upon reaction with 4-ethynylanisole in *t*-BuOH by addition of Cu(OAc)$_2$ and ordered in accordance with increasing yields in the CuAAC by time[227]. b) Nitrogen based donor-ligands. Efficiency is tested upon reaction with 4-ethynylanisole in *t*-BuOH by addition of Cu(OAc)$_2$ and ordered in accordance with increasing yields in the CuAAC by time [227]. c) Nitrogen based donor-ligands. Efficiency is tested upon reaction with 7-ethynylcoumarin in phosphate buffer:DMF by addition of CuSO$_4$ and sodium ascorbate and ordered in accordance with increasing reaction rate *V* provided in the CuAAC, which are adapted from [185].

The extent of the acceleration-effect depends on the physical proximity of the donating nitrogen, responsible for the pre-organization of the copper(I)-acetylide and the reactive azide-moiety. Thus, insignificant acceleration is provided from pyridine functionalized methyl azides in *meta-* and *para-* position (compare **I** – **III**, *V* [nM^{-1} s^{-1}] = 0.01 – 0.59). Similar observations are made for reactants, which are restricted in their mobility such as 8-azidoquinoline (**IV**, 0.22 nM^{-1} s^{-1}), where the fixed position of the azide prevents the internal chelation. In turn, the addition of a mobile methylene spacer in-between the rigid aromatic system and the reactive azide group is enabling the full potential of the chelation-assistance effect. For instance, usage of the 2-(2-azidoethyl)pyridine (**VII**, 19.87 nM^{-1} s^{-1}) leads to an increased reaction rate by ~ $2 \cdot 10^3$ and is also slightly more active in comparison to picolyl azide (**VI**, 13.35 nM^{-1} s^{-1}) as a consequence of a better movement of the azide-group. Even superior reaction rates are obtained by adapting the polydentate(triazole)- and polydentate(benzimidazole)- composition of the most efficient external ligands to the ca-CuAAC ligand design (see **VIII** – **XII**, 37.29 – 402.54 nM^{-1} s^{-1}). Hence, employing **VIII** – **X** in the ca-CuAAC causes the reactions to quantitatively convert within mere seconds (37.29 – 46.14 nM^{-1} s^{-1}). The fastest known ligand up to date (**XII**, 402.54 nM^{-1} s^{-1}) is also substituted with a bulky *tert*-butyl group and an acid-moiety in the sidechain to enhance the solubility in aqueous media and to further prevent the alkyne homocoupling. Accordingly, the modified bis(triazole)-based **XII** shows slight improvement in reaction-rate compared to the unmodified benzimidazolium analogue (**XI**, 171.25 nM^{-1} s^{-1}), which still achieves fast conversions in the ca-CuAAC.

General trends observed in the chelation-assisted CuAAC

The low yields obtained by sulfur- (**I'**) and oxygen- (**II'**) auxiliary ligands are attributed to their lower Lewis basicities in comparison to the nitrogen-ligands (**III'**) (see Figure 18a). As a consequence, a weaker binding of the Lewis acidic Cu(II) is assumed, resulting in an insufficient activation of the azide group, limiting the acceleration effect originated by sulfur- and oxygen- ligands (**I'** and **II'**)[227]. Subsequently, the favorable kinetics that occur with nitrogen-auxiliary ligands make them the preferred choice in the CuAAC. Accordingly, applying picolyl azides allows for a tremendous reduction of the required copper-amount and thus lowers the toxicity level to such an extent that efficient labeling of proteins is enabled (compare **IV'** and **V'** in Figure 18b)[43, 228]. Precise studies revealed that electron-donating groups (OMe) (**VI'**) attached to the pyridine-ring improved the kinetic outcome in the CuAAC (in comparison to **V'**), while electron-withdrawing groups (Cl (**VII'**), F) act *vice versa* (see Figure 18b). This is attributed to the reduced donor-capacity of the nitrogen-atom, while the higher the capacity the better the coordination of the copper(I)-acetylide, which facilitates the reaction-rate. Hence, the increase
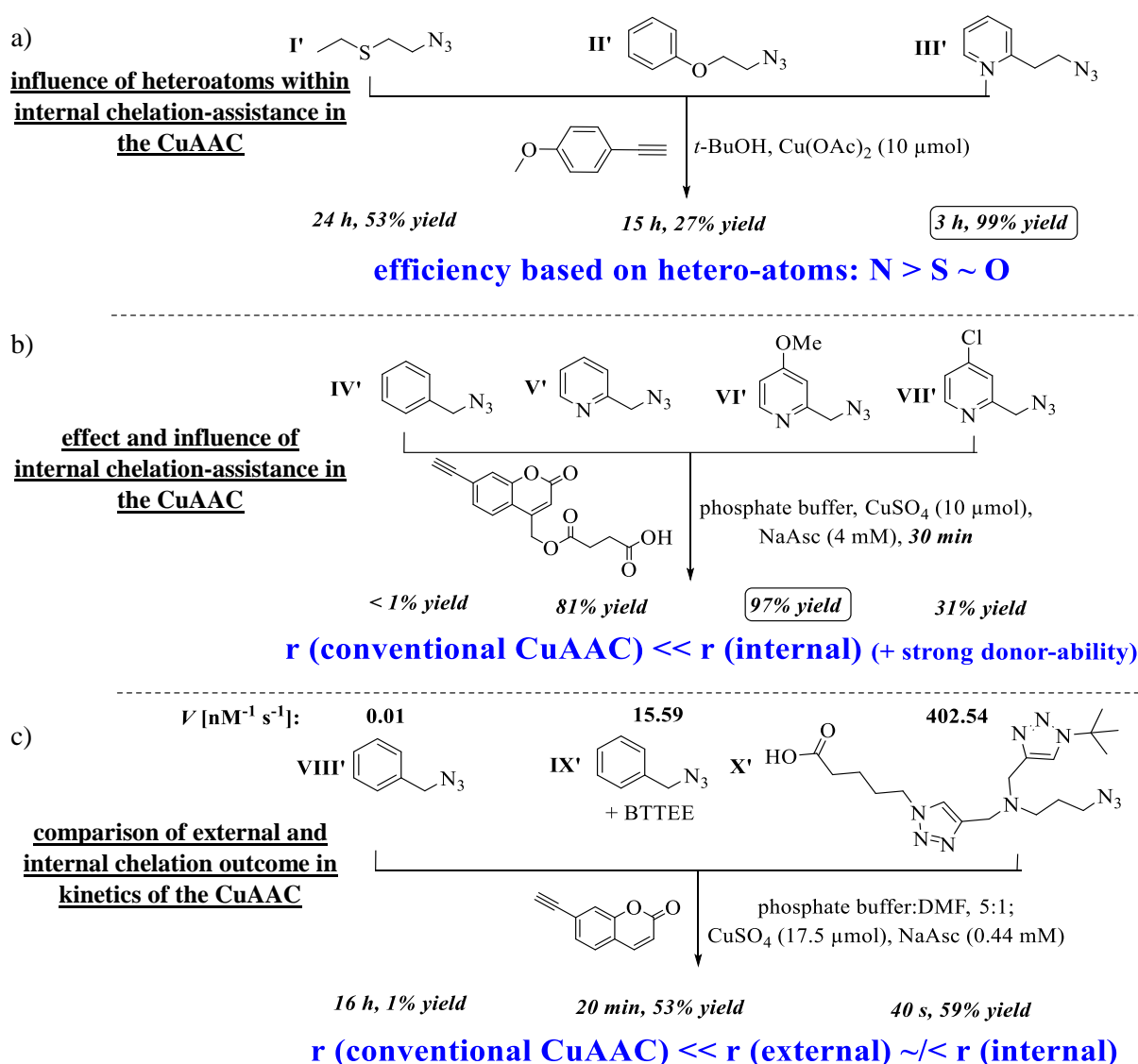
Figure 18. Beneficial outcome in kinetics when reactants, capable of internal-chelation are applied in the CuAAC. a) Performance of internal-chelation assisted ligands in the CuAAC with different hetero-atoms such as nitrogen (N), sulfur (S) and oxygen (O). Results are adapted from [227]. b) Effect of the rate acceleration in the CuAAC by usage of internal chelation-assisted ligands (picolyl azide) and the influence by electron- donating/withdrawing groups compared to conventional ligands (benzyl azide) without chelation-assistance. Results are adapted from [43]. c) Differences in rate of conventional (benzyl azide), ligand-accelerated (external: BTTEE) and the internal chelation-assisted CuAAC. Results are adapted from [185].

of copper(I)- concentration close to the reaction-center is another reason for an outstanding acceleration in the CuAAC. Accelerated processes achieved by internal chelation-assistance is at least similar or even superior compared to acceleration-effects originated by external ligands such as THPTA or BTTEE[185], applied to convert aromatic- or aliphatic azides, making the internal chelation-assistance the fastest CuAAC version up to date[43] (see Figure 18c). For instance, the reaction rates V [nM^{-1} s^{-1}] of the conversion of benzyl azide (**VIII'**) without further supplements, benzyl azide in presence of the external ligand BTTEE (**IX'**) or the newest chelation-assisted internal ligand (**X'**) with 7-ethynyl-coumarin are compared[185]: while the conventional CuAAC of pure benzyl azide provides the least reaction rate (**VIII'**: 0.01 nM^{-1} s^{-1}), an acceleration by more than 1500-fold (**IX'**: 15.59 nM^{-1} s^{-1}) is observed by the addition of the external ligand BTTEE, being even exceeded by additional 26-fold when employing the internal chelation-assisted ligand (**X'**: 402.54 nM^{-1} s^{-1}).

1.2 Covalent crosslinking systems for autonomous self-healing (SH) approaches

Self-healing in material science describes the ability of a material to regain a specific property, which has been lost as a consequence of failure[229]. Recognizing any input of damage and the simultaneous availability of the appropriate response, e.g. rapid formation of a covalent network via crosslinking multivalent reactants, is the characteristic of autonomous self-healing materials. Non-autonomous approaches, however, require external stimuli such as light or temperature to trigger self-healing[230]. These biomimetic materials try to copy the principle of curing liquids in nature[231]. Similar to humans, when blood is filling the gap as a consequence of a cut in our skin and thus inducing self-healing, synthetic liquids diffuse into the crack, react with each other and seal the fracture point in the material. Such a concept can be realized by implementation of multivalent polymers capable of conducting the required crosslinking within a host-material. The created network combines the cracked areas and thus prevents the failure of the material (see Figure 19a).
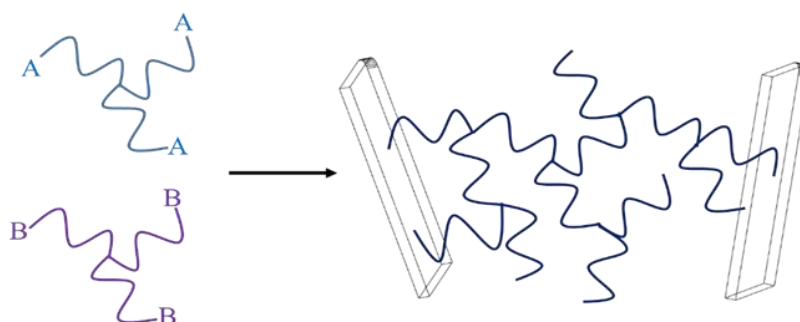
Figure 19. Crosslinking of two complementary functionalized multivalent polymers to form a macromolecular network inside the gap of two cracked surfaces.

Besides the ability to form a dense network, emerging from a high thermodynamic gain in reaction, the reactants have to resist adverse conditions. For instance, very high tolerance to other functional groups in an adjacent environment, a long storage life-time and the capacity to maintain a liquid-flow-behavior even at low temperatures is simultaneously required. These criteria are particular fulfilled for the CuAAC, making it the ideal chemistry to develop autonomous self-healing approaches at low temperatures[6]. For the first time the CuAAC crosslinking is used to prepare resin type structures upon reaction of trivalent azides and alkynes to link metallic surfaces (e.g., copper) by non-covalent interactions, exerted by the formed triazoles or unreacted acetylenes, respectively. (see Figure 20a)[232]. The strength of the adhesion formation is further investigated, applying a plethora of multivalent azides and alkynes to the CuAAC, mediated by metallic copper plates in presence of Cu(I) catalysts[233]. In a second approach a bulk step growth polymerization of bivalent azides and alkynes through the CuAAC is conducted (see Figure 20b)[234-235], while utilizing homogeneous [CuBr(PPh₃)₃] (T_P = 96 °C) the

CuAAC is more efficient than heterogeneous Cu/C (T_P = 140 °C). In a third approach the efficiency of the CuAAC mediated crosslinking, varying both, the monomer architecture (A-D) and the Cu(I)-catalyst source (E-F), has been systematically researched (see Figure 20c).[6] A large variety of low molecular weight monomers of star shaped architecture (A) together with various Cu(I)-sources are subjected to DSC measurements in order to find optimal conditions to conduct the CuAAC crosslinking. Hence, **II** (R = (CH$_2$)$_2$-CH$_3$) in combination with **III** (R = Et) in presence of [Cu(PPh$_3$)$_3$]F shows a conversion at T_p = 50 °C.[236] Upon melt-rheology experiments low molecular weight **IV** and polymeric star shaped **VII** (M_n ~ 4 000 g/mol) in presence of [Cu(PPh$_3$)$_3$]Br turned out to provide the fastest crosslinking (gelation time = 380 min) at 40 °C.[42] As efficient crosslinking is often limited by insufficient diffusion of reactants, liquid reactants of different molecular weights (M_n ~ 5 – 35 kg/mol) and functional group density (3 – 21 groups/chain) are developed (B-D).[40, 44] Thus, network-formation of **VI** (M_n ~ 6 500 g/mol) with PIB-based alkyne **VIII** (M_n ~ 6 300 g/mol) through the CuAAC is accomplished within 290 minutes at room temperature.[40] Further changing from star shaped alkyne **VIII** to random poly(propargyl acrylate-*co-n*-butyl acrylate) **XI** (M_n ~ 7 000 g/mol) increases the number of functional groups per chain from three to approximate eight, resulting in an increased efficiency in the subsequent CuAAC (gelation time = 104 min, RT) (approach C). Decreasing the molecular weight of polymers (**VI** and **XI**) leads to decreased gelation times, which is attributed to the increased molecular mobility.
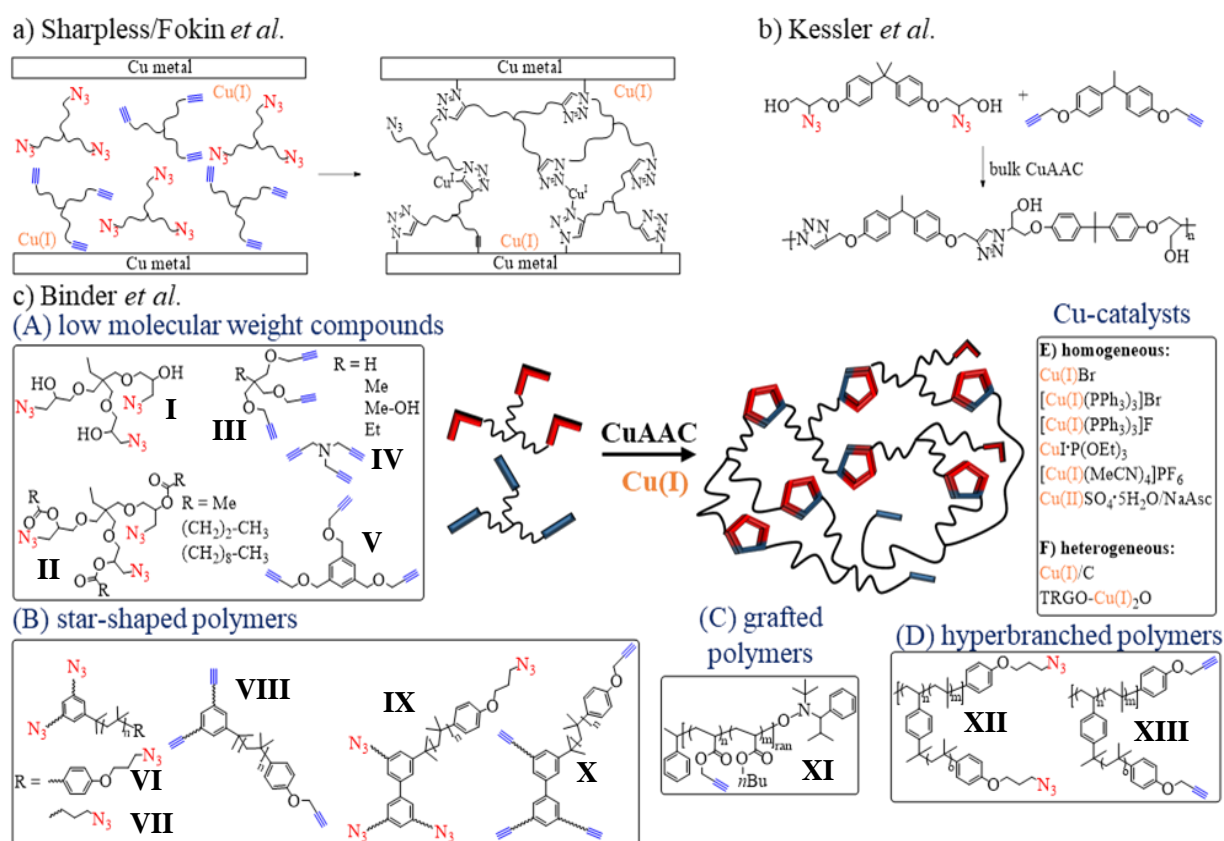
Figure 20. The CuAAC for crosslinking approaches; a) bulk polycondensation of bivalent structures; b) multivalent monomers, forming adhesives upon contact with Cu(I) ions generated from Cu(0) surface; c) systematical screening of multivalent azides and alkynes (A-D) as healing agents and Cu(I)-catalysts (E-F) for a capsule-based system.

A similar effect towards auto-acceleration[82, 107] of the CuAAC (e.g., **VI** + **VIII** + [Cu(PPh$_3$)$_3$]Br) is observed, resulting in an acceleration of up to 3.8 for the more mobile **VI$_a$** (M_n ~ 5.5 kg/mol) or 2.1 for the more rigid **VI$_b$** (M_n ~ 30 kg/mol) with progressive conversion, respectively[40]. The gelation time required for crosslinking PIBs through the CuAAC is further reduced to 33 minutes at room temperature by introducing a hyperbranched version of spherical shaped **XII** (M_n ~ 34 100 g/mol) and **XIII** (M_n ~

35 300 g/mol) with up to nine arms containing the functional monomer groups (approach D).[44] Besides this change of architecture for kinetic improvement, further attempts have been made, including the change from homogeneous (E) to heterogeneous catalysts (F)[45, 49-50, 152, 236-241]. In total, these researches are systematically improving the efficiency of the CuAAC crosslinking approaches to develop autonomous sensing[48, 51, 242] (for a more detailed discussion see chapter 1.3) and low temperature self-healing systems (for more details see discussion of entry 9A and 9B of Table 2 this chapter).[6, 39, 240]

In order to design a covalent self-healing approach, crosslinking chemistry needs to be implemented into a material, which is first described by White *et al.*, using the capsule based system in 2001 (see Figure 21).[243] Their system consists of dicyclopentadiene (DCPD), protected by encapsulation in urea-form-aldehyde shells to prevent degradation and premature crosslinking. Upon rupture of the scaffolding epoxy matrix (see Figure 21a) and the embedded capsules the healing content is released (see Figure 21b), thus closing the crack upon contact of the monomers and the Grubbs catalyst, triggering ring-opening-metathesis-polymerization (ROMP) (see Figure 21c and Table 2, entry 1 for healing chemistry). This healing-process recovers 75% in toughness of the virgin material.
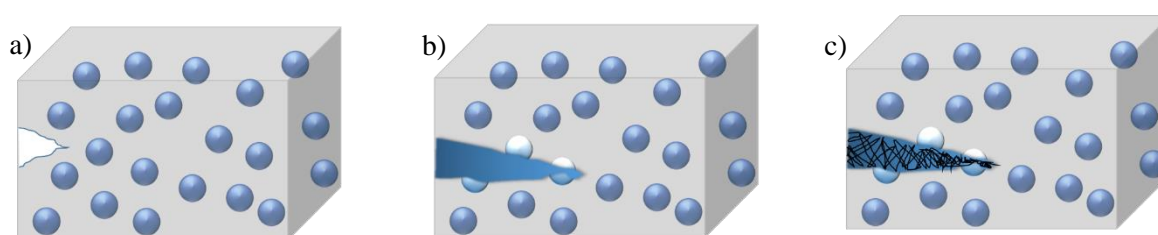
Figure 21. Schematic representation of a self-healing system, corresponding to White *et al.*[243] a) Crack appears at the left side of the specimen, consisting of epoxy-matrix, embedding Grubbs first catalyst and UF-capsules, containing DCPD-monomers. b) Upon proceeding crack size capsules are ruptured and are thus releasing their healing-content. c) The DCPD-monomer is getting polymerized when getting into contact with the catalyst and in turn sealing the crack.

This crucial trigger caused the development of a plethora of covalent SH approaches, aiming to increase SH-efficiency, thus opening an access to our everyday life[230, 244] (see Table 2). Even though, healing efficiency is defined as the restoration of a specific material property and is summarized in one specific percentage, it is noteworthy that performance of covalent SH approaches is a very complex process, depending on a variety of influencing parameters[229]. A rough distribution of the dependency can be ordered as in the following: First, the chemical concept applied, second, the temperature the experiment is conducted at and third, the examined property. In order to create the covalent SH approach particulate fillers need to be embedded into a host material, requiring the compatibility of both. Therefore, the microcapsules have to possess an adequate strength to ensure protection of the reactive components, proper dispersion in the scaffolding matrix and a long shelf-time stability, but also the correctly tuned fragility to break upon stress, if required[245-246]. These characteristics can be adjusted in terms of density, thickness, size and architecture of the microcontainers (capsule or vascular interwoven channels)[247]. Exact dosage and volume fraction of the external healing containers embedded in the host material is decisive to improve healing efficiency.[248-249] The addition of microcontainers to a final material is affecting the mechanical performance, which can lead to increased fracture toughness or a reduced mechanical strength.[245] Catalysts, which are often added to enhance the activity of crosslinking, need high stability concerning degradation as observed for Ru-carbene catalysts[250], which are commonly applied in olefin-metathesis capsule based SH approaches. Furthermore, a good dissolution of the catalyst is required to ensure a well dispersion and thus the ability to conduct crosslinking throughout the host material.[251] Considerations have to be expanded upon applicability tests to the SH material, when stress-induced, approaching crack is rupturing the microcontainers, releasing the liquid healing agents to the cracked area via capillary effects, which upon mixing can seal the crack by covalent crosslinking[252]. In this process, both the diffusion and the crosslinking are rate-determining steps, which

strongly depend on the temperature (usually at or below RT) and the composition of the crosslinking components (chain length, rigidity, chemistry of reactive groups) applied. The material rehabilitation is also dependent on the appearing crack- and the available healing volume[247]. In order to qualitatively and quantitatively evaluate the healing performance, strong efforts have been made for adaption of appropriate methods, techniques and specimen geometries.[253] A collection of the present mechanical self-healing concepts for polymers and their dependency on their chemical and matrix composition as well as the healing- temperature and efficiencies can be found in Table 2.[230, 246]

Table 2. Autonomous self-healing systems based on the formation of covalent networks in dependence of matrix, temperature and healing-efficiency.

	self-healing concept	conditions
A)	**capsule-based systems**	
1	*ROMP – DCPD*	epoxy-matrix, healing recovery: 90% at RT after 10 hours[254-255]
2	*thiol - isocyanate*	epoxy-matrix, healing recovery: 54% at RT after 5 days[256]
3	*maleimide - based*	epoxy-matrix (furan-functionalized), healing recovery: 71% at RT after 1 day[257]
4A	*siloxanes – DBTL*	epoxy-matrix, healing recovery: 24% at 50 °C after 1 day[258]
4B	*siloxanes – Pt-catalyst*	PDMS-matrix, healing recovery: 100% at RT after 2 days[259]
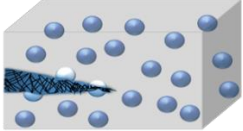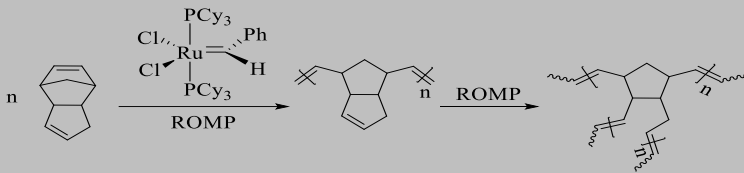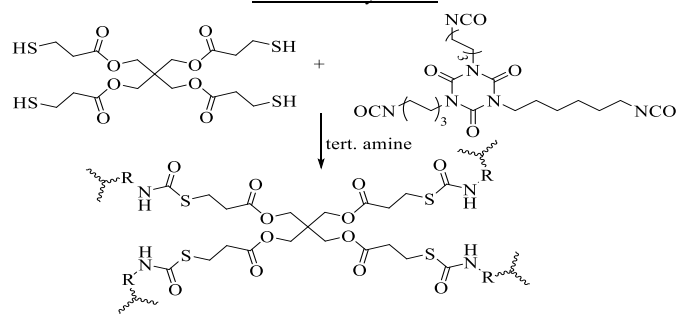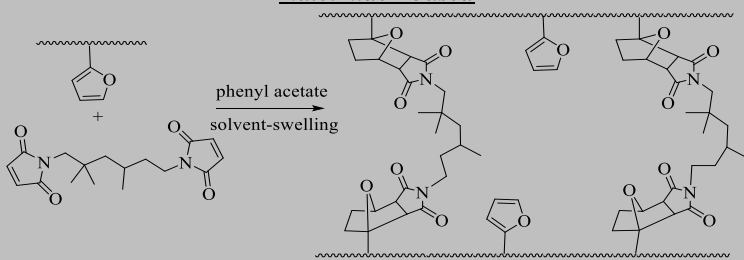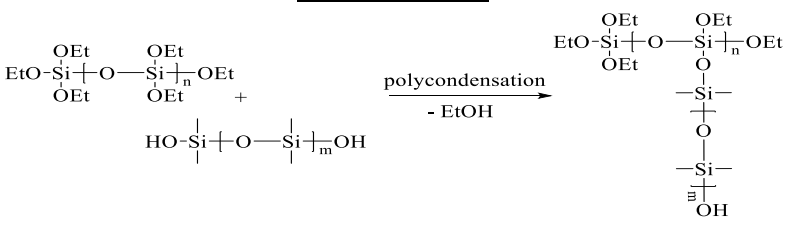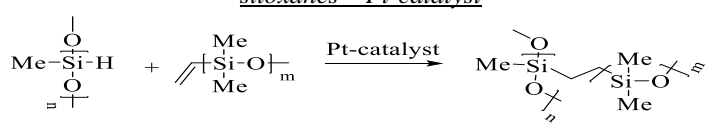
5	*amine - epoxy*	epoxy-matrix, healing recovery: 77% at RT after 1 day[260], by applying EPON-815H and EPIKURE 3274: healing recovery: 91% at RT after 1 day[261]
6	*thiol - epoxy*	epoxy-matrix, healing recovery: 86% at - 10 °C after 36 hours[262]
7A	*CuAAC*	PIB-matrix, healing recovery: 91% at RT after 5 days[39]
7B		epoxy nanocomposite, healing recovery: 100% at RT after 36 hours[240]
B)	**vascular based systems**	
8	*isocyanates*	closed-cell isocyanurate foam, healing recovery: 100% at RT after 1 day[263]
9	*cyanoacrylates*	polyester, healing recovery: 97% at RT after 1 day[264]

The original first autonomic SH-approach consisting of the DCPD-ROMP system compounded to an epoxy-thermoset, which is chosen due to its good adhesion to various materials, recovered 75% of fracture toughness at RT.[243] By varying the microcapsule and catalyst concentration the healing performance is increased to over 90% and completed within 10 hours (see Table 2, entry 1).[254-255] Employing the thiol-isocyanate chemistry requires residual amines inside of the host-epoxy material to catalyze the crosslinking reaction (see Table 2, entry 2)[256]. A two-capsule based approach is designed, where the tetradentate thiol-component and the tridentate isocyanate agents are separately encapsulated (melamine-formaldehyde and UF shells). Upon rupture of the microcapsules and a healing time of five days a moderate 54% of the virgin fracture toughness is recovered at RT, which is attributed to the high viscosity of the healing agents, spatial distribution of the microcapsules and an insufficient healing volume. Incorporation of multimaleimide (MMI) filled UF-capsules into an epoxy-amine thermoset leads to a 71% recovery of the initial load after fracture by DA-crosslinking and the swelling of phenyl acetate, which is added to dissolve the MMI (see Table 2, entry 3)[257].

The siloxane based healing approach achieves healing efficiencies of just 24% at 50 °C within the epoxy matrix (see Table 2, entry 4A)[258], whereas the similar chemistry provides 100% healing efficiency within a PDMS matrix at room temperature (see Table 2, entry 4B)[259], due to the same composition of the healing agents and the host material, leading to a good miscibility. Hence, a lot of efforts have been made to design epoxy-thermosets capable of autonomous healing by epoxy-based healing strategies, providing healing performance of up to 91% via nucleophilic ring-opening by either residual[266-267] or supplemented amines[260-261] for crosslinking reactions (see Table 2, entry 5). Significant improvement is achieved by the addition of a thiol component to the epoxy concept, leading to the design of the lowest temperature self-healing approach recorded so far (see Table 2, entry 6)[262]. Healing efficiencies of 86% at – 10 °C are achieved, indicating a good liquid-flow behavior of the healing agents, maintaining their high reactivity just in presence of a tertiary amine catalyst. However, thiols tend to react with a versatile pool of functional groups, thus lacking a sufficient storage life and are one of the most odorous components existing, e.g. the perception threshold of ethanethiol is about 1 mg/t and thus added to liquefied gases as odor sensor. Hence, these systems are rarely applicable in real-life systems.

Furthermore, the CuAAC crosslinking is employed when subjecting a specimen of a high molecular weight PIB-matrix (M_n = 250 000 g/mol), containing azido telechelic three-arm star PIBs (M_n =

3 900 g/mol) and low molecular weight liquid alkynes, encapsulated separately to micron-sized UF-capsules, to tensile-stretch measurements (see Table 2, entry 7A).[39] Before strain experiments have started optical micrographs clearly show the appearance of unruptured capsules, being finely dispersed inside the host material. Measuring the tensile storage modulus reveals the loss of 30% in strength, after 150% strain is applied to the specimen, containing 15wt% of capsules. Subsequent storage of the specimen at RT or at 60 °C for five days leads to an increase of the storage modulus to 91% or 107%, respectively.

A systematical screening of healing agents and Cu(I)-sources leads to an improved crosslinking efficiency in the CuAAC[39-40, 42, 44-45, 48-50] (for a more detailed discussion see Figure 20c), resulting in a superior CuAAC capsule based epoxy nanocomposite with graphene filler in terms of SH performance (see Table 2, entry 7B).[240] The added graphene filler is acting as both the catalyst to conduct the CuAAC crosslinking and a reinforcement agent to counterbalance the reduced tensile strength, caused by the addition of capsules, which establish the SH ability into the epoxy composite. In depth, two different approaches (I, II) are investigated, consisting of two-capsule based (I) and one-capsule based (II) concepts. Approach I uses liquid, three-arm star-shaped and low molecular weight azides and alkynes, separately encapsulated in poly(urea-formaldehyde) shells of ~ 400 nm size, which are uniformly dispersed (15wt% in total) in the epoxy nanocomposite along with a Cu(I)-source as the CuAAC catalyst. While the expected loss of the Young's modulus from 1240 MPa (neat epoxy) to ~ 1110 MPa caused by the addition of capsules (15wt%) in presence of homogeneous $[Cu(PPh_3)_3]Br/F$, reinforcement by addition of Cu_2O-TRGO filler is more than counterbalancing material fatigue, increasing the Young's modulus to 1440 MPa, which is attributed to an efficient load transfer of GO and epoxy by adhesion[268]. Notching the specimen (approach I + Cu(I)-TRGO) leads to a decrease of the storage modulus E' from 2150 MPa to 1900 MPa, of which 91% is recovered by treating the specimen at 60 °C for a period of six hours[240].

An improved healing performance is achieved by applying the one-capsule based approach II, in which only the azide component is encapsulated in comparatively smaller poly(vinyl formal) (PVF) capsules of ~ 100 nm size. The alkyne component, however, is uniformly dispersed in the matrix. The capsule loading to the specimen is significantly reducing the mechanical integrity by a continuous decrease of the Young's modulus from E' = 1440 MPa (neat specimen) to 910 MPa (20wt% capsule-loading). This reduction is also counterbalanced by the addition of Cu(I)-TRGO to the epoxy composite, possessing a Young's modulus of 1560 MPa at 15wt% capsule-loading and providing full recovery in healing performance after 36 hours at room temperature. Healing efficiency is improved with increasing capsule loading, thus 20% recovery at 5wt%- in comparison to 60% at 10wt%- and finally 100% recovery at 15wt%- and 20wt%- capsule loading at RT after 48 hours is detected. It is assumed, that 5wt% and 10wt% capsule loading is providing insufficient healing volume to fill the crack plane completely, limiting the healing performance. Considering the contrasting effects of both mechanical fatigue with increasing capsule-loading and the difference in healing, an optimal loading of 15wt% is recommended. Furthermore, the homogeneous $[Cu(PPh_3)_3]Br/F$ catalysts provide 75% recovery after being stored at RT for 36 hours, thus also being less efficient in terms of healing performance compared to the heterogeneous Cu(I)-TRGO (100% recovery). These results demonstrated that with regard to mechanical integrity and the healing performance the heterogeneous Cu(I)-TRGO is superior to the commercial and homogeneous $[Cu(PPh_3)_3]Br/F$ catalysts. This is primarily caused by the scaffolding properties, emerging from the graphene sheets, which effectively prevent an agglomeration of the copper(I) nanoparticles (size ~ 25 nm)[45, 269], improving the long-time capability of such a SH nanocomposite. In contrast, homogeneous catalysts tend to form agglomerates within the epoxy matrix, limiting their SH performance with increasing time[240].

The vascular based approaches can also lead to healing-efficiencies of more than 90%, while two of them utilize isocyanates (100%, see Table 2, entry 8)[263] and cyanoacrylates as healing agents (97%, see Table 2, entry 9)[264]. The complex SH-mechanism, consisting of the acylhydrazine/methacrylates approach, is one of the best concepts to date to provide large volume SH, filling gaps that exceed 35 mm in diameter and recover 62% of total absorbed energy of the initially impacted damage (see Table 2, entry 10)[265]. However, the required dense network of the pipelines introduced into the material significantly affects the virgin property of the host material, limiting the application field of the vascular based concepts.

A capsule based approach, exploiting the CuAAC crosslinking healing agents (offering various open opportunities to be discovered), might lead to the design of an orthogonal SH-material, able to address the major challenge most of the autonomous SH approaches cannot compete with until now: the ability to provide highly efficient crosslinking reactions at temperatures below 20 °C, since lower temperatures cause most of these reactions to stagnate. For instance, successfully implementing SH materials to aircrafts, flying at an altitude of about 8 000 – 12 000 meters, dominated by temperatures of -50 to -80 °C, could lead to the prevention of expensive repair-costs, emerging from otherwise unhindered growing micro-cracks.[270]

1.3 Mechanochemical sensing

Efficient damage sensing can be a powerful tool to reduce extensive repairs of manufactures. In the form of radiation at the damaged area a precise localization of the failure in material is signalized and leads to a deeper understanding in the operating principle and the reason of failure. One way to address this issue is the utilization of mechanochemistry, able to give a chemical response to a mechanical impact, often leading to the failure of materials. The chemical response either consists of a structural transformation in the chemical composition, causing a change of the properties such as color-change (see Figure 22a) or of the collapse into reactive components, which are able to conduct a second (= desired) reaction (see Figure 22b)[271]. The mode of action and the beneficial outcome is based on the structural composition of such mechanophores: the enclosure of a labile bond close to the center of long polymer chains enables the efficient transmittance of the mechanical force to the active core.
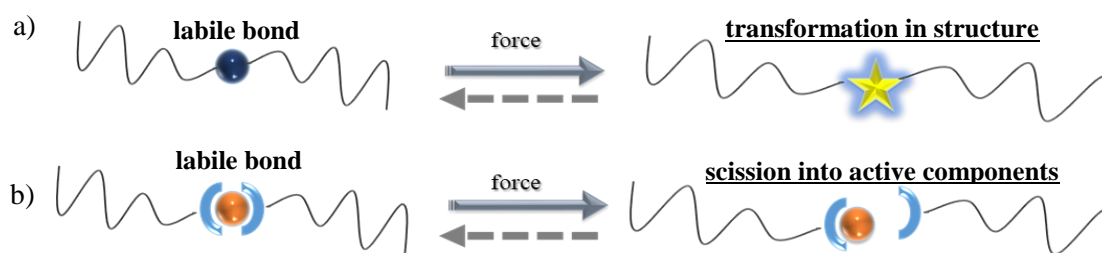
Figure 22. General principles of mechanophoric structural elements enclosed in the midst of long polymer chains. a) By impact of a force the labile core undergoes chemical transformation to a new structure (ring-opening, isomerization, etc.), simultaneously changing its property (e.g. emitting of light). b) By impact of a force the labile center is decomposed by scission into reactive components.

Subsequently, mechanochemical response can be triggered in numerous ways, generally distinguishing between bulk- and solution- activation. Applying US in solution evokes the creation of cavitation bubbles, that are able to trigger the mechanochemical activation by collapse[272]. Efficiency of scission is dependent on the US-intensity, the solvent, the temperature and the concentration of the mechanocatalyst[273]. Solvents of high vapor pressure reduce the efficiency of cavitation bubble collapse and thus the activation of the mechanocatalyst. Accordingly, US-activation of mechanochemistry is improved at lower temperatures, leading to a better force transmission[274].

The second and simultaneously largest pool of mechanochemical structures is designed by anchoring the mechanophores via supramolecular or covalent bonds[275] to the surrounding matrix material or by co-crystallization[276] of the polymer handles with the matrix polymers. If stress in the form of tensile stretch[277], torsional shear force[278] or compression[279] is applied to these bulk-materials, their mechanochemical composition will lead to the chemical response.

General observations for optimal activation are made for solution and solid state materials: applying longer polymer-chains results in an improved activation of the mechanocatalyst due to a more efficient force transmission of the incoming impact to the labile bond. In depth, the potential energy of a chemical bond is described by the Morse potential: if the bond is stretched by an external force (F_{ext}) its dissociation energy barrier (D_e) is lowered by the amount of F_{ext} applied to the system, resulting in a new temporary dissociation barrier D_e' (see Figure 23).[280-286] In accordance to the thermally activated barrier to scission (TABS)-theory implementing the Constrained Geometries simulate External Force (CoGEF) method the mechanochemical scission can appear even at lower temperatures (illustrated by the horizontal lines), when D_e' is low enough. Exploiting mechanophores (in solution) to ultra-sonication leads to the collapse of cavitation bubbles, causing the coil-to-stretch transformation of the polymer chains. Short chains will return to the random coil formation rapidly, whereas longer chains require longer relaxation times, allowing for an improved cavitation and thus activation of the mechanophores in solution[285]. In the solid state an increased and sufficient entanglement of the longer polymer chains ensures a better force transmission. Falling below the critical length of polymer chains, required for efficient activation, disturbs the mechanochemical response immediately. For an optimal transmittance of the mechanical impact to the labile core a central positioning into the polymer chains is crucial. A discrepancy of more than ± 15% leads to a tremendous drop in activation of the mechanophore, getting worse with growing distance up to complete absence of a chemical response[287]. Hence, living polymerization techniques are favored for synthesis of polymer-chains to ensure low PDI-values, leading to polymer chains of equal length, able to center the labile bond.
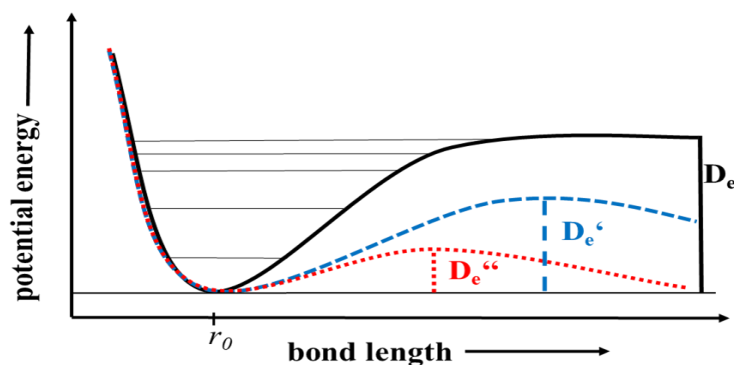
Figure 23. Morse-potential of a chemical bond, illustrating the change in energy potential in turn of mechanical input. The energy barrier for bond dissociation D_e (black curve) is lowered to D_e' (blue curve) or D_e'' (red curve) by increasing external force (F_{ext}) with F_{ext} (D_e'') > F_{ext} (D_e').

The mode of action of mechanophoric systems is described by Moore *et al.* in 2007, when impact of ultra-sonication triggers the linkage of benzocyclobutene polymer and *N*-(1-pyrene)-maleimide via mechanical ring opening followed by cycloaddition[277, 281].

Sensing materials based on mechanochemistry are designed by implementation of functional groups, such as mechanochromophores. Spiropyrane[279], spirothiopyrane[288] and the dimers of coumarin[289] and anthracene[290] belong to the mechanochromophores, emitting radiation via mechanoluminescence, whereas 1,2-dioxetanes[291] undergo a transformation to excited structures, able to drop their energy-level via a chemiluminescent mechanism (see Figure 24). The principle of mechanochromophores is based on the chemical transformation in turn of mechanical impact, which leads to a change in color

(see Figure 24a-d). Thus, colorless spiropyran (SP) changes to purple merocyanine (MC) by applying US (see Figure 24a). In case of spirothiopyran, when oxygen is exchanged by a sulfur atom, the color-change appears greenish by isomerization of spirothiopyran (STP) to thiomerocyanine (TMC) instead (see Figure 24b). The collapse of the cyclobutane ring of the non-fluorescent dimers of coumarin (see Figure 24c) or anthracene moiety (see Figure 24d) leads to the decomposition in their highly fluorescent monomers. Treating a solution containing 1,2-dioxetanes with US leads to the decomposition in excited ketones of a singlet or a triplet spin configuration, emitting light directly or by energy transfer to acceptors in close proximity, forming adamantanone (see Figure 24e).
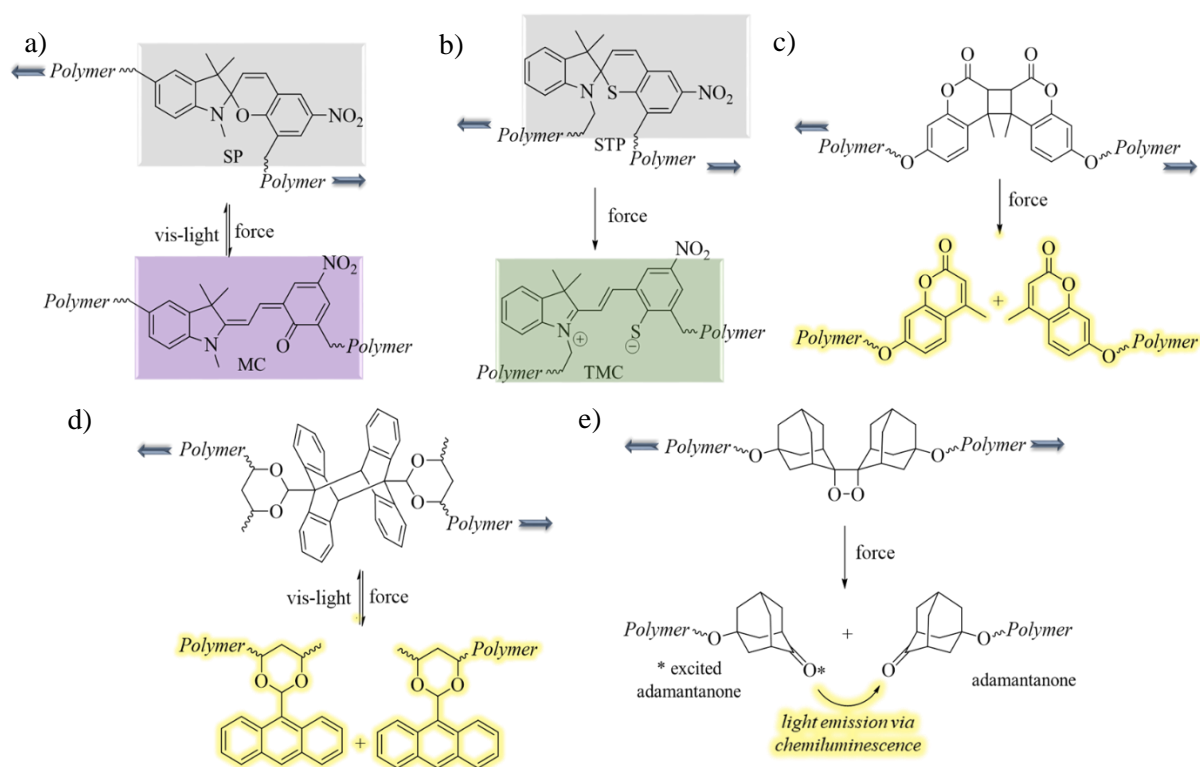
Figure 24. Mechanosensing activated via force. a) Chemical transformation of colorless SP to purple MC by impact of US. b) Chemical isomerization of colorless STP to greenish TMC by US in solution or stretch in solid state. c, d) Decomposition of non-fluorescent coumarin dimer (c) or anthracene dimer (d) in highly fluorescent monomers by impact of either US or crack. e) Decomposition of 1,2-dioxetane into excited and non-excited adamantanone. Excited adamantanone emits light by dropping its energy level to the initial state of adamantanone via chemiluminescence.

Using NHC-metal complexes is advantageous, based on their positive stabilization effects and thus better resistance to dissociation processes[292]. The otherwise unstable, but very reactive carbenes are stabilized by the exchange of adjacent carbon- or hydrogen-atoms with nitrogen-atoms, leading to the formation of stable crystals with a carbenic structure, which were isolated for the first time in 1991[293]. The occurring stabilization is mainly attributed to three different effects: 1.) The nucleophilicity of the σ-orbital is lowered by the negative inductive effect, originated by the adjacent nitrogen-atoms. 2.) The electrophilicity of the empty π-orbitals is lowered by the positive mesomeric effect of the free-electron pairs of the nitrogen-atoms and 3.) additional stabilization is caused by an aromatization, according to the Hückl's rule (see Figure 25a)[294]. The conversion of Cu(I)-salts and NHC-ligands at basic conditions can lead to the formation of Cu(I)-bis-NHC-complexes. The metal-NHC-complex is stabilized by strong σ-donation, originated by the carbene structure and the weak π-back donation of the central and electron-rich Cu(I) (see Figure 25b)[295]. The active center is stereoelectronically shielded, which leads to an improved resistance to oxygen, moisture and heat and can further be adjusted by the various kinds of ligands (see Figure 8e-g in chapter 1.1.1 and Figure 14 in chapter 1.1.3.3) attached to the NHC-moieties.
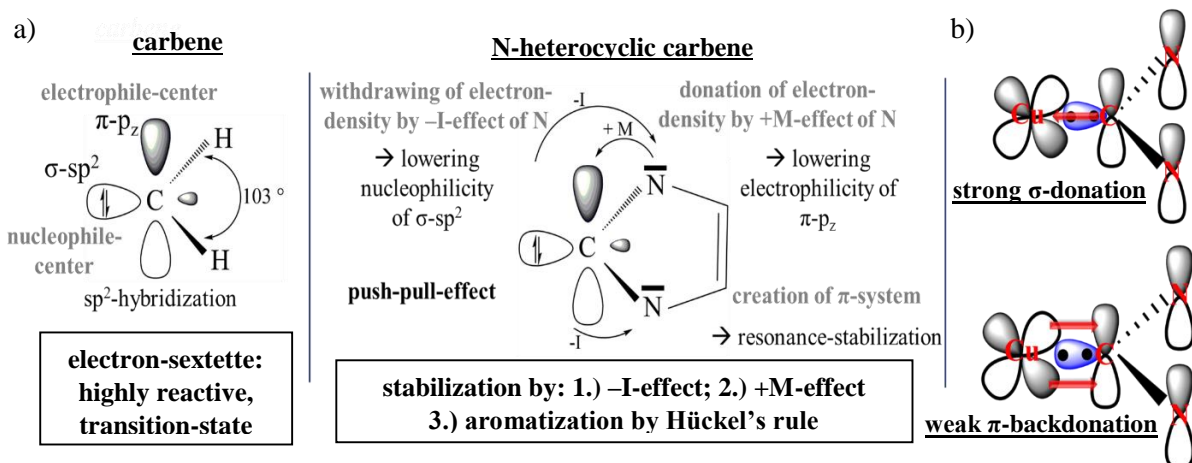
Figure 25. a) Stabilization of the reactive carbene structure by adjacent nitrogen-atoms. b) Stabilization of the Cu(I)-NHC complex by strong σ-donation and weak π-back donation.

The group of Sijbesma *et al.* is the first to apply the structural element of NHC to mechanochemistry based approaches (see Figure 26a, approach A-C)[285]. In this specific case, the impact of an external force leads to a chemical response as a consequence of the released active species. Applying US to a bis(pTHF-NHC)-silver(I) complex (**I**) induces the scission of the core, consisting of AgPF$_6$ and the previously attached NHC-polymer-chains (see Figure 26a, approach A)[283, 296-297]. The mechanochemical triggered release of the NHC-ligand is inducing the transesterification of benzyl alcohol and vinyl acetate to form benzyl acetate[284, 298]. Second, a bis(pTHF-NHC)-ruthenium(II) catalyst (**II**) is developed, cleaving one NHC shielding ligand under scission, thus gaining one free coordination site at the ruthenium complex (see Figure 26a, approach B)[299]. Hence, ROMP of a norbornene derivative[276, 299] or a ring-closing metathesis (RCM) of diethyl diallylmalonate (DEDAM)[298, 300] is conducted upon ultra-sonication impact in solution or upon compression in the solid state, when the norbornene derivative and the mechanocatalyst **II** (M_n = 34 000g/mol) are incorporated to a semi-crystalline pTHF matrix (M_n = 170 000 g/mol)).[276] The pTHF handles attached to the bis(NHC)-ruthenium(II) complex are able to co-crystallize with the surrounding matrix as consequence of their similarities in chemical composition (melting point ≈ 40 – 44 °C, degree of crystallinity ≈ 46 – 54%), which is improving the efficiency of the external force transmittance applied to the material by subsequent compression cycles. Thus, up to 25% of the monomer content is polymerized to poly(norbornene) after subjecting the specimen to five compression cycles (approximate linear increase after each compression cycle is observed). Third, a bis(pTHF-NHC)-palladium(II) complex (**III**) is designed, which collapses into the corresponding carbene, acting as a base to deprotonate a spiroadamantyl-substituted phenolic 1,2-dioxetane (see Figure 26a, approach C).[301] The high-energy intermediate emits blue light upon decomposition under ambient conditions, thus illustrating another approach of mechanically triggered chemiluminescence.

Mechanochemical approaches based on bis(NHC)-Cu(I) complexes for the CuAAC
Furthermore, bis(NHC)-metal complexes are designed, able to conduct the CuAAC of benzyl azide and phenylacetylene in solution upon ultra-sonication (see Figure 26b, approach D)[48, 302]. The impact of the mechanical force is inducing the release of one of the NHC-ligands, gaining one free coordination site at the copper(I)-center. In turn, the alkyne (phenylacetylene) can be attached, followed by the formation of the desired copper(I)-acetylide complex, subsequently following the normal catalysis cycle of the CuAAC (see Figure 4, chapter 1.1) to finally provide the triazole product. The influence of the rigidity of the polymeric handles to the cleaving process is investigated either by the chemical composition of the polymeric backbone or by their different degree of polymerization (DP). Hence, PIB- (**IV**), PS- (**V**)

and pTHF- (**VI**) based Cu(I)-mechanocatalysts of different molecular weights are subjected to subsequent ultra-sonication experiments. An increased DP improves the cleaving of a NHC-ligand and in turn the catalytic efficiency of the mechanocatalyst, thus enhancing the conversion from 11% to 28% after 10 sonication cycles from the lowest (**IV**, M_n = 4 750 g/mol) to the highest molecular weight (**IV**, M_n = 17 200g/mol) catalysts, composed of PIB. In case of PS, the "click" conversion is increasing from 23% (**V**, M_n = 6 800 g/mol) to 52% (**V**, M_n = 13 600 g/mol), due to an initially higher stiffness (T_g (PS) ≈ 100 °C > T_g (PIB) ≈ -80 °C) of its chemical composition, providing almost twice the conversion in the CuAAC compared to the most efficient PIB-mechanophore (**IV**, M_n = 17 200g/mol, DP ≈ 107), counterbalancing the lower DP (**V**, M_n = 13 600 g/mol, DP ≈ 190). The highest „click" conversion of 97% is provided upon ultra-sonication using the pTHF based Cu(I)-mechanocatalyst (**VI**, M_n = 15 600g/mol). However, in appropriate control experiments **VI** also afforded 24% conversion in absence of mechanical impact, contrary to the totally latent mechanocatalysts **IV** and **V**.
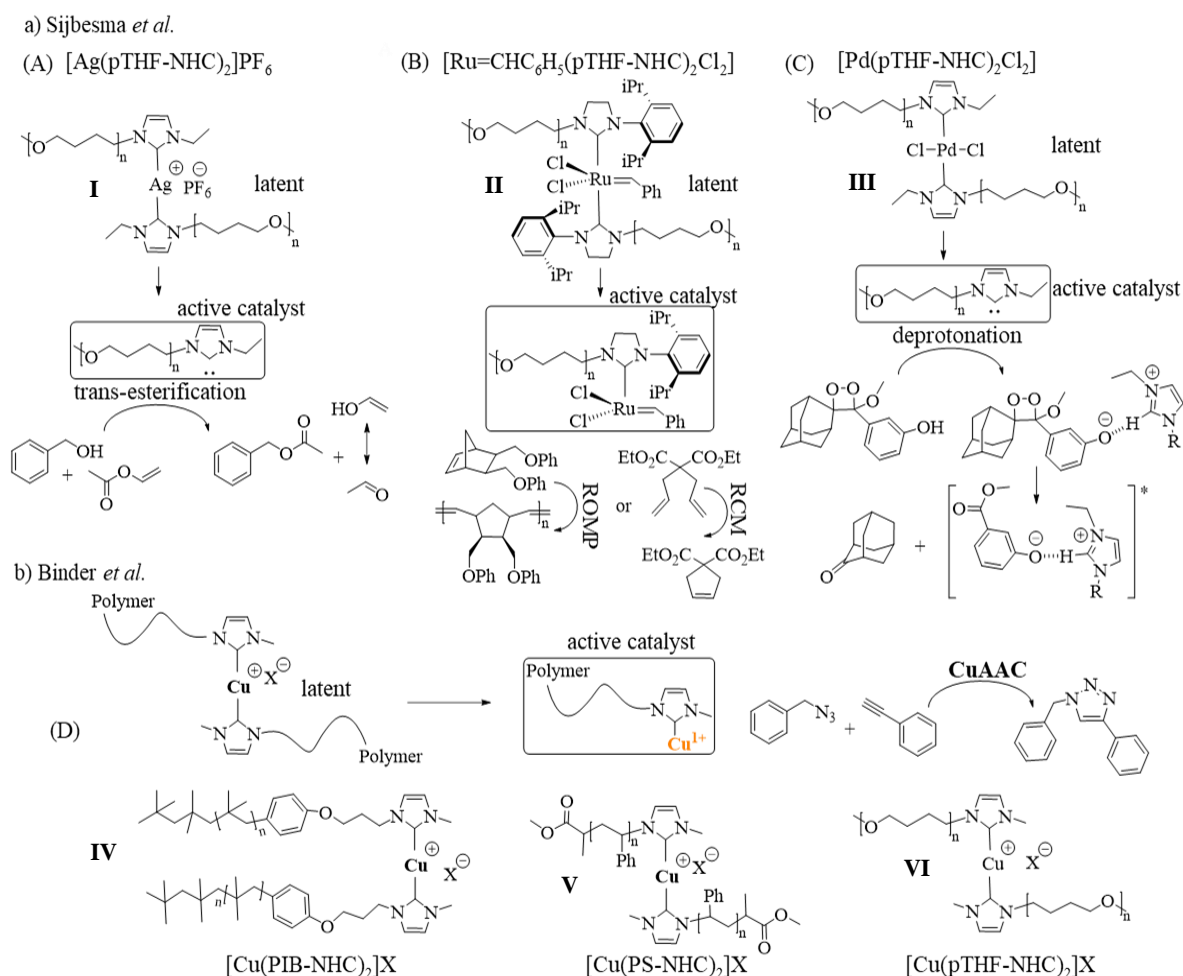
Figure 26. Application of bis(NHC)-transition metal complexes for mechanochemical approaches upon ultra-sonication: a) (A) trans-esterification of benzyl alcohol and vinyl acetate, applying (**I**); (B) ROMP of norbornene or RCM of DEDAM, applying (**II**); (C) deprotonation of spiroadamantyl-substituted phenolic 1,2-dioxetane, which under decomposition emits blue light; b) the CuAAC of benzyl azide and phenylacetylene (D), applying **IV**-**VI**.

Finally, a mechanochemical triggered the CuAAC sensing approach is developed (see Figure 27)[48]. The bis(NHC)-copper(I) catalysts (**I**-**V**) of different architecture, coumarin azide and phenylacetylene are embedded into a high molecular weight pTHF-matrix (M_n = 112 000 g/mol) (see Figure 27, concepts A-D).[48] Upon compression of such sensing pellets an increase of fluorescence intensity is observed, which is caused by the formation of the highly fluorescent triazole-product as an outcome of the released copper(I)-monocarbene species, able to conduct the fluorogenic "click" reaction. Different polymeric

architectures are studied recently (**II-V**) to investigate the efficiency of the force transmitting scaffold on the activation behavior of the mechanocatalysts.[242] The pellet, containing none copper(I)-source or **I** (see Figure 27, concept A), provided almost no conversions (< 1.0%) in subsequent "click" reactions upon compression impact. On the one hand, this illustrates that the CuAAC is not triggered by pressure-accelerated AAC, on the other hand, that mechanocatalysts cannot be activated if handles, attached to the NHC-moieties, are too short to provide sufficient transmittance of the external force to overcome the activation barrier D_e. Furthermore, subjecting pellets, containing **II** or **III**, to 60 °C for 72 hours in absence of mechanical impact led to an insignificant change of the fluorescence intensity (conversion < 1.0%) and thus excluded an activation of the mechanocatalysts by thermal treatment. The linear approach, applying PIB-based Cu(I)-mechanocatalyst **II** (M_n = 17 200g/mol, $T_g \approx$ -80°C) or the stiffer PS-based Cu(I)-mechanocatalyst **III** (M_n = 13 600g/mol, $T_g \approx$ 100 °C), provided 7.2% and 7.9% conversion in the CuAAC, respectively (see Figure 27, concept B). The more efficient PS-backbone is chosen for the chain-extended- (C) and the network approach (D). Both the higher content of potentially activatable Cu(I)-centers (3-4 times) and the higher DP of **IV** (M_n = 13 600 g/mol, DP $\approx$ 190) in comparison to **III** (DP $\approx$ 107) explain the tremendous increase of "click" conversion to 44.2% in subsequent experiments (see Figure 27, concept C). Even though DP is lower in network based Cu(I)-mechanocatalyst (DP between each Cu(I)-center $\approx$ 10-12) compared to the chain-extended **VI** (DP $\approx$ 190), the force emitted to each mechanophore is higher in turn of possible redirection by the crosslinking points of the network (D), while only the parallel and anti-parallel chains in the chain-extended approach (C) can participate in the activation process[303]. Similar conversion in the mechanochemical CuAAC of 44.1% is detected, applying the network-based Cu(I)-mechanocatalyst **V** composed of poly(styrene)-stat-1-methyl-3-(4-vinylbenzyl)imidazol-2-ylidene]copper(I) linked units (see Figure 27, concept D).[242]
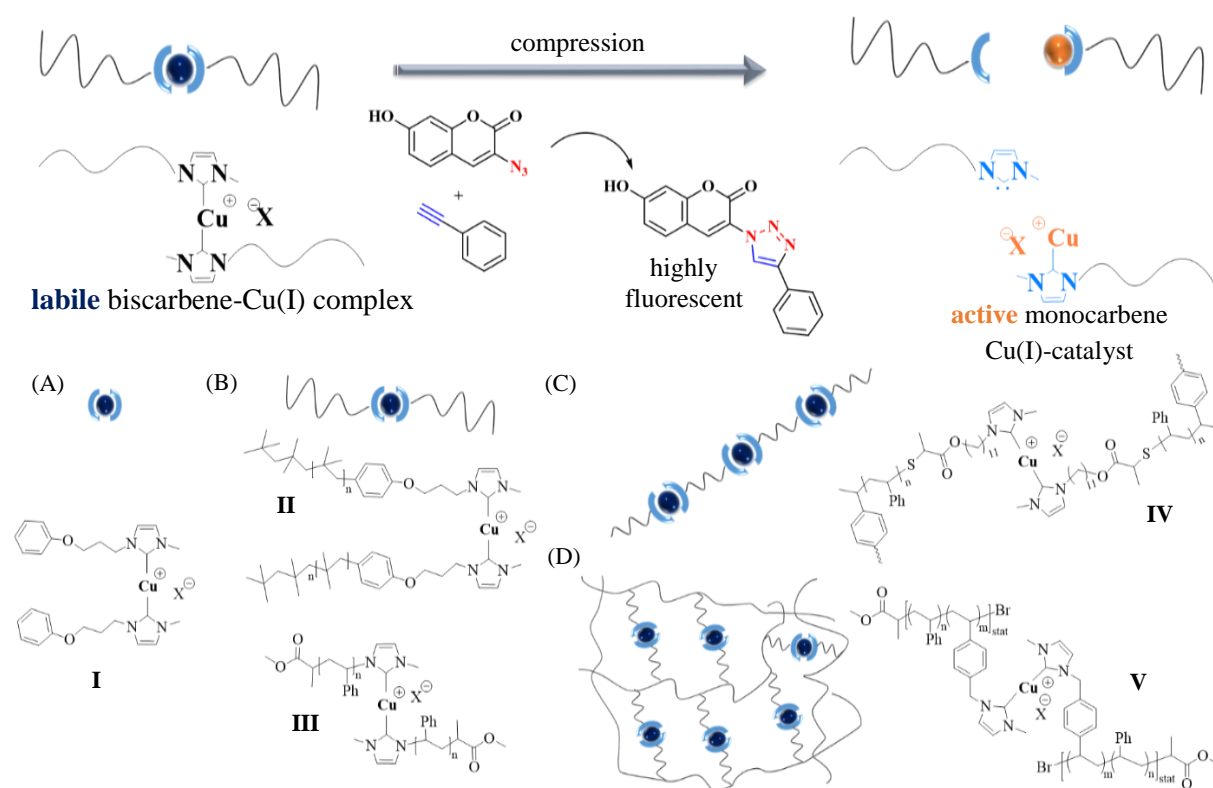
Figure 27. Application of bis(NHC)-transition metal complexes for mechanochemical approaches upon compression: for conducting a highly fluorescent CuAAC within a final material (high molecular weight pTHF), applying bis(NHC)-Cu(I) catalysts of different architecture: (A) low molecular weight (**I**); (B) linear PIB (**II**) and PS (**III**); (C) chain-extended PS (**IV**); (D) network PS-stat-1-methyl-3-(4-vinylbenzyl) copolymer based bis(NHC) Cu(I)-mechanocatalyst (**V**).

2 Aim of the thesis

2.1 Objective and motivation

The aim of this thesis was the development of a crosslinking chemistry, usable for autonomous self-healing approaches, applicable at sub-ambient conditions. For this purpose, appropriate reactants, suiting a ca-CuAAC mechanism, should be designed, the reaction rates determined and finally the SH-capability tested within a host-material (see Figure 28). In order to find optimal conditions to accelerate the SH-approach, both homogeneous and heterogeneous copper(I) catalysts should be investigated. This includes the conception and testing of NHC-Cu(I)-mechanocatalysts of different rigidities in order to design the autonomous and capsule-free sensing approach. The induced failure of the bulk material and the subsequent healing should be visualized by sensing agents.
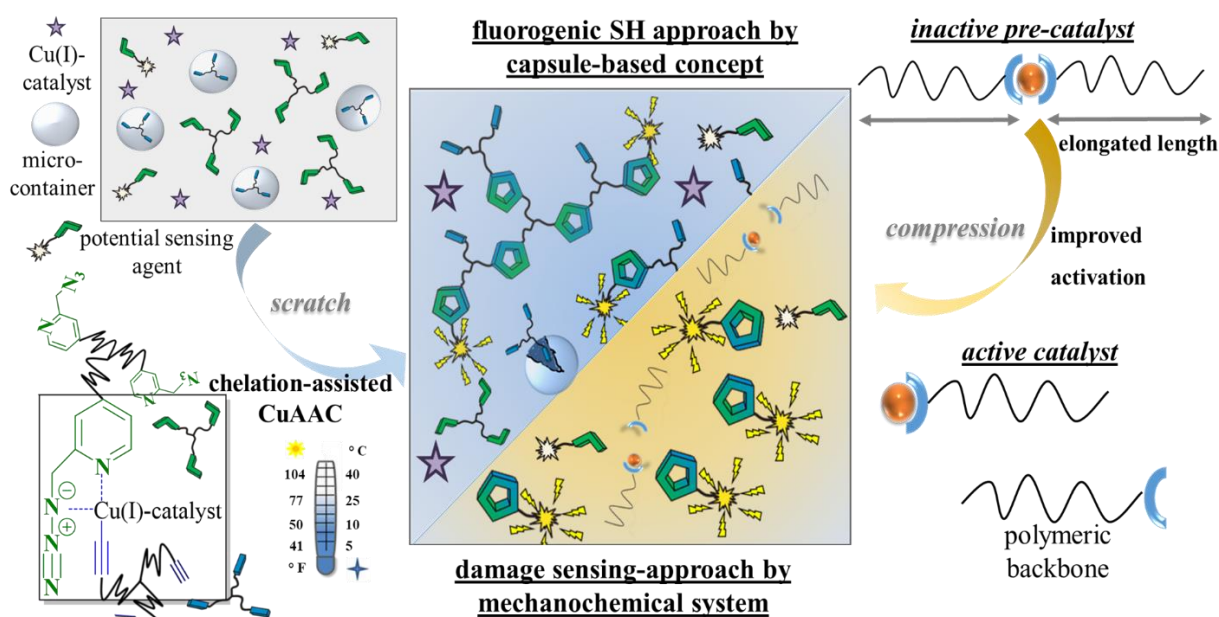
Figure 28. Design of a capsule-based fluorogenic SH approach based on the ca-CuAAC, supported by homogeneous or heterogeneous catalysts. Conception of an autonomous and capsule free sensing approach, utilizing a Cu(I)-mechanocatalyst.

Most of the common autonomous SH approaches lack of sufficient efficiency at sub-ambient conditions (< 20 °C). Appropriate reagents should provide high orthogonality and rapid crosslinking, describing the characteristics of a "click"-reaction.[1, 3-4, 8, 16, 21, 31, 34-35, 232-233, 304] Among them, the ca-CuAAC of newest generation of azides and terminal alkynes is the most versatile tool, promising rapid conversions of the reactants at almost any conditions.[43, 185, 227-228] Therefore, adequate multivalent components should be developed and the crosslinking efficiency in solution and in the melt should be studied. Furthermore, homogeneous catalysts, providing a good availability of all components and in turn high reaction rates and heterogeneous catalysts, enabling "a green" recyclability of the catalyst[123], should be designed and tested upon efficiency within the concept. Premature reaction of the healing agents in the scaffolding matrix should be prevented either by micro-container protection[39, 229-230, 240, 243, 245-246], permuted in a one-capsule-based approach, or by utilization of a latent Cu(I)-mechanocatalyst[48, 242, 302]. The latter concept can be employed as a capsule free version, due to the inactivity of the catalyst under neat conditions. Catalyst activation should be accomplished upon mechanical impact to the host material. The efficiency of the activation can be tuned by the polymer handles attached to the labile bond, consisting of NHC-Cu(I), while longer polymer chains should provide an improved activation[242, 280, 283-286]. A new synthesis strategy should be developed, enabling the design of a high molecular weight polymer-NHC precursor, addressing higher activation efficiency of subsequent mechanocatalysts to provide sensing within the material, triggered by compression impact.

2.2 Concept

Low molecular weight picolyl azides should be selected to confirm and improve the ca-CuAAC rate, when converted with phenylacetylene in solution by *in situ* NMR experiments. Therefore, the influence of both homogeneous and heterogeneous catalysts should be studied. For that purpose, copper(I) modified thermally reduced graphene oxide (Cu-TRGO) should be synthesized as a heterogeneous catalyst via a three-step synthesis. In the first step, a commercially available graphite should be chemically oxidized, followed by the implementation of Cu(II)-nanoparticles by ion exchange on the previously created imperfections of the graphene-oxide. Finally, thermal reduction should provide the heterogeneous Cu(I)-catalyst, able to conduct the CuAAC "click" reactions. Furthermore, the crosslinking efficiency in solution should be tested by DSC measurements. For this purpose, picolyl azides should be modified with a carboxylic group, enabling the attachment to the alcoholic groups of the star-shaped precursors via esterification. Consequently, the attachment of picolyl azides to a trivalent alcohol of low molecular weight should be accomplished, before testing the reactivity with star-shaped alkyne moieties (see Figure 29). Reaction conditions should be optimized, varying between homogeneous and heterogeneous Cu(I)-catalysts. The kinetics of the network-formation of the high-molecular weight components should be monitored by melt rheology experiments, varying the temperature-profile to sub-ambient conditions (< 20 °C). Thus, the star-shaped precursor of PIB should be synthesized via LCCP of isobutylene, utilizing mono-, bi- and trivalent initiators. Subsequent endgroup transformation to the desired picolyl azides should afford the highly reactive reagent. As its crosslinking counterpart trivalent alkyne-PIB should be used and both polymers should maintain their liquid flow-behavior by controlling their molecular weight ($T_g \sim$ -80 °C, $M_n \sim$ 6 000 g/mol).
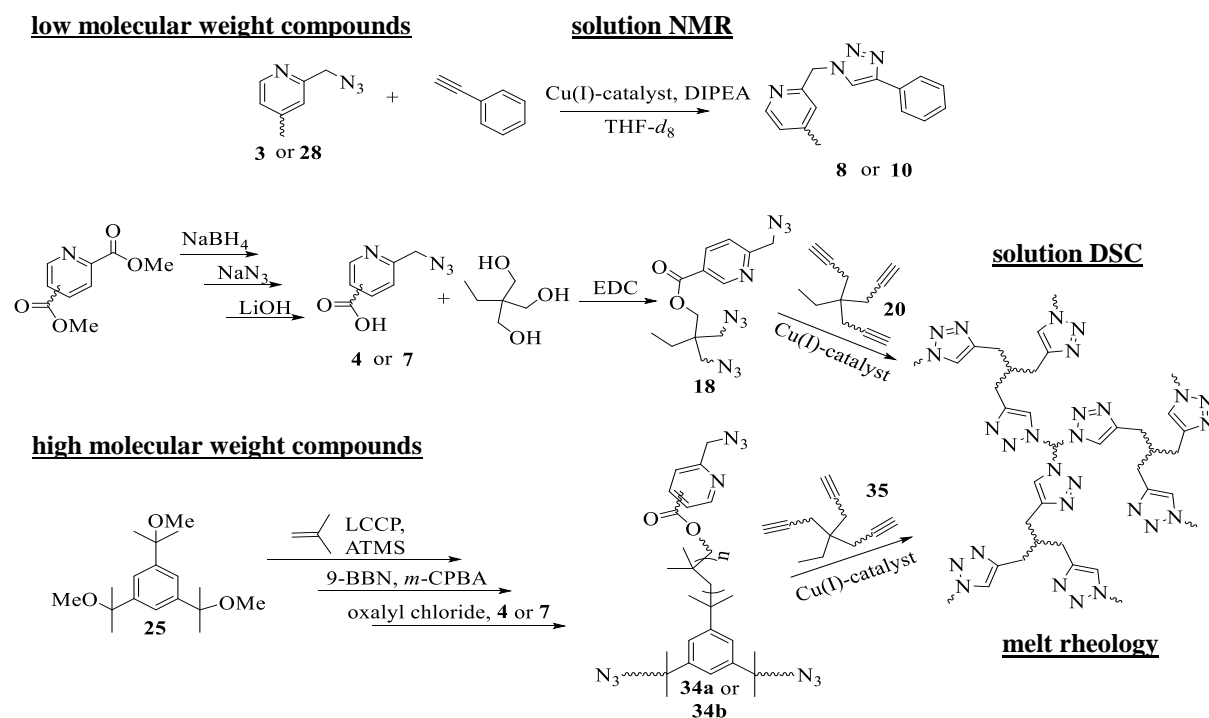
Figure 29. Concept for kinetic investigations of the chelation-assisted CuAAC of low-molecular and high molecular weight systems for efficient crosslinking at lower temperatures.

Star-shaped picolyl azido telechelic PIB, urea-formaldehyde (UF) capsules, containing the trivalent alkyne, the Cu(I)-catalyst and a sensing tool should be compounded to either poly(dimethylsiloxane) (PDMS) or high molecular weight PIB (see Figure 30A) to accomplish the SH approach. SH capability of the final material should be determined by performing scratch experiments. The approaching crack

will rupture the capsules, leading to the release of the healing agents, monitored by the increase of the fluorescence-intensity, which is indicating the simultaneous formation of the network. For this purpose, coumarin azide should be synthesized and implemented to the system, able to act as a sensing tool.

Optimized activation efficiency of mechanocatalysts should be achieved by tuning the length of the appropriate polymer handles, using a new CTA, allowing to conduct RAFT of styrene and *n*-butyl acrylate, while the introduction of NHC is enabled simultaneously. The influence of the different rigidities to the efficiency of bond-cleaving should be examined by both, varying the nature of the polymeric backbone (PS or P-nBuA) and the molecular weight of the polymer handles. Therefore, PS- and P-*n*BuA-NHC precursors of at least three different molecular weights should be synthesized, ranging from 2 000 g/mol to 30 000 g/mol. Treatment of the NHC telechelic polymers with a base and a copper(I)-source should afford the desired mechanophores. The activation behavior of the Cu(I)-mechanocatalysts should be investigated in solution upon ultra-sonication and within the host-material upon compression. The latter approach should be accomplished by compounding the catalyst, coumarin azide and phenylacetylene to a high molecular weight pTHF. Hence, compression induced activation of the Cu(I)-mechanocatalysts should be executed, proving the autonomous sensing behavior of the final material, triggered by the subsequent fluorogenic CuAAC (see Figure 30B).
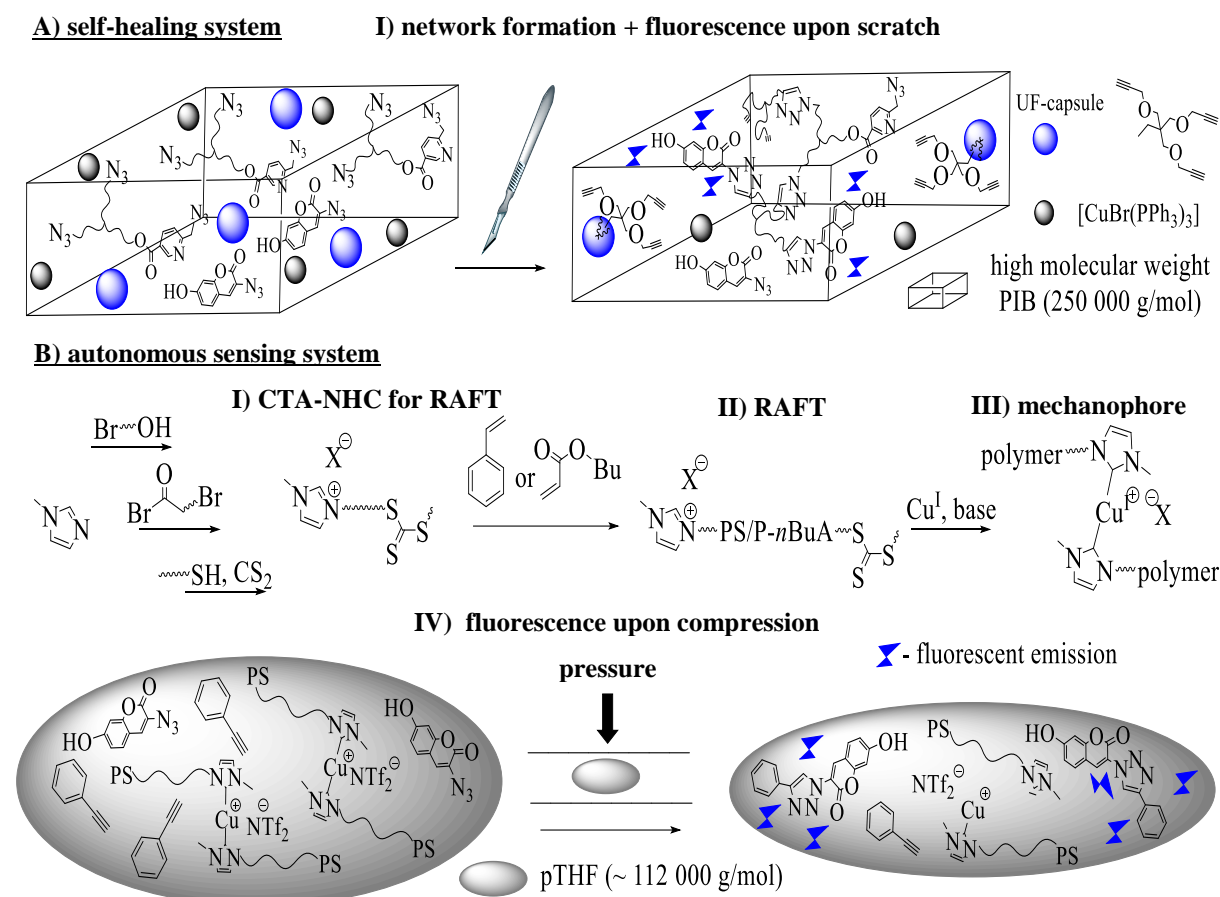
Figure 30. Concept to investigate materials in self-healing (A) or sensing-behavior (B). A) Self-healing approach, consisting of star-shaped picolyl azido telechelic PIB, coumarin azide, Cu^I-source and star-shaped alkyne telechelic PIB (encapsulated in UF-microcontainers) compounded to high-molecular weight PIB. Scratching the specimen evokes the release of the alkyne to undergo network formation with the azide components upon contact with the Cu(I)-catalyst, which leads to an increase of fluorescence-intensity by formation of the "click" product. B) Design of an autonomous sensing-system: I) Synthesis of CTA-NHC for RAFT of styrene or *n*-butyl acrylate (II) and further transformation (III) to polymeric Cu(I)-mechanocatalyst. Mechanocatalyst, phenylacetylene and coumarin azide are compounded to a high molecular weight pTHF matrix, which upon compression (IV) leads to an increase of fluorescence intensity, due to scission of the mechanocatalyst into the active Cu^I-monocarbene species, conducting the fluorogenic CuAAC.

3   Results and discussion

Parts of the results and discussion as well of the experimental part were already published in *"Chelation-assisted CuAAC in star-shaped polymers enables fast self-healing at low temperatures"* (Neumann, S.; Döhler, D.; Ströhl, D., Binder, W.H. *Polym. Chem.* **2016**, *7*, 2342. DOI: 10.1039/c5py01818h) - Published by The Royal Society of Chemistry and were in parts adapted with permission from The Royal Society of Chemistry (Copyright 2016).

3.1 Design of a low temperature and fluorogenic SH approach

Rapid crosslinking components were synthesized, suiting the ca-CuAAC mechanism in order to design an autonomous SH approach, giving response to damage-impact even at lower temperatures. First of all, the synthesis of an azide, containing the chelation-assisted responsible part – the nitrogen atom, carrying at least one free electron pair in close proximity to the active group had to be accomplished. Followed by the determination of the performance in the ca-CuAAC in solution monitored by *in situ* NMR experiments. Furthermore, the presence of a second functionality, allowing the attachment of the desired property to the star-shaped precursors, was indispensable. Accordingly, two different regioisomers of carboxylic picolyl azides (**4** and **7**) were designed and further attached to the alcoholic groups of mono-, bi- and trivalent PIB (high molecular weight approach) as well as to low-molecular weight 2-(hydroxymethyl)-2-ethylpropane-1,3-diol. The crosslinking rates were investigated either in solution (via DSC) and in the melt state (via rheology). Additionally, the influence of homogeneous and heterogeneous copper(I) catalysts was studied, while the latter had to be synthesized. Finally, the best crosslinking system was compounded to scaffolding matrix (PIB), providing an autonomous SH material, which upon scratch conducted the fluorogenic "click" formation.

3.1.1 Chelation-assisted CuAAC of picolyl azides in solution
3.1.1.1 Synthesis and characterization of picolyl azides (4, 7)

Synthesis of picolyl components was done according to Ting *et al.*[43, 228]. The design considered two key aspects, which need to be fulfilled, if aiming for the ca-CuAAC capable crosslinking components: first, at least one nitrogen atom had to be in close proximity to the active azide moiety -N_3, being perfectly addressed by the composition of picolyl azides, additionally allowing for excellent mobility of the azide group, due to the existent methylene-spacer in between the azide and the pyridine-ring (see Figure 31). Secondly, a second functional group was required in order to attach the desired property to alcoholic precursors. Therefore, the carboxylic-acid moiety was introduced to the pyridine-ring, enabling the attachment of mono- to multivalent alcohols via esterification reactions. Two different regioisomers (2,4- and 2,5-) of picolyl azides were synthesized within this work. Synthesis strategy for both regioisomers was almost the same, while esterification was just required in case of 2,4-regioisomer (**1**), in turn of the commercial availability of the 2,5-derivative. The most critical step in this synthesis
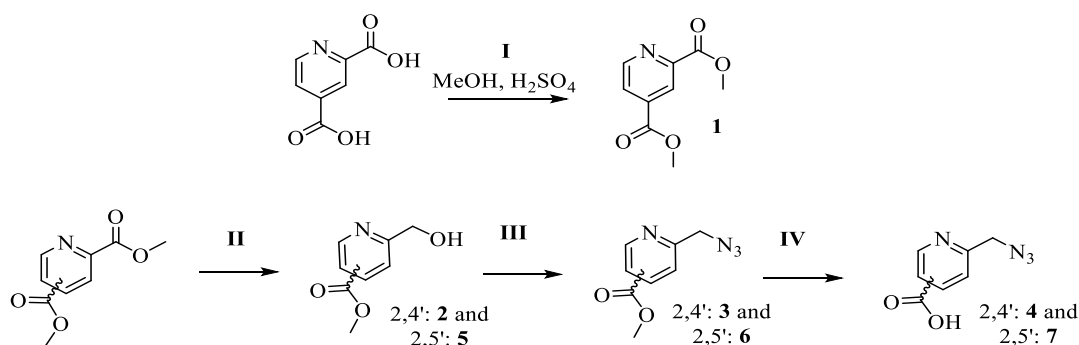
Figure 31. Synthetic route to obtain 2,4'- and 2,5'-regioisomers of chelation-assisted CuAAC suitable picolyl azide moieties.

route was the selective reduction (**II**) of the methyl ester to an alcohol, which was located in *ortho*-position to the nitrogen-atom of the pyridine-ring. Besides the desired conversion, the undesired reduction of the second methyl ester group was also prominent. The inherent chemical structure of the 2,4- di-substituted pyridine derivative (**1**) shifted the electron deficient point of the aromatic ring, emerging from the nitrogen-atom, from α- to γ- position, causing similar reactivities for both ester moieties and thus led to reduced yields of **2** (~ 30%) as consequence of the formation of the double-reduced side-product.

Therefore, the 2,5-regioisomer was employed, since β- position was not conjugated with the hetero-atom inside the ring, eliminating the undesired side-reaction. Subsequently, 2-(6-hydroxymethyl)-pyridine-5-carboxylic acid methyl ester (**5**) was obtained in gram-scales within short time-scales, by increasing the appropriate (average) yield from ~ 30% (**2**) to ~ 75% (**5**). Successful conversion to **5** was confirmed in ¹H-NMR spectroscopy, when the signal at δ = 4.03 ppm, belonging to the methyl-ester at α- position, was shifted to δ = 4.82 ppm of the resulting methylene group attached to the newly introduced hydroxy group (see Figure 32a). The following nucleophilic substitution (**III**) was promoted by conversion of the alcoholic group to the mesylate ester, before sodium azide was added. The increased nucleophilicity of the mesylate, due to resonance stabilization of the leaving group, caused high yields of 80% for subsequent substitution to 2-(6-azidomethyl)-pyridine-5-carboxylic acid methyl ester (**6**). Successful introduction of the azide moiety was verified by both, spectrometry- (ESI-ToF-MS) and spectroscopy- methods as NMR and IR. Thus, in NMR-spectrum the signal of the methylene group attached to the azide-moiety was now shifted to δ = 4.57 ppm (see Figure 32b), while in IR-
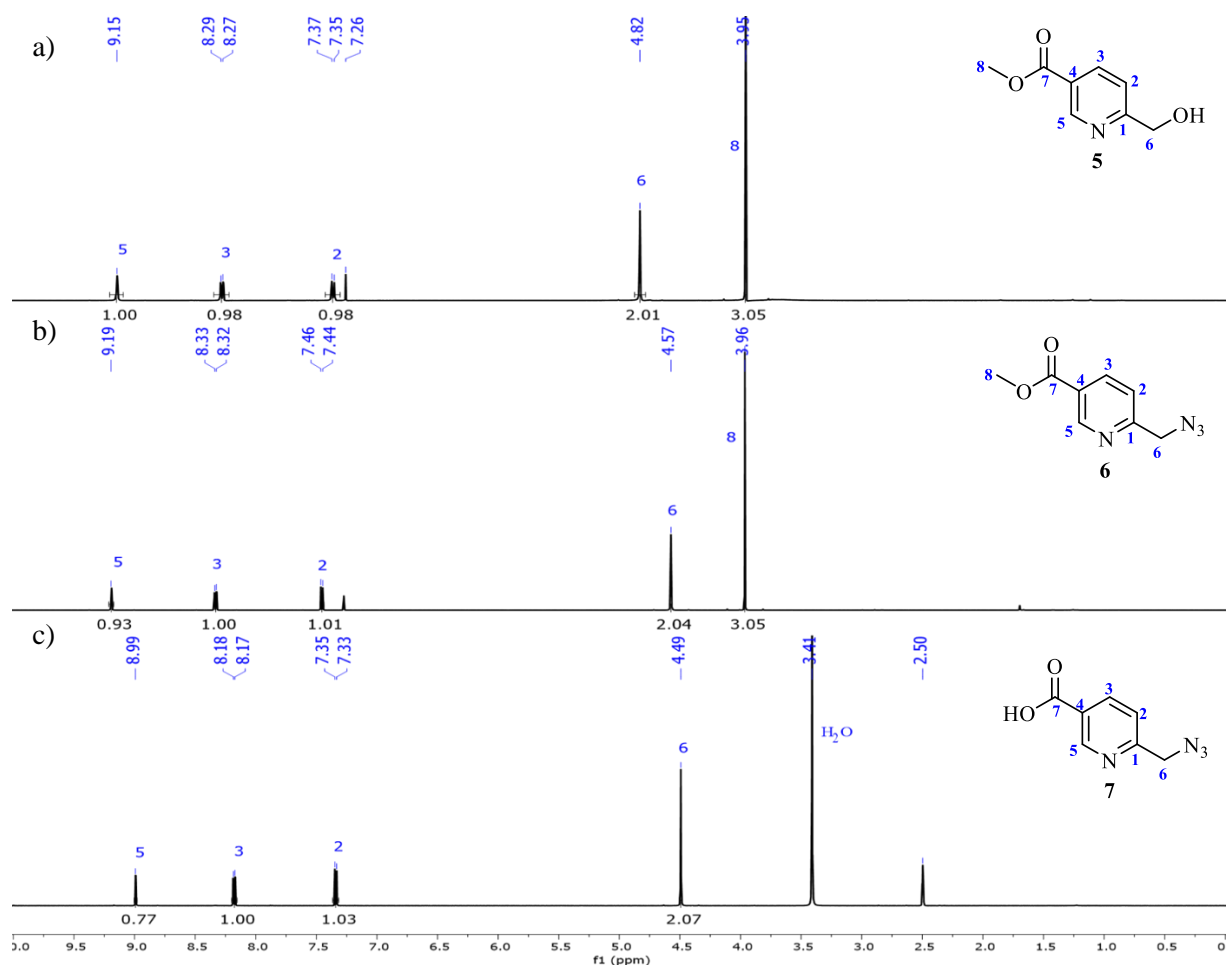
Figure 32. ¹H-NMR-spectrum of a) 2-(6-hydroxymethyl)-pyridine-5-carboxylic acid methyl ester **5** in C*D*Cl₃; b) 2-(6-azidomethyl)-pyridine-5-carboxylic acid methyl ester **6** in C*D*Cl₃; c) 2-(6-azidomethyl)-pyridine-4-carboxylic acid **7** in DMSO-*d₆*.

spectrum the azide vibration at $v = 2113$ cm^{-1} was newly detected. In the last step, hydrolysis (**IV**) was performed similar to the 2,4-analogue, applying LiOH to adjust the required basic conditions in the aqueous solution, affording **7** in quantitative yields. The missing signals at $\delta = 3.05$ ppm (^{1}H-NMR-spectrum) (see Figure 32c) and at $\delta = 52.6$ ppm (^{13}C-NMR-spectrum) of the before present methyl-ester group proved the successful completion of the reaction, which was confirmed by a measured loading of $m/z = 179.0664$ g/mol (simulated: $m/z = 179.0564$ g/mol) in ESI-ToF-MS analysis. Detailed spectra can be found in the appendix 7.1.

3.1.1.2 In-situ NMR of the ca-CuAAC applying picolyl azides

To achieve a highly efficient and fast self-healing process via the chelation-assisted CuAAC, different reaction setups, including the change of the copper(I) source and the addition of *N,N*-di-isopropylethylamine (DIPEA) as a base, were investigated via *in situ* NMR measurements (see Figure 33). 2-(6-Azidomethyl)-pyridine-4-carboxylic acid methyl ester (**3**) and phenylacetylene served as ideal low molecular weight substrates for *in situ* NMR-studies, containing the azide, the alkyne, the copper(I) source and DIPEA (Table 3, entries 5–8), separately dissolved in deuterated THF. For better comparison the same experiments were conducted when **3** was exchanged with polymeric PIB-analogue **28**. Mixing of all components in a NMR-tube defined the starting point of every single experiment (see Table 3), allowing the quantification of the reaction progress.
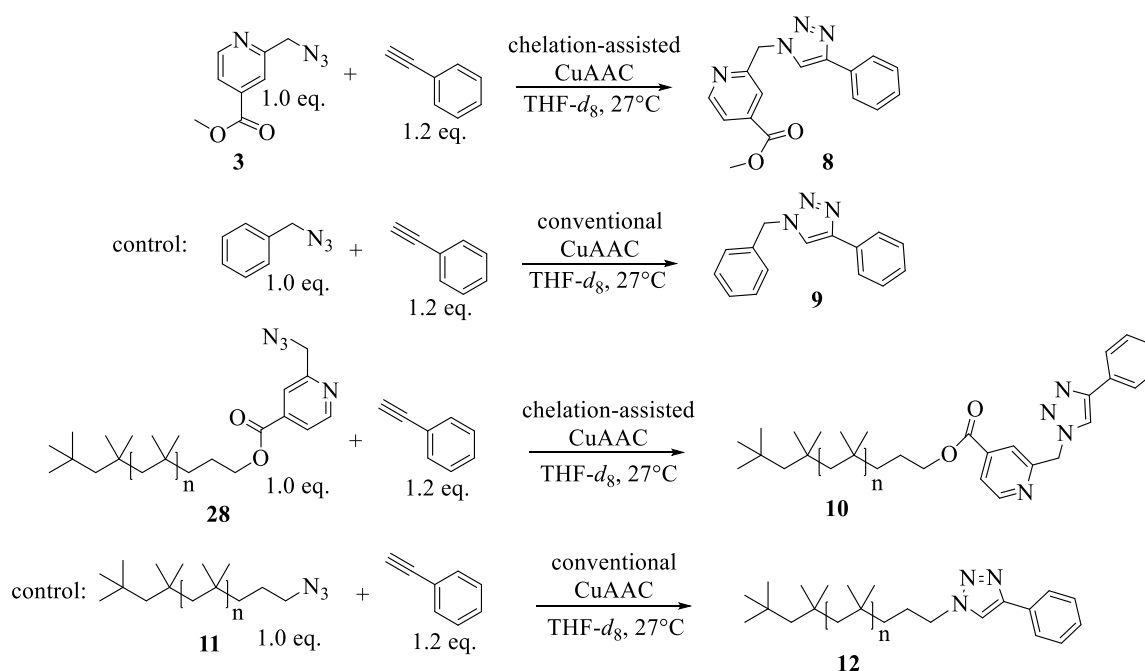
Figure 33. Experimental setup for *in situ* NMR investigations.

Conversion of every single measurement was determined by the ratio of the integrals of the methylene-group attached to the azido-group (e.g., **3**: at $\delta = 4.54$ ppm) and the integrals of the methylene-group attached to the triazole-ring (e.g., **8**: at $\delta = 5.79$ ppm) according to equation 1:

$$conversion = \frac{integral\ of\ resonance\ d}{(integral\ of\ resonance\ d + integral\ of\ resonance\ a)} \cdot 100\ \% \ (\boldsymbol{e1})$$
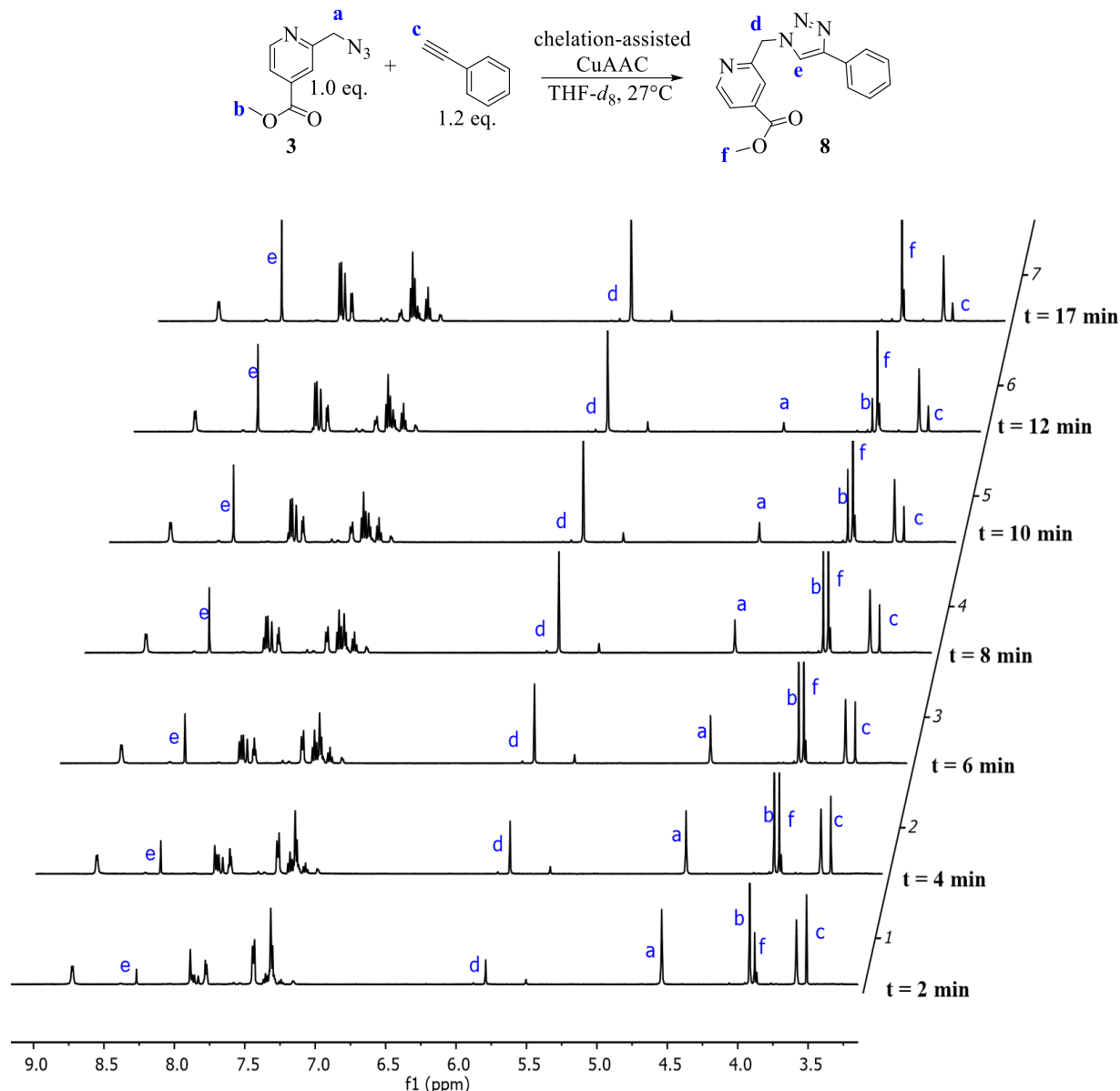
Figure 34. *In situ* NMR measurement of the chelation-assisted CuAAC of picolyl azide (**3**) and phenylacetylene conducted in THF-*d₈* in presence of CuBr and DIPEA (0.01 eq.) (Table 3, entry 6).

NMR-experiments were conducted at different period of times and the signals of the reactants and the product (**8**) were assigned (see Figure 34). First of all, applying **3** in presence of [Cu(CH₃CN)₄]PF₆ (Table 3, entry 1) or Cu(OAc) (Table 3, entry 2) and phenylacetylene resulted in conversions of 32% and 82% within one day and thus turned out to be too slow for fast self-healing applications. Amongst the tested Cu(I)-catalysts, CuBr delivered the best results, leading to quantitative conversion within nine hours at 27 °C (Table 3, entry 3). Thus, CuBr was chosen to run the reaction in the presence of DIPEA, which can promote the formation of a Cu(I)-acetylide species in the first step and therefore initially the "click" reaction. In the first NMR spectrum, measured five minutes after mixing all components, no NMR resonances of the starting material can be found (Table 3, entries 4 and 5). Even with just 1 mol% DIPEA the reaction went to completion within 17 minutes (Table 3, entry 6). The conventional CuAAC, employing benzyl azide instead of picolyl azide (**3**) showed no conversion of **9** at the same time, increasing slowly to 7% after 110 minutes (Table 3, entry 14), which was caused by the missing chelation-assistance acceleration. [CuBr(PPh₃)₃] was also tested as catalyst due to its increased solubility in THF[235], due to the attached triphenylphosphane ligands. Contrary, [CuBr(PPh₃)₃] showed a lower

conversion (10% after 2 hours) in the presence of 1 mol% DIPEA (Table 3, entry 7) compared to pure CuBr. Thus, it is presumed that DIPEA is not just promoting the formation of the initially required Cu(I)-acetylide by acting as a base, but also further disintegrates unreactive CuBr clusters[8], delivering an ideal catalyst system for fast "click"-reactions in solution. Change of homogeneous Cu(I)-sources to heterogeneous Cu(I)-TRGO provided 94% conversion within one day and was not as efficient as CuBr (Table 3, entry 8). However, change to commercially available Cu/charcoal catalyst resulted in a poor conversion (< 1%) within nine hours (Table 3, entry 9).

In case of monovalent picolyl azido telechelic PIB (**28**) complete conversions can be observed in 42 minutes in lonely presence of CuBr (Table 3, entry 12). Further acceleration was achieved by the addition of DIPEA (1 mol%), leading to a full conversion within four minutes (Table 3, entry 13). [CuBr(PPh$_3$)$_3$] demonstrated again weak performance in solution, when compared to CuBr, resulting in a poor conversion of 32% within one day (Table 3, entry 10), being just slightly improved by utilization of [CuF(PPh$_3$)$_3$] and 64% within 11 hours (Table 3, entry 11). Utilization of the conventional CuAAC mechanism, exchanging picolyl azide with azide group in **11** (Table 3, entry 15) further suppressed the conversion of **12** to 9% and was thus more than three times less in comparison to the chelation-assisted mechanism.

Table 3. (A) The chelation-assisted CuAAC of 2-(6-azidomethyl)-pyridine-4-carboxylic acid methyl ester **3** ($c = 104$ mM) or monovalent picolyl azido telechelic PIB **28** ($c = 104$ mM) and phenylacetylene ($c = 125$ mM) at 27 °C in deuterated THF, applying different Cu(I)-catalysts investigated via *in situ* NMR-measurements. (B) The CuAAC of benzyl azide or monovalent azido telechelic PIB (**11**) and phenylacetylene, exploiting the same conditions of (A).

entry	azide	catalyst	[DIPEA] [eq.]	time	conversion [%]
A)	**NMR experiments applying the ca-CuAAC of either 3 or 28 and phenylacetylene**				
1	**3**	[Cu(CH$_3$CN)$_4$]PF$_6$[a]	–	24 h	32
2	**3**	Cu(OAc)[a]	–	16 h	82
3	**3**	CuBr[a]	–	9 h	> 99
4	**3**	CuBr[a]	1.2[d]	< 5 min[g]	> 99
5	**3**	CuBr[a]	0.1[e]	< 5 min[g]	> 99
6	**3**	CuBr[a]	0.01[f]	17 min	> 99
7	**3**	[CuBr(PPh$_3$)$_3$][b]	0.01[f]	2 h	10
8	**3**	Cu-TRGO[c]	–	24 h	94
9	**3**	Cu/charcoal[a]	–	9 h	< 1
10	**28**	[CuBr(PPh$_3$)$_3$][a]	–	24 h	32
11	**28**	[CuF(PPh$_3$)$_3$][a]	–	11 h	64
12	**28**	CuBr[a]	–	42 min	> 99
13	**28**	CuBr[a]	0.01[f]	< 4 min[g]	> 99
B)	**NMR control experiments applying the CuAAC of either benzyl azide or 11 and phenylacetylene**				
14	**benzyl azide**	CuBr[a]	0.01[f]	110 min	7
15	**11**	[CuBr(PPh$_3$)$_3$][a]	–	24 h	9

a) 0.1 equivalents of the catalyst were added; b) 0.05 equivalents of the catalyst were added; c) 0.02 equivalents of the catalyst were added; d) $c = 125$ mM; e) $c = 10.4$ mM; f) $c = 1.04$ mM; g) the first NMR-spectrum showed complete conversion.

Selected spectra of *in situ* NMR experiments to determine the "click" conversions after different periods of time (illustrated in Table 3) can be found in the appendix 7.2.

3.1.2 Synthesis and characterization of graphene based copper(I)-catalysts
3.1.2.1 Cu-TRGO (15) and Cu-TREGO (17)
In order to increase the reaction rate of the ca-CuAAC heterogeneous Cu(I)-catalysts were applied. Implementing Cu(I)-nanoparticles onto graphene layers was accomplished to combine the substantial advantageous characteristics of the support material such as recyclability and the beneficial outcome in

reaction acceleration for the ca-CuAAC originated by the Cu(I)-NPs. Starting from graphite respectively yielded in the synthesis of the desired heterogeneous catalysts by two different methods. Separation of the graphite-layers was accomplished either by chemical oxidation using the Hummers method[164] or by exfoliation of graphene, applying an additional electrical field, providing graphene-oxide sheets each.[238] The distance of the layers is increased and the functional groups are established on the surface of the graphene layer by both methods (see Figure 35). Cu(II)-nanoparticles were introduced by treating an aqueous solution of ultra-sonication dispersed graphene-oxide with Cu(OAc)$_2$, resulting in the exchange of protons versus Cu^{II}-cations. Reducing the catalytically inactive Cu(II)-species to Cu^I-nanoparticles in an oven at 600 °C afforded the thermally reduced copper(I) graphene oxide (Cu-TRGO) (**15**) and the thermally reduced copper(I) exfoliated graphene oxide (Cu-TREGO) (**17**).
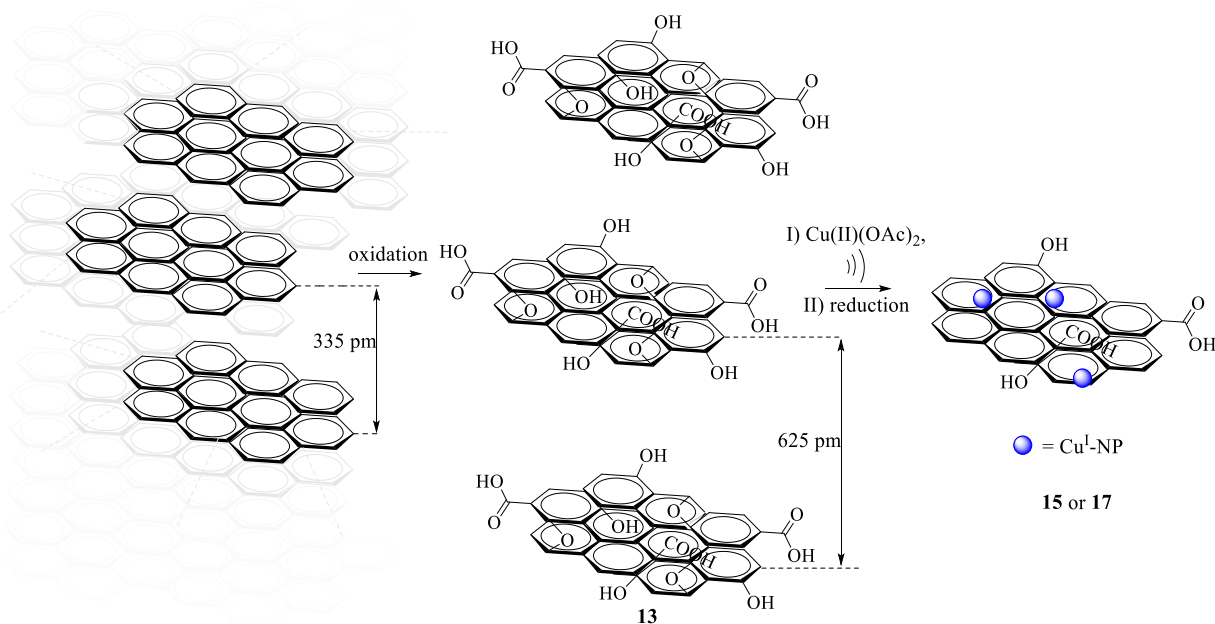
Figure 35. Synthesis of Cu-TRGO (**15**) and Cu-TREGO (**17**).

Successful conversions were monitored by XRD-measurements. Theta scan of the graphite shows peak-position belonging to the graphite-layers at $2\Theta = 25.600$ °, shifting to $2\Theta = 11.168$ ° with a second order peak located at $2\Theta = 22.068$ ° for graphene-oxide (**13**), demonstrating a complete conversion for the chemical method (see Figure 36a, top). In case of exfoliated graphene (provided by Prof. Feng's group) residual graphite can be observed, occurring at $2\Theta = 26.454$ °, beside the graphene-peak located at $2\Theta = 12.677$ °, limiting thus the concentration of the functional groups required for anchoring the Cu(I)-NPs (see Figure 36a, bottom).[238] Introduction of Cu(I)-NPs onto graphene-layers was detected by the shift of theta to $2\Theta = 26.288$ ° in case of Cu(I)-TRGO (**15**) (see Figure 36b, top) and $2\Theta = 26.501$ ° for Cu(I)-TREGO (**17**), overlapping the still present signal of the residual graphite, appearing at the same position (see Figure 36b, bottom). Additional peaks appear at $2\Theta = 35.97$ ° and 42.69 ° and belong to Cu$_2$O and to Cu^0 respectively, verifying the presence of Cu-particles.
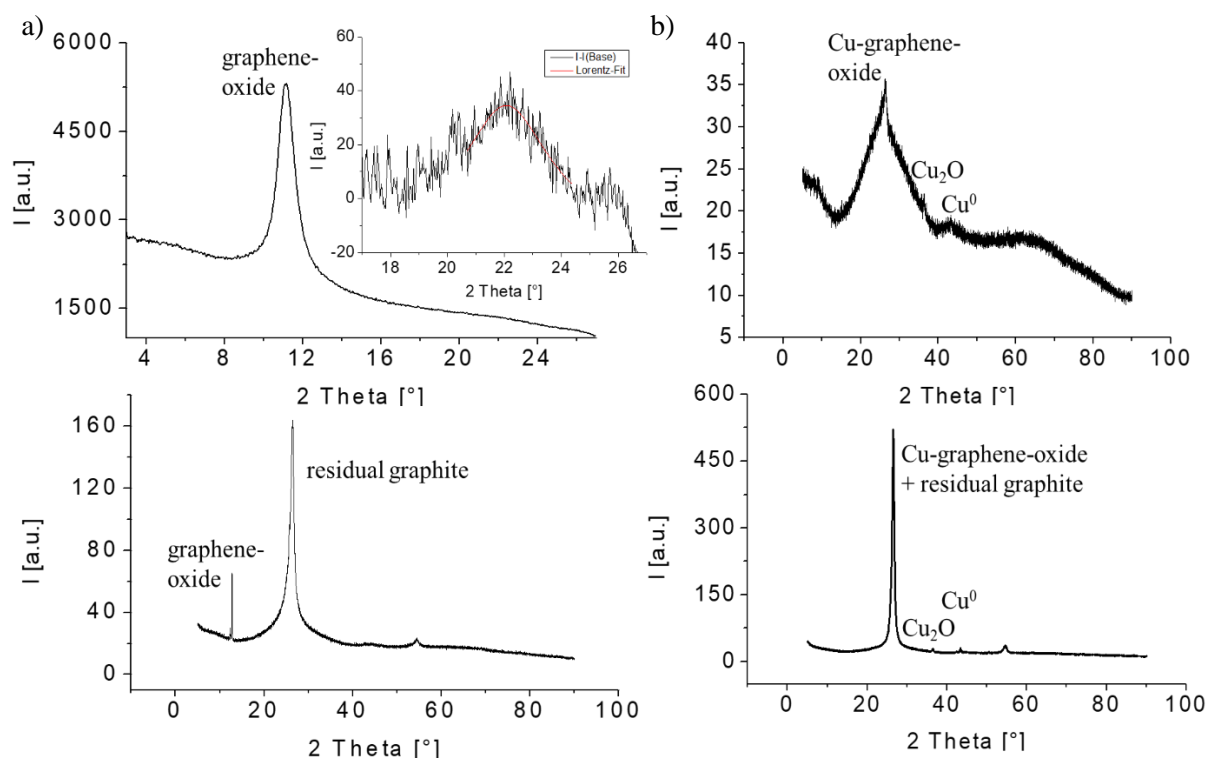
Figure 36. XRD-graphs of a) graphene-oxide (**13**) and superimposed area, showing the first order and second order-peaks (top) and of exfoliated graphene, showing residual graphite peak beside the graphene peak (bottom). b) XRD-graphs of Cu-TRGO **15** (top) and Cu-TREGO **17** (bottom).

FAAS-measurements were conducted to determine the exact amount of Cu-particles of the heterogeneous catalysts. A Cu-content of 6.8 wt% Cu/C for Cu-TRGO (**15**) and of 5.2 wt% Cu/C for Cu-TREGO (**17**) was measured. The minor amount of copper of Cu-TREGO (**17**) was caused due to a reduced concentration of the functional groups, emerging from the insufficient oxidation process (compare Figure 36a, top and bottom). Presence of Cu-particles was further confirmed by transmission electron microscopy (TEM)-images, illustrating nanoparticles in the size of $d = 10 - 100$ nm anchored to the carbon-sheets in the size of $d = 1 - 5$ μm. TEM-images can be found in the appendix 7.3.

3.1.3 Crosslinking investigations of star-shaped picolyl azides in the ca-CuAAC
3.1.3.1 Synthesis and characterization of trivalent picolyl azide (18)
In order to develop an efficient SH-material upon the ca-CuAAC, the responsible picolyl azide moiety (**7**) had to be attached to a star-shaped precursor, enabling the investigation of the crosslinking behavior. Thus, 2-(hydroxymethyl)-2-ethylpropane-1,3-diol was used, promising excellent conversion, since a good mobility of every single alkyl chain without bulky substituents and a good reactivity of the primary alcohol-groups were given. For the functionalization Steglich's method was applied, exchanging *N,N'*-dicyclohexylcarbodiimide (DCC) by 3-(ethyliminomethyleneamino)-*N,N*-dimethylpropan-1-amine (EDC) (see Figure 37a).[305] The resulting 1-ethyl-3-(3-dimethylaminopropyl)urea (EDU) can be removed more easily by washing with water, when compared to the otherwise produced 1,3-dicyclohexylurea (DCU). Column-chromatography was accomplished to remove the excess of **7**, *N,N*-dimethylpyridin-4-amine (DMAP) and still present alcoholic side-products, providing the tris-picolyl azide **18**, suitable for the chelation-assisted CuAAC. The successful introduction of the picolyl azide moieties was confirmed by the aromatic signals at $\delta = 9.15$ ppm, 8.26 ppm and 7.42 ppm in ^{1}H-NMR-spectra (see Figure 37b), confirmed by the azide vibration at $\nu = 2095$ cm^{-1} in IR-spectrum (see appendix 7.4). Purity and thus complete conversion of all three alcoholic groups can be verified in NMR-spectra

via the shift of the appropriate methylene signal from δ = 3.73 ppm to δ = 4.55 ppm[306]. All signals in ^{13}C-NMR spectrum can be assigned to the desired structure, approving the high purity of the product (see Figure 37c), validated by the mass detected in ESI-ToF-MS of m/z = 637.1976 g/mol (simulated: m/z = 637.1994 g/mol) (see appendix 7.4).
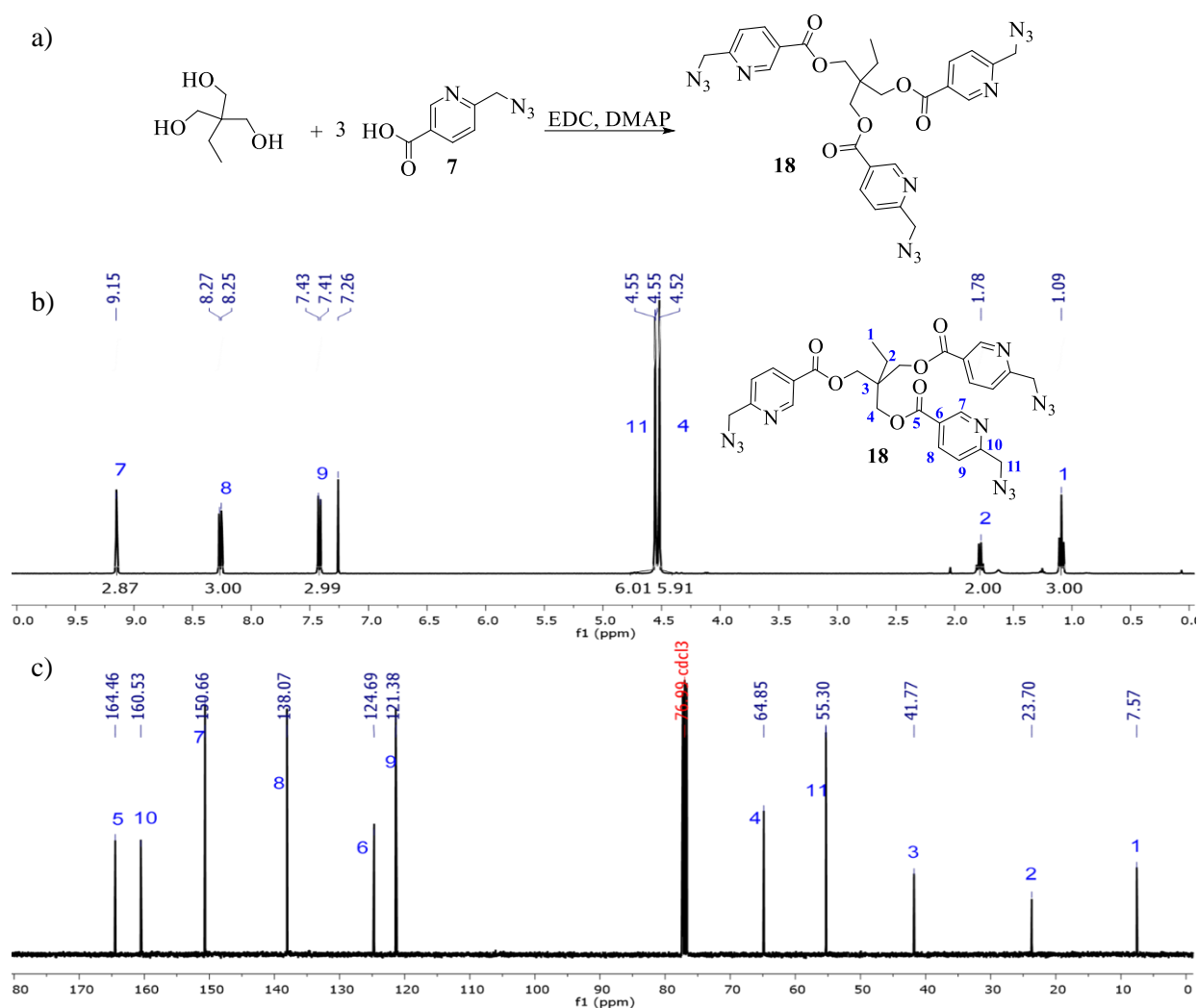
Figure 37. a) Synthesis of trivalent picolyl azide (**18**) via Steglich esterification of 2-(hydroxymethyl)-2-ethylpropane-1,3-diol with picolyl azide (**7**). b) ^{1}H-NMR spectrum of **18** in C*D*Cl$_3$. c) ^{13}C-NMR spectrum of **18** in C*D*Cl$_3$.

3.1.3.2 DSC of NHC-Cu(I)-catalysts and multivalent picolyl azides (solution crosslinking)

The difference in kinetics of the CuAAC and the chelation-assisted CuAAC was further investigated by DSC-measurements. Previous studies of crosslinking the CuAAC, using a non-chelation-assisted trivalent azide (**19**)[49] (see Figure 38a), were compared to the crosslinking approach based on the ca-CuAAC, converting star-shaped **18** with a trivalent alkyne (**20**) to form a network (see Figure 38b). The efficiency of various catalysts, including homogeneous and heterogeneous ones were probed. Continuously, the thermal activation of the previously synthesized homogeneous bis(NHC)-Cu(I)-catalysts (**21** and **22**) was tested (see Figure 38c).

The crosslinking efficiency of **19** and **20** in the CuAAC and **18** + **20** in the ca-CuAAC varying the Cu(I)-source was detected by comparison of T_{Peak} of the uncatalyzed and the catalyzed experiments (see Table 4). In absence of a catalyst the thermal Huisgen reaction was conducted at temperatures, which were in the range of the reported literature values of 120 – 133 °C (see Table 4, entry 1 and 6).[56] The CuAAC of **19** and **20** in presence of a homogeneous Cu(I)-source led to a reduced T_{Peak} of 74 °C ([CuBr(PPh$_3$)$_3$])

(see Table 4A, entry 2) or of 66 °C ([CuF(PPh$_3$)$_3$]) (see Table 4A, entry 3). In comparison, less efficiency was provided, applying heterogeneous Cu-TRGO (**15**) instead, increasing T_{Peak} slightly to 85 °C (see Table 4A, entry 4). Insignificant change of T_{Peak} to 76 °C was observed, applying Cu-TREGO (**17**) (see Table 4A, entry 5). Thus, heterogeneous catalysts were less efficient than the homogeneous catalysts in triggering the CuAAC of crosslinking reactants (see Figure 38a).
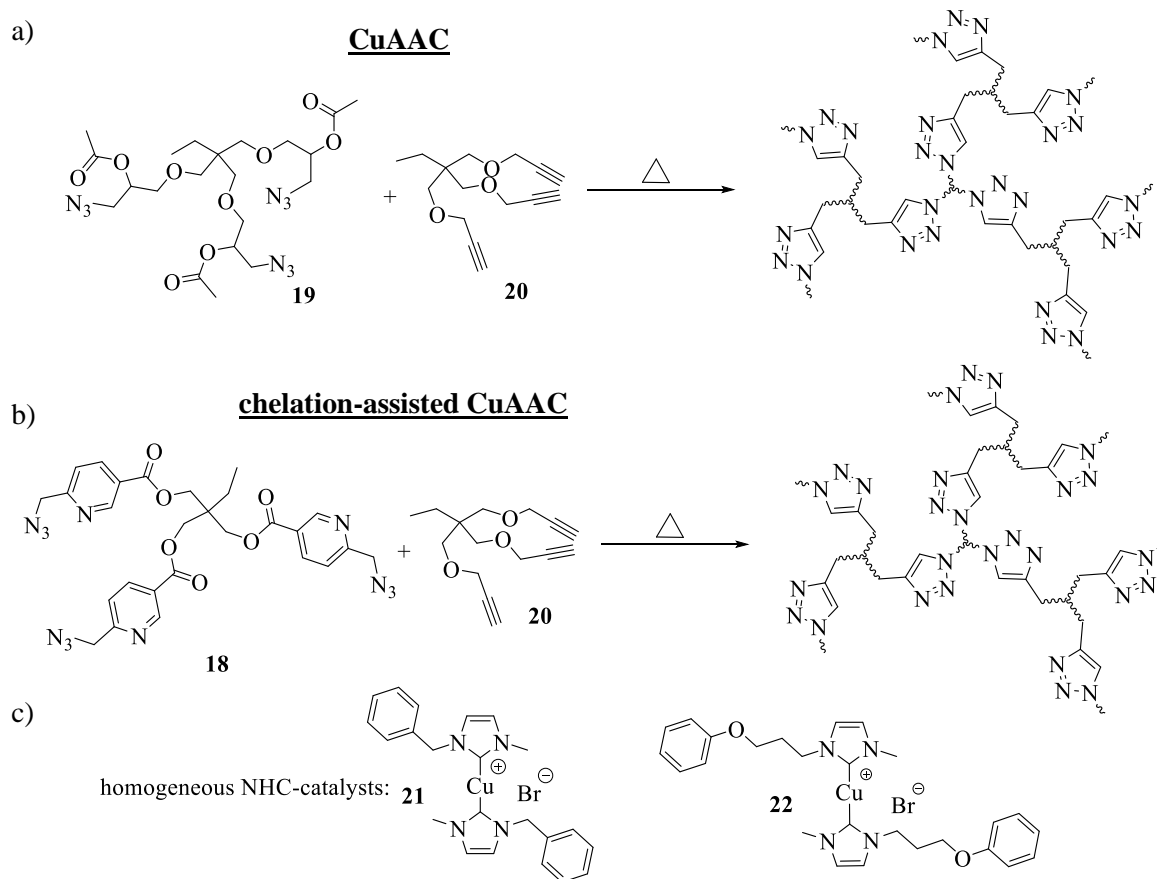
Figure 38. DSC-experiments of a) CuAAC suitable azide (**19**) and trivalent alkyne (**20**) and b) chelation-assisted CuAAC suitable azide **18** and trivalent alkyne (**20**). c) Thermal activation of the homogeneous NHC-catalysts (**21** and **22**) was verified via DSC-experiments of the ca-CuAAC.

Switch to the ca-CuAAC mechanism, employing trivalent picolyl azide (**18**) required the addition of a solvent (anhydrous chlorobenzene (50 wt%)), ensuring proper diffusion of the substances, as a consequence of the solid appearance of **18** (see Figure 38b). A continued reduction of T_{Peak} to 59 °C ([CuBr(PPh$_3$)$_3$]) (see Table 4B, entry 7) or 41 °C ([CuF(PPh$_3$)$_3$]) (see Table 4B, entry 8) was observed, lowering the reaction temperature by ~ 20 °C compared to the conventional CuAAC. The beneficial pre-organization of the Cu(I)-acetylide to close proximity of the azide-group led to the improved acceleration in catalysis. Highest efficiency was provided in presence of heterogeneous Cu-TRGO with a measured peak T of 38 °C (see Table 4B, entry 9). The thermal activation of the latent and homogeneous NHC-catalysts (**21** and **22**) was probed (see Figure 38b-c), revealing that the inactive biscarbene-Cu(I) unit cannot be abolished by the thermal treatment (see Table 4B, entry 10-12). In turn, scission into the active monocarbene-Cu(I)-species was inhibited, leading to a T_{Peak} similar to a non-catalytic reaction at approximately ~ 120 °C (see Table 4B, compare entry 6 with entry 10-12). The addition of a base such as 1,8-diazabicyclo[5.4.0]undec-7-ene (DBU) or 1,5-diazabicyclo[4.3.0]non-5-ene (DBN) led to a significant reduce of T_{Peak} (see Table 4B, entry 13-16). It is assumed that one Cu-carbene-bond is cleaved off by the base-treatment, releasing the active Cu(I)-monocarbene species, able to conduct the crosslinking "click" reaction. In particular the combination of the NHC-catalyst (**22**) in

presence of DBU demonstrated to be most efficient, leading to a start of the „click"-reaction at $T_{ON} =$ 4 °C (see Table 4B, entry 16). The reaction setups, which were already starting below 35 °C (see Table 4B, entry 8, 9, 15 and 16) simultaneously provided the lowest "click" conversions, varying between 11% to 40%. This was presumably referred to the delay time in turn of the device-related measurement setup: the crosslinking reaction already started upon mixing the components with the Cu(I)-catalyst, while it took in total approximately ~ 2 – 3 minutes (= delay time) to subject the samples into the crucibles, to close the latter with lids and to transfer it to the oven (driven by the device ~ 1.5 minutes), before the hole sample was cooled (from RT) and finally heated to start the measurement.

Table 4. DSC investigations of (A) the CuAAC of star-shaped azide (**19**) or (B) the ca-CuAAC of trivalent azide (**18**) with trivalent alkyne (**20**).

entry	catalyst		base	T_{ON} [°C] at 5 K/min	T_P [°C] at 5 K/min	ΔH_m [kJ/mol]	conversion [%]
	composition	mol%					
A)	CuAAC of tris-azide (**19**) and tris-alkyne (**20**)[a]						
1[c]	without	-	-	91	133	-205.3	78
2[c]	[CuBr(PPh₃)₃]	3	-	59	74	-185.4	71
3[c]	[CuF(PPh₃)₃]	3	-	39	66	-191.0	73
4	Cu-TRGO (**15**)	3	-	64	85	-78.2	30
5	Cu-TREGO (**17**)	3	-	55	76	-77.6	30
B)	chelation-assisted CuAAC of tris-azide (**18**) and tris-alkyne (**20**)[b]						
6	without	-	-	92	121	-209.8	80
7	[CuBr(PPh₃)₃][c]	3	-	44	59	-139.6	53
8	[CuF(PPh₃)₃][c]	3	-	27	41	-76.5	29
9	Cu-TRGO[a]	3	-	20	38	-105.8	40
10	**21**	3	-	90	125	-126.3	48
11	**21**	10	-	90	126	-223.8	85
12	**22**	10	-	90	126	-149.6	57
13	**21**	10	DBN[d]	45	91	-231.5	88
14	**21**	10	DBU[d]	45	77	-159.3	61
15	**22**	10	DBN[d]	30	64	-58.4	22
16	**22**	10	DBU[d]	4	40	-28.5	11

a) Azide and alkyne mixture (1:1) was dissolved in DCM and stirred before the solvent was evaporated to ensure proper diffusion of the components. The mixture (5 – 10 mg) was transferred to the crucible and mixed with Cu(I)-catalyst by spatula. In b) additional chlorobenzene (0.5 wt%) was added; c) unpublished work of the working group, see chapter 4.1; d) 10 mol% compared to the reactants was added.

The extent of the network formation was estimated by comparing the literature-value of enthalpies of reactions of entirely converted phenylacetylene and benzyl azide with 1 mol% [CuBr(PPh₃)₃] ($\Delta H_m =$ 262 kJ/mol[49]) and those detected by own measurements. Selected DSC-spectra can be found in the appendix 7.5.

3.1.3.3 Synthesis and characterization of star-shaped picolyl azido telechelic PIBs (34a/b)

Star-shaped polymers, possessing a low T_g, were required to ensure a proper diffusion of the reactants, enabling an efficient crosslinking at low temperatures (< 20 °C) in absence of solvents. Thus, PIBs (T_g ≈ -80 °C)[39] of different valence were synthesized via LCCP of isobutylene, applying either 2-chloro-2,4,4-trimethyl-pentane (TMPCl) (**23**), 5-tert-butyl-1,3-bis(1-chloro-1-methylethyl)-benzene (DCCl) (**24**) or 1,3,5-tris(2-methoxyisopropyl)benzene, (tricumyl methoxy, TriCuOMe) (**25**) as initiators (see Figure 39). Allyl-terminated PIBs (**26**, **29**, **32**) were provided in a one-pot synthesis by quenching the polymerization with allyltrimethylsilane (ATMS) and were subsequently converted to hydroxy groups by treatment with 9-BBN and *m*-CPBA in a second step. The molecular weights were limited to 3 000 – 6 000 g/mol, maintaining the beneficial advantage of a liquid flow-behavior. The hydroxy telechelic

PIBs (**27**, **30**, **33**) were now used as alcoholic-precursors for anchoring the ca-CuAAC responsible group.
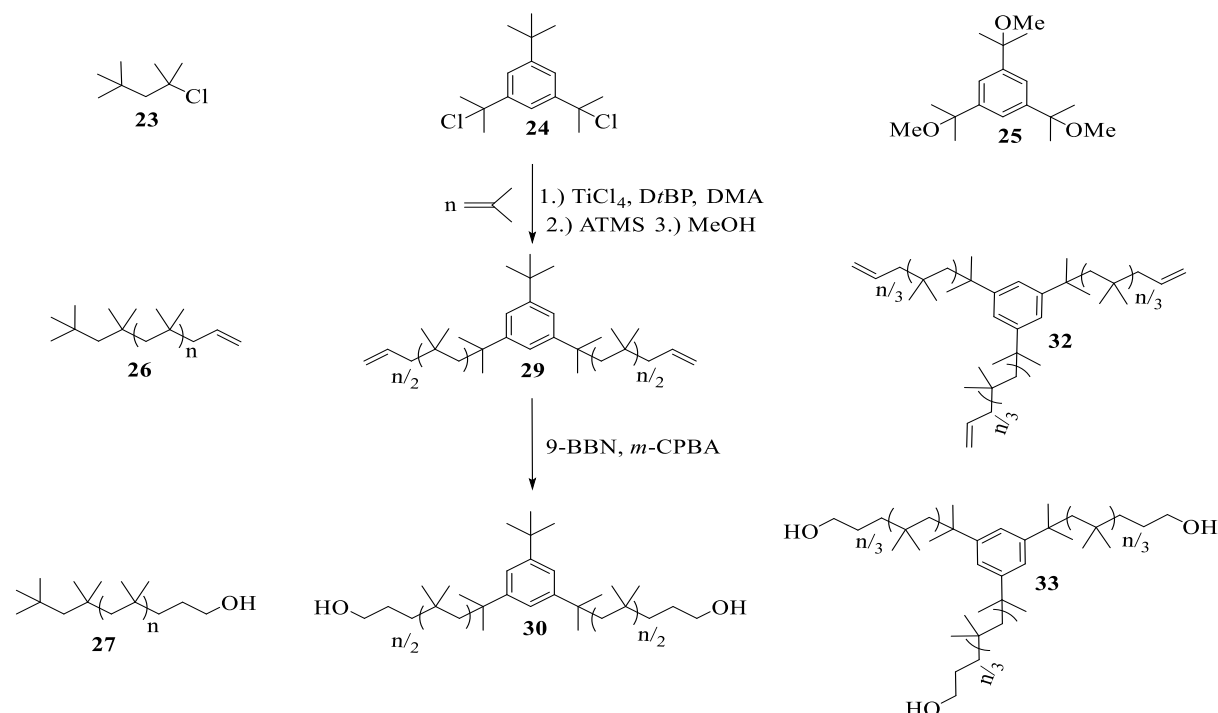
Figure 39. Synthesis of mono-, bi- and trivalent hydroxy telechelic PIB precursor (**27**, **30**, **33**) synthesized via LCCP of isobutylene, applying TMPCl (**23**), DCCl (**24**) and TriCuOMe (**25**) as initiators and ATMS as quenching-agent in a one-pot synthesis. Followed by the conversion to the desired alcoholic groups by treatment with 9-BBN and *m*-CPBA in a second step.

In contrast to the synthesis-route of **18**, the Steglich esterification remained insufficient in case of mono- to multivalent hydroxy telechelic PIBs. Accordingly, the reactivity of **4** or **7** was increased by treatment with oxalyl chloride in DCM. In a one-pot synthesis the previously synthesized acid chloride, EDC·HCl and DMAP were added to the polymeric precursors, affording the picolyl azido telechelic PIBs (**28**, **31**, **34a** and **34b**) (see Figure 40).
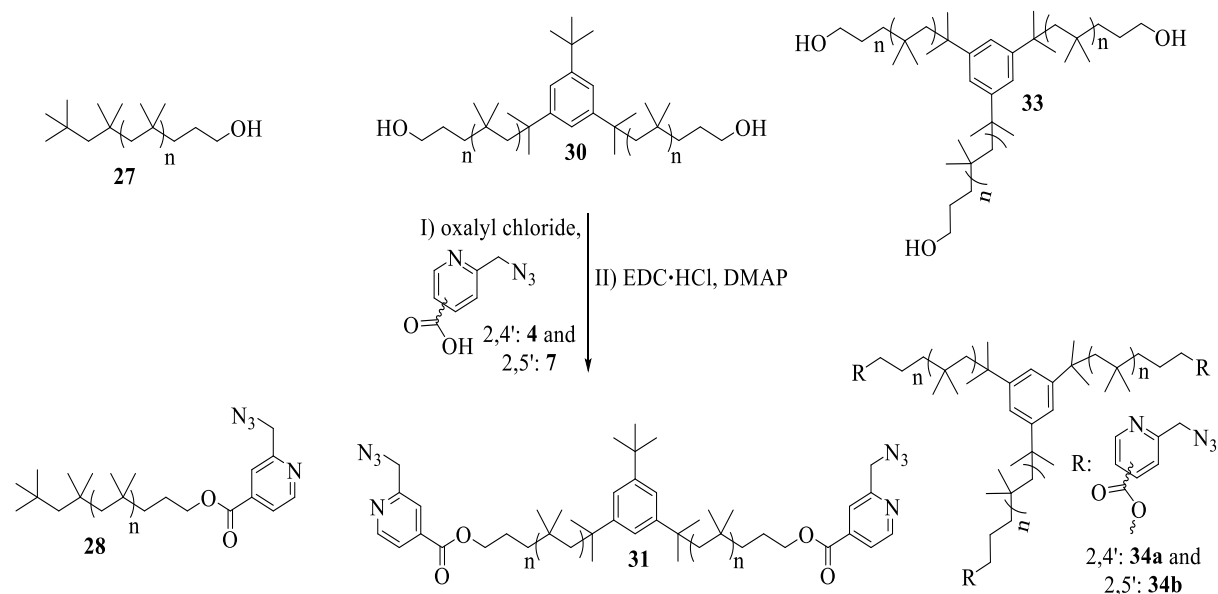
Figure 40. Synthesis of the chelation-assisted CuAAC suitable polymers based on PIB (**28**, **31**, **34a/b**).

The molecular weight of the polymers was limited to < 7000 g/mol, verified via GPC- and NMR-measurements, showing also a narrow distribution of the obtained molecular weights, illustrated by the low PDI-values of 1.1 – 1.3 (see Table 5).

Table 5. Overview of analytical data of the synthesized PIBs.

PIB-allyl			PIB-OH			PIB-picolyl-N$_3$		
$M_{n(GPC)}$[a) [g/mol]	$M_{n(NMR)}$[b) [g/mol]	PDI[a)	$M_{n(GPC)}$[a) [g/mol]	$M_{n(NMR)}$[c) [g/mol]	PDI[a)	$M_{n(GPC)}$[a) [g/mol]	$M_{n(NMR)}$[d) [g/mol]	PDI[a)
26: 3 000	3 100	1.16	**27**: 2 700	3 700	1.19	**28**: 3 000	4 100	1.17
29: 3 500	3 400	1.18	**30**: 3 300	3 900	1.22	**31**: 4 000	4 100	1.21
32: 4 500	6 300	1.34	**33**: 5 000	7 300	1.32	**34a**: 6 500	6 600	1.33
						34b: 5 800	6 800	1.31

a) GPC-measurement was performed in THF and PIB-standards were used for the calibration. b) Calculated, according to the ratio of the signals at δ = 5.84 ppm of the allylic head group and δ = 1.11 ppm of the repetitive unit (two CH$_3$-groups), considering the relation of the initiator-part at **26**: δ = 0.99 ppm (15 H); **29**: δ = 0.79 ppm (12 H); **32**: δ = 0.80 ppm (18 H). c) Calculated, according to the ratio of the signals at δ = 3.61 ppm of the CH$_2$-moiety attached to the hydroxy-group and δ = 1.11 ppm of the repetitive unit (two CH$_3$-groups), considering the relation of the initiator-part at **27**: δ = 0.99 ppm (15 H); **30**: δ = 0.79 ppm (12 H); **33**: δ = 0.80 ppm (18 H). d) Calculated, according to the ratio of the signals at δ = 4.33 ppm of the CH$_2$-moiety attached to the ester group and δ = 1.11 ppm of the repetitive unit (two CH$_3$-groups), considering the relation of the initiator-part at **28**: δ = 0.99 ppm (15 H); **31**: δ = 0.79 ppm (12 H); **34/34b**: δ = 0.80 ppm (18 H).

Successful introduction of the picolyl azide moieties was verified by NMR- and IR- spectroscopy and MALDI-ToF-MS. The progress of the reaction was comprehensible, focusing on the transformation of the end group signals in NMR-spectroscopy (see Figure 41). The allylic signals, (of **26**) appearing at δ = 5.85 ppm and δ = 5.03 ppm (see Figure 41a), shifted in the first instance to the triplet-signal at δ = 3.61 ppm, corresponding to the methylene group, carrying the alcoholic unit (of **27**) (see Figure 41b) and finally to δ = 4.33 ppm of the methylene group, containing the picolyl azide moiety (of **28**) (see Figure 41c).
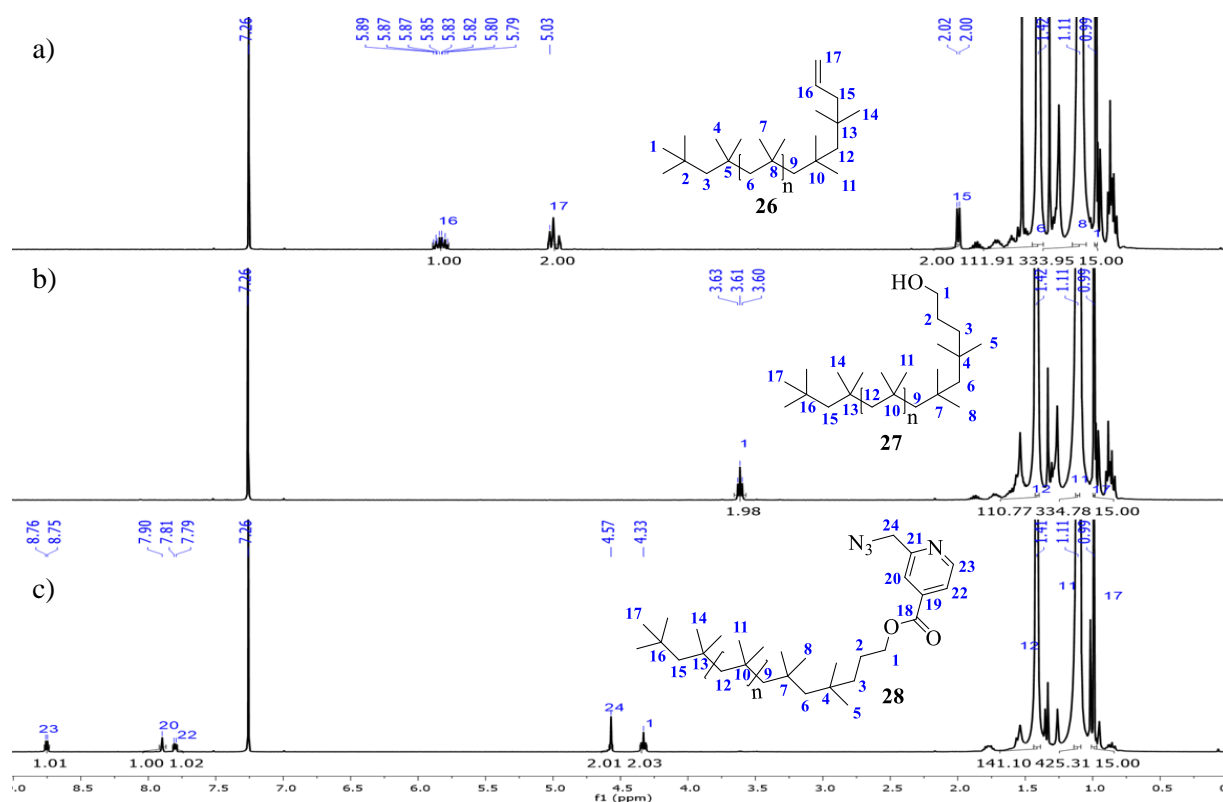
Figure 41. ^{1}H-NMR spectra in CDCl$_3$ of a) allyl telechelic PIB (**26**); b) hydroxy telechelic PIB (**27**); c) picolyl azido telechelic PIB (**28**).

For the bi- and trivalent PIBs the same characterization-methods were applied, confirming the successful synthesis of the crosslinkers suitable for the chelation-assisted CuAAC. Conversion of all arms for the bivalent azido telechelic PIB (**31**) and the trivalent **34a** was complete, when compliance of the following two characteristics was given: first, the entirely disappearance of the triplet signal at $\delta = 3.61$ ppm and secondly by the matching integrals of the signals, corresponding to the initiator part (for instance $\delta = 7.13 – 7.17$ ppm) and the signals, belonging to the end group (e.g., $\delta = 7.44 – 9.19$ ppm) (see Figure 42a and 42b). In case of **34b** the separation of the final product from semi-converted contaminants remained insufficient. A repeatedly conducted reaction in order to accomplish a full conversion and further purification by column chromatography and repeated precipitation in MeOH afforded a mixture, consisting of azido- and hydroxy- functionalized PIBs. In consequence **34b** was mixed with hydroxy telechelic PIB to an extent of 20%, according to the ratio of the corresponding integrals (CH_2-OH at $\delta = 3.61$ ppm and CH_2-OR-N_3 at $\delta = 4.32$ ppm) in NMR-spectra (see Figure 42c). Hence, it was estimated, that **34b** would provide less performance in the subsequent crosslinking experiments compared to the star-shaped azido telechelic PIB (**34a**). The star-shaped PIBs (**34a** and **34b**) were distinguished in ^{1}H-NMR spectra, differing in the position of the aromatic protons, as a consequence of their dissimilar regiostructures (see Figure 42b and 42c). Thus, the aromatic signals of the pyridine-ring for the 2,4-analogue (**34a**) appeared at $\delta = 8.76$ ppm, $\delta = 7.90$ ppm and $\delta = 7.80$ ppm, in contrast to those of **34b** located at $\delta = 9.20$ ppm, $\delta = 8.34$ ppm and $\delta = 7.46$ ppm.
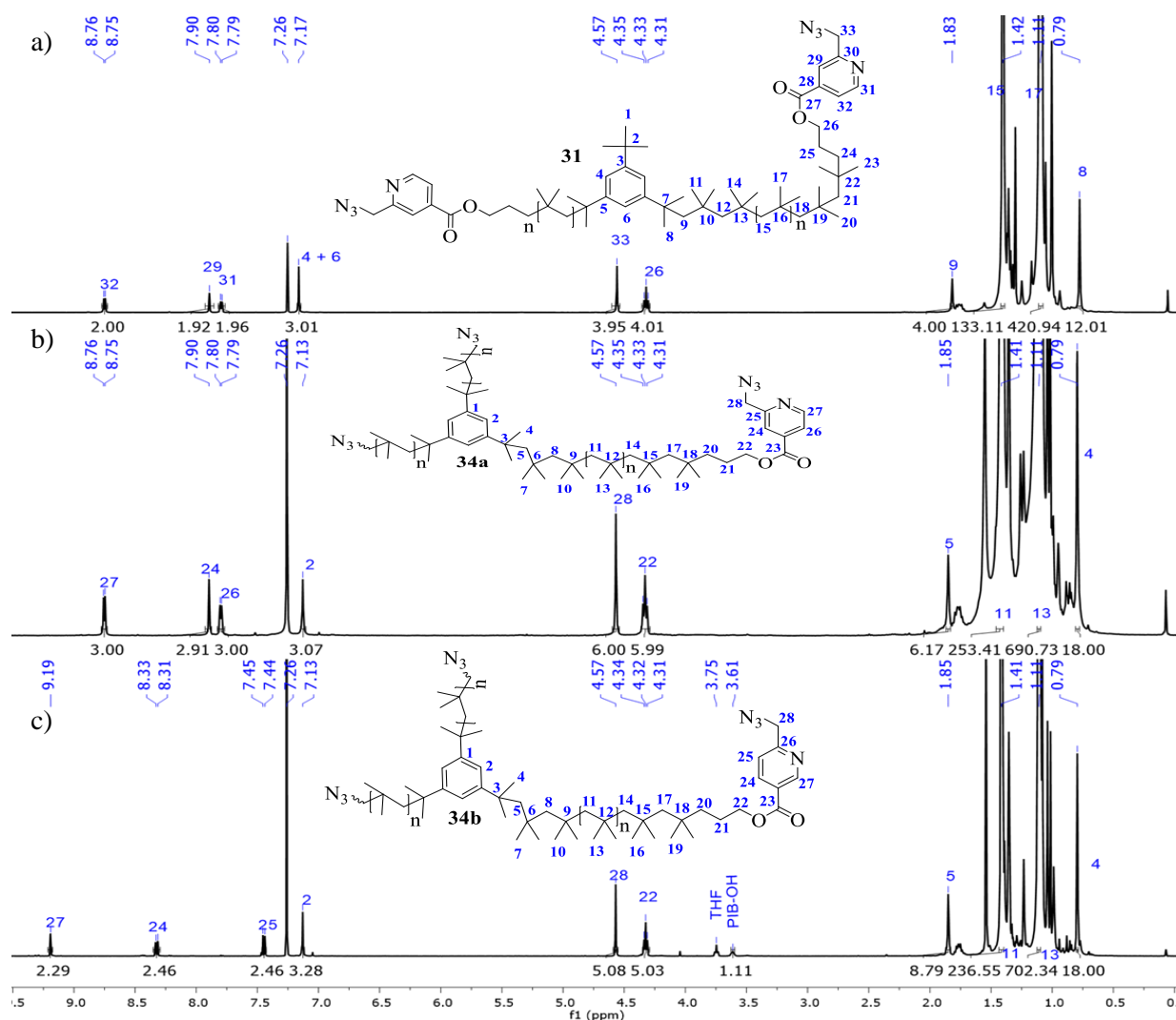
Figure 42. ^{1}H-NMR spectra in C*D*Cl3 of a) bivalent azido telechelic PIB (**31**); b) trivalent 2,4-azido- telechelic PIB (**34a**); c) trivalent 2,5-azido- telechelic PIB (**34b**).

A MALDI-ToF-MS analysis proved the attachment of the desired picolyl azido moiety to the monovalent PIB (**28**) (see Figure 43a-c) and the trivalent PIB (**34a**). The *m/z*-distance of each signal was 56 g/mol, belonging to the molecular weight of the repetitive unit of isobutylene (see Figure 43b). The structure of the monovalent PIB (**28**) was detected by two different series, while the first one with its maximum at 2348.375 g/mol was identified as the desired picolyl azido telechelic PIB (**28**) with additional silver cation, matching well with its simulation of 2348.259 g/mol (error 49 ppm) ([M+Ag]$^+$ (C$_4$H$_8$)$_{34}$C$_{18}$H$_{28}$N$_4$O$_2$Ag$^+$) (see Figure 43c). The second series could again be assigned to the picolyl azido telechelic PIB (**28**) with additional sodium trifluoroacetic acid and proton with the absolute maximum at 2320.693 g/mol, fitting well with its simulation of 2320.272 g/mol (error 181 ppm) ([M+NaTFA+H]$^+$ (C$_4$H$_8$)$_{33}$C$_{18}$H$_{29}$N$_4$O$_2$C$_2$F$_3$O$_2$Na$^+$) (see Figure 43c). The limited resolution of the MALDI-ToF-MS was preventing the inspection of the compliance of the isotopic patterns of the measured and the simulated spectra. The existence of the picolyl azide moiety for all the PIBs (**28**, **31**, **34a** and **34b**) of various valence was additionally detected via IR-measurements, showing the azide vibration for each of them at $v = 2103$ cm^{-1} – 2105 cm^{-1}. ^{1}H-NMR-spectra of precursor PIBs of a bivalent and a trivalent composition, MALDI-ToF-spectrum of **34a** and IR-spectrum can be found in the appendix 7.6.
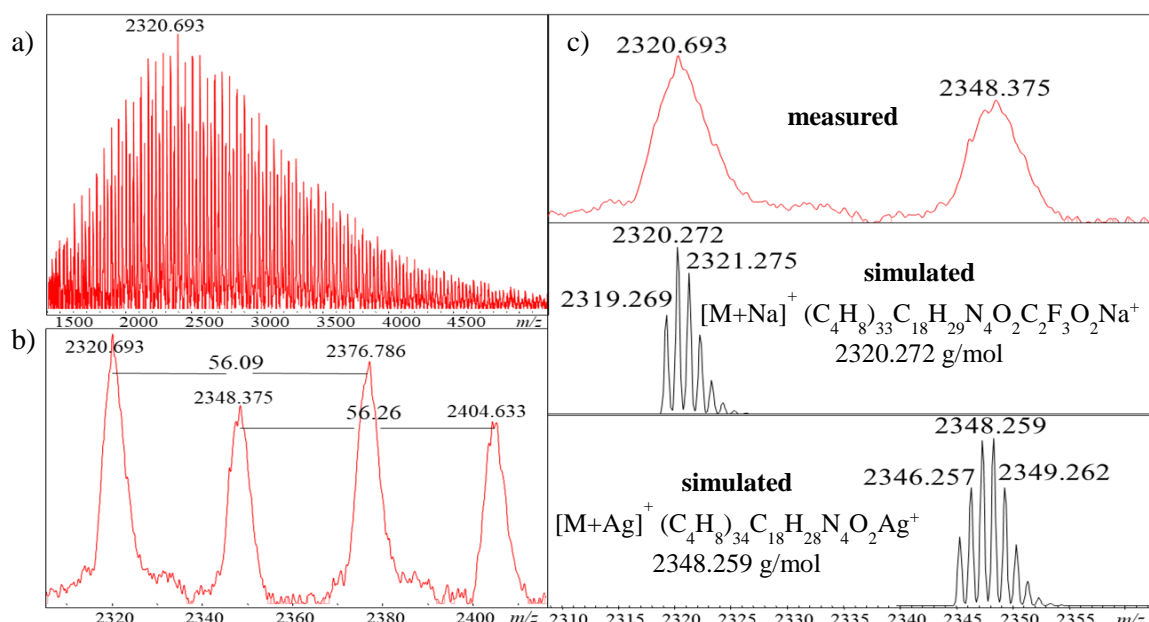
Figure 43. MALDI-ToF-MS of picolyl azido telechelic PIB (**28**). a) Full spectrum of **28**, showing two series. b) Superimposed area of spectrum of **28**, showing distance between peaks of both series of 56 g/mol. c) Measured peaks and their simulated isotopic pattern, belonging to the displayed structures.

3.1.3.4 Rheology of ca-CuAAC PIBs for crosslinking in the melt

The crosslinking behavior of the obtained azido telechelic PIBs (**34a**, **34b**) was monitored by melt rheology measurements. Thus, either azido component **34a** or **34b** was mixed with the star-shaped PIB-alkyne (**35**) (see Figure 44), varying the conditions (like catalyst or temperature), allowing a comprehensive comparison to previous results, applying the conventional CuAAC based systems.[40, 42, 44, 47] Since the use of CuBr in solution delivered full conversion in the shortest period of time it was also tested in melt rheology experiments. Although 1 mol% of DIPEA was added, the network formation took 870 minutes (gelation time, see Table 6, entry 1), which was mainly attributed to oxidation of the catalyst during the rheology experiment. In accordance with literature[39-40, 42, 44] [CuBr(PPh$_3$)$_3$] was probed as an alternative catalyst, despite its relatively poor performance in the initial low molecular weight compound tests. Consequently, this system showed significantly shorter gelation times of 255 – 266 min (Table 6, entries 2 and 3) and was slightly better than the comparable conventional CuAAC (290 min, RT) approach[40]. Change of the counterion of the catalyst from bromide to fluoride

presumably led to an improved solubility of the catalyst within the mixture[307] and thus to further tremendous reduction of the gelation-times, accomplishing crosslinking within 15 minutes at room temperature (Table 6, entry 4). This system was even faster than the crosslinking hyperbranched PIB-polymers (20 °C, 33 minutes) converted via the conventional CuAAC.[44] Change from the 2,4- (**34a**) to the 2,5-isomer (**34b**) nearly doubled the crosslinking time to 29 minutes at 20 °C (Table 6, entry 5), which was caused by its lower amount of crosslinking capable groups. However, rapid crosslinking was also provided at 10 °C, forming the network within 71 minutes (Table 6, entry 6). Further reduction of the temperature to 5 °C caused the condensation of water-droplets in the inner system of the device, leading to the deactivation of the catalyst. In turn, the increased gelation time of 663 minutes at 5 °C was not only caused by the lower temperature, reducing the crosslinking rate, but also by the condensation of water, decomposing the Cu(I)-catalyst (Table 6, entry 7).
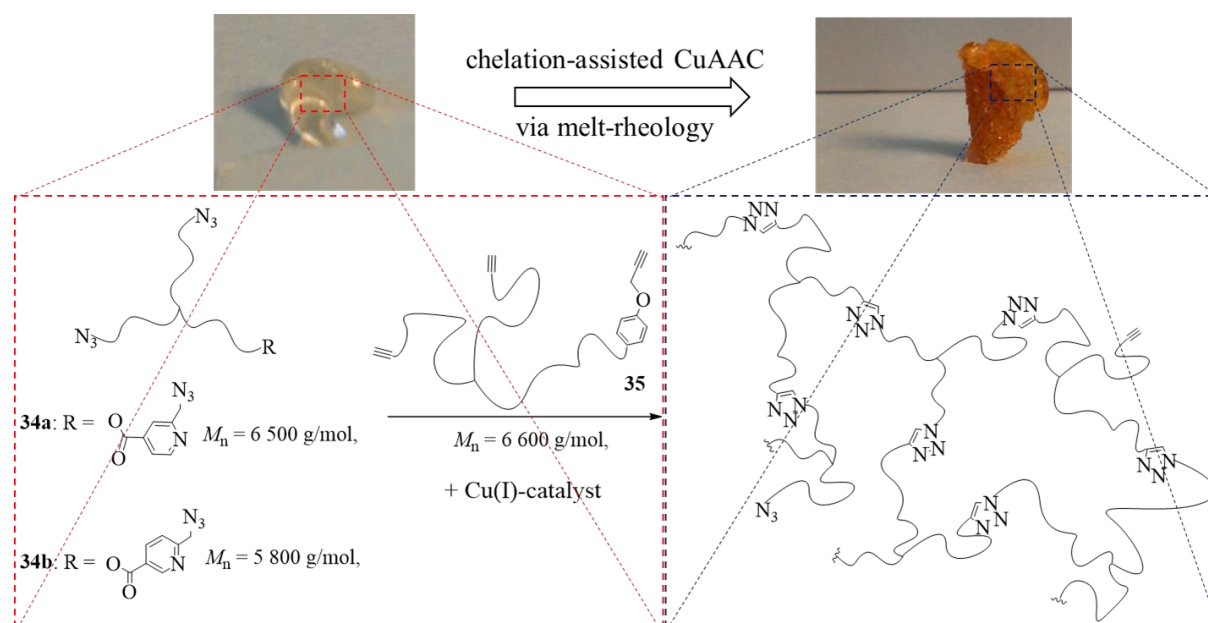
Figure 44. Melt-rheology of star-shaped picolyl azido telechelic PIBs (**34a** and **34b**) and multivalent alkyne telechelic PIB (**35**) in presence of a Cu(I)-catalyst to form a macromolecular network by the chelation-assisted CuAAC crosslinking.

Table 6. Network formation of the star-shaped picolyl azido telechelic PIBs (**34a** or **34b**) (4 mmol) and PIB-alkyne (**35**) (4 mmol), using the chelation-assisted CuAAC monitored via melt rheology measurements.[a)]

entry	PIB-azide	catalyst	T [°C]	$t_{(Gel)}$[d)] [min]	c_M [M]	c_{Cu} [M] (*10^{-2})	k_0 [M^{-3} min^{-1}]	$k_{crossover}$ [M^{-3} min^{-1}]	r_0 [M min^{-1}]
1[b)]	**34a**	CuBr	20	870	0.254	2.54	-	-	-
2[b)]	**34a**	[CuBr(PPh₃)₃]	20	255	0.254	2.54	2 200	7 300	0.092
3[c)]	**34a**	[CuBr(PPh₃)₃]	20	266	0.254	2.54	400	1 000	0.017
4	**34a**	[CuF(PPh₃)₃]	20	15	0.254	2.54	_e)	_e)	_e)
5	**34b**	[CuF(PPh₃)₃]	20	29	0.200	2.00	3 100	9 100	0.050
6	**34b**	[CuF(PPh₃)₃]	10	71	0.200	2.00	2 500	7 500	0.041
7	**34b**	[CuF(PPh₃)₃]	5	663	0.200	2.00	_f)	_f)	_f)

a) **34a** or **34b** was mixed with **35** (1:1) and dissolved in anhydrous DCM, followed by evaporation of the solvent. The mixture was subjected to the device and the catalyst (0.1 eq. per functional group) dissolved in CHCl₃ (20 μL) was added as stock-solution to start the measurement. b) 0.01 eq. of DIPEA was added; c) 0.1 eq. of DIPEA was added; d) determined via melt rheology, $G'' = G'$ at $\omega = 10$ Hz; e) reaction was too fast for determination; f) water was disturbing the measurement.

The rate constants near the gel point were calculated using equation 2[40, 308-309]:

$$k = \frac{e^{(k't)} - 1}{t \cdot [A]_0 \cdot [Cu]^2} \qquad \textbf{(e2)}$$

For all the performed crosslinking reactions an acceleration of the reaction rates with progressing time was observed (see Figure 45). This autocatalytic effect was caused by an increasing concentration of the formed triazole rings during the proceeding crosslinking reactions, since these heterocyclic rings could act as internal ligands, capable of chelating copper[40, 82]. Further, the auto-acceleration of the chelation-assisted CuAAC originated by the newly formed triazole rings should not be as strong as in the classical CuAAC, due to the presence of the internal pyridine ligand already at the very beginning of each reaction. Indeed, the acceleration factors of the chelation-assisted CuAAC varied from 2.9–3.3 (see Figure 45 and Table 6, entries 2, 5 and 6) and were therefore lower compared to the classical CuAAC approach, utilizing polymers with comparable molecular weights (acceleration factor of 3.8).[40]
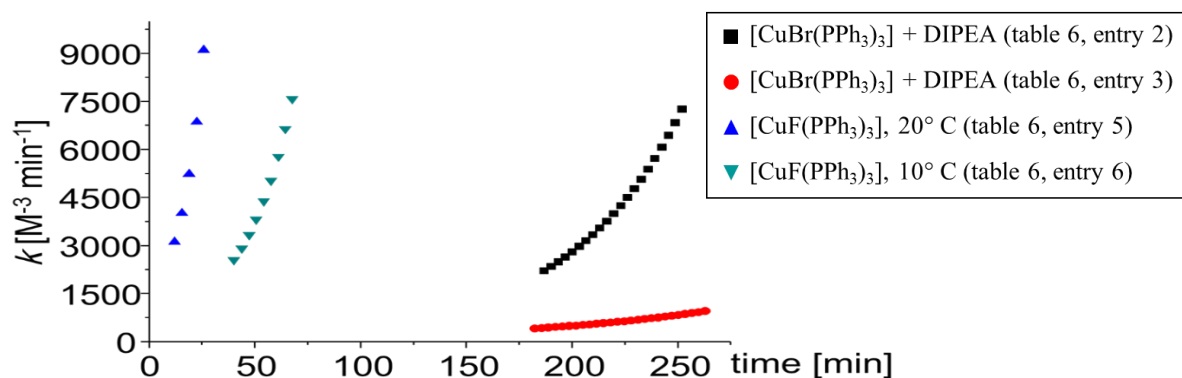
Figure 45. Rate-constants k vs. time, displaying the auto-acceleration-effect of the ca-CuAAC of **34a** + **35** (black squares and red dots) and of **34b** + **35** (blue and green triangles) with proceeding reaction-progress (see Table 6).

Although the difference in the acceleration of the chelation-assisted CuAAC and the classical CuAAC was moderate, a substantial distinction in the calculated rate constants resulted. While the classical CuAAC started with a rate constant of $k_0 \sim 700$ M^{-3} min^{-1},[40] up to fourfold higher k_0 values (2200–3100 M^{-3} min^{-1}) were observed for the crosslinking reactions, following the chelation-assisted CuAAC mechanism from the very beginning (Table 6, entries 2, 5 and 6). In entry 3 (see Table 6), the rate constant k_0 was ~ 400 M^{-3} min^{-1} and was therefore just 1/5 of k_0 in entry 2 (see Table 6), leading, however, to identical gelation times of ~ 260 minutes for both experiments. For crosslinking **34b** + **35** in the presence of the most active catalyst [CuF(PPh$_3$)$_3$], k_0-values of ~ 2500–3100 M^{-3} min^{-1} (Table 6, entries 5 and 6) were observed already at the very beginning of the reaction, resulting in strongly reduced gelation times (29–71 minutes) even at 10 °C.

Network strand densities v_x were determined for the final crosslinked materials according to equation (3)[310-311]:

$$G_N = v_x RT = \frac{\rho RT}{M_c} \left(1 - \frac{2M_c}{M_n}\right) \qquad \textbf{(e3)}$$

where G_N is the measured plateau modulus at $\omega = 100$ Hz, ρ is the density of the polymer mixture, M_n is the average molecular weight of the polymer mixture, R is the universal gas constant (8.3145 J mol^{-1} K^{-1}), T is the temperature in K and M_c is the average molecular weight between two network points. By assuming a complete conversion, the maximum network strand density $v_{x,max}$ was calculated. The experimental network strand density $v_{x,exp}$ was determined, using the experimentally determined plateau moduli. Relation of the experimental and the maximum network strand density provided information about the amount of the formed network points during the crosslinking and thus the completeness of the reaction (see Table 7). Both the plateau modulus G_N (1 x 10^4 Pa) and the calculated network strand density $v_{x,exp}$ (4 mol/m^3 = 1.6% network density) were low, using CuBr as a catalyst (Table 7, entry 1),

which was in agreement with only slight changes observed in the viscosity during the network formation, indicating incomplete crosslinking, presumably due to oxidation instability of the catalyst during the melt rheology experiment. Exchange of CuBr to more oxidation stable [CuBr(PPh$_3$)$_3$] catalyst resulted in increased network strand densities of up to 46 mol/m^3, corresponding to a network density of 18.5% (Table 7, entries 2 and 3). The network density was further doubled to 40.2% (network strand density: 102 mol/m^3) by change to the most active catalyst, namely [CuF(PPh$_3$)$_3$] (Table 7, entry 4), which was in accordance with the observed short gelation time (15 minutes) caused by the better solubility of [CuF(PPh$_3$)$_3$] in organic media in contrast to [CuBr(PPh$_3$)$_3$].[307] Network strand densities decreased to 36 – 45 mol/m^3 (network density: 20 – 25%), employing isomer **34b**, which was referred to the dead ends, consisting of hydroxy groups, unable to conduct the CuAAC crosslinking (Table 7, entries 5 and 6).

Table 7. Calculated network densities based on equation (3) for crosslinking of **34a** or **34b** + **35** (1:1, 4 mmol).

entry	catalyst	T [°C]	PIB-azide	G_N [Pa][a]	$v_{x,max}$ [mol m^{-3}]	$v_{x,exp}$ [mol m^{-3}]	$v_{x,exp}/v_{x,max}$ [%]
1	CuBr	20	**34a**	1 x 10^4	254	4	1.6
2	[CuBr(PPh$_3$)$_3$]	20	**34a**	1.03 x 10^5	254	43	16.9
3	[CuBr(PPh$_3$)$_3$]	20	**34a**	1.13 x 10^5	254	46	18.1
4	[CuF(PPh$_3$)$_3$]	20	**34a**	2.48 x 10^5	254	102	40.2
5	[CuF(PPh$_3$)$_3$]	20	**34b**	8.73 x 10^4	181	36	19.9
6	[CuF(PPh$_3$)$_3$]	10	**34b**	1.07 x 10^5	181	45	24.9
7	[CuF(PPh$_3$)$_3$]	5	**34b**	6.05 x 10^4	181	26	14.4

a) Constant value (= plateau) at ω = 100 Hz.

IR-measurements of the finally obtained networks showed significant reduce up to disappearance of the azide vibration at $v \sim 2100$ cm^{-1} (for entry 2-7 of Table 7), indicating a full conversion of the azide. While the azide vibration for the crosslinking attempt, using CuBr as a catalyst (Table 7, entry 1) was still present, explaining the low network strand density of 1.6%. Determination of the apparent rate constant k' and selected IR-spectra can be found in the appendix 7.7.

3.1.4 Detection of SH-PIB via fluorogenic scratch experiments

The evaluated crosslinking kinetics in the melt promised potential efficiency in the subsequent autonomous SH-approach, applying the benefits from the ca-CuAAC suiting components (**34b**). A sensing agent was designed, which should visualize the healing within the host-material. Successful synthesis of coumarin azide (**36**) was verified via NMR- and IR- analysis and ESI-ToF-MS (for spectra see appendix 7.8). Embedding of SH-components to PDMS and to various blends of PDMS and PIB failed, caused by the rejection of the two different polymer compositions (for experimental details see chapter 4.2.8.1.), thus an alternative was required. Therefore, a high molecular weight PIB ($M_n \sim$ 210 000 g/mol) was used as a matrix material, which was not restricted to mixing limitations. Photographs of the compounding attempts can be found in the appendix 7.9.

Autonomous self-healing within the polymer material was probed via a fluorogenic dye, able to measure the damage induced "click" reaction. The specimen contained the star-shaped picolyl azido telechelic PIB (**34b**, 5 wt%), micron-sized UF-capsules filled with a trivalent alkyne (2,2-bis(prop-2-2-ynyloxymethyl)-1-(prop-2-ynyloxy)butane (**20**), 10 wt%), the Cu(I)-source [(CuBr(PPh$_3$)$_3$], 2 wt%) and the non-fluorescent azido coumarin dye (**36**, 2.5 wt% of **34b**). Scratching the specimen (**37a**) evoked the rupture of the capsules, which in turn released their inner content, inducing the healing reaction upon contact with the Cu(I)-catalyst and the azido components. The fluorescence emission generated in the

subsequent "click"-reaction was measured, emerging from the elongation of the conjugated π-system by the formation of the coumarin-triazole product (see Figure 46 and Figure 47a).
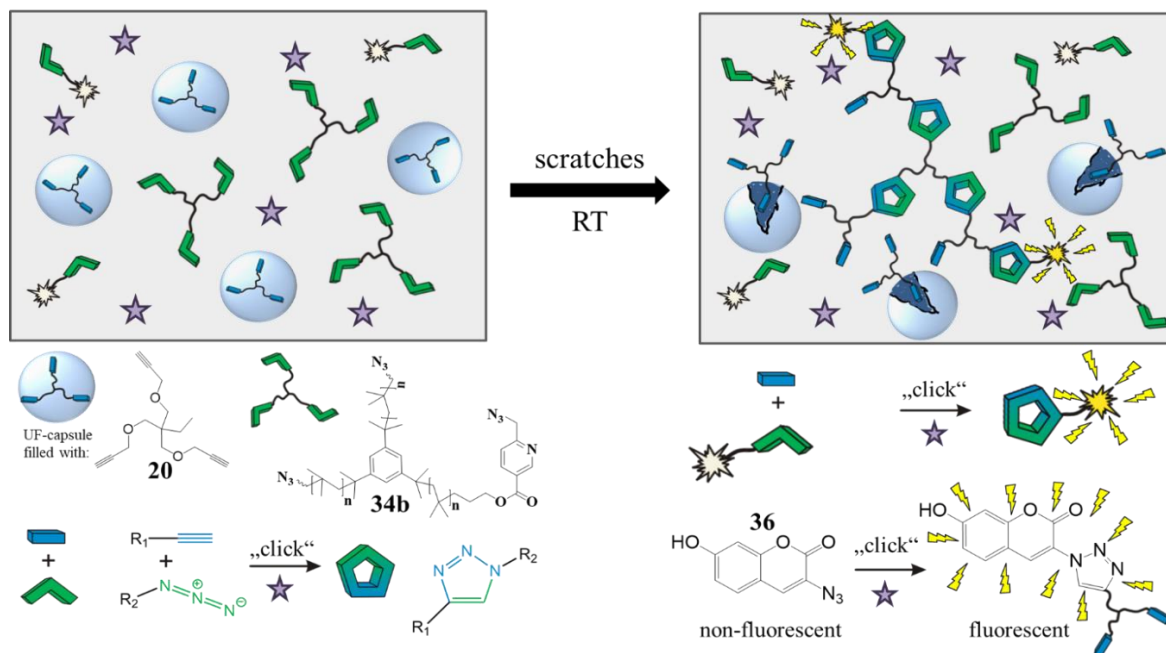
Figure 46. Fluorogenic "click"-reaction within SH-PIB-specimen (**37a**). Star-shaped picolyl azido telechelic PIB (**34b**), UF-capsules filled with the trivalent alkyne (**20**), [CuBr(PPh₃)₃] and the fluorogenic azido coumarin dye (**36**) were incorporated into a high molecular weight PIB matrix. Micron-sized capsule breaking was evoked by scratches, in turn the alkyne-moiety (**20**) was released and thus enabled to undergo "click"-reaction with **34b** and azido coumarin (**36**), leading to the formation of the highly fluorescent triazole-product.

The fluorogenic "click"-reaction was investigated for 24 hours at room temperature, monitoring the *in situ* fluorescence (excitation: 330 nm, emission: 450 nm) (see Figure 47a). The observed increase in the fluorescence intensity was related to the fluorogenic "click"-reaction indicative of the healing, representing the autonomous SH-approach. In turn, the alkyne (**20**) conducted "click" reactions with both, the star-shaped picolyl azido telechelic PIB **34b** and the azido coumarin dye (**36**), which was
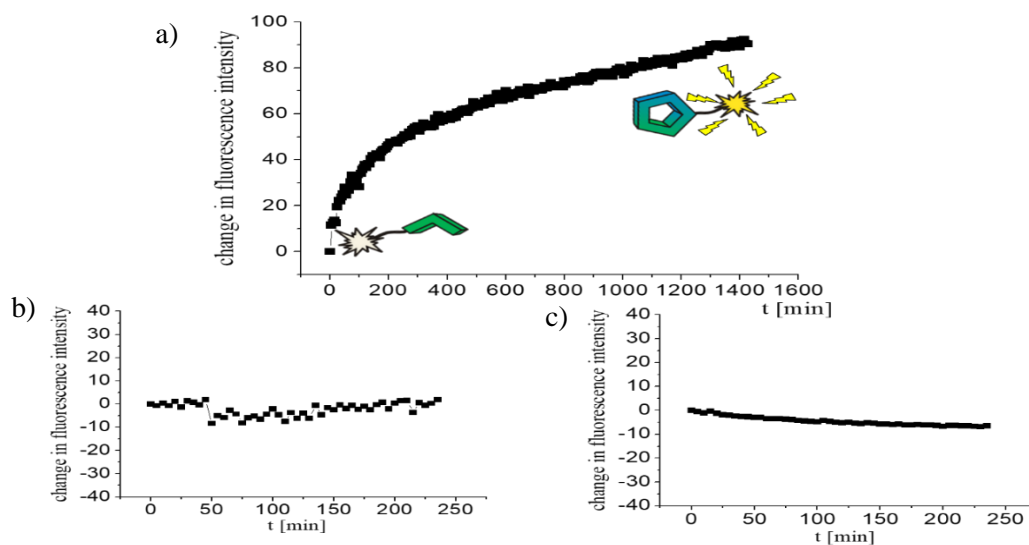
Figure 47. Fluorescence-measurements of a) self-healing-specimen (**37a**), containing star-shaped picolyl azido PIB (**34b**), UF-capsules filled with **20**, [CuBr(PPh₃)₃] and azido coumarin (**36**). Scratching the specimen **37a** with a razor-blade resulted in subsequent change in fluorescence-intensity, measured over a period of 24 hours at room temperature. b) Same specimen (**37a**) in absence of scratches. c) Scratching the specimen without Cu(I)-catalyst (**37b**) led to no change in fluorescence intensity.

visualized by the formation of the fluorogenic coumarin triazole product. In control experiments, missing either the impact of scratches (**37a**) (see Figure 47b) or the Cu(I)-source (**37b**) (see Figure 47c), no increase of fluorescence intensity was observed as a consequence of prevented "click" reactions.

3.2 Design of a capsule-free sensing approach based on mechanocatalysts

The design of an autonomous sensing approach independent of the need of micro-container protection to prevent premature reactions, initiated the development of a mechanocatalyst. The latent catalyst shall be activated just in turn of mechanical impact, providing the chemical response. A very specific design of the mechanocatalyst is required to ensure best force transmission to the most latent bond. Therefore, the labile bond shall be centered between two long polymer chains of equal length. Hence, the beneficial characteristics of RAFT shall be employed to provide large amounts of either PS or P-*n*BuA of at least three different molecular weights, ranging from 2 000 g/mol to 30 000 g/mol. These polymers shall be attached to mechanophoric precursors such as *N*-heterocyclic carbenes (NHC), ideally in a one pot polymerization strategy. Thus, limitations in functionalization of especially long polymer chains can be circumvented, which was commonly observed in previous synthesis strategy, subjecting bromo-functionalized polymer chains to quaternization reactions with *N*-methylimidazole.[48, 302] It was assumed, that the bulkiness of polymer chains longer than 15 000 g/mol were hampering an efficient quaternization, resulting in very low yields of the desired NHC telechelic polymers. Therefore, a new CTA, able to conduct RAFT and to simultaneously introduce the NHC to the polymer chain at once shall be synthesized, potentially enabling the accessibility to high molecular weight mechanocatalysts. In detail, the effect in weakening the labile bond by partially stretching long polymer chains in turn of incoming force, leading to the activation of the mechanocatalyst, is stronger than compared to the effect originated by short polymer chains, according to the TABS-theory implementing the CoGEF method[280-283]. The dissociation energy barrier (typical values for bis(NHC)-Cu-mechanophores range from $D_e = 400 – 900$ pN[48, 283]) in the Morse potential can be lowered, tuning the molecular weight of the polymer handles attached to the mechanocatalyst, which in turn can improve the bond-scission efficiency and thus the activity of the catalyst. Finally, a Cu(I)-source shall be enclosed by polymeric NHC-ligands, delivering a system, which can be activated by incoming external stress. The compression induced scission of the latent catalyst into the active monocarbene-Cu(I)-species shall start the fluorogenic "click" reaction of phenylacetylene and coumarin azide within a host-material, proving its potential application as an autonomous sensing approach.

3.2.1 Synthesis and characterization of chain-transfer agents (CTAs) (40, 43, 44, 46)

A CTA going to be used to conduct RAFT, acting as a radical control agent by establishing the equilibrium between dormant and active species, can be composed of four different classes of substances such as dithiobenzoate, dithiocarbamate, xanthogenate and trithiocarbonate. In this thesis imidazolium modified trithiocarbonates were selected as CTA, since they open the opportunity to simultaneously conduct RAFT polymerization and to introduce the mechanophoric precursor at once. Thus, a new attempt to synthesize CTA-imidazolium as ionic liquid (IL) was probed (see Figure 48), while methyl-imidazolium was in the first instance treated with 11-bromo-undecanol, introducing the ionic-liquid character located at the nitrogen-atom of **38**, being confirmed via assignment of all signals in ¹H-NMR-spectra. The introduced chlorine was exchanged with bis(trifluoromethane)sulfonimide anion in the next step, initiating the reversal of the solubility behavior of **39**. Thus, excess of water-soluble **38** was removed by water extraction of the organic phase, containing the mixture of the desired product (**39**) and **38**. The thio-bromo "click" reaction in the last step provided the CTA-imidazole (**40**), according to NMR-spectrum and ESI-ToF-MS in a yield of 96%.
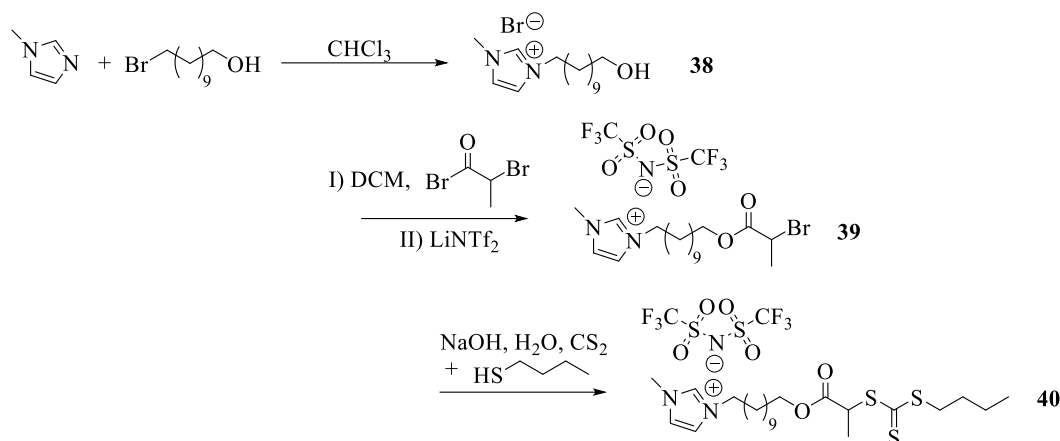
Figure 48. Synthesis route to obtain CTA-imidazole (**40**).

In ¹H-NMR-spectrum the introduction of the butyl trithiocarbonate group was verified by the appearing signal at $\delta = 3.35$ ppm, belonging to the methylene group next to the trithiocarbonate (see Figure 49a), being validated in ¹³C-NMR spectrum by the signal at $\delta = 222.1$ ppm, corresponding to the thiocarbonyl group (see Figure 49b). The presence of the imidazolium-unit was proved by the signals at $\delta = 8.79$ ppm, $\delta = 7.29$ ppm and $\delta = 7.27$ ppm, matching with their total integral of three to the corresponding structural elements. The successful implementation of the bis(trifluoromethane)sulfonimide anion was detected in ¹³C-NMR spectrum by the apparent quartette at $\delta = 124.6 - 115.0$ ppm. Coupling of the appropriate ¹³carbon atom with its three adjacent ¹⁹fluoro atoms caused the splitting of this resonance into a quartet. ESI-ToF-MS verified both, the cationic and anionic structure (spectra can be found in the appendix 7.10). In positive mode the peak maximum at 473.230 g/mol was assigned to the desired cationic structure, fitting well with its simulation of 473.232 g/mol (error: 4 ppm) ($[M]^+$ $C_{23}H_{41}N_2O_2S_3^+$). The in the negative mode apparent peak at 280.014 g/mol was assigned to the bis(trifluoromethane)sulfonimide anion, matching well with its simulation of 279.918 g/mol (error: 343 ppm) ($[NTf_2]^-$ $C_2F_6NO_4S_2^-$).
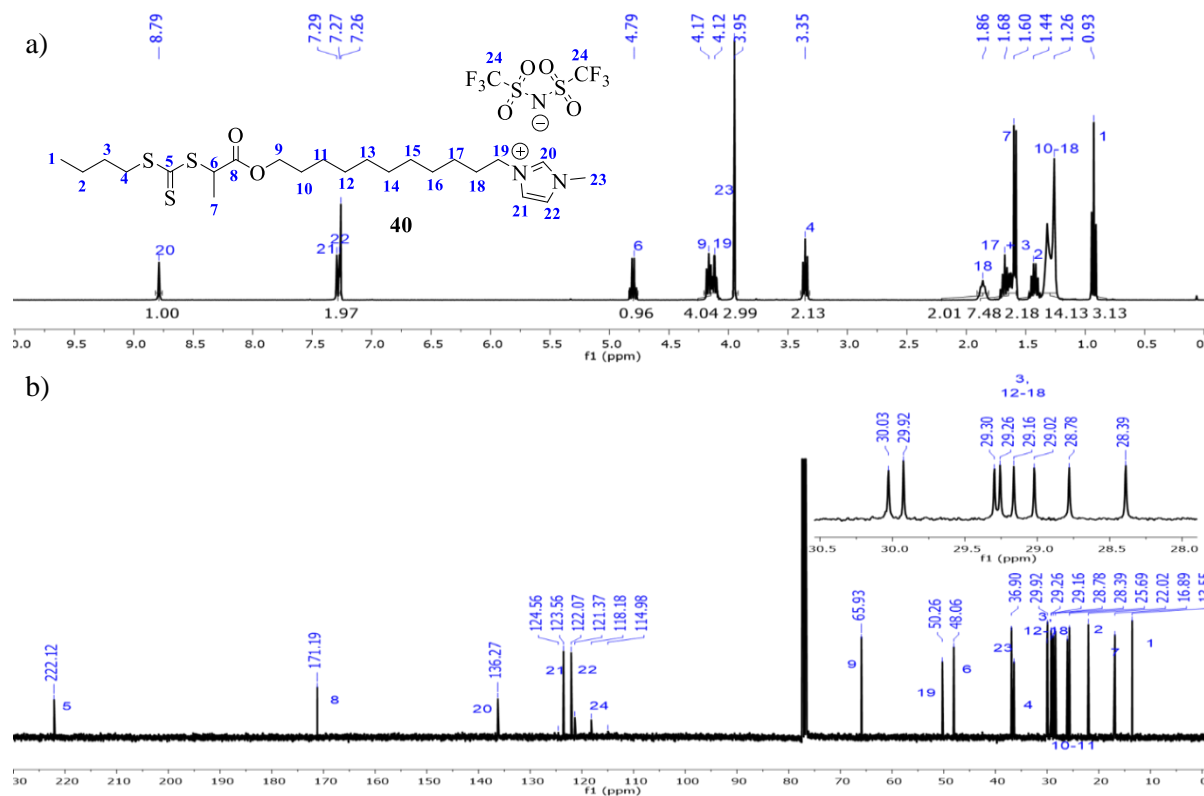
Figure 49. a) ¹H-NMR spectrum of **40** in C*D*Cl₃; b) ¹³C-NMR spectrum with superimposed area (right corner) of **40** in C*D*Cl₃.

Previous synthesis strategy started with the treatment of methyl-imidazolium with chloro-propanol, followed by the addition of a tertiary bromide acid, leading to an incomplete conversion in the following thiol-bromo "click" reaction (see Figure 50). Thus, CTA-IL (**43**) contained also after purification with column-chromatography starting material **42**, according to ^{1}H-NMR-spectra of up to 30% and was not used further within this work. For experimental spectra see appendix 7.10.
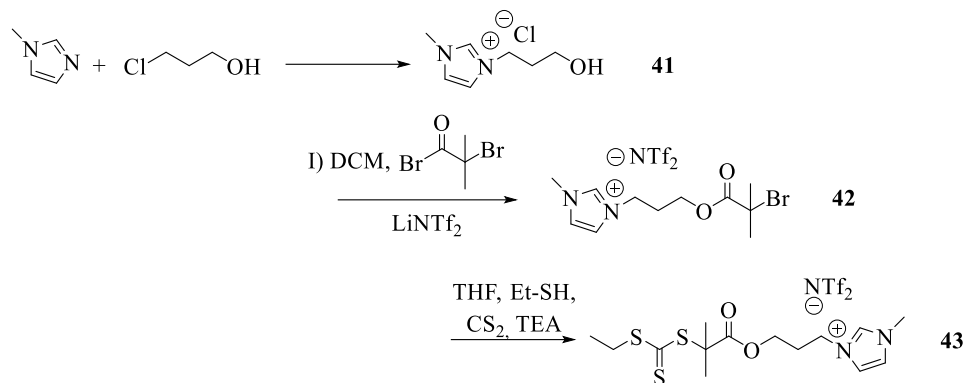
Figure 50. Synthesis attempt to obtain CTA-IL (**43**).

In turn, a new synthesis strategy was required, leading to the conduction of test experiments, investigating the influence of the chain-length attached to the trithiocarbonate-group and the substitution grade of the carbon atom linked to the bromo position upon efficiency in conversion. Thus, both ethyl (see Figure 51a and Figure 51b) and butyl mercaptan (see Figure 51c and Figure 51d) were converted either with secondary or tertiary acid bromides.
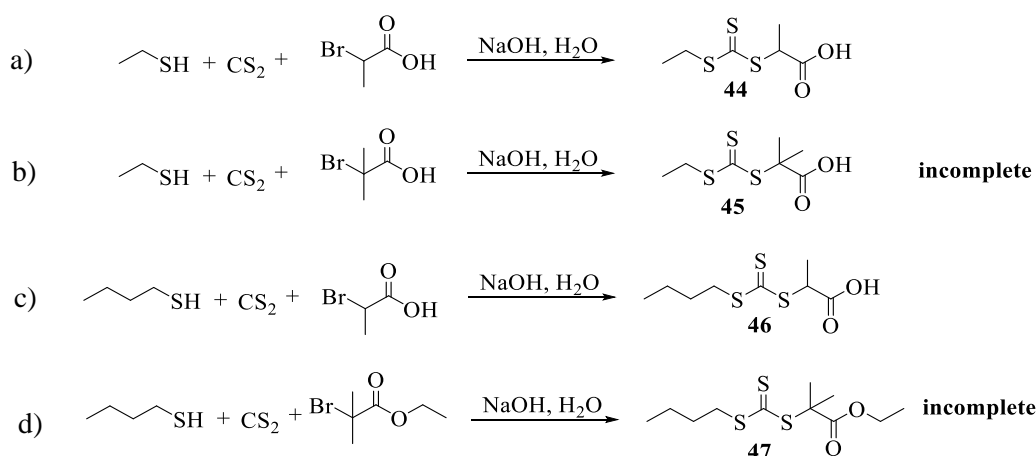
Figure 51. Investigation of influence of the chain-length of the thiol-component and substitution grade of the acid reactant to the outcome in subsequent thiol-bromo "click" reaction. a) Successful conversion of ethyl-thiol + secondary bromide; b) incomplete conversion of ethyl-thiol + tertiary bromide; c) successful conversion of butyl-thiol + secondary bromide; d) incomplete conversion of butyl-thiol + tertiary bromide.

Control-experiments indicated an insignificant influence of the chain-length, but a substantial outcome to the completion of the thiol-bromo "click" reaction originated by the substitution grade of the carbon atom. Consequently, only the attempts, applying secondary bromo-components, afforded pure ethyl-CTA (**44**) and butyl-CTA (**46**), evidenced by ^{13}C-NMR-spectra, assigning all the appearing signals to the corresponding structures (see appendix 7.10). In contrast, test experiments, applying the tertiary bromide acids instead, resulted in incomplete conversions (**45** and **47**) as a consequence of the limited accessibility of the bromo group in the subsequent "click" reaction (see Figure 51b and 51d). Complete analysis screening of **40** – **47** can be found in the appendix 7.10.

3.2.2 Synthesis and characterization of RAFT-PS (48, 49a-m)

The RAFT- technique, counting to the controlled radical polymerization methods, was applied to provide polymers of similar molecular weights (low PDI) as a consequence of the introduced equilibrium between dormant and active radical species.[312] The essential equilibrium is established by the addition of a CTA such as trithiocarbonate components, reducing the reactive radical species originated by the use of initiators as 2,2′-azobis(2-methylpropionitrile) (AIBN) (see Figure 52a). A couple of vinyl-monomers, including styrene are capable of auto-initiation at elevated temperatures (~ 120 °C)[313-314], starting with the Diels-Alder-cycloaddition, followed by re-aromatization and subsequent formation of the initiating radical-species (see Figure 52b).
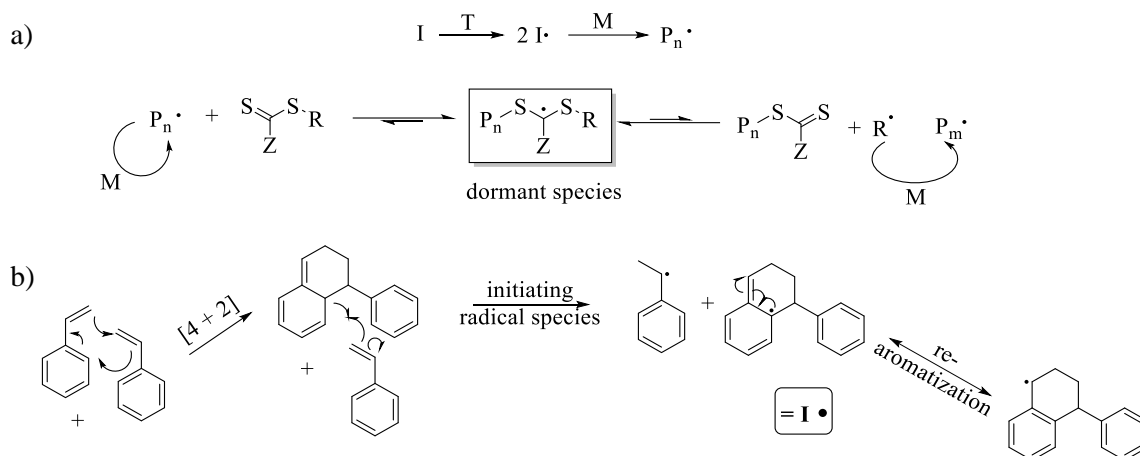
Figure 52. a) General mechanism of RAFT polymerization, starting with the origination of radicals by thermal decomposition of the radical initiator (I) in initiator radical (I·). Followed by monomer (M) polymerization, resulting in growing polymer chain (P$_n$·), controlled by the CTA (trithiocarbonate). The established equilibrium is shifted to the dormant species, reducing the active radical species P$_n$·, (left sided) or R· (right sided). b) Probable mechanism of auto-initiation of styrene: at elevated T (~ 120 °C) two styrene monomers can undergo [4+2] cycloaddition (Diels-Alder reaction), forming the first radicals under involvement of a third monomer. The dimeric structure is providing the initiating species (I·) after re-aromatization process, qualified to start the RAFT-polymerization in absence of initiator and solvent.

Therefore, in bulk polymerization the addition and subsequent removal of an external initiator and a solvent is no longer required, facilitating the purification of the polymer. In order to establish the optimal force transmission of mechanical impact to the latent bond, forwarded by the polymeric backbone, the influence of its rigidity to the scission efficiency of the latent bond was investigated. The rigidity of the backbone was varied by either employing two different composition of polymers (see also chapter 3.2.3) and by synthesizing at least three different molecular weights of each polymer. CTA-imidazole (**40**) was added to mediate the RAFT polymerization and to introduce simultaneously the NHC-moiety as end group, according to the literature.[315-317] A bunch of different PS (**49a** – **m**), varying in their molecular weights of 3 000 g/mol – 42 000 g/mol, were afforded, adjusting the ratio between CTA-imidazole (**40**) and the amount of styrene (see Figure 53b and Table 8). The PDI-values were in the scope of 1.07 – 1.23, confirming, in combination with the detected linear chain-growth of the polymers, the livingness of the performed polymerizations. Separation of the products from excess of monomer was achieved by precipitation in ice-cold MeOH, allowing to get rid of CTA-imidazole (**40**) additionally. The polymerization was in the first instance accomplished in toluene and in presence of AIBN as initiator at 80 °C, providing PS (e.g., **49a**) of low yields $\eta = 5 – 14\%$ (see Table 8A, entry 2). The mismatch of the calculated molecular weight from NMR (20 400 g/mol) and from GPC (10 900 g/mol) indicated incomplete conversions.
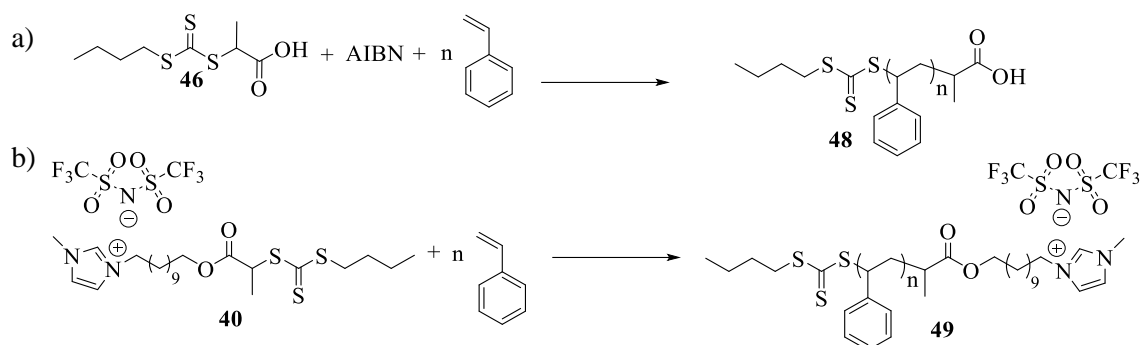
Figure 53. RAFT-polymerization of styrene to afford PS with a) –COOH (**48**) as end group and b) -imidazole (**49**) as end group.

Likewise, moderate results were observed, when CTA-imidazole (**40**) was changed to CTA-COOH (**46**), providing PS (**48**) (see Figure 53a and Table 8A, entry 1). Therefore, the conditions were changed, e.g. when polar solvents such as acetonitrile and dioxane were applied instead of nonpolar toluene (see Table 8A, entry 3 and 4) the miss-match of the molecular weights determined by NMR and GPC for PS (**49b** – **49c**) was fixed and the yields increased up to $\eta = 32$ % (see Table 8A, entry 4). Consequently, the removal of the solvent and AIBN, employing the bulk-polymerization (T = 120 °C) completed the search for optimal RAFT-conditions, affording the desired good yields of $\eta = 67 - 73$ % for PS (**49d** – **49f**) (see Table 8B, entry 5 – 7).[315] Among all synthesized PS, three of different molecular weight (**49d** = 5 900 g/mol, **49e** = 11 500 g/mol and **49f** = 25 300 g/mol) were chosen for further investigations. Detailed information of the remaining PS (**49g** – **49m**) can be found in the chapter 4.3.2 and the appendix 7.11.

Table 8. Synthesis details of selected RAFT-polymerization of styrene.

entry	polymer	CTA	$M_{n(GPC)}$[a] [g/mol]	$M_{n(NMR)}$[b] [g/mol]	PDI	solvent	T [°C]	yield [%]
A)	**RAFT-polymerization using AIBN for initiation in solution**							
1	**48**	**46**	3 000[c]	4 200[d]	1.23	toluene	80	6
2	**49a**	**40**	10 900	20 400	1.24	toluene	80	13
3	**49b**	**40**	4 000	4 500	1.16	MeCN	80	23
4	**49c**	**40**	11 400	14 500	1.16	dioxane	80	32
B)	**RAFT-polymerization conducted in bulk in absence of AIBN**							
5	**49d**	**40**	5 900	6 000	1.07	/	120	70
6	**49e**	**40**	11 500	11 100	1.17	/	120	67
7	**49f**	**40**	25 300	26 000	1.15	/	120	68

a) GPC-measurements were performed in HPLC-grade DMF with the addition of LiNTf$_2$ ($c = 10.0$ mM) and molecular weight was determined by calibration with external PS-standards ($M_P \sim 1\,000 - 115\,000$ g/mol) and detection of refractive-index. b) Calculated by the ratio of initiator at $\delta = 3.28$ ppm and repetitive unit at $\delta = 7.24 - 6.32$ ppm. c) GPC-measurements were performed in HPLC-grade THF and molecular weight was determined by calibration with external PS-standards ($M_P \sim 1\,000 - 115\,000$ g/mol) and detection of refractive-index. d) Calculated by the ratio of initiator at $\delta = 3.26$ ppm and repetitive unit at $\delta = 7.24 - 6.32$ ppm.

PS (**48** and **49**) were characterized by GPC- and NMR- analysis, ESI-ToF-MS and MALDI-ToF-MS. For **48** the attachment of the trithiocarbonate group from the initiator part and COOH as head-group was confirmed in MALDI-ToF-MS, detecting two different species with a distance of 104 g/mol each, corresponding to styrene as the repetitive unit of the polymeric backbone (see Figure 54a-b). The absolute maximum was detected at 5171.477 g/mol, belonging to the desired structure with potassium

as cation, fitting well with the simulation of 5171.933 g/mol (error: 88 ppm) ([M+K]$^+$ (C$_8$H$_8$)$_{47}$C$_8$H$_{14}$O$_2$S$_3$K$^+$) (see Figure 54c). The second series could be identified as the carboxylic PS (**48**) with two additional potassium cations, caused by an additional exchange of one proton versus potassium, leading to a peak maximum at 5209.511 g/mol, matching well with the simulation of 5209.899 g/mol (error: 73 ppm) ([M-H+2K]$^+$ (C$_8$H$_8$)$_{47}$C$_8$H$_{13}$O$_2$S$_3$K$_2^+$) (see Figure 54c).
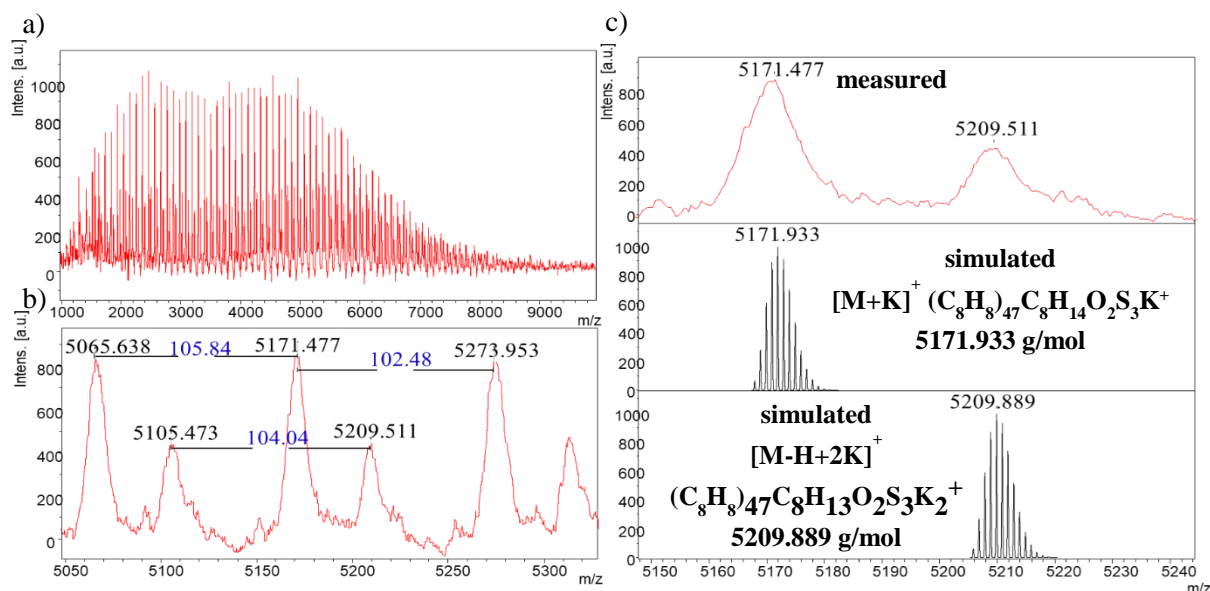
Figure 54. MALDI-ToF-MS of PS-COOH (**48**). a) Full spectrum of **48**, showing two series. b) Superimposed area of spectrum of **34**, showing distance between peaks of both series of 104 g/mol. c) Measured peaks and their simulated isotopic pattern, belonging to the displayed structures.

^{1}H-NMR-analysis verified the complete structure of PS-COOH (**48**) by assigning all signals to the apparent composition of the polymer (^{1}H-NMR-spectrum can be found in the appendix 7.11). In NMR-spectra of **49** singlets at δ = 8.85, 7.56, 7.52 and 3.92 ppm can be assigned to the successful introduction of the imidazole ligand and thus, the presence of the potential mechanophoric precursor unit (see Figure 55a). NMR signals of the polystyrene-backbone can be found at δ = 7.24 – 6.32 ppm, corresponding to the aromatic unit of the polymer and as an additional multiplet at δ = 2.44 − 1.18 ppm, belonging to the aliphatic part of the repetitive unit. ESI-ToF-MS of **49d** proved the attachment of the complete initiator part to the polymeric structure (see Figure 55b-c). The absolute maximum at 2556.284 g/mol of the main series could be assigned to the cationic part of the polymer, fitting well with the simulation of 2556.490 g/mol (error: 81 ppm) ([M]$^+$ (C$_8$H$_8$)$_{20}$C$_{23}$H$_{41}$N$_2$O$_2$S$_3^+$) (see Figure 55c). Matching of both isotopic pattern proved the correlation of the measured and simulated spectra. The apparent difference in the molecular weight determined by GPC/NMR (M_n ~ 6 000 g/mol, see Table 8B, entry 5) with the one displayed in ESI-ToF-MS (M_n ~ 2 600 g/mol, see Figure 55) of **49d** resulted from detection limitations in ESI-ToF-MS-analysis. Thus, MALDI-ToF-measurements were applied for high molecular weight PS, providing the compliance in measured and calculated molecular weights, but missing the isotopic pattern resolution instead. The minor series in ESI-ToF-MS remained unidentified (see Figure 55b), being repeatedly observed for all MALDI-ToF-MS and ESI-ToF-MS of PS-NHCs (**49a -49m**). Selected spectra for the components can be found in the appendix 7.11.
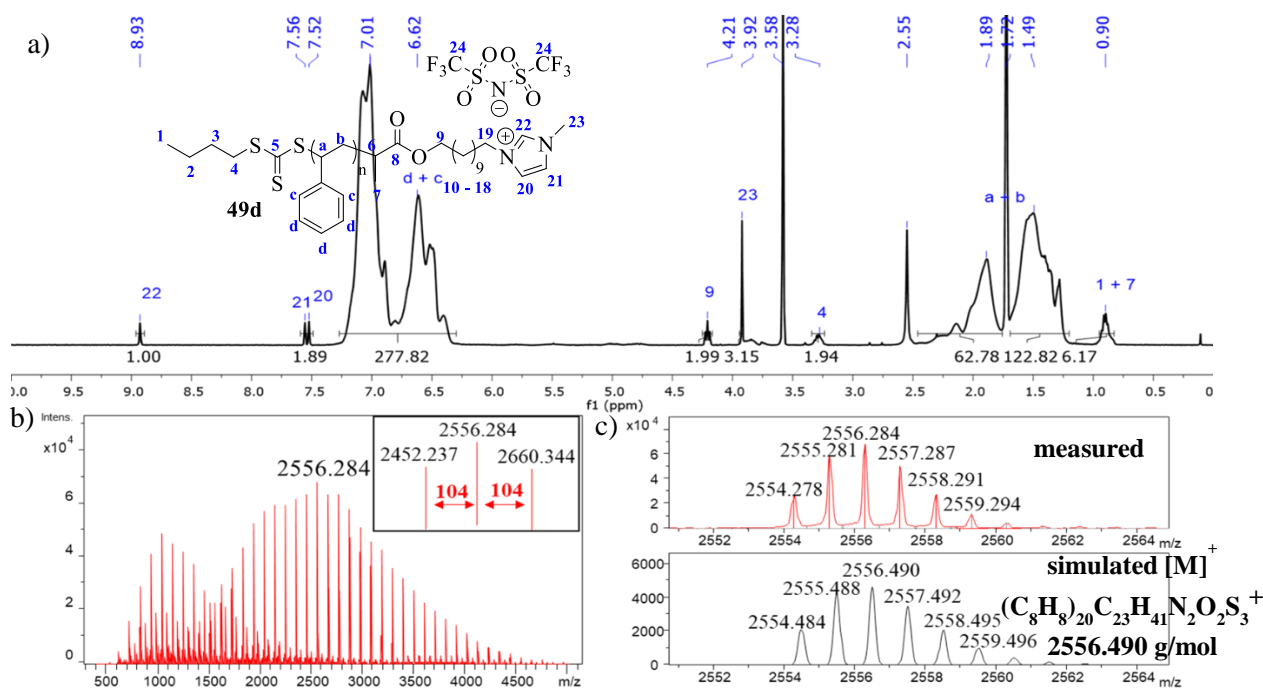
Figure 55. Characterization of PS-NHC (**49d**). a) ^{1}H-NMR spectrum of **49d** in THF-d_8. b) Full ESI-ToF-MS of **36d**, showing three series and a distance of 104 g/mol, belonging to the repetitive unit of PS. c) Measured peaks (top) and their simulated isotopic pattern (bottom), belonging to the displayed structure.

3.2.3 Synthesis and characterization of RAFT-P-*n*BuA (50, 51a-j)

The rigidity of the polymeric backbone was also varied, polymerizing a second monomer such as *n*-butyl acrylate, providing P-*n*BuA of lower glass transition-temperature ($T_g \sim 219$K) compared to poly(styrene), possessing an approximated $T_g \sim 373$ K. RAFT-polymerization was carried out, applying either CTA-COOH (**46**) to conduct a control-polymerization (see Figure 56a) or CTA-imidazole (**40**), allowing for the simultaneous introduction of the mechanophoric precursor (see Figure 56b).
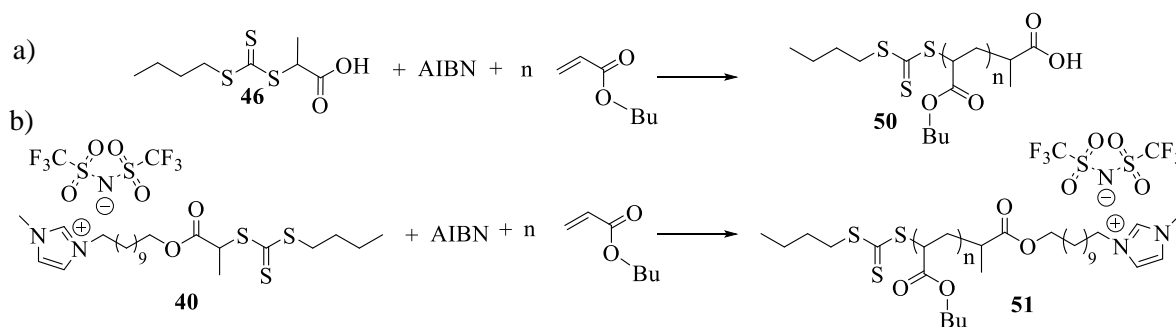
Figure 56. RAFT-polymerization of *n*-butyl acrylate to afford P-*n*BuA with a) –COOH (**50**) as end group or b) -imidazole (**51**) as end group.

In the first instance, RAFT-polymerization was conducted in toluene, according to previous experiments in our own working group.[316] Contrary to literature results, P-*n*BuA (**51a**) of a low yield $\eta \sim 10\%$ and a moderate PDI-value of 1.6 was afforded (see Table 9A, entry 2), which was attributed to the different composition of the CTAs. Thus, more polar solvents such as acetonitrile and dioxane were exploited, increasing the yields of P-*n*BuA (**51b-c**) up to 41%, decreasing the obtained PDI-values (1.35 – 1.48), but still missing a perfect match of molecular weight determined via GPC and calculated by NMR (molecular weight difference = 3 500 – 4 000 g/mol) (see Table 9A, entry 3 and 4). Performing the RAFT-polymerization in DMF resulted in P-*n*BuA (**50**, **51d-f**) with low PDI-values of 1.21 – 1.30, good conformity of the determined molecular weights by NMR and GPC and very high yields in the range of

$\eta = 66 - 93\%$ (see Table 9A, entry 1, 5, 6 and 7). In order to synthesize at least three different molecular weights, the ratio of CTA:M (10:500, 10:1 000, 10:2 000) was varied, accomplishing P-nBuA of molecular weights in between 12 700 – 37 100 g/mol, still missing thus the low-molecular weight polymers. Accordingly, bulk polymerization of n-butyl acrylate at 120 °C[318] was tested, avoiding the requirement of a solvent or the addition of AIBN (see Table 9B, entry 8 and 9), finally affording the desired low-molecular weight P-nBuA (**51h**) (M_n = 2 300 g/mol) in a moderate yield of 42% and a very good PDI value of 1.13 (see Table 9B, entry 9). Experimental data of the remaining P-nBuA (**51i-j**) can be found in chapter 4.3.2 and the appendix 7.12.

Table 9. Synthesis details of RAFT-polymerization of n-butyl acrylate.

entry	polymer	CTA	$M_{n(GPC)}$[a] [g/mol]	$M_{n(NMR)}$[b] [g/mol]	PDI	solvent	T [°C]	yield [%]
A)	**RAFT-polymerization using AIBN for initiation in solution**							
1	**50**	**46**	12 700[c]	13 500[d]	1.19	DMF	65	91
2	**51a**	**40**	9 600	13 700	1.62	toluene	70	10
3	**51b**	**40**	12 100	14 600	1.35	MeCN	80	41
4	**51c**	**40**	11 200	15 300	1.48	dioxane	80	25
5	**51d**	**40**	13 400	13 900	1.21	DMF	65	80
6	**51e**	**40**	21 800	23 800	1.23	DMF	65	66
7	**51f**	**40**	25 600	24 400	1.30	DMF	65	93
B)	**RAFT-polymerization conducted in bulk in absence of AIBN**							
8	**51g**	**40**	16 000	16 900	1.15	/	120	51
9	**51h**	**40**	2 300	2 100	1.13	/	120	42

a) GPC-measurements were performed in HPLC-grade DMF with the addition of LiNTf$_2$ (c = 10.0 mM) and molecular weight was determined by calibration with external PBMA-standards ($M_P \sim 0.8$ kg mol^{-1} – 111 kg mol^{-1}) and detection of the refractive-index. b) Calculated by the ratio of the methylene-group of the initiator at δ = 3.39 ppm and repetitive unit at δ = 4.12 – 3.94 ppm, of which the integral-value of 2 was subtracted, due to overlay with methylene-group of initiator-part. c) GPC-measurements were performed in HPLC-grade THF and molecular weight was determined by calibration with external PBMA-standards ($M_P \sim 0.8$ kg mol^{-1} – 111 kg mol^{-1}) and detection of the refractive-index. d) Calculated by the ratio of the methylene-group of the initiator at δ = 3.34 ppm and the repetitive unit at δ = 4.16 – 3.83 ppm.

Polymers were characterized by MALDI-ToF-MS, GPC- and NMR- analysis. All parts of the chain transfer agent and the polymeric backbone can be assigned in NMR-spectrum (see Figure 57a): beside the signals, belonging to the imidazolium unit (for discussion see chapter 3.2.2), the remaining CTA-part was assigned to the multiplet at δ = 4.85 ppm and the two apparent triplets at δ = 4.21 ppm and at δ = 3.39 ppm. Signals of the repetitive unit composed of n-butyl acrylate were found as multiplets at δ = 4.04 ppm, corresponding to the methylene group in adjacency of the carboxylic ester moiety and at δ = 0.95 ppm, belonging to the terminally methyl group and the abundant multiplets between δ = 2.40 – 1.24 ppm of the remaining backbone. The complete proof of the structure (e.g. for **51h**) was verified in MALDI-ToF-MS, detecting one series with its absolute maximum at 2011.391 g/mol, fitting well with the simulation of 2011.241 g/mol (error: 75 ppm) and its isotopic pattern ([M]$^+$ for (C$_7$H$_{12}$O$_2$)$_{12}$C$_{23}$H$_{41}$N$_2$O$_2$S$_3$$^+$) (see Figure 57b-c). The measured molecular weight ($M_n \sim 2$ 000 g/mol) was matching well compared with these one obtained via GPC- and NMR- measurement ($M_n \sim 2$ 200 g/mol). The distance of 128 g/mol of each peak was assigned to the repetitive unit, belonging to n-butyl acrylate (see Figure 57b). Selected spectra for the remaining P-nBuA (**51a-j**), including P-nBuA-COOH (**50**), can be found in the appendix 7.12.
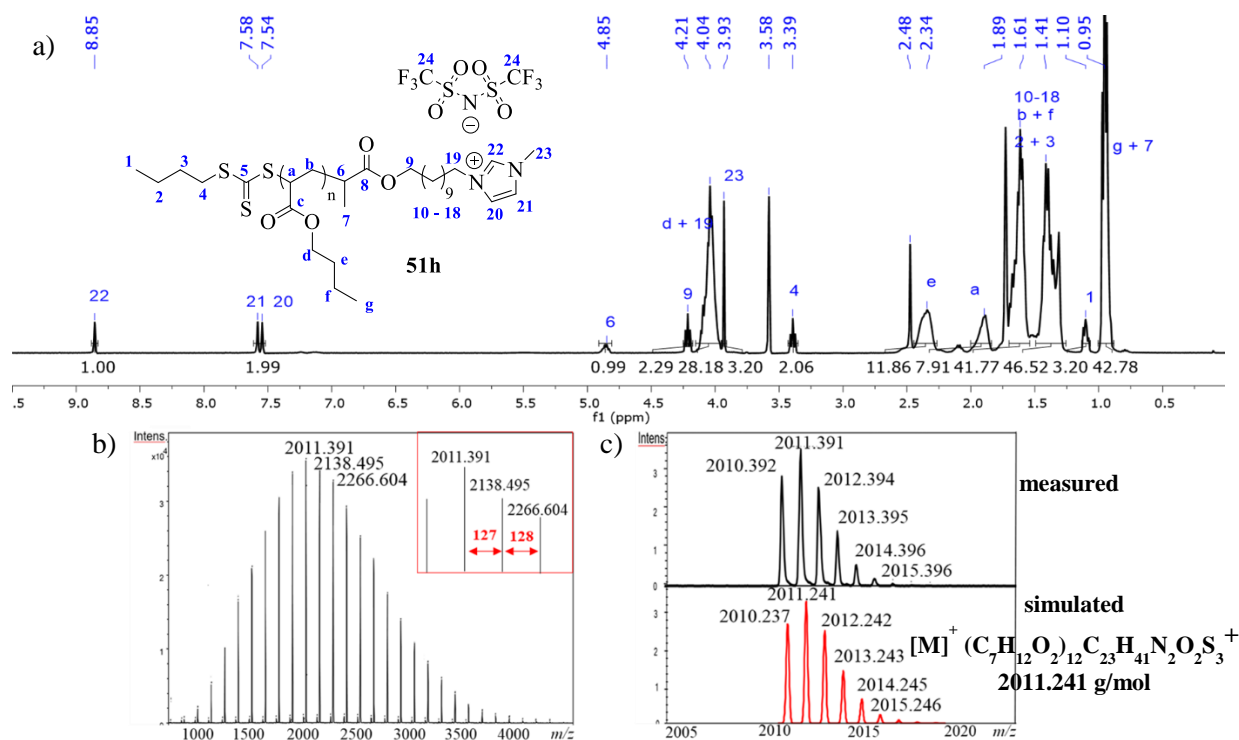
Figure 57. Characterization of P-*n*BuA-NHC (**51h**). a) ^{1}H-NMR spectrum of **51h** in THF-*d$_8$*; b) Full MALDI-ToF-MS of **51h**, showing one series. Superimposed area showing a distance of peaks of 128 g/mol, corresponding to the repetitive unit of *n*-butyl acrylate. c) Measured peak (top) and its simulated isotopic pattern (bottom), belonging to the displayed structure.

3.2.4 Synthesis and characterization of PS-mechanocatalysts (52a-f)

The synthesized PS (**49d-f**) and P-*n*BuA (**51d, 37f, 37h**) of different molecular weights each were now applied as precursors to afford mechanocatalysts, able to conduct the CuAAC reactions. The following polymers were subjected to the subsequent transformation (see Figure 58), starting with low-molecular PS (**49d**) of 5 900 g/mol and P-*n*BuA (**49h**) of 2 300 g/mol, slightly increased by 5 000 – 10 000 g/mol in case of PS (**49e**) (M_n ~ 11 500 g/mol) and P-*n*BuA (**51d**) (M_n ~ 13 400 g/mol) and being stopped by additional 10 000 g/mol for PS (**51f**) (M_n ~ 25 300 g/mol) and P-*n*BuA (**51f**) (M_n ~ 25 600 g/mol).
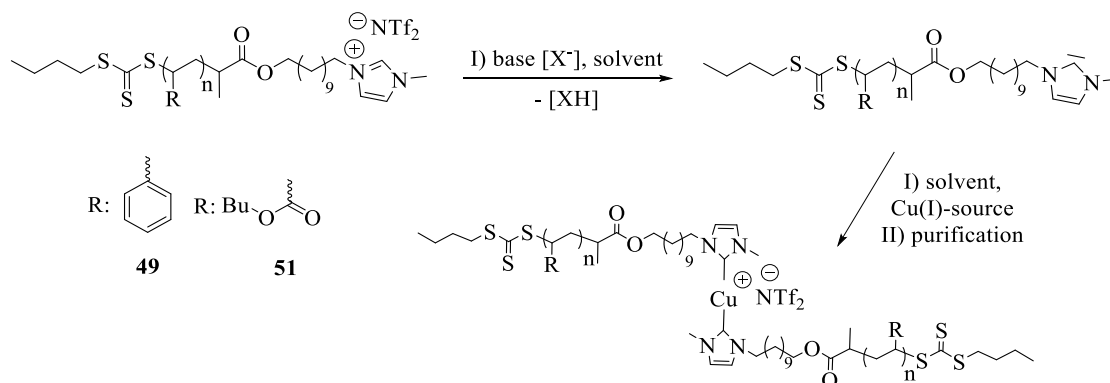
Figure 58. Synthesis attempts to form the Cu(I)-mechanocatalyst by deprotonating the imidazole and adding the Cu(I)-source to build the desired biscarbene structure.

Synthetic strategy started with deprotonation of the proton in between the two nitrogen atoms of the imidazolium-unit by addition of a base in accordance with literature.[48] A complete deprotonation (pK_a (in water) of NHC-polymer = 19 – 23)[319-321], without affecting the polymeric backbone nor the carboxylic-ester group, connecting the polymer-chain with the NHC unit, was crucial, thus applying either sodium *tert*-butoxide (NaO^{t}Bu) (pK_a (in water) = 19)[322] or potassium 1,1,1-trimethyl-*N*-

(trimethylsilyl)silanaminide (KHMDS) (p$K_{a\text{ (in water)}}$ = 26)[323]. Both belong to the class of non-nucleophilic bases, but differ in their corresponding pK_a-values and were known to minimalize disturbing side-reactions towards mechanophore synthesis of NHC telechelic PIB, pTHF and PS precursor[302]. It was shown, that a not adequate combination of the polymer and the base can lead to decomposition of the formed biscarbene structure or the elimination of *N*-methylimidazole, leaving an external double bond at the end of the polymer. In case of PS-NHC this was minimal for NaO^{t}Bu, being the major choice within this work. Secondly, by the addition of [Cu(MeCN)$_4$]PF$_6$ the Cu(I)-catalyst was located in the center of the two polymer-arms tied by the carbene bond as NHC-Cu-NHC mechanocatalyst. The formation of the mechanophore unit was controlled by *in situ* GPC measurements by doubling of the molecular weight and confirmed by NMR-measurements, displaying the shift of NC*HCH*N protons attached to the imidazole-ring.

In case of PS efficient transformation was accomplished in MeCN, verified by doubling of the molecular weight in GPC and the disappearance of NC*H*N resonance at δ = 8.93 ppm and the shift of NC*HCH*N resonances from δ = 7.56 – 7.52 ppm to δ = 6.25 – 6.22 ppm. Same experiments conducted in THF, toluene and mixtures were preventing the formation of the biscarbene structure, according to GPC and NMR (no doubling in molecular weight and no shift of protons). Furthermore, polymers (PS) of up to 6 000 g/mol were completely dissolved in MeCN, while longer chains remained as solidified particles in the solution, thus forming a suspension. The dissolving power of non-polar PS decreased with increasing chain length in pure MeCN, preventing a complete transformation of NHC telechelic PS to bis(NHC)-Cu(I)-mechanocatalyst. When added a few µL of THF or toluene, in order to re-establish a pure solution to increase transformation efficiency, the formation of the biscarbene structure was disturbed immediately (according to GPC and NMR). In turn, PS mechanophore synthesis was conducted in pure and anhydrous MeCN, providing mixtures of the desired bis-NHC structure and of the unreacted NHC telechelic precursor in different ratios. Especially for the highest molecular weight of PS-NHC (**49f**) with 25 300 g/mol and thus a low dissolving amount in MeCN, the formed biscarbene content was low (approximately 23%), while for the lower molecular weights (**49d-f**) (5 900 – 11 500 g/mol) 55 – 77% biscarbene was formed. In order to separate the precursor from the desired mechanocatalyst substantial purification was attempted. Separation by preparative GPC was the only purification method, providing mechanophores (**52a-c**) of high purity for 12 000 g/mol (**52a**) (see Figure 59a), 23 000 g/mol (**52b**) (see Figure 59b) and 50 500 g/mol (**52c**) (see Figure 59c) in very low isolated
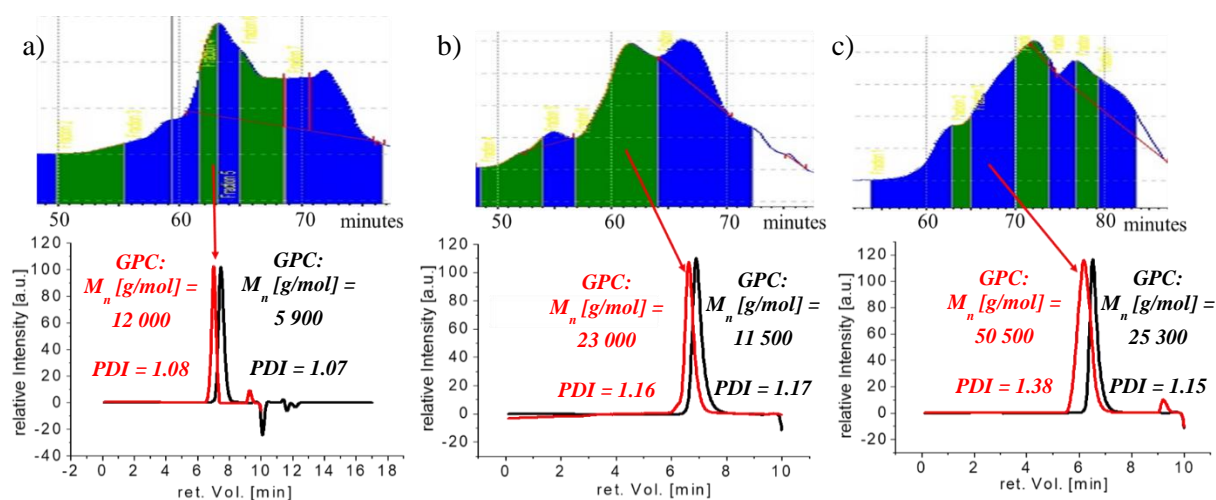
Figure 59. Preparative GPC was conducted in pure HPLC-grade DMF, while analytical GPC was conducted in HPLC-grade DMF with the addition of LiNTf$_2$ (c = 10.0 mM) and molecular weights were determined by calibration with external PS-standards (M_P ~ 1 000 – 115 000 g/mol) and detection of the refractive-index. a) Preparative GPC of **52a** (top) and analytical GPC (bottom) of **52a** (red) and **49d** (black). b) Preparative GPC of **52b** (top) and analytical GPC (bottom) of **52b** (red) and **49e** (black). c) Preparative GPC of **52c** (top) and analytical GPC (bottom) of **52c** (red) and **49f** (black).

yields of 4 – 7%. This was caused by the experimental issues of the preparative GPC, requiring high temperatures (55 °C) and high pressures (> 10 bar) to ensure proper eluent flow during the purification procedure (preparative GPC, DMF as a solvent). The longer the polymer mixture was exposed to these conditions the more the ratio of the molecular weight distribution was shifted to the single polymer chain structure (= precursor), detected via strong shift from the high molecular weight peak to the low molecular weight one with increasing time (complete disappearing of the doubled molecular weight peak within three hours was observed at these conditions). When the eluent solvent was changed from DMF to THF, in turn allowing more moderate conditions, an immediate decomposition of the bis-NHC-structure appeared, visualized by the greenish discoloration of the solution and verified by NMR- and GPC-measurements. Other purification attempts such as precipitation in $CHCl_3$ or MeOH as well as column-chromatography (either Al_2O_3, silica or diatomaceous earth) remained insufficient. Most frequently the biscarbene proof in NMR disappeared (e.g., applying column-chromatography), indicating the unsteady composition of the mechanocatalyst with its fragile core. Only the precipitation of mechanocatalyst mixtures in acetonitrile was removing the excess of the base and the $[Cu(MeCN)_4]PF_6$ without decomposing the biscarbene structure. Thus, mixtures of bis-NHC-Cu(I)-mechanocatalyst and NHC telechelic PS precursor (**52d-f**) in different ratios (23 – 76% biscarbene content) for three different molecular weights (10 100 – 38 700 g/mol) were afforded (see Table 10B). The experimental proof can be found in the appendix 7.13. In total six different mechanocatalysts were synthesized for PS, subdivided in pure ones (**52a-c**), obtained by preparative GPC in low amounts (see Table 10A) and mixtures of the same three molecular weights purified by simple precipitation in acetonitrile (**52d-f**), providing moderate purity (23 – 76% biscarbene content) and high yields ($\eta = 45 – 71\%$) (see Table 10B). Accordingly, perfect doubling of the molecular weight (and low PDI-values: 1.08 – 1.38) was just accomplished in case of preparative GPC purification, whereas the precipitation method afforded decreased molecular weights and increased PDI-values (1.36 – 1.73) (see Table 10). For further experimental details, see also chapter 4.3.3.

Table 10. Overview of synthesized mechanocatalysts based on PS.

polymer	start-PS	$M_{n(GPC)}$[a] of **36** [g/mol]	PDI	$M_{n(GPC)}$[a] [g/mol] of **52**	PDI	biscarbene content [%][b]	isolated yield [%]
A)	**pure mechanophores purified by preparative GPC**						
52a	**49d**	5 900	1.07	12 000	1.08	100	4
52b	**49e**	11 500	1.17	23 000	1.16	100	7
52c	**49f**	25 300	1.15	50 500	1.38	100	5
B)	**mechanophore mixtures purified by precipitation in MeCN**						
52d	**49d**	5 900	1.07	10 100	1.36	55	45
52e	**49e**	11 500	1.17	19 200	1.73	76	57
52f	**49f**	25 300	1.15	38 700	1.53	23	71

a) Analytical GPC was conducted in HPLC-grade DMF with the addition of $LiNTf_2$ ($c = 10.0$ mM) and molecular weights were determined by calibration with external PS-standards ($M_P \sim 1\,000 – 115\,000$ g/mol) and detection of refractive-index. b) Determined via ^{1}H-NMR and the ratio of imidazole-protons of precursor located at $\delta = 7.56 – 7.52$ ppm and imidazole-protons, belonging to the biscarbene structure at $\delta = 6.25 – 6.23$ ppm. Presumably apparent monocarbene structure was not taken into account, in turn of overlapping signals of suspected structure with multiplet at $\delta = 7.24 – 6.34$ ppm, belonging to the aromatic part of the repetitive unit.

Mechanophore structure was proven by the combination of the doubled molecular weight detected in GPC-analysis and the shift for the protons attached to the imidazolium-ring from $\delta = 7.56 – 7.52$ ppm

(precursor) to $\delta = 6.25 - 6.22$ ppm (biscarbene structure) monitored via ^{1}H-NMR-measurement (see Figure 60).
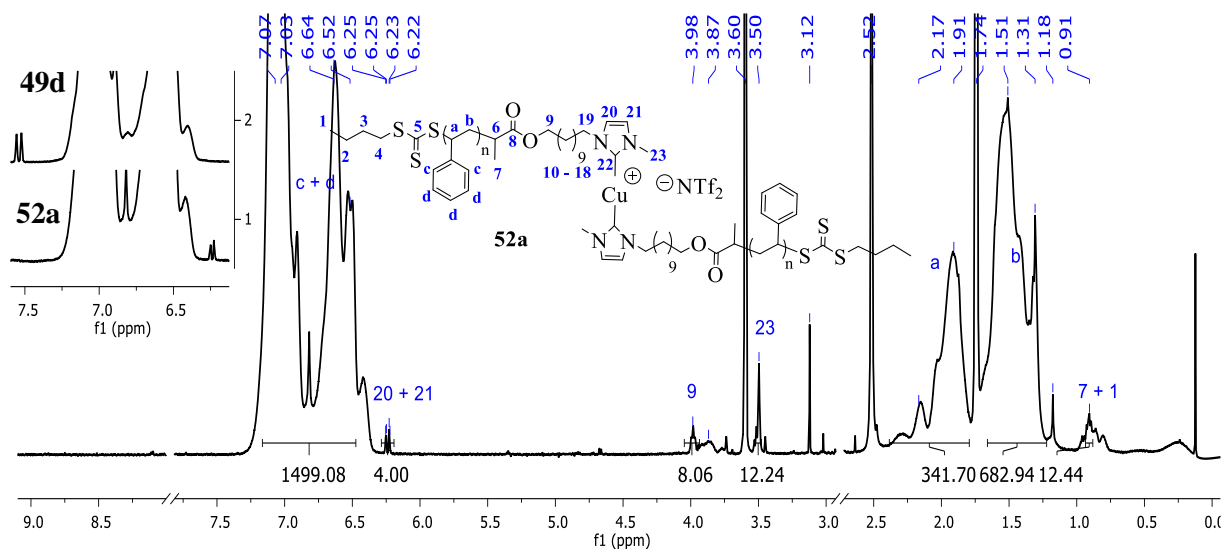
Figure 60. ^{1}H-NMR spectrum of **52a** in THF-d_8. Residues of DMF were cut out. Superimposed spectrum of stacked precursor **49d** (top) and **52a** (bottom).

Synthetic attempts to provide P-*n*BuA mechanophores remained insufficient, even though different condition-setups were investigated, varying the solvents (MeCN, THF, mixture), the temperature (T = -40 °C – +20 °C) and the amount of bases (0.5 – 2.3 eq.) (for experimental details see chapter 4.3.3. and appendix 7.13). It was assumed, that the high polarity of the P-*n*BuA backbone in combination with the apparent trithiocarbonate group tended to promote side-reactions at basic conditions as detected in NMR-spectrum, missing the shift of the NC*H*C*H*N resonances, even though doubling of the molecular weight was detected in GPC. Presumably, the trithiocarbonate group was hydrolysed, forming an elongated disulfide-bridged polymer, preventing the desired formation of the mechanocatalyst (see Figure 61).
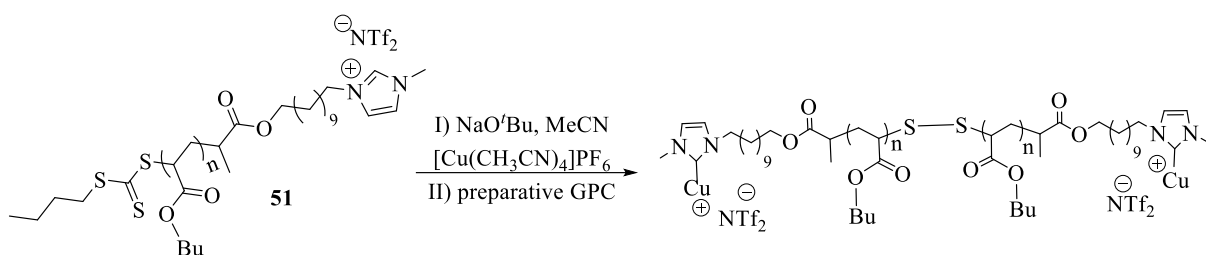
Figure 61. Synthesis of disulfide bridged P-*n*BuA preventing the formation of the desired mechanophore structure.

3.2.5 Activation of mechanocatalysts in solution and bulk state

Testing of the mechanocatalysts (**52a-f**) in solution and bulk state required appropriate experiments and sufficient amount of the catalyst. Limited amounts of the pure mechanocatalysts (**52b-c**) prevented their proper use in the final material, thus **52a** was the only pure mechanocatalyst available to design the autonomous sensing material. While reserves of mechanocatalyst-mixtures (**52d-f**) allowed for their investigation in both, the solution and the bulk state.

3.2.5.1 Ultra-sonication experiments of mechanocatalysts

The efficiency of the synthesized mechanocatalysts (**52d-f**) was probed in solution by conducting the CuAAC of benzyl azide (75 mM) and phenylacetylene (75 mM) and monitoring the "click" conversion by *in situ* ^{1}H-NMR measurements. The exposure of the system to ultra-sonication shall cleave the

weakest bond of the mechanocatalyst, releasing the active monocarbene-Cu(I)-species, able to catalyze the „click"-reaction (see Figure 62), subsequently following the normal CuAAC mechanism[48, 218-219, 302] (see Figure 4, chapter 1.1). The cleaving efficiency in solution upon ultra-sonication depends on the coil-to-stretch transformation of the polymer handles caused by the collapse of the cavitation bubbles, which can be tuned by the sonication power, the polymer concentration, the temperature and the molecular weight of the polymer handles.[273] In order to investigate only the influence of polymer handles to cleaving efficiency the experimental setup was adopted from literature[302], exploiting the same experiment conditions. In absence of ultra-sonication all coordination sites of the latent Cu(I)-catalyst should be occupied, preventing the alkyne-coordination and thus the „click"-reaction.
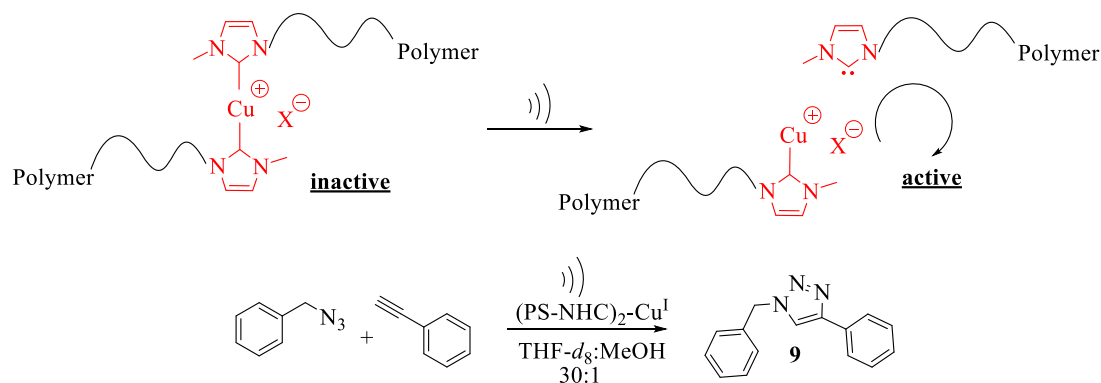
Figure 62. Mechanophoric activation by ultra-sonication, releasing the catalytic active Cu(I)-monocarbene species, able to conduct the „click"-reaction of benzyl azide and phenylacetylene.

At first, **52d** (0.01 eq., 10 100 g/mol, 55% biscarbene content) was subjected to ultra-sonication experiment conducted in a THF:MeOH, 30:1 mixture, providing a continuous increase of the conversion with increasing time and US-cycles. "Click" conversions of 36% after the third US-cycle, 62% after the fifth US-cycle and 75% after the tenth US-cycles were calculated via ^{1}H-NMR measurements, comparing the CH_2 resonances of $\delta = 4.34$ ppm (N$_3$) and $\delta = 5.58$ ppm (triazole) and the increasing triazole resonance at $\delta = 8.10$ ppm (see Table 11B, entry 7). Contrary, a "click" conversion of 13% before US was applied, led to verification via control experiments. In absence of US, employing the mechanocatalysts (**52d-f**), complete conversions within 18 hours were afforded (see Table 11A, entry 1-3). This was presumably caused by two different reasons: first, residual monocarbene-Cu(I) species might be left within the mixtures of **52d-f**, indicated by the bimodal distribution in GPC. The experimental verification in NMR is not possible, due to overlapping of the resonances of the repetitive PS-unit at $\delta = 7.27 – 6.35$ ppm with the potential signals of NCHCHN of the monocarbene structure.[302] Second, the labile bond of **52d-f** was too fragile to persist in solution in terms of the dissociation energy barrier in the Morse potential[280-285]. However, these catalysts missed the required latency to be applied as mechanocatalysts as was similar observed, using a mechanocatalyst with pTHF-handles[302]. It was further tried to weaken the polymer-solvent interaction[272, 274, 324] by change from THF to DMF:MeOH, 30:1 mixtures. The "click" conversion of the CuAAC conducted in DMF:MeOH, 30:1 control experiments (absence of US), applying mechanocatalysts (**52d-f**), was indeed lower (80% in 24 hours) than in THF (100% after 18 hours), but was still missing the required latency (see Table 11A, entry 4-6) to be further investigated in US solution experiments. Experimental data can be found in the appendix 7.14.

Table 11. Conversion of phenylacetylene and benzyl azide in THF-d_8 or DMF-d_7 in presence of a Cu(I)-mechanocatalyst (**52**), applying ultra-sonication or not (control experiments)[a].

entry	Cu(I)-catalyst	$M_{n(GPC)}$ [g/mol]	solvent	T [°C]	US	conversion [%][b]			
A	**control-experiments without US**					t [h]	1	2	18	24
1	**52d**	10 100	THF:MeOH	20	off	-	-	100	100
2	**52e**	19 200	THF:MeOH	20	off	-	-	100	100
3	**52f**	38 700	THF:MeOH	20	off	-	-	100	100
4	**52d**	10 100	DMF:MeOH	20	off	2	-	-	80
5	**52e**	19 200	DMF:MeOH	20	off	4	20	-	-
6	**52f**	38 700	DMF:MeOH	20	off	2	-	-	-
B	**mechanochemical activation with US**					US-cycles	0	3	5	10
						t [h]	0	7.5	12.5	25
7	**52d**	10 100	THF:MeOH	0	on	13	36	62	75

a) For all reactions an equimolar concentration (c = 75 mM) of benzyl azide and phenylacetylene in the mentioned solvent mixture (30:1) was adjusted. The concentration of the Cu(I)-mechanophore (**52d-f**) was adjusted to c = 0.75 mM (0.01 equivalents). b) Conversion was calculated by determining the increasing triazole-resonance at δ = 8.10 ppm and the CH_2 resonance of the triazole product at δ = 5.58 ppm. Comparison of triazole-resonance with the CH_2-resonance of benzyl azide at δ = 4.34 ppm afforded the conversion to different period of times, when the aliquot was taken and ^{1}H-NMR-experiments were conducted.

3.2.5.2 Detection of sensing pTHF-pellets via fluorogenic compression experiments (activated via mechanocatalysts)

The afforded strain rates to activate linear mechanocatalysts in solution are higher than in the solid state, leading to a commonly observed less performance of the same catalyst in the solid state compared to their solution efficiency[48, 272, 325]. Thus, the mechanocatalyst mixtures **52d-f** can eventually develop their full potential better in the solid approach, than in solution. The effect of the increasing molecular weight of the polymer handles to the catalytic efficiency within a host-material was studied by monitoring the fluorogenic CuAAC of coumarin azide (**36**) and phenylacetylene within a scaffolding pTHF-matrix upon compression impact according to literature conditions[48, 242] (see Figure 63).

improved scission efficiency of Cu(I)-mechanocatalysts leads to an increase of the catalytic efficiency in the CuAAC
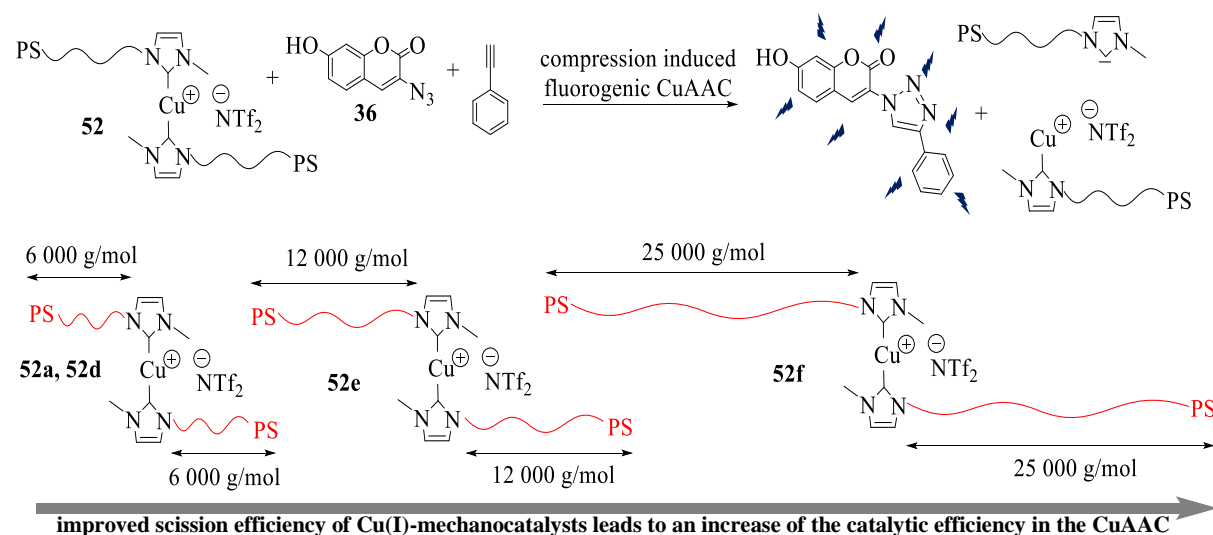
Figure 63. Activation of mechanophores (**52**) upon compression leads to release of the active Cu(I)-monocarbene species, able to conduct the fluorogenic CuAAC. Cleaving-efficiency should increase with increasing molecular weight of the polymer handles attached to the labile bond.

High molecular weight pTHF[299] ($M_{n(GPC)}$ = 112 000 g/mol; crystallinity 68%), coumarin azide (**36**) and phenylacetylene (c = 1.56 · 10^{-4} mmol$_{dye}$/mg$_{sample}$) were dissolved in anhydrous THF and continuously stirred, affording a good distribution of the components within the scaffolding matrix. To prevent

premature decomposition of the (PS-NHC)$_2$-Cu(I)-mechanocatalysts (**52a**, **52d–f**) complete evaporation of THF was required, before the catalyst (dissolved in DMF) was added to the crude and viscous mixture. The remaining solvent was removed under reduced pressure and the complete specimen (**53a-d**) were allowed to crystallize for one week in the dark at − 40 °C (47 − 61% crystallinity determined via DSC, see also chapter 4.3.6.1.), since crystalline regions within host-material were known to improve the mechanochemical force transmission[276]. Gentle pressing with a spatula was forming the pTHF pellet, which upon compression should induce the scission of the latent catalyst into the active Cu(I)-monocarbene-species, able to conduct the fluorogenic CuAAC. The reaction progress was monitored before the pellet was subjected to the hydraulic press (0th cycle), followed by the 1st, 2nd, 3rd, 5th, 10th and 20th compression-cycle, applying 10 tons of pressure (corresponding to 0.74 GPa) for 30 minutes (see Figure 64 for calculated "click" conversions and chapter 4.3.6.2. for experimental data). The increasing fluorescence-intensities, emitted at $\lambda = 432$ nm, were compared with previously documented calibration-curves[48], allowing to determine the "click"-conversion (see Table 12) after each compression cycle (for detailed information of calibration see appendix 7.15).

Table 12. Calculated "click"-conversions for the 20th fluorescence-compression cycle for each pTHF pellet (**53a-d**), containing the mechanocatalysts (**52a, 52d-f**), coumarin azide **36** and phenylacetylene.

| entry | pTHF -pellet | mechanocatalyst | | | | fluorescence intensity [a.u.]$^{c)}$ | "click"-conversion [%]$^{d)}$ |
		No.	$M_{n(GPC)}$ [g/mol]$^{a)}$	$m^{b)}$	n_{pure} [μmol]		
1	**53a**	**52a**	12 000 (100 %)	6.4 wt%	1.2	227	21.8 ± 0.8
2	**53b**	**52d**	10 100 (55 %)	11.0 wt%	1.2	112	11.1 ± 1.1
3	**53c**	**52e**	19 200 (76 %)	14.8 wt%	1.2	170	16.2 ± 0.3
4	**53d**	**52f**	38 700 (23 %)	19.2 wt%	0.2	143	13.1 ± 1.2

a) Values in brackets represent the amount of Cu(I) bis(NHC) complex according to ^{1}H-NMR analysis. b) Values represent wt% of the mechanocatalyst (or mixture) in the pTHF pellet. c) Average value of multiple determined fluorescence spectra at three different positions of the sample after excitation at $\lambda = 382$ nm and fluorescence emission at $\lambda = 432$ nm. d) Calculated according to eq. 5, assuming a maximum concentration of the fluorescence dye of $1.56 \cdot 10^{-4}$ mmol$_{dye}$/mg$_{sample}$ (see appendix 7.15).

The highest fluorescence intensity of 227 was detected after the 20th compression cycle of pellet **53a**, containing the pure mechanocatalyst **52a** (M_n = 12 000 g/mol, 100% biscarbene), corresponding to a "click" conversion of p = 21.8% (see Table 12, entry 1 and Figure 64). For specimen **53b-d** mechanocatalyst mixtures **52d-f** were applied and their wt%-amount within the pellets was increased (up to 19.2 wt% for **53d**) in order to keep the same concentration of activatable catalyst (1.2 μmol). Limitations in mixing of pTHF matrix and PS-mechanocatalysts and the low biscarbene content (23%) of the highest molecular weight mechanocatalyst **52f** led to the tremendous reduce of concentration of the latent catalyst (0.2 μmol) within pellet **53d**. However, the trend that cleaving-efficiency was improved with increasing molecular weight of polymer handles was still significant. Pellet **53b** (55% biscarbene content), containing the lowest molecular weight catalyst (10 100 g/mol) was providing halve the „click"-conversion (p = 11.1%, fluorescence intensity: 112) of pellet **53a**, containing the same catalyst in 100% purity (see Table 12, entry 2 and Figure 64), which was caused by the "dead" amount of the catalyst upon mechanochemical activation. However, doubling of the chain length (from 6 000 g/mol to 12 000 g/mol), applying the mechanocatalyst mixture **52e** (M_n = 19 200 g/mol, 76% biscarbene) in pellet **53c**, afforded an increase in conversion to p = 16.2% (fluorescence intensity: 170) (see Table 12, entry 3 and Figure 64). Additional doubling of the molecular weight of the

mechanocatalyst (38 700 g/mol, 23% biscarbene content in **52f**), subjecting pellet **53d** to compression cycles, afforded a moderate fluorescence intensity of 143, representing a "click" conversion of p = 13.1% (see Table 12, entry 4 and Figure 64). The marginal reduction in "click" conversion was founded in the tremendous decrease of mechanocatalyst content in **53d** (n_{pure} = 0.2 μmol), being less than one fifth compared to the other pTHF pellets **53a-c** (n_{pure} = 1.2 μmol).
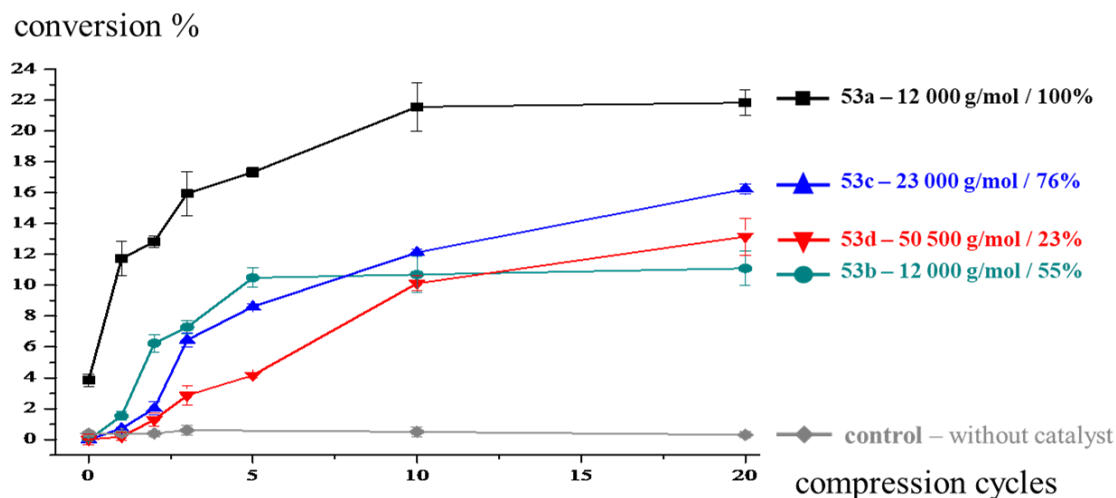
Figure 64. Graph of „click"-conversions determined after each compression cycle by fluorescent measurement by comparing to calibration curve of sensing-pellets (**53a–d**) (black, blue, red and green curve, value% represents the bis(NHC)-Cu(I) content within the mechanocatalyst) and of control specimen[48] without catalyst (grey curve).

Neither the specimen missing the mechanocatalyst (see Figure 64, grey curve adopted from[48]) nor the ones (**53b-d**) missing the mechanical impact provided any increase in "click" conversion (see Figure 64, blue, red and green curve at 0th cycle), proving the mechanochemical activation was induced by compression impact.[48] Just in case of pTHF pellet (**53a**), containing the pure mechanocatalyst (**52a**) an increase of fluorescence-emission was detected before any compression was applied, which was presumably caused during the crystallization of the scaffolding pTHF-matrix (see Figure 64, black curve at 0th cycle). The documentation and detection of the process by a UV-lamp (λ = 366 nm and 254 nm) clearly visualized the progress of the reaction by an increasing fluorescence-emission after each compression cycle (see Figure 65).
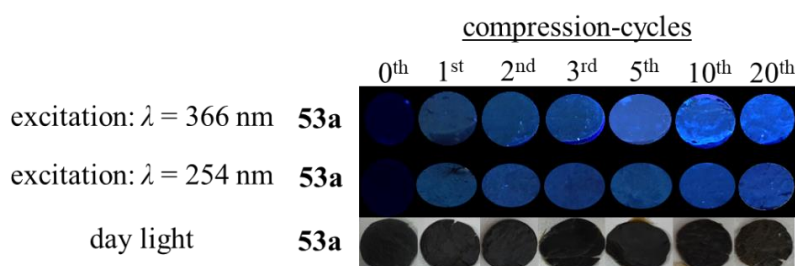
Figure 65. Photographs of pTHF pellet (**53a**) after each compression cycle and excitation by UV-lamp (λ = 366 nm or 254 nm) and photographs taken at day light.

Summed up, an autonomous and capsule free sensing approach triggered by compression impact was accomplished. The material (**53a**), containing the pure mechanocatalyst (**52a**), afforded the highest "click"-conversion of p = 21.8%, representing its capability for stress-reporting systems. While pTHF pellets (**53b-d**), consisting of mechanocatalyst-mixtures (**52d-f**), provided less efficiency in catalysis, but were demonstrating the dependency of the mechanocatalyst activation from the chain length anchored to the labile bond (bis(NHC)-Cu(I)). The longer the polymer chain the better the activation of the catalyst and the higher the "click" conversion was, indicated by a higher fluorescence intensity.

4 Experimental part

4.1 Materials and methods

The following reactions were carried out under dry argon atmosphere, using common Schlenk techniques unless noted. All solvents were purchased in technical grade and were distilled before further use. THF was predried over potassium hydroxide, while toluene was predried over calcium chloride. Final drying was done by heating under reflux over sodium/benzophenone until the blue color persists. Dichloromethane (DCM) was predried over calcium chloride and dried finally by refluxing over calcium hydride for several hours. Dimethylformamide (DMF), acetonitrile (MeCN), triethylamine (TEA) and butyronitrile were dried by refluxing over calcium hydride and freshly distilled prior use. *n*-Hexane was predried over KOH and freshly distilled over sodium and KOH under a nitrogen atmosphere prior to use.

All chemicals were used as received without further purification unless noted. 2,4-Pyridinecarboxylic acid hydrate was purchased from TCI. Calcium chloride (ultra dry 99.9%), 2,4-dihydroxy benzaldehyde (98%) were purchased from Alfa Aesar, lithium hydroxide from Lachema, hydrochloric acid (37%) from Grüssing, oxalyl chloride from Merck, high molecular weight poly(isobutylene) (250 000 g/mol) from BASF and 4-(dimethylamino)pyridine from Fluka. Copper(I)bromide was obtained from Sigma Aldrich and washed with glacial acetic acid followed by dry ethanol and finally by dry diethyl ether, before it was dried in high vacuum and stored in a Schlenk tube within the glove box prior to use. Copper(I)acetate, copper charcoal (3 wt%), tris(triphenylphosphine)copper(I) bromide, tris(triphenylphosphine)copper(I) fluoride, potassium hexamethyldisilazide (KHMDS, 95%), sodium *tert*-butoxide (NaO*t*Bu, 97%), tetrakis(acetonitrile)copper(I) hexafluorophosphate ([Cu(MeCN)$_4$]PF$_6$, 97%), *N*-methylimidazole (97%), sodium iodide (99.9%), 1,4,7,10,13-pentaoxacyclopentadecane (15-crown-5-ether, 98%), phenylacetylene (98%), copper(II) sulfate pentahydrate, sodium ascorbate, anhydrous sodium acetate (99%), sodium nitrite (99%), sodium azide (99.5%), methyl trifluoromethanesulfonate (98%) and 2,6-di-*tert*-butylpyridine (97%) were purchased from Sigma Aldrich. Graphite flakes (KFL 99.5, min 20% > 100 μm) were received from Kropfmühl AG. *N*-Acetylglycine as well as acetic anhydride (99%) were purchased from VWR. Column chromatography was performed, using Merck silica gel 60 (230 – 400 mesh). Thin-layer chromatography (TLC) was carried out on Merck TLC aluminum sheets (silica gel 60 F254). Spots on TLC plates were visualized either by UV light with a wavelength of 254 or 366 nm or by oxidizing agents such as "blue stain", consisting out of Ce(SO$_4$)$_2$·4H$_2$O (1 g) and (NH$_4$)$_6$Mo$_7$O$_{24}$·4H$_2$O (1 g) dissolved in a mixture of distilled water (90 mL) and concentrated sulfuric acid (6 mL).

The synthesis of azido telechelic PIB (**11**) ($M_{n(GPC)}$ = 2 800 g/mol, $M_{n(NMR)}$ = 3 000 g/mol, PDI = 1.2) was done according to literature[326] by Dr. Florian Herbst, synthesis of ((2-((2-acetoxy-3-azidopropoxy)methyl)-2-ethylpropane-1,3-diyl) bis(oxy))bis(3-azidopropane-1,2-diyl) diacetate (**19**) was done according to literature[49, 236, 327] by Neda Kargarfard, synthesis of 2,2-bis(prop-2-2-ynyloxymethyl)-1-(prop-2-ynyloxy)butane (**20**) was done according to literature[42] by Jan Freudenberg, synthesis of the homogeneous low molecular weight bis(NHC)-catalysts (**21**, **22**) was done according to literature[48] by Michel Biewend, synthesis of mono- (**23**)[328-329], bi- (**24**)[330] and trivalent initiator (**25**)[331] for LCCP[331-333] of isobutylene and subsequent endgroup transformation from allylic to hydroxy moiety[334-335] was done according to literature during my master's degree, synthesis of star-shaped PIB-alkyne (**35**) (M_n = 6 600 g/mol, PDI = 1.4) was done according to literature[40] by Dr. Diana Döhler, the synthesis and encapsulation of (2,2-bis(prop-2-2-ynyloxymethyl)-1-(prop-2-ynyloxy)butane (**20**) in urea–formaldehyde microcapsules with an average hydrodynamic diameter of 6–8 μm, using an oil-in-water emulsion technique, was done according to literature[39, 42, 336-337] by Wilton Osim, synthesis of

high molecular weight pTHF (M_n = 112 000 g/mol)[48] and performance of calibration measurements of fluorogenic dye (**54**) within pTHF matrix[48] was done by Dr. Philipp Michael and thankfully received for conducting experiments. Exfoliated graphene[238] was thankfully provided by the working group of Prof. Feng. Parts of the DSC-experiments were conducted by Dr. Ali Shaygan Nia[49], Neda Kargarfard[236] and Moritz Schüller (unpublished work) and displayed within this work for better comparison of the present work.

NMR spectra were recorded on a Varian Gemini 2000 (400 MHz) or on a Varian Unity Inova 500 (500 MHz) at 27 °C. Deuterated chloroform (C*D*Cl$_3$), deuterated dimethylformamide (DMF-*d$_7$*), deuterated methanol (MeO*D*) or deuterated tetrahydrofuran (THF-*d$_8$*) were used as solvents. All chemical shifts are given in ppm and referred to the residual solvent signals. MestReNova software (version 6.0.2-5475) was used for interpretation of the NMR spectra.

Rheology experiments were performed on an Anton Paar (Physica) MCR 101/SN 80753612 at either 20 °C or 10 °C. For regulating the sample temperature, thermoelectric cooling/heating in a Peltier chamber under a dry oxygen atmosphere was applied. For all measurements parallel plates with a diameter of 8 mm were used. Frequency measurements were performed within the linear viscoelastic range. For the evaluation of the data, RheoPlus/32 software (V 3.40) and OriginPro8 were used.

Fluorescence measurements were performed on a Cary Eclipse Fluorescence Spectrophotometer from Agilent Technologies. The excitation wavelength was set to 330 nm (or 360 nm) while detecting the fluorescence emission from 350 to 650 nm for scratch-SH approach (or 380 – 650 nm for compression sensing approach). The samples were fixed in a solid sample holder between two object slides out of quartz glass. All fluorescence experiments were repeated at least three times. For the evaluation of the data, Cary Eclipse Scan Applications Software (v. 1.2 (147)) and Origin Pro8G (v. 8.0951) were used.

For inline FTIR-measurements a Bruker Vertex 70 MIR spectrometer equipped with an ATR-FTIR diamond probe was used. Opus 6.5 was used for analyzing the data.

Differential scanning calorimetry (DSC) measurements were performed on a differential scanning calorimeter 204F1/ASC Phoenix from Netzsch. Crucibles and lids made of aluminum were used. Measurements were performed in a temperature range from -100 to 250 °C, using a heating rate of 5 K/min. As purge gas a flow of dry nitrogen (20 mL/min) was used for all experiments. For evaluation of data the Proteus Thermal Analysis Software (Version 5.2.1) and OriginPro8 were used.

Gel permeation chromatography (GPC) measurements were performed on a Viscotek GPCmax VE 2002 using a HH$_{RH}$ Guard-17369 and a GMH$_{HR}$-N-18055 column in THF at 40 °C and the detection of the refractive index was performed with a VE 3580 RI detector of Viscotek. For external calibration, PIBstandards (320 g/mol to 578 000 g/mol) from Viscotek were used. The concentration of all samples was 3 mg/mL and the flow rate was 1 mL/min. GPC measurements of polymers, containing ionic-groups, were performed on a Viscotek GPCmax VE 2001, using a GMH$_{HR}$-N-18055 column in DMF with LiNTF$_2$ (10 mM) at 60 °C and the detection of the refractive index was performed with a VE3580 RI detector of Viscotek at 30 °C, using a flow rate of 1 mL/min. PS standards (1.0 kg/mol – 170 kg/mol) from Malvern and poly(butyl methacrylate) (PBMA) standards (0.8 kg/mol – 111 kg/mol) from PSS were used for external calibration of analytic and preparative GPC. Preparative GPC was used to separate the biscarbene from the monocarbene complexes and was performed on a VWR HITACHI Chromaster, using a KD-2002.5 column from Shodex in DMF at 55 °C. The detection of the refractive index was performed with a RI detector from VWR at 50 °C. The concentration of the samples was adjusted to 50 – 100 mg/mL and the flow rate was 0.7 mL/min.

Electrospray Ionization – Time of Flight Mass Spectrometry (ESI-ToF-MS) was performed on a Bruker Daltonics microTOF via direct injection with a flow rate of 180 μL/h, using the positive mode with an acceleration voltage of 4.5 kV. Samples were prepared by dissolving the sample in THF or MeOH, adjusting concentrations of 0.1 mg/mL for neutral components by addition of NaI or of 0.001 mg/mL for positive charged ionic-components without the addition of a salt.

Matrix Assisted Laser Desorption Ionization – Time of Flight Mass Spectrometry (MALDI-ToF-MS) were conducted on a Bruker Autoflex III system. The ionization was accomplished via a smart beam laser (355 nm, 532 nm, 808 nm and 1064 nm ± 5 nm; 3 ns pulse width; up to 2500 Hz repetition rate) and an acceleration voltage of 20 kV. The molecules were detected as positive ions either in reflector or linear mode and the baseline subtraction as well as the smoothing of the recorded spectra were performed, using a three point Savitzky-Golay algorithm. The sample preparation was done spotting the polymer solution in a 2 mg/mL concentration in THF together with trans-2-[3-(4-tert-butylphenyl)-2-methyl-2-propenylidene] malononitrile (DCTB) as matrix in a 20 mg/mL concentration in different ratios of matrix:analyte:salt on the MALDI target. LiTFA, AgTFA or NaTFA were used as salts.

For transmission electron microscopy (TEM) the samples (Cu-TRGO and Cu-TREGO) were dispersed in isopropanol, using a sonication bath and spread onto a Cu grid coated with a Carbon-film. After 1 min, excess liquid was blotted off with filter paper. The dried specimens were examined with an EM 900 transmission electron microscope (Carl Zeiss Microscopy GmbH, Oberkochen, Germany). Micrographs were taken with a SSCCD SM-1k-120 camera (TRS, Moorenweis, Germany).

XRD measurement were performed, using a Bruker AXS D8 advanced X-ray diffractometer with $Cu_{K\alpha}$ ($\lambda = 0.15406$ nm) radiation in the 2θ range between 5–80° with a scan rate of 2°/min.

For synthesis of TRGO-Cu_2O and TREGO-Cu_2O a glass tube oven from Nabertherm, Mod. RSR-B120 / 750 / 11 was used.

Flame atomic absorption spectroscopy (FAAS) measurements were recorded via an instrument of Analytik Jena AG novAA 350 #113A0641 Tech: Flame. For analysis of data Software-Version ASpect LS 1.4.1.0 was used. Calibration was accomplished by external and plotting methods. To determine the copper content samples were burnt to ashes at 800 °C and subsequently diluted with nitric acid (2 M, 50.0 mL). Followed by mixing with 0.2wt% potassium chloride solution (0.4 g KCl dissolved in 200.0 mL bidest. water, ratio 1:1), providing the sample, which was measured.

Ultra-sonication experiments were conducted under inert conditions with a Sonics VCX 500 ultra-sonic processor at a frequency of 20 kHz equipped with a long full wave solid probe (254 mm) out of titanium alloy (Ti-Al-4V) with a diameter of 13 mm, an internally threaded stainless steel adapter (fitting to the full wave long 13 mm probe at nodal point) and a 10 mL reaction vessel with two additional 14/20 side necks, which was temperate at 20 °C by an external cooling bath. 30% of the maximal amplitude of 125 μm was used, corresponding to a sonication intensity of 8.75 W/cm^2 in a THF/MeOH 30:1 mixture, while the energy input was determined as 21 kJ per applied ultra-sonication cycle, consisting out of 90 min sonication with a pulse sequence of 5 s on and 10 s off.

The compression experiments were conducted on the automatic hydraulic Atlas Power Presses T15 from Specac together with an Atlas 13 mm evacuable pellet die applying 10 tons' pressure.

4.2 Synthesis of a low temperature and fluorogenic SH approach
4.2.1 Synthesis of picolyl azides (4, 7)
4.2.1.1 Synthesis of 2-(6-azidomethyl)-pyridine-4-carboxylic acid (4)[43, 228, 338-340]
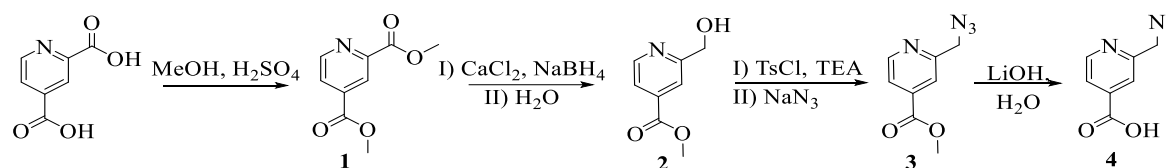
Scheme 1. Synthetic route to obtain 2-(6-azidomethyl)-pyridine-4-carboxylic acid (**4**).

2,4-Pyridinedicarboxylic acid monohydrate (10.9 mmol, 2.0 g) was suspended in methanol (12.0 mL) and concentrated sulfuric acid (12.0 mmol, 640 µL) was added. The solution was refluxed for 48 hours and subsequently allowed to cool to room temperature. The mixture was treated with saturated aqueous sodium bicarbonate solution until $pH = 7$ was achieved. The solvent was removed under reduced pressure. The residue was suspended in chloroform (30.0 mL) and was filtered and the organic layer was washed with a saturated solution of sodium chloride for several times. The organic layer was dried over magnesium sulfate and concentrated under reduced pressure to provide 2,4-pyridinedicarboxylic acid dimethyl ester (**1**) in a yield of 82%. R_f (ethyl acetate) = 0.61.

<u>^{1}H-NMR (CDCl$_3$, 400 MHz):</u> δ = 8.90 (dd, 1H, $^3J_{H,H}$ = 4.9 Hz, $^5J_{H,H}$ = 0.6 Hz, CH), 8.64 (dd, 1H, $^4J_{H,H}$ = 1.5 Hz, $^5J_{H,H}$ = 0.8 Hz, CH), 8.03 (dd, 1H, $^3J_{H,H}$ = 4.9 Hz, $^4J_{H,H}$ = 1.6 Hz, CH), 4.03 (s, 3H, CH_3), 3.98 (s, 3H, CH_3).

<u>^{13}C-NMR (CDCl$_3$, 100 MHz):</u> δ = 165.1 (C=O), 164.8 (C=O), 150.8 (CH$_{aromat}$), 149.1 (C-COOMe), 138.8 (C-COOMe), 126.4 (CH$_{aromat}$), 124.4 (CH$_{aromat}$), 53.2 (CH$_3$), 53.0 (CH$_3$).

2,4-Pyridinedicarboxylic acid dimethyl ester (**1**) (3.8 mmol, 750 mg) and ultra dry calcium chloride (99.99%, 17.1 mmol, 1.9 g) were dissolved in anhydrous tetrahydrofuran (6.0 mL) and anhydrous methanol (12.0 mL). The solution was cooled to −5 °C and subsequently sodium borohydride was added in small portions (5.6 mmol, 225 mg, (3 × 75 mg)). The reaction was complete after ~ 160 minutes and quenched with ice-cold water (15.0 mL). The solution was extracted with chloroform (3 × 40.0 mL) and the combined organic layers were dried over magnesium sulfate. The solvent was removed under reduced pressure to afford 2-(6-hydroxymethyl)-pyridine-4-carboxylic acid methyl ester (**2**) in a yield of 66%. R_f (ethyl acetate) = 0.41.

<u>^{1}H-NMR (CDCl$_3$, 400 MHz):</u> δ = 8.70 (d, 1H, $^3J_{H,H}$ = 5.1 Hz, CH), 7.83 (s, 1H, CH), 7.75 (dd, 1H, $^3J_{H,H}$ = 5.1 Hz, $^4J_{H,H}$ = 0.7 Hz, CH), 4.83 (s, 2H, CH_2-OH), 3.96 (s, 3H, CH_3).

<u>^{13}C-NMR (CDCl$_3$, 100 MHz):</u> δ = 165.5 (C=O), 160.4 (C-CH$_2$OH), 149.4 (CH$_{aromat.}$), 138.1 (C-COOMe), 121.6 (CH$_{aromat.}$), 119.8 (CH$_{aromat.}$), 64.2 (CH$_2$-OH), 52.7 (CH$_3$).

2-(6-Hydroxymethyl)-pyridine-4-carboxylic acid methyl ester (**2**) (0.3 mmol, 50 mg) was dissolved in anhydrous dichloromethane (6.6 mL), followed by the addition of triethylamine (1.5 mmol, 207 µL) and 4-methylbenzene-1-sulfonyl chloride (0.5 mmol, 87 mg). After stirring for two hours the solvent was removed under reduced pressure. The residue was dissolved in anhydrous tetrahydrofuran (3.3 mL) and sodium azide (3.0 mmol, 193 mg) was added. The reaction was stirred for further 24 hours at room temperature, subsequently followed by dilution with ethyl acetate (30.0 mL) and water (30.0 mL). After extraction of the aqueous layer with ethyl acetate (three times 30.0 mL), the combined organic layers were washed with a saturated solution of sodium chloride and dried over magnesium sulfate. The crude

product was purified by chromatography (SiO$_2$, *n*-hexane/ethyl acetate 4:1, R$_f$ = 0.65 in *n*-hexane/ethyl acetate 1:1), providing 2-(6-azidomethyl)-pyridine-4-carboxylic acid methyl ester (**3**) in a yield of 69%.

<u>^{1}H-NMR (CDCl$_3$, 400 MHz):</u> δ = 8.74 (*d*, 1H, $^3J_{H,H}$ = 5.0 Hz, C*H*), 7.89 (*s*, 1H, C*H*), 7.79 (*dd*, 1H, $^3J_{H,H}$ = 5.0 Hz, $^4J_{H,H}$ = 1.4 Hz, C*H*), 4.56 (*s*, 2H, C*H*$_2$-N$_3$), 3.96 (*s*, 3H, C*H*$_3$).

<u>^{13}C-NMR (CDCl$_3$, 100 MHz):</u> δ = 165.3 (*C*=O), 157.0 (*C*-CH$_2$N$_3$), 150.5 (*C*H$_{aromat.}$), 138.4 (*C*-COOMe), 122.1 (*C*H$_{aromat.}$), 121.1 (*C*H$_{aromat.}$), 55.4 (*C*H$_2$-N$_3$), 52.8 (*C*H$_3$).

<u>IR (bulk) [cm^{-1}]:</u> 2955 (w), 2105 (s), 1732 (s), 1603 (w), 1563 (w), 1438 (w), 1292 (m), 1214 (m), 1111 (w), 762 (w).

2-(6-Azidomethyl)-pyridine-4-carboxylic acid methyl ester (**3**) (2.6 mmol, 500 mg) was dissolved in methanol (10.0 mL), followed by the addition of a 1.0 M aqueous solution of lithium hydroxide (7.8 mmol, 7.8 mL). The reaction was stirred for 25 minutes at room temperature. Neutralization was achieved with the addition of a 1.0 M solution of aqueous hydrogen chloride. The solvent was removed under reduced pressure and the product was dried under high vacuum until constant weight to obtain 2-(6-azidomethyl)-pyridine-4-carboxylic acid (**4**) in a quantitative yield.

<u>^{1}H-NMR (DMSO-d_6, 400 MHz):</u> δ = 8.51 (*d*, 1H, $^3J_{H,H}$ = 4.9 Hz, C*H*), 7.74 (*s*, 1H, C*H*), 7.66 (*dd*, 1H, $^3J_{H,H}$ = 4.9 Hz, $^4J_{H,H}$ = 1.1 Hz, C*H*), 4.48 (*s*, 2H, C*H*$_2$-N$_3$).

<u>^{13}C-NMR (DMSO-d_6, 100 MHz):</u> δ = 167.2 (*C*OOH), 155.7 (C-CH$_2$N$_3$), 149.5 (*C*H$_{aromat.}$), 149.2 (*C*-COOH), 123.1 (*C*H$_{aromat.}$), 122.4 (*C*H$_{aromat.}$), 55.1 (*C*H$_2$-N$_3$).

<u>IR (bulk) [cm^{-1}]:</u> 3354 (s), 2099 (s), 1603 (s), 1553 (m), 1425 (m), 1393 (m), 1335 (w), 1269 (w), 703 (w).

4.2.1.2 Synthesis of 2-(6-azidomethyl)-pyridine-5-carboxylic acid (7)[43, 228, 338-340]
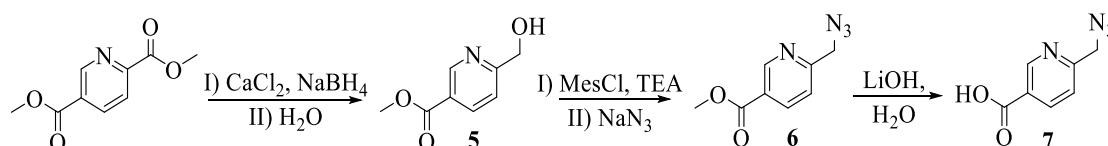
Scheme 2. Synthetic route to obtain 2-(6-azidomethyl)-pyridine-5-carboxylic acid (**7**).

In a two-neck flask calcium chloride (414.5 mmol, 46.0 g) was dried, applying vacuum and simultaneous heating of the powder with a heating gun for 30 minutes. The anhydrous calcium chloride was suspended in dry tetrahydrofuran (200.0 mL) and dry methanol (400.0 mL), followed by the addition of 2,5-pyridinedicarboxylic acid dimethyl ester (205 mmol, 20.0 g) and cooled to 0 °C. Subsequently, sodium borohydride was added in small portions (4 x 103 mmol, 4 x 3.9 g) and the mixture was stirred for further two hours at 0 °C. The reaction was monitored by TLC (SiO$_2$, R$_f$ = 0.63 in ethyl acetate). Once the reaction went to completion, cooled water (400.0 mL) was added and the reaction mixture was extracted with chloroform (4 x 300.0 mL). The combined organic phases were washed with water (3 x 200.0 mL), dried over sodium sulfate and filtered. The solvent was removed under reduced pressure, obtaining 2-(6-hydroxymethyl)-pyridine-5-carboxylic acid methyl ester (**5**) as a colorless solid in a yield of 79%.

<u>^{1}H-NMR (500 MHz, CDCl$_3$):</u> δ = 9.16 (*d*, $^4J_{H,H}$ = 2.1 Hz, 1H, C*H*), 8.29 (*dd*, $^3J_{H,H}$ = 8.1 Hz, $^4J_{H,H}$ = 2.1 Hz, 1H, C*H*), 7.38 (*d*, $^3J_{H,H}$ = 8.1 Hz, 1H, C*H*), 4.83 (*s*, 2H, C*H*$_2$-OH), 3.96 (*s*, 3H, C*H*$_3$), 3.69 (*bs*, 1H, O*H*).

^{13}C-NMR (125 MHz, C*D*Cl$_3$): δ = 165.6 (*C*=O), 163.5 (*C*-CH$_2$OH), 149.9 (*C*H$_{aromat}$), 137.7 (*C*H$_{aromat}$), 124.9 (*C*-COOMe), 120.0 (*C*H$_{aromat}$), 64.3 (*C*H$_2$OH), 52.4 (*C*H$_3$).

ESI-ToF-MS (direct injection, NaI in MeOH 1.0 mg/mL, 0.1 mg/mL) [m/z]: [M+Na]$^+$ C$_8$H$_9$NO$_3$Na$^+$: simulated: 190.0475 g/mol, measured: 190.0441 g/mol.

In a two-neck flask **5** (23.9 mmol, 4.0 g) was suspended in dry DCM (240.0 mL) and cooled to 0 °C. Followed by the addition of methanesulfonyl chloride (25.8 mmol, 2.0 mL) and dry triethylamine (101.0 mmol, 14.0 mL), the mixture was stirred for 60 seconds at 0 °C. The solvent was removed under reduced pressure at 0 °C and the residue was suspended in dry THF (240.0 mL). Sodium azide (126.9 mmol, 8.25 g) was added and the reaction mixture was stirred for further 24 hours at room temperature. The suspension was filtered and the solvent was removed under reduced pressure at 40 °C. The crude product was diluted with water (100.0 mL) and ethyl acetate (200.0 mL). The aqueous phase was extracted with ethyl acetate (3 x 100.0 mL). The combined organic phases were washed with saturated sodium chloride solution (2 x 50.0 mL), dried over sodium sulfate and filtered. The solvent was removed under reduced pressure at 40 °C. The residue was purified by column chromatography (SiO$_2$; R$_f$ = 0.62 in *n*-hexane/ethyl acetate 2:1), obtaining 2-(6-azidomethyl)-pyridine-5-carboxylic acid methyl ester (**6**) as slightly yellow solid in a yield of 81%.

^{1}H-NMR (500 MHz, C*D*Cl$_3$): δ = 9.18 (*d*, $^4J_{H,H}$ = 1.4 Hz, 1H, C*H*), 8.32 (*dd*, $^3J_{H,H}$ = 8.1 Hz, $^4J_{H,H}$ = 2.2 Hz, 1H, C*H*), 7.45 (*d*, $^3J_{H,H}$ = 8.1 Hz, 1H, C*H*), 4.57 (*s*, 2H, C*H*$_2$-N$_3$), 3.96 (*s*, 3H, C*H*$_3$).

^{13}C-NMR (125 MHz, C*D*Cl$_3$): δ = 165.4 (*C*=O), 160.0 (*C*-CH$_2$N$_3$), 150.8 (*C*H$_{aromat}$), 138.1 (*C*H$_{aromat}$), 125.3 (*C*-COOMe), 121.3 (*C*H$_{aromat}$), 55.4 (*C*H$_2$N$_3$), 52.6 (*C*H$_3$).

ESI-ToF-MS (direct injection, NaI in MeOH 1.0 mg/mL, 0.1 mg/mL) [m/z]: [M+Na]$^+$ C$_8$H$_8$N$_4$O$_2$Na$^+$: simulated: 215.0539 g/mol, measured: 215.0471 g/mol.

IR (bulk) [cm^{-1}]: 3413 (w), 3062 (w), 2961 (w), 2113 (s), 1713 (s), 1597 (m), 1437 (m), 1309 (s), 1283 (s), 1120 (m), 758 (w).

In a two-neck flask **6** (10.1 mmol, 1.9 g) was suspended in water (40.0 mL) and methanol (40.0 mL). Lithium hydroxide monohydrate (46.1 mmol, 1.9 g) was added and the solution was stirred for 30 minutes at room temperature. Subsequently, the pH-value was adjusted to 3 by the addition of diluted hydrochloric acid (1.0 M) and methanol was removed under reduced pressure at 40 °C. The aqueous solution was extracted with DCM (5 x 40.0 mL). The combined organic phases were dried over sodium sulfate, filtered and the solvent was removed under reduced pressure. 2-(6-Azidomethyl)-pyridine-4-carboxylic acid (**7**) was afforded as a slight brownish solid in a yield of 87%.

^{1}H-NMR (400 MHz, DMSO-*d*$_6$): δ = 13.41 (*bs*, 1H, COO*H*), 8.99 (*d*, $^4J_{H,H}$ = 2.1 Hz, 1H, C*H*), 8.18 (*dd*, $^3J_{H,H}$ = 7.9 Hz, $^4J_{H,H}$ = 2.0 Hz, 1H, C*H*), 7.34 (*d*, $^3J_{H,H}$ = 7.9 Hz, 1H, C*H*), 4.49 (*s*, 2H, C*H*$_2$-N$_3$).

^{13}C-NMR (100 MHz, DMSO-*d*$_6$): δ = 167.6 (*C*=O), 156.0 (*C*-CH$_2$N$_3$), 151.0 (*C*H$_{aromat}$), 137.9 (*C*H$_{aromat}$), 134.7 (*C*-COOH), 121.7 (*C*H$_{aromat}$), 54.8 (*C*H$_2$-N$_3$).

ESI-ToF-MS (direct injection, NaI in MeOH 1.0 mg/mL, 0.1 mg/mL) [m/z]: [M+H]$^+$ C$_7$H$_7$N$_4$O$_2$$^+$: simulated: 179.0564 g/mol, measured: 179.0664 g/mol.

IR (bulk) [cm^{-1}]: 3074 (s), 2108 (s), 1607 (s), 1589 (s), 1562 (m), 1401 (s), 1368 (s), 1347 (m), 1265 (w), 777 (w).

4.2.2 *In situ* NMR investigations of picolyl azides
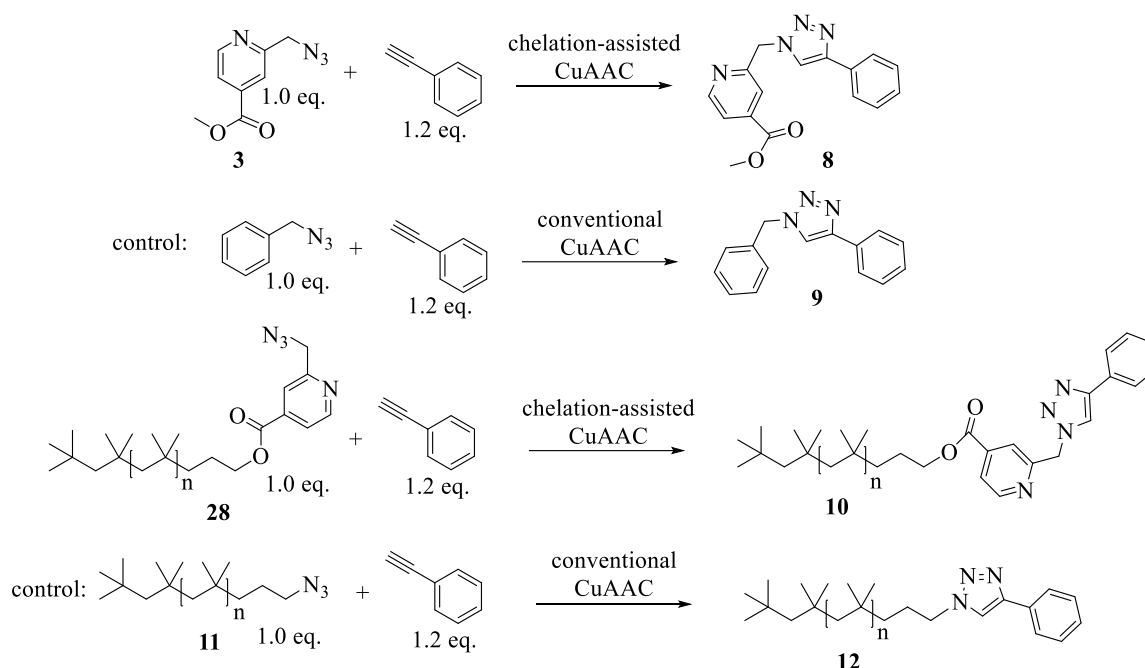
Scheme 3. *In-situ* NMR investigations of the chelation-assisted CuAAC and the conventional CuAAC in deuterated THF.

To determine the conversion efficiency of the ca-CuAAC 2-(6-azidomethyl)-pyridine-4-carboxylic acid methyl ester **3** (78 μmol, 15 mg, 1.0 equivalent) or monovalent picolyl azido telechelic PIB **28** (4.6 μmol, 15.0 mg, 1.0 equivalents) was dissolved in THF-d_8 (0.35 mL), while phenylacetylene (94 μmol, 10.3 μL, 1.2 eq.), the catalyst (0.05 or 0.1 eq.) and DIPEA (0.01, 0.1 or 1.2 eq.) (Table 13, entries 5–8) were separately dissolved in THF-d_8 (0.40 mL). When using 0.01 eq. of DIPEA, a stock solution in THF-d_8 was prepared. Mixing of the azide-containing solution and the alkyne-containing solution was the starting point for the *in situ* NMR experiments. The first NMR-experiment was recorded directly after mixing the solutions. Further experiments were conducted at different defined periods of time, while the corresponding conversion was calculated for each NMR-experiment by comparing the integrals of the CH_2-moiety attached to the azide (educt, e.g **3:** δ = 4.54 ppm) and the CH_2-moiety attached to the triazole ring (product, e.g **8:** δ = 5.79 ppm). Complete disappearing of the CH_2-moiety attached to azide-component represented the complete conversion to **8** or **10**. The same setup was used for control experiments of the CuAAC, exploiting either benzyl azide or azido telechelic PIB (**11**), leading to the formation of **9** or **12**, respectively (see Table 13).

<u>^{1}H-NMR of **8** (tetrahydrofuran-d_8, 400 MHz):</u> δ = 8.72 (*d*, 1H, $^3J_{H,H}$ = 4.8 Hz, N-C*H* of pyridine ring), 8.26 (*s*, 1H, C*H* of triazole-ring), 7.87 (*d*, 2H, $^3J_{H,H}$ = 7.4 Hz, C*H* of phenyl ring), 7.83 (*s*, 1H, C*H* of pyridine ring), 7.78 (*d*, 1H, $^3J_{H,H}$ = 4.9 Hz, C*H* of pyridine ring), 7.45 – 7.21 (*m*, 3H, C*H* of phenyl ring), 5.79 (*s*, 2H, C*H$_2$*-triazole), 3.88 (*s*, 3H, C*H$_3$*).

<u>ESI-ToF-MS of **8** (direct injection, NaI in THF 0.1 mg/mL, 0.1 mg/mL) [m/z]:</u> [M+Na]$^+$ C$_{16}$H$_{14}$N$_4$O$_2$Na$^+$: simulated: 317.1009 g/mol, measured: 317.1150 g/mol; 2nd peak was found for [2M+Na]$^+$ C$_{32}$H$_{28}$N$_8$O$_4$Na$^+$: simulated: 611.2126 g/mol, measured: 611.1289 g/mol.

<u>^{1}H-NMR of **9** (tetrahydrofuran-d_8, 400 MHz):</u> δ = 8.09 (*s*, 1H, C*H* of triazole-ring), 7.84 (*d*, 2H, $^3J_{H,H}$ = 7.7 Hz, C*H* of phenyl ring), 7.46 – 7.19 (*m*, 8H, C*H* of phenyl ring), 5.58 (*s*, 2H, C*H$_2$*-triazole).

<u>^{1}H-NMR of **10**</u> (tetrahydrofuran-d_8, 400 MHz): δ = 8.73 (s, 1H, N-C*H* of pyridine ring), 8.27 (s, 1H, C*H* of triazole-ring), 7.89 – 7.84 (m, 3H, C*H* of pyridine ring + C*H* of phenyl ring), 7.79 (d, 1H, $^3J_{H,H}$ = 5.0 Hz, C*H* of pyridine ring), 7.46 – 7.22 (m, 3H, C*H* of phenyl ring), 5.78 (s, 2H, C*H$_2$*-triazole), 4.28 (t, 2H, $^3J_{H,H}$ = 6.8 Hz, C*H$_2$*-O-C=O), 1.49 (s, C*H$_2$* of repetitive unit), 1.16 (s, C*H$_3$* of repetitive unit), 1.02 (s, 15H, C*H$_3$* groups of initiator).

<u>MALDI-ToF-MS of **10**</u>: While using different matrices, salts and ionization methods, no matching spectrum could be found.

<u>IR of **10**</u> (bulk) [cm^{-1}]: 2950 (s), 2893 (s), 1732 (w), 1472 (m), 1389 (m), 1365 (m), 1228 (m), 949 (w), 909 (w), 760 (w), 735 (w), 694 (w), 631 (m).

<u>^{1}H-NMR of **12**</u> (tetrahydrofuran-d_8, 400 MHz): δ = 7.99 – 7.22 (m, 6H, C*H* of phenyl ring$_{(product + educt)}$ + C*H* of triazole ring), 4.36 (t, 2H, $^3J_{H,H}$ = 7.3 Hz, C*H$_2$*-triazole), 3.23 (t, 2H, $^3J_{H,H}$ = 7.0 Hz, C*H$_2$*-N$_3$), 3.07 (s, 1H, C≡C*H*) 1.42 (s, C*H$_2$* of repetitive unit), 1.11 (s, C*H$_3$* of repetitive unit), 0.99 (s, 15H, C*H$_3$* groups of initiator).

Table 13. (A) Chelation-assisted CuAAC with 2-(6-azidomethyl)-pyridine-4-carboxylic acid methyl ester **3** (m = 15 mg, c = 104 mM) or monovalent picolyl azido telechelic PIB **28** (m = 234 mg, c = 104 mM) and phenylacetylene (m = 9.6 mg, c = 125 mM) at 27 °C in deuterated THF, applying different Cu(I)-catalysts investigated via *in situ* NMR-measurements. (B) CuAAC of benzyl azide or monovalent azido telechelic PIB (**11**) and phenylacetylene, exploiting the same conditions of (A).

entry	azide	catalyst	$m_{catalyst}$ [mg]	[DIPEA] [eq.]	time	conversion [%]
A)	**NMR experiments applying the ca-CuAAC of either 3 or 28 and phenylacetylene**					
1	**3**	[Cu(CH$_3$CN)$_4$]PF$_6$[a)]	2.9	–	24 h	32
2	**3**	Cu(OAc)[a)]	1.0	–	16 h	82
3	**3**	CuBr[a)]	1.1	–	9 h	> 99
4	**3**	CuBr[a)]	1.1	1.2 (c = 125 mM)	< 5 min[d)]	> 99
5	**3**	CuBr[a)]	1.1	0.1 (c = 10.4 mM)	< 5 min[d)]	> 99
6	**3**	CuBr[a)]	1.1	0.01 (c = 1.04 mM)	17 min	> 99
7	**3**	[CuBr(PPh$_3$)$_3$][b)]	3.6	0.01 (c = 1.04 mM)	2 h	10
8	**3**	Cu-TRGO[c)] (4.8 wt%)	2.1	–	24 h	94
9	**3**	Cu/charcoal[a)] (3 wt%)	16.5	–	9 h	< 1
10	**28**	CuBr(PPh$_3$)$_3$[a)]	7.3	–	24 h	32
11	**28**	CuF(PPh$_3$)$_3$ [a)]	6.8	–	11 h	64
12	**28**	CuBr[a)]	1.1	–	42 min	> 99
13	**28**	CuBr[a)]	1.1	0.01 (c = 1.04 mM)	< 4 min[d)]	> 99
B)	**NMR control experiments applying the CuAAC of either benzyl azide or 11 and phenylacetylene**					
14	**benzyl azide**	CuBr[a)]	1.1	0.01 (c = 1.04 mM)	110 min	7
15[e]	**benzyl azide**	Cu-TRGO[c)] (4.8 wt%)	2.1	–	48 h	70
16	**11**	[CuBr(PPh$_3$)$_3$][a)]	7.3	–	24 h	9

a) 0.1 equivalents of catalyst were added. b) 0.05 equivalents of catalyst were added. c) 0.02 equivalents of catalyst were added. d) First NMR-spectrum showed complete conversion. e) Results are adapted from[45].

4.2.3 Synthesis of graphene-based copper(I)-catalysts (15, 17)

Within this work two different heterogeneous Cu(I)-catalysts were obtained. Synthesis of Cu-TRGO was accomplished by starting with graphite and following the Hummers method to obtain graphene-oxide, which was further modified with Cu(II) and reduced in an oven to finally afford catalytically active Cu-TRGO (**15**).[45, 164] Applying identical procedure to exfoliated graphene provided the second heterogeneous catalyst Cu-TREGO (**17**).

4.2.3.1 Synthesis of Cu-TRGO (15)
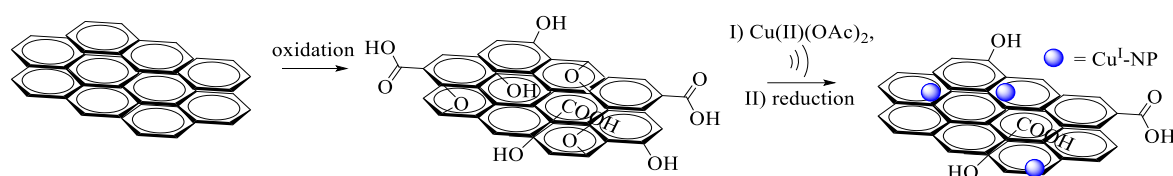
Scheme 4. Synthesis of Cu-TRGO (**15**).

In a three-neck flask graphite (12.0 g) was suspended in concentrated sulfuric acid (96%, 390.0 mL) and sodium nitrite (72.5 mmol, 5.0 g) was added. The suspension was cooled to 0 °C and potassium permanganate (191.0 mmol, 30.0 g) was added in small portions to ensure that the temperature was always kept below 5 °C. The greenish slurry was allowed to warm up to room temperature within two hours and was further stirred for 24 hours. The highly viscous suspension was dropped carefully into a big beaker filled with distilled water (1.0 L) and ice (300.0 g). Subsequently, an aqueous solution of hydrogen peroxide (3 wt%, 300.0 mL) was added and the mixture was stirred over night at room temperature. After intensive vacuum filtration of several days, the remaining residue was washed with an aqueous solution of $HCl:H_2O_2$, 1:1 (5 wt% each of them, 300.0 mL), followed by filtration. This procedure was repeated for five times, until there was no more visible bubbling when pouring the aqueous mixture to the crude product. In turn, the suspension was washed with distilled water. The superfine distributed layers were separated from the solution by centrifugation and simple decanting. This washing step was repeated until the supernatant was of neutral $pH = 7$. The remaining residue was freeze-dried, affording graphene-oxide (**13**).

<u>XRD (wide-angle, PD = 9.85 cm, T = 29 °C):</u> first peak: $2\Theta = 11.168$ °, second peak: $2\Theta = 22.068$ °.

<u>TEM:</u> 1 – 5 μm sized carbon sheets.

Graphene-oxide **13** (1.0 g) and copper(II) acetate (1.65 mmol, 300.0 mg) were suspended in distilled water (300.0 mL) by ultra-sonication for 30 minutes. The suspension was stirred for 24 hours. The crude product was filtered and washed with water, followed by washing with acetone. Freeze-drying of the solid provided graphene-oxide, which was modified with copper(II) (**14**). In the next step, **14** was reduced in an oven at 600 °C, affording copper(I) thermally reduced graphene-oxide (Cu-TRGO, **15**).

<u>XRD (wide-angle, PD = 9.85 cm, T = 29 °C):</u> first peak: $2\Theta = 26.288$ °.

<u>TEM:</u> 1 – 5 μm sized carbon sheets + 10 – 100 nm sized particles.

<u>FAAS:</u> Cu-content = 6.8 wt% Cu/carbon.

4.2.3.2 Synthesis of Cu-TREGO (17)
Exfoliated graphene was synthesized according to published procedure (see chapter 4.1.).[238]

<u>XRD (wide-angle, PD = 9.85 cm, T = 29 °C):</u> first peak: $2\Theta = 12.677$ °, second peak: $2\Theta = 26.454$ °.

<u>TEM:</u> 1 – 5 μm sized carbon sheets.

Exfoliated graphene (1.0 g) and copper(II) acetate (1.65 mmol, 300.0 mg) were suspended in distilled water (300.0 mL) by ultra-sonication for 30 minutes. The suspension was stirred over night. The crude product was washed with water, followed by washing with acetone. Freeze-drying of the solid provided

exfoliated-graphene-oxide modified with copper(II) (**16**). In the next step **16** was reduced in an oven at 600 °C, obtaining copper(I) thermally reduced exfoliated graphene-oxide (Cu-TREGO, **17**).

XRD (wide-angle, PD = 9.85 cm, T = 29 °C): first peak: 2Θ = 26.501 °.

TEM: 1 – 5 μm sized carbon sheets + 10 – 100 nm sized particles.

FAAS: Cu-content = 5.2 wt% Cu/carbon.

4.2.4 Synthesis of trimethylolpropane-tris-(pyridine-2-(6-azidomethyl)-5-carboxylat) (18)
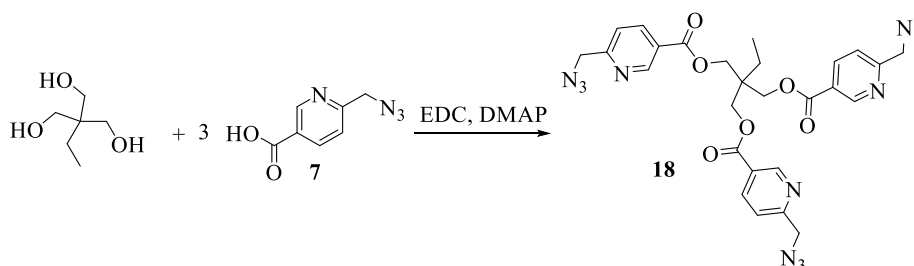
Scheme 5. Synthesis of trimethylolpropane-tris-(pyridine-2-(6-azidomethyl)-5-carboxylat) (**18**).

2-(Hydroxymethyl)-2-ethylpropane-1,3-diol (3.4 mmol, 456.0 mg) and **7** (11.22 mmol, 2.0 g) were suspended in dry DCM (100.0 mL), before DMAP (3.1 mmol, 380.0 mg) was added. The reaction mixture was cooled down to 0 °C, subsequently EDC (12.3 mmol, 2.370 g) was added and the reaction was allowed to warm up to room temperature. The solution was stirred for 24 hours. The solvent was removed under reduced pressure and the obtained residue was diluted with DCM (100.0 mL) and water (100.0 mL). The organic phase was washed twice with a saturated solution of sodium carbonate (50.0 mL) and water (2 x 50.0 mL). The organic phase was dried over sodium sulfate, filtered and the solvent was removed under reduced pressure. Purification was done by column chromatography (SiO$_2$; R$_f$ = 0.4 in *n*-hexane/ethyl acetate 3:2), providing trimethylolpropane-tris-(pyridine-2-(6-azidomethyl)-5-carboxylat) (**18**) as a slightly yellow solid in a yield of 84%.

^{1}H-NMR (500 MHz, C*D*Cl$_3$): δ = 9.15 (*dd*, $^4J_{H,H}$ = 2.2 Hz, $^5J_{H,H}$ = 0.8 Hz, 3H, C*H*), 8.26 (*dd*, $^3J_{H,H}$ = 8.1 Hz, $^4J_{H,H}$ = 2.2 Hz, 3H, C*H*), 7.42 (*dd*, $^3J_{H,H}$ = 8.1 Hz, $^5J_{H,H}$ = 0.8 Hz, 3H, C*H*), 4.56 (*s*, 6H, C*H*$_2$-N$_3$), 4.52 (*s*, 6H, C*H*$_2$-O-C=O), 1.78 (*q*, $^3J_{H,H}$ = 7.6 Hz, 2H, C*H*$_2$) 1.09 (*t*, $^3J_{H,H}$ = 7,6 Hz, 3H, C*H*$_3$).

^{13}C-NMR (125 MHz, C*D*Cl$_3$): δ = 164.5 (*C*=O), 160.5 (*C*-CH$_2$N$_3$), 150.7 (*C*-7), 138.1 (*C*-8), 124.7 (*C*-6), 121.4 (*C*-9), 64.9 (*C*-4), 55.3 (*C*H$_2$-N$_3$), 41.8 (*C*-3), 23.7 (*C*H$_2$), 7.6 (*C*H$_3$).

ESI-ToF-MS (direct injection, NaI in THF 0.1 mg/mL, 0.1 mg/mL) [m/z]: [M+Na]$^+$ C$_{27}$H$_{26}$N$_{12}$O$_6$Na$^+$: simulated: 637.1990 g/mol, measured: 637.1976 g/mol.

IR (bulk) [cm^{-1}]: 2973 (w), 2095 (s), 1710 (s), 1596 (m), 1386 (m), 1260 (s), 1109 (s), 1022 (m), 956 (m), 756 (s).

4.2.5 DSC investigations of picolyl azides (+ NHC-Cu(I)-catalysts)[49]
For DSC investigation **18** (36 μmol, 22.0 mg), trivalent alkyne **20** (36 μmol, 9.0 mg) and anhydrous chlorobenzene (50 wt%) were dissolved in anhydrous DCM (5.0 mL), ensuring a proper diffusion of all components. The solvent was removed under reduced pressure at 0 °C. The flask, containing the mixture, was cooled to – 5 °C. After dispersing the Cu(I)-source (0.03 equivalents = 1 mol% per functional group), the mixture was directly transferred to a DSC-crucible. The crucible was subjected

to the DSC-apparatus and its oven. Subsequently, the crucible and the reference crucible were cooled to – 20 °C with a cooling rate of 20 K/min. Followed by heating to 160 °C, applying a heating rate of 5 K/min. The observed exothermic peak represents the CuAAC "click"-reaction of the components to the final network (see Table 14).
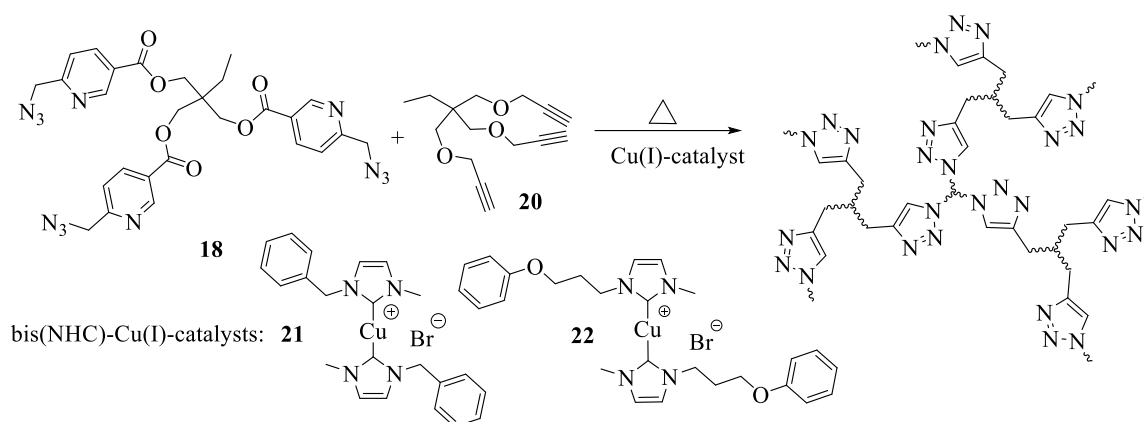
Scheme 6. DSC investigation of network formation of the trivalent azide (**18**) and the trivalent alkyne (**20**), applying the chelation-assisted CuAAC mechanism and different kinds of Cu(I)-catalysts.

Table 14. DSC investigations of „clicking" picolyl azide (**18**) with trivalent alkyne (**20**) to form a network upon the ca-CuAAC.

entry	catalyst	mol% of **18**	base [eq.]	T_{ON} [°C] at 5 K/min	T_P [°C] at 5 K/min
1	without	-	-	90	120
2[a]	[CuBr(PPh₃)₃]	3	-	44	59
3[a]	[CuF(PPh₃)₃]	3	-	27	41
4[a]	Cu-TRGO	3	-	20	38
5	**21**	3	-	90	125
6	**21**	10	-	90	126
7	**22**	10	-	90	126
8	**21**	10	DBN (0.1)	45	91
9	**21**	10	DBU (0.1)	45	77
10	**22**	10	DBN (0.1)	30	64
11	**22**	10	DBU (0.1)	4	40

a) Unpublished work of the working group, see chapter 4.1.

The chelation-assisted CuAAC mechanism was compared with the conventional CuAAC, conducting the same DSC experiments, applying a trivalent terminal azide (**19**) instead of **18** (see scheme 7).
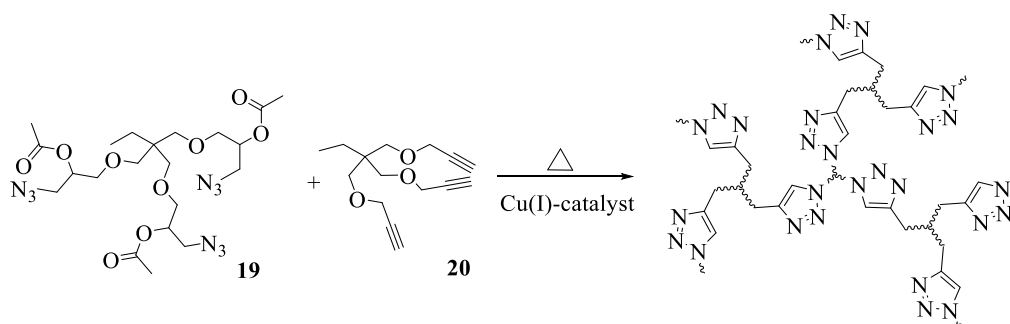
Scheme 7. DSC investigation of network formation of the trivalent azide (**19**) and the trivalent alkyne (**20**), applying the conventional CuAAC mechanism and different Cu(I)-catalysts.

For DSC investigation trivalent azide **19** (112 mmol, 62.4 mg) and trivalent alkyne **20** (112 mmol, 27.8 mg) were dissolved in anhydrous DCM (5.0 mL) to ensure proper diffusion of all components. The solvent was removed under reduced pressure. After dispersing the Cu(I)-source (0.03 equivalents =

1 mol% per functional group), the mixture was directly transferred to a DSC-crucible. The crucible was applied to the DSC-apparatus and its oven. Subsequently, the crucible and the reference crucible were cooled to – 20 °C with a cooling rate of 20 K/min. Followed by heating to 160 °C, applying a heating rate of 5 K/min. The observed exothermic peak represents the CuAAC "click"-reaction of the components to the final network (see Table 15).

Table 15. DSC investigations of „clicking" trivalent azide (**19**) with trivalent alkyne (**20**) to form a network upon the CuAAC.

entry	catalyst	mol% of **19**	T_{ON} [°C] at 5 K/min	T_P [°C] at 5 K/min
1[a)]	without	-	91	133
2[a)]	[CuBr(PPh$_3$)$_3$]	3	59	74
3[a)]	[CuF(PPh$_3$)$_3$]	3	39	66
4	Cu-TRGO (**15**)	3	64	85
5	Cu-TREGO (**17**)	3	55	76

a) Values were adapted from literature[236], see chapter 4.1.

4.2.6 Synthesis of picolyl azido functionalized PIBs (28, 31, 34a-b)

Synthesis of star-shaped picolyl azido telechelic PIBs (**34a**, **34b**) was done, using 1,3,5-tris(2-hydroxy-2-propyl)-benzene (**25**) as initiator in the living carbocationic polymerization (LCCP) of isobutylene according to the literature followed by quenching with allyltrimethylsilane (ATMS) and further end group transformation to the corresponding alcohol according to known procedures.[332-334, 340-341]

4.2.6.1 Synthesis of initiators for LCCP of isobutylene (23-25)
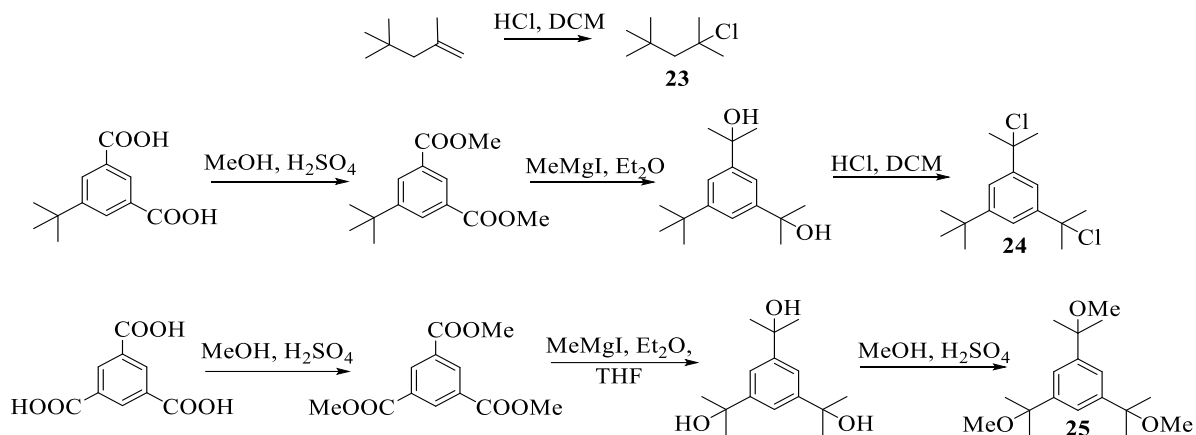
Scheme 8. Synthesis of initiators for LCCP of isobutylene. TMPCl (**23**) for monovalent, DCCl (**24**) for bivalent and TriCuOMe (**25**) for trivalent initiation.

For synthesis details of the monovalent initiator 2-chloro-2,4,4-trimethyl-pentane (TMPCl) (**23**), the bivalent initiator 5-*tert*-butyl-1,3-bis(1-chloro-1-methylethyl)-benzene (DCCl) (**24**) and the trivalent initiator 1,3,5-tris(2-methoxyisopropyl)benzene, (tricumyl methoxy, TriCuOMe) (**25**) for the LCCP of isobutylene see chapter 4.1.

4.2.6.2 Synthesis of picolyl azido telechelic PIBs (28, 31, 34a/b)[335, 340]
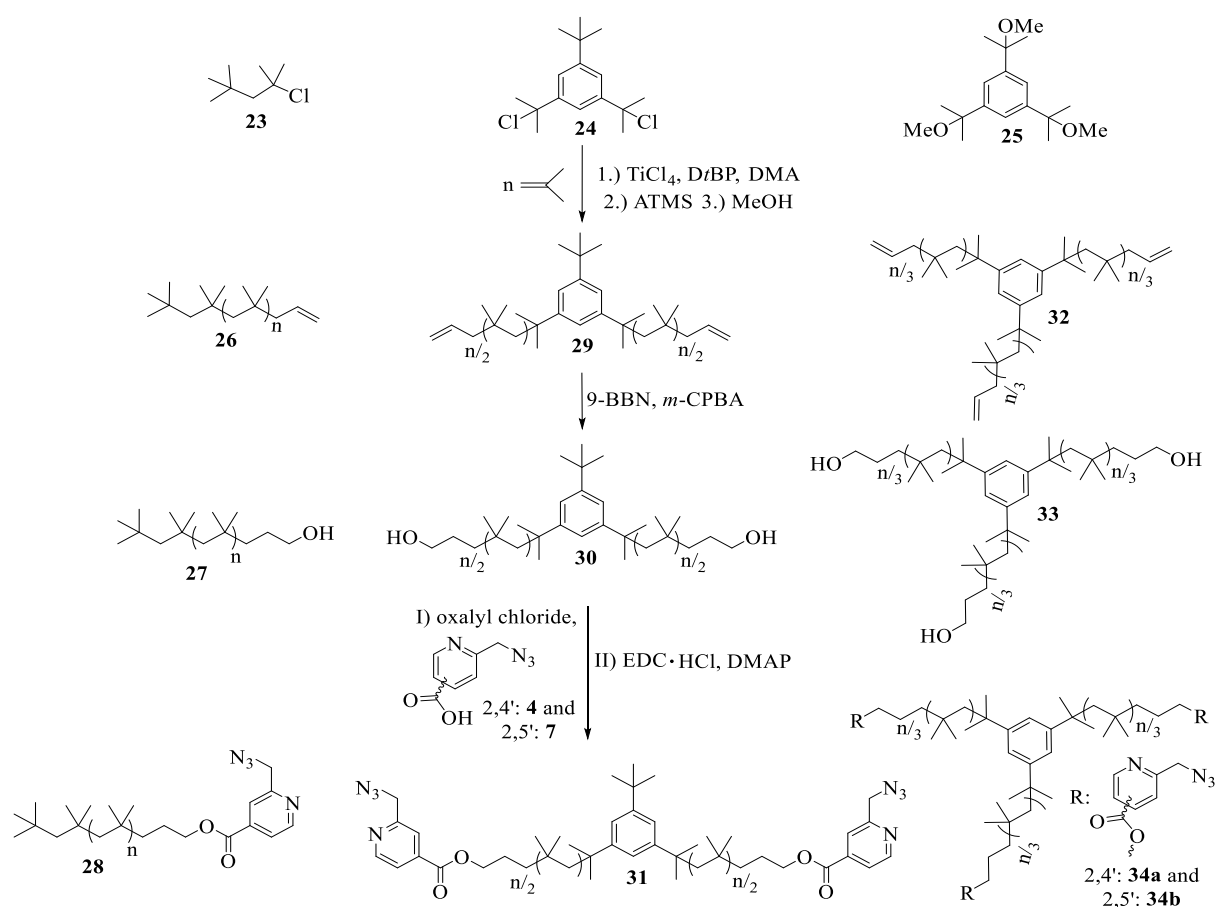
Scheme 9. Synthesis of picolyl azido telechelic PIBs (**28**, **31**, **34a/b**).

In previous investigations the allyl-functionalized PIB precursor (**26**, **29**, **32**) and subsequent transformation to hydroxy telechelic PIBs (**27**, **30**, **33**) were prepared according to the literature.[332-334, 341] In the following 2-(6-azidomethyl)-pyridine-4-carboxylic acid (**4**) (4 eq. per functional group) was dissolved in anhydrous dichloromethane (5.0 mL), followed by the addition of oxalyl chloride (4 eq. per functional group). The reaction was heated under reflux for five hours and then allowed to cool to room temperature. Subsequently, either **27**, **30** or **33** (1 eq.) and 4-(dimethylamino)pyridine (0.5 – 0.6 eq. per functional group) were dissolved in dichloromethane (2.0 – 5.0 mL) and added to the solution. Finally, *N*-(3-dimethylaminopropyl)-*N'*-ethylcarbodiimide hydrochloride (1.5 – 1.6 eq. per functional group) was added to the ice-cooled reaction mixture, which was then heated under reflux for three days. For the exact amount of reactants used to transform hydroxy telechelic PIBs (**27**, **30**, **33**) to picolyl azido telechelic PIBs (**28**, **31**, **34a/b**) see Table 16. In the next step the solution was diluted with dichloromethane (30.0 mL) and filtered. The organic layer was washed with a saturated solution of ammonium chloride (15.0 mL) and dried over sodium sulfate. Filtration, followed by evaporation of the solvent under reduced pressure afforded the crude product, which was purified by dissolving in *n*-hexane and precipitation in 15-fold excess of methanol. The final polymer was dried under high vacuum until a constant weight, providing the picolyl azido telechelic PIBs (**28**, **31**, **34a/b**). For the characterization data of monovalent telechelic PIBs (**26-28**) see Table 17, for bivalent telechelic PIBs (**29-31**) see Table 18 and for trivalent telechelic PIBs (**32-34a/b**) see Table 19.

Table 16. Experimental conditions of PIB transformation from hydroxy- to picolyl azide moiety.

No.	polymer n [μmol]	polymer m [mg]	**4**[a] or **7**[b] n [μmol]	**4**[a] or **7**[b] m [mg]	oxalyl chloride n [μmol]	oxalyl chloride V [μL]	DMAP n [μmol]	DMAP m [mg]	EDC·HCl n [μmol]	EDC·HCl m [mg]
27	56	150	197[a]	35	197	17	31	4	90	17
30	30	100	240[a]	42	240	21	30	4	96	18
33	58	350	674[a, b]	120	674	56	88	11	263	50

a, b) Transformation of hydroxy- group to picolyl azido moiety was performed with both 2,4-regioisomer (**4**) and 2,5-regioisomer (**7**).

Table 17. Characterization data of monovalent telechelic PIB.

polymer	$M_{n(theoretical)}$ [g/mol]	$M_{n(GPC)}$[a] [g/mol]	$M_{n(NMR)}$ [g/mol]	PDI[a]	yield [%]
26	3 500	3 000	3 100[b]	1.16	96
27	3 500	2 700	3 700[c]	1.19	84
28	3 700	3 000	4 100[d]	1.17	89

a) GPC-measurement was performed in THF and PIB-standards were used for the calibration. b) Calculated, according to the ratio of signals at $\delta = 5.84$ ppm of the allylic head group and $\delta = 1.11$ ppm of the repetitive unit (two CH_3-groups), considering the relation of the initiator-part at $\delta = 0.99$ ppm (15 H). c) Calculated, according to the ratio of signals at $\delta = 3.61$ ppm of the CH_2-moiety attached to hydroxy-group and $\delta = 1.11$ ppm of the repetitive unit (two CH_3-groups), considering the relation of the initiator-part at $\delta = 0.99$ ppm (15 H). d) Calculated, according to the ratio of signals at $\delta = 4.33$ ppm of the CH_2-moiety attached to the ester group and $\delta = 1.11$ ppm of the repetitive unit (two CH_3-groups), considering the relation of the initiator-part at $\delta = 0.99$ ppm (15 H).

<u>1H-NMR of **28** (CDCl$_3$, 500 MHz):</u> $\delta = 8.75$ (*d*, 1H, $^3J_{H,H} = 5.0$ Hz, CH), 7.90 (*s*, 1H, CH), 7.80 (*d*, 1H, $^3J_{H,H} = 5.0$ Hz, CH), 4.57 (*s*, 2H, CH_2-N$_3$), 4.33 (*t*, 2H, $^3J_{H,H} = 6.8$ Hz, CH_2-O-C=O), 1.42 (*s*, CH_2 of repetitive unit), 1.11 (*s*, CH_3 of repetitive unit), 0.99 (*s*, 15H, CH_3 groups of initiator).

<u>MALDI-ToF-MS of **28** [DCTB, AgTFA or NaTFA] [m/z]:</u> Two monovalent azido telechelic PIB species were found with additional silver cation as [M+Ag]$^+$ for (C$_4$H$_8$)$_{34}$C$_{18}$H$_{28}$N$_4$O$_2$Ag$^+$ simulated 2348.259 g/mol, found 2348.375 g/mol; with additional sodium trifluoroacetic acid and proton cation as [M+NaTFA+H]$^+$ for (C$_4$H$_8$)$_{33}$C$_{18}$H$_{28}$N$_4$O$_2$C$_2$F$_3$O$_2$NaH$^+$ simulated 2320.272 g/mol, found 2320.655 g/mol.

<u>IR of **28** (bulk) [cm^{-1}]:</u> 2950 (s), 2892 (s), 2103 (w), 1734 (w), 1471 (m), 1389 (m), 1365 (m), 1229 (m), 949 (w), 923 (w), 763 (w).

Table 18. Characterization data of the bivalent telechelic PIB.

polymer	$M_{n(theoretical)}$ [g/mol]	$M_{n(GPC)}$[a] [g/mol]	$M_{n(NMR)}$ [g/mol]	PDI[a]	yield [%]
29	3 000	3 500	3 400[b]	1.18	97
30	3 000	3 300	3 900[c]	1.22	93
31	3 400	4 000	4 100[d]	1.21	60

a) GPC-measurement was performed in THF and PIB-standards were used for the calibration. b) Calculated, according to the ratio of signals at $\delta = 5.84$ ppm of the allylic head group and $\delta = 1.11$ ppm of the repetitive unit (two CH_3-groups), considering the relation of the initiator-part at $\delta = 0.79$ ppm (12 H). c) Calculated, according to the ratio of signals at $\delta = 3.61$ ppm of the CH_2-moiety attached to hydroxyl-group and $\delta = 1.11$ ppm of the repetitive unit (two CH_3-groups), considering the relation of the initiator-part at $\delta = 0.79$ ppm (12 H). d) Calculated, according to the ratio of signals at $\delta = 4.33$ ppm of the CH_2-moiety attached to the ester group and $\delta = 1.11$ ppm of the repetitive unit (two CH_3-groups), considering the relation of the initiator-part at $\delta = 0.79$ ppm (12 H).

<u>1H-NMR of **31** (CDCl$_3$, 500 MHz):</u> $\delta = 8.75$ (*d*, 2H, $^3J_{H,H} = 5.1$ Hz, CH), 7.90 (s, 2H, CH), 7.80 (*d*, 2H, $^3J_{H,H} = 5.1$ Hz, CH), 7.17 (*s*, 3H, CH of initiator), 4.57 (*s*, 4H, CH_2-N$_3$), 4.33 (*t*, 4H, $^3J_{H,H} = 6.8$ Hz, CH_2-O-C=O), 1.83 (*s*, 4H, CH_2), 1.41 (*s*, CH_2 of repetitive unit), 1.11 (*s*, CH_3 of repetitive unit), 0.79 (*s*, 12H, CH_3 of initiator).

<u>IR (bulk) of **31** [cm^{-1}]:</u> 2950 (s), 2894 (s), 2104 (w), 1734 (w), 1471 (s), 1389 (s), 1365 (s), 1230 (s), 1112 (w), 949 (w), 923 (w), 762 (w), 717 (w), 686 (w).

The synthetic route to obtain **34b** was the same as described for **34a**, now applying esterification agent **7** instead of its stereo-analogue **4**. The conversion was 80%, meaning that product **34b** was still mixed with unconverted **33** to an extent of 20 %. The final polymer was dried under high vacuum until a constant weight, providing trivalent azido telechelic PIB (**34b**) in a yield of 57%.

Table 19. Characterization data of trivalent telechelic PIB.

polymer	$M_{n(theoretical)}$ [g/mol]	$M_{n(GPC)}$[a)][g/mol]	$M_{n(NMR)}$ [g/mol]	PDI[a)]	yield [%]
32	6 000	4 500	6 300[b)]	1.34	85
33	6 000	5 000	7 300[c)]	1.32	76
34a	6 500	6 500	6 600[d)]	1.33	52
34b	6 500	5 800	6 800[d)]	1.31	57

a) GPC-measurement was performed in THF and PIB-standards were used for the calibration. b) Calculated, according to the ratio of signals at $\delta = 5.84$ ppm of the allylic head group and $\delta = 1.11$ ppm of the repetitive unit (two CH_3-groups), considering the relation of the initiator-part at $\delta = 0.80$ ppm (18 H). c) Calculated, according to the ratio of signals at $\delta = 3.61$ ppm of the CH_2-moiety attached to hydroxyl-group and $\delta = 1.11$ ppm of the repetitive unit (two CH_3-groups), considering the relation of the initiator-part at $\delta = 0.80$ ppm (18 H). d) Calculated, according to the ratio of signals at $\delta = 4.33$ ppm of the CH_2-moiety attached to the ester group and $\delta = 1.11$ ppm of the repetitive unit (two CH_3-groups), considering the relation of the initiator-part at $\delta = 0.80$ ppm (18 H).

<u>^{1}H-NMR of **34a**</u> (CDCl$_3$, 500 MHz): $\delta = 8.76$ (d, 3H, $^3J_{H,H} = 5.0$ Hz, CH), 7.90 (s, 3H, CH), 7.80 (dd, 3H, $^3J_{H,H} = 5.0$ Hz, $^4J_{H,H} = 1.1$ Hz, CH), 7.13 (s, 3H, CH of initiator), 4.57 (s, 6H, CH_2-N$_3$), 4.33 (t, 6H, $^3J_{H,H} = 6.8$ Hz, CH_2-O-C=O), 1.85 (s, 6H, CH_2), 1.41 (s, CH_2 of repetitive unit), 1.11 (s, CH_3 of repetitive unit), 0.80 (s, 18H, CH_3 of initiator).

<u>MALDI-ToF-MS of **34a**</u>: [M+Ag]$^+$ for (C$_4$H$_8$)$_{88}$C$_{45}$H$_{54}$N$_{12}$O$_6$Ag$^+$ simulated 5903.856 g/mol, found 5903.266 g/mol.

<u>IR (bulk) of **34a**</u> [cm^{-1}]: 2950 (s), 2892 (s), 2103 (w), 1734 (w), 1472 (m), 1390 (m), 1365 (m), 1229 (m), 949 (w), 923 (w), 763 (w), 662 (w), 632 (w).

<u>^{1}H-NMR of **34b**</u> (CDCl$_3$, 400 MHz): $\delta = 9.20$ (s, 3H, CH), 8.34 (dd, 3H, $^3J_{H,H} = 8.1$ Hz, $^4J_{H,H} = 2.1$ Hz, CH), 7.46 (d, 3H, $^3J_{H,H} = 8.1$ Hz, CH), 7.14 (s, 3H, CH of initiator), 4.58 (s, 6H, CH_2), 4.34 (t, 6H, $^3J_{H,H} = 6.7$ Hz, CH_2), 1.86 (s, 6H, CH_2), 1.43 (s, CH_2 of repetitive unit), 1.12 (s, CH_3 of repetitive unit), 0.81 (s, 18H, CH_3 of initiator).

<u>IR (bulk) of **34b**</u> [cm^{-1}]: 2950 (s), 2893 (s), 2105 (w), 1729 (w), 1598 (w), 1471 (m), 1389 (m), 1365 (m), 1284 (w), 1229 (m), 1119 (w), 1025 (w), 949 (w), 924 (w), 758 (w), 632 (w).

4.2.7 Investigation of network-formation via rheology at low temperatures[40, 47, 308-311, 340]
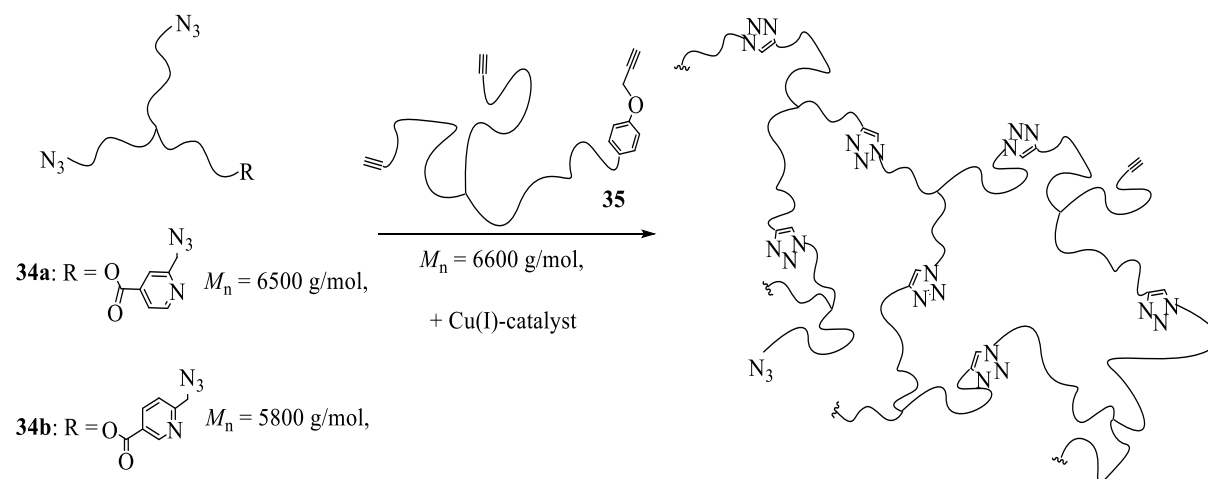
Scheme 10. Crosslinking experiments of star-shaped PIBs (**34a** and **34b**) and **35** at different temperatures.

For crosslinking experiments the picolyl azido functionalized and star-shaped PIB **34a** or **34b** (30.0 mg, 1.0 eq.) and the alkyne functionalized and star-shaped PIB (**35**) (26.0 mg, 1.0 eq.) were put in a vial and dissolved in anhydrous CHCl₃. After mixing both solutions and evaporation of the solvent under reduced pressure, the obtained polymer mixture was dried under high vacuum. The catalyst (CuBr, [CuBr(PPh₃)₃] or [CuF(PPh₃)₃]) (0.1 eq. per functional group) was dissolved in CHCl₃ (20 μL) and added as a stock solution to the polymer blend. In cases of CuBr and [CuBr(PPh₃)₃], *N,N*-diisopropylethylamine (DIPEA) (0.01 or 0.1 eq. per functional group) was additionally added as a stock solution. Subsequently, the reaction mixture was mixed with a spatula and was immediately put on the rheometer plate. Crosslinking experiments were performed with a strain γ of 0.1% and with an angular frequency ω ranging from 100 to 1 rad s⁻¹. Gelation times were determined as a crossover of the storage (G') and loss modulus (G'') at 10 rad s⁻¹. Each measurement was stopped when the values of loss and storage modulus stayed constant (to two decimal places) for at least one hour. This time was considered as the total time. The determined plateau moduli corresponded to the storage moduli measured at this total time at 100 Hz. Measurements were conducted at different temperatures (see Table 20).

Table 20. Network formation of star-shaped azido telechelic PIBs (**34a** or **34b**) and PIB-alkyne (**35**) using the chelation-assisted CuAAC to enable fast self-healing at low temperatures (10 °C) monitored via melt rheology measurements.

ent.	poly-mer	catalyst	DIPEA [eq.]	T [°C]	$t_{(Gel)}$[a] [min]	c_M [M]	c_{Cu} [M] (*10⁻²)	k_0 [M⁻³ min⁻¹]	$k_{crossover}$ [M⁻³ min⁻¹]	r_0 [M min⁻¹]
1	**34a**	CuBr	0.01	20	870	0.254	2.54	-	-	-
2	**34a**	[CuBr(PPh₃)₃]	0.01	20	255	0.254	2.54	2 200	7 300	0.092
3	**34a**	[CuBr(PPh₃)₃]	0.1	20	266	0.254	2.54	400	1 000	0.017
4	**34a**	[CuF(PPh₃)₃]	-	20	15	0.254	2.54	_[b]	_[b]	_[b]
5	**34b**	[CuF(PPh₃)₃]	-	20	29	0.200	2.00	3 100	9 100	0.050
6	**34b**	[CuF(PPh₃)₃]	-	10	71	0.200	2.00	2 500	7 500	0.041
7	**34b**	[CuF(PPh₃)₃]	-	5	663	0.200	2.00	_[c]	_[c]	_[c]

a) Determined via melt rheology, $G'' = G'$ at ω = 10 Hz. b) Reaction was too fast for determination. c) Water was disturbing the measurement.

IR of network (bulk) [cm⁻¹]: 2950 (s), 2892 (s), 1731 (w), 1599 (w), 1471 (m), 1389 (m), 1365 (m), 1292 (w), 1229 (m), 1118 (w), 1033 (w), 949 (w), 924 (w), 828 (w), 722 (w), 694 (w).

4.2.8 Synthesis of 3-azido-7-hydroxy-coumarin (36)[342]
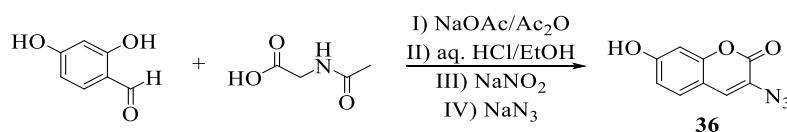
Scheme 11. Synthesis of 3-azido-7-hydroxy-coumarin (**36**).

Acetic anhydride (150.0 mL) was filled in a three-neck flask equipped with a reflux-condenser, a gas-tap and a stopper. 2,4-Dihydroxybenzaldehyde (30.0 mmol, 4.15 g, 1.0 eq.), *N*-acetyl-glycine (30.0 mmol, 3.53 g, 1.0 eq.) and anhydrous sodium acetate (120.0 mmol, 9.15 g, 4.0 eq.) were carefully added to the stirred solution. The mixture was heated to reflux for six hours, followed by pouring it to an ice-bath (750.0 mL). The brownish residue was filtered by suction-filtration and washed with cold distilled water for several times. The crude product was diluted with HCl (36 wt%)/EtOH 2:1 (90.0 mL) and heated until reflux for one hour. Subsequently, ice-cooled water (40.0 mL) was added and the reaction-mixture was cooled to 0 °C. Sodium nitrite (60.0 mmol, 4.16 g, 2.0 eq.) and sodium azide (90.0 mmol, 5.85 g, 3.0 eq.), each of them dissolved in water (10.0 mL), were added to the stirred

solution over a period of two hours, keeping the temperature below 5 °C. The mixture was stirred for further 15 minutes at room temperature. In the next step the product was separated by filtration, followed by washing with water for several times. Final drying in high vacuum provided 3-azido-7-hydroxy-coumarin (**36**) as brownish solid in a yield of 16%. Experimental spectra can be found in the appendix 7.8.

^{1}H-NMR (DMSO-d_6, 400 MHz): δ = 10.52 (*s*, 1H, O*H*), 7.58 (*s*, 1H, C*H*), 7.47 (*d*, 1H, $^3J_{H,H}$ = 8.5 Hz, C*H*), 6.80 (*dd*, 1H, $^3J_{H,H}$ = 8.5 Hz, $^4J_{H,H}$ = 2.3 Hz, C*H*), 6.75 (*d*, 1H, $^4J_{H,H}$ = 2.2 Hz, C*H*).

^{13}C-NMR (DMSO-d_6, 100 MHz): δ = 160.3 (*C*-OH), 157.3 (*C*-O-C=O), 152.7 (*C*=O), 129.1 (*C*H), 127.8 (*C*H), 121.1 (*C*-N$_3$), 113.8 (*C*H), 111.3 (*C*$_{quart.}$), 102.0 (*C*H).

ESI-ToF-MS (direct injection, without addition of salt, THF 0.01 mg/mL) [*m/z*]: [M-H]$^-$ C$_9$H$_4$N$_3$O$_3$$^-$: simulated: 202.026 g/mol, measured: 202.025 g/mol.

IR (bulk) [cm^{-1}]: 3300 (w), 3050 (w), 2113 (s), 1679 (s), 1600 (s), 1454 (w), 1372 (m), 1342 (s), 1317 (s), 1299 (s), 1257 (s), 1213 (s), 1154 (s), 1123 (s), 1065 (m), 922 (m), 856 (s), 836 (s), 750 (s), 625 (s), 583 (m).

4.2.9 Synthesis and testing of the autonomous SH approach (PIB-matrix)
4.2.9.1 Synthesis of high molecular weight PIB SH-system (37a)[39, 240, 340]

Scheme 12. Embedding procedure of SH-components to high molecular weight PIB.

The scaffolding matrix of the SH-specimen (3 g) consisted of high molecular weight PIB ($\sim$ 210 000 g/mol, 2.49 g), which was dissolved in *n*-hexane (40.0 mL) overnight. To this highly viscous mixture, star-shaped picolyl azido telechelic PIB (**34b**) (5 wt%, 146.0 mg) dissolved in *n*-hexane (1.0 mL), UF-capsules, containing (2,2-bis(prop-2-2-ynyloxymethyl)-1-(prop-2-ynyloxy)butane (**20**) (10 wt%, 300.0 mg), [CuBr(PPh$_3$)$_3$] (2 wt%, 60.0 mg) and 3-azido-7-hydroxy-coumarin **36** (2.5 wt% of **34b**, 4.0 mg) were added. The components were homogeneously mixed by using a VORTEX-GENIE® touch mixer. The pressure was reduced carefully to 150 mbar and kept at this level for at least ten minutes to get rid of air-bubbles. The viscous mixture was poured into a mold and kept at 50 °C overnight. A specimen of approximate dimensions of 5 mm × 13 mm × 0.8 mm was cut out with a razor blade, yielding **37a**. For control experiments a second specimen was synthesized without catalyst ([CuBr(PPh$_3$)$_3$]), therefore the amount of high molecular weight PIB was increased to 2.55 g, representing **37b**.

In previous attempts pure PDMS-matrices and PDMS-PIB-blends as embedding materials were tested unsuccessfully (see Table 21). At first, optimal conditions (vacuum, form and size of mold) needed to be found to obtain air-bubble free specimen (Table 21, entry 1-4). Followed by attempts to introduce

UF-capsules, applying a layer by layer strategy (Table 21, entry 5-6), leading to rejection of the layers or the collection of capsules at the ground of the mold. Further attempts were made, using PDMS-PIB blends (90:10 or 95:5), which however led in all cases to rejection of the different matrix compositions (Table 21, entry 7-11). Thus, PIB-matrix was applied, affording a neat specimen (Table 21, entry 12), which was also compatible with capsule- and PIB fillers (Table 21, entry 13), enabling the synthesis of the SH specimen **37a** (Table 21, entry 14) and the control specimen **37b** (Table 21, entry 15). For photographs of different attempts see also appendix 7.9.

Table 21. Embedding attempts of SH-components to different polymer-matrices to finally obtain a SH-specimen.

entry	polymer	catalyst	matrix	alkyne	attempts	observations
1	-	-	PDMS	-	temperature curing	bubbles in matrix
2	-	-	PDMS	-	vacuum over night	destroyed matrix
3	-	-	PDMS	-	vacuum (2 min)[a]	neat thin blank
4	-	-	PDMS	-	stretched deep mold	insufficient curing
5	-	-	PDMS	-	double layer + round mold[b]	neat layers reject each other
6	-	-	PDMS	10 wt%	triple layer (neat-alkyne-neat)	capsules collect at the ground
7	-	-	PDMS-PIB, 95:5	-	test of compatibility	rejection
8	-	-	PDMS-PIB, 90:10	-	test of compatibility	rejection
9	-	2.0 wt%	PDMS-PIB, 95:5	15 wt%	test of compatibility	rejection
10	-	-	PDMS-PIB, 95:5	15 wt%	test of compatibility	rejection
11	-	0.7 wt%	PDMS-PDMS:PIB, 95:5-PDMS	10 wt%	test of compatibility (triple layer)	rejection
12	-	-	PIB	-	vacuum (2 min), round deep mold	neat blank
13	5.0 wt%	2.0 wt%	PIB	10 wt%	random PIB used	neat test specimen
14	5.0 wt%	2.0 wt%	PIB	10 wt%	SH specimen[c]	neat **37a**
15	5.0 wt%	-	PIB	10 wt%	control-specimen[c]	neat **37b**

a) Once, the problem of appearing bubbles inside the matrix was solved, this procedure was applied to all following attempts. b) Drying in deep round mold was more efficient than in stretched mold, thus the round mold was used for all following attempts. c) Coumarin azide (**36**) (2.5 wt% of **34b**) was added.

4.2.9.2 Detection of SH via fluorogenic scratch-experiment (PIB-system)[51, 340]

Scheme 13. Scratch experiments of SH-specimen monitored via fluorescence measurements.

The specimen (**37a**), containing the star-shaped picolyl azido telechelic PIB (**34b**, 5 wt%, 146 mg), micron-sized UF-capsules with an average hydrodynamic diameter of $6 - 8$ μm filled with a trivalent alkyne (2,2-bis(prop- 2-2-ynyloxymethyl)-1-(prop-2-ynyloxy)butane (**20**) (10 wt%, 300 mg), the Cu(I)-source ([CuBr(PPh$_3$)$_3$], 2 wt%, 60 mg) and 3-azido-7-hydroxy-coumarin **36** (2.5 wt% of **34b**, 4 mg) was

scratched several times with a razor blade. The specimen was subsequently put in between two glass quartz plates and fixed within the sample holder. The measured fluorescence emission was increasing in consequence of the formation of the highly fluorogenic "click" product (λ_{ex} = 330 nm, λ_{em} = 450 nm). The fluorogenic "click"-reaction within the PIB-matrix was measured every five minutes over a course of 24 hours at room temperature. Same procedure was employed to control-specimen **37b** (without Cu(I)-catalyst). In a second control experiment, using unscratched specimen **37a**, measurement was performed every five minutes over a period of six hours.

4.3 Synthesis of an autonomous and capsule-free sensing approach
4.3.1 Synthesis of CTAs for RAFT polymerization
4.3.1.1 Synthesis of CTA-IL (40, 43)[343-345]

Scheme 14. Synthetic route to obtain CTA-IL (**40**).

N-Methylimidazole (50.4 mmol, 4.0 mL) and 11-bromo-undecanol (55.4 mmol, 13.9 g) were dissolved in chloroform and heated under reflux for 24 hours. The solvent was evaporated subsequently under reduced pressure and the crude product was washed with diethyl ether (three times x 10.0 mL). The highly viscous oil was dissolved in DCM (15.0 mL) and dried over sodium sulfate. Followed by filtration and removing of the solvent under reduced pressure. Drying at high vacuum afforded 3-(11-hydroxyundecyl)-1-methylimidazolium bromide (**38**) as a colorless oil in a yield of 92%.

<u>^{1}H-NMR (DMSO-d_6, 400 MHz):</u> δ = 9.19 (*s*, 1H, N-C*H*-N), 7.78 (*t*, 1H, $^3J_{H,H}$ = 7.8 Hz, C*H*), 7.71 (*t*, 1H, $^3J_{H,H}$ = 7.8 Hz, C*H*), 4.29 (*t*, 2H, $^3J_{H,H}$ = 5.1 Hz, O*H*), 4.14 (*t*, 2H, $^3J_{H,H}$ = 7.2 Hz, N-C*H*$_2$), 3.84 (*s*, 3H, C*H*$_3$), 3.34 (*q*, 2H, $^3J_{H,H}$ = 6.4 Hz, C*H*$_2$-OH), 1.76 (*quint*, 2H, $^3J_{H,H}$ = 7.3 Hz, C*H*$_2$), 1.36 (*quint*, 2H, $^3J_{H,H}$ = 6.4 Hz, C*H*$_2$), 1.28 − 1.18 (*m*, 14H, C*H*$_2$).

<u>^{13}C-NMR (DMSO-d_6, 100 MHz):</u> δ = 136.5 (N-*C*H-N), 123.5 (*C*H), 122.2 (*C*H), 60.6 (*C*H$_2$-OH), 48.7 (N-*C*H$_2$), 35.7 (*C*H$_3$), 32.5 (*C*H$_2$), 29.3, 29.0, 28.9, 28.9, 28.8, 28.3, 25.5, 25.4.

<u>ESI-ToF-MS (direct injection, without addition of salt, MeOH 0.001 mg/mL) [m/z]:</u> [M]$^+$ C$_{15}$H$_{29}$N$_2$O$^+$: simulated: 253.227 g/mol, measured: 253.230 g/mol.

3-(11-Hydroxyundecyl)-1-methylimidazolium bromide (**38**) (45.0 mmol, 15.0 g, 1.0 eq.) was dissolved in anhydrous DCM and 2-bromo-propionic acid bromide (135.0 mmol, 29.1 g, 3.0 eq.) was added in drops over a period of 30 minutes. The reaction was allowed to stir for 48 hours at room temperature. The solvent was evaporated under reduced pressure and the crude product was diluted with water (20.0 mL), followed by the addition of lithium bis(trifluoromethane)sulfonimide (49.5 mmol, 14.2 g, 1.1 eq.). The resulting suspension was extracted five times with DCM (each 20.0 mL). The combined

organic layers were dried over magnesium sulfate and filtered. Removing the solvent under reduced pressure provided 3-(11-(2-brompropionyloxy)undecyl)-methyl-1-imidazolium bis(trifluoromethane)sulfonimide (**39**) as a colorless oil in a yield of 87%.

<u>^{1}H-NMR (CDCl$_3$, 400 MHz):</u> δ = 8.75 (*s*, 1H, N-C*H*-N), 7.31 (*t*, 1H, $^3J_{H,H}$ = 1.8 Hz, C*H*), 7.29 (*t*, 1H, $^3J_{H,H}$ = 1.8 Hz, C*H*), 4.36 (*q*, 2H, $^3J_{H,H}$ = 6.9 Hz, H$_3$C-C*H*), 4.20 − 4.09 (*m*, 4H, C*H*$_2$), 3.94 (*s*, 3H, N-C*H*$_3$), 1.90 − 1.81 (*m*, 2H, C*H*$_2$), 1.81 (*d*, 2H, $^3J_{H,H}$ = 6.9 Hz, HC-C*H*$_3$), 1.65 (*quint*, 2H, $^3J_{H,H}$ = 6.6 Hz, C*H*$_2$), 1.41 − 1.20 (*m*, 14H, C*H*$_2$).

<u>^{13}C-NMR (CDCl$_3$, 100 MHz):</u> δ = 170.3 (*C*=O), 136.1 (N-CH-N), 123.6 (*C*H), 122.2 (*C*H), 119.9 (*q*, *J* = 321.2 Hz, *C*F$_3$), 66.1 (*C*H$_2$-O), 50.2 (N-*C*H$_2$), 40.4 (H$_3$C-*C*H), 36.3 (N-*C*H$_3$), 30.0 (*C*H$_2$), 29.3, 29.2, 29.1, 29.0, 28.8, 28.3, 26.1, 25.6, 21.7 (HC-*C*H$_3$).

<u>^{19}F-NMR (CDCl$_3$, 375 MHz):</u> δ = -79.00 (C*F*3).

<u>ESI-ToF-MS (direct injection, without addition of salt, THF 0.001 mg/mL) [*m/z*]:</u> (positive mode) [M]$^+$ C$_{18}$H$_{32}$N$_2$O$_2$Br$^+$: simulated: 387.164 g/mol, measured: 387.166 g/mol. (negative mode) [NTf$_2$]$^-$ C$_2$F$_6$NO$_4$S$_2^-$: simulated: 279.918 g/mol, measured: 279.951 g/mol.

1-Butanethiol (361 mg, 4.5 mmol, 1.1 eq.) was dissolved in a mixture of distilled water (3.0 mL), aqueous sodium hydroxide solution (0.36 g, 50 wt%) and acetone (1.0 mL) and stirred at room temperature for 30 min. Subsequently, the solution was cooled to 0 °C and carbon disulfide (343 mg, 4.5 mmol, 1.1 eq.) was added dropwise and stirred for further 30 min at room temperature. The yellowish solution was cooled below 10 °C and **39** (2.74 g, 4.1 mmol, 1.0 eq.) was added in the countercurrent of argon. Distilled water (3.0 mL) was added and the reaction mixture was stirred overnight at room temperature. The solution was diluted with water (5.0 mL), extracted with dichloromethane (DCM) (3 x 20.0 mL) and the combined organic layers were dried over magnesium sulfate. The solvent was removed under reduced pressure, providing the crude product, which was finally purified by column chromatography on silica (solvent mixture DCM/MeOH 4:1, TLC: R$_f$ = 0.1 in pure DCM), obtaining 1-((11-(3-methylimidazolium)un-decyloxy)carbonyl)ethyl butyl carbonotrithioate bis(trifluormethyl)sulfonimide (**40**) as a yellow oil in yields of 96%.

<u>^{1}H-NMR (CDCl$_3$, 400 MHz):</u> δ = 8.79 (*s*, 1H, N-C*H*-N), 7.29 (*t*, 1H, $^3J_{H,H}$ = 1.6 Hz, C*H*), 7.27 (*t*, 1H, $^3J_{H,H}$ = 1.7 Hz, C*H*), 4.79 (*q*, 2H, $^3J_{H,H}$ = 7.4 Hz, H$_3$C-C*H*), 4.17 (*t*, 2H, $^3J_{H,H}$ = 7.5 Hz,O-C*H*$_2$), 4.12 (*dt*, 2H, $^3J_{H,H}$ = 6.7, $^4J_{H,H}$ = 3.5 Hz, N-C*H*$_2$), 3.95 (*s*, 3H, N-C*H*$_3$), 3.35 (*dt*, 2H, $^3J_{H,H}$ = 7.3, $^4J_{H,H}$ = 1.0 Hz, S-C*H*$_2$), 1.86 (*quint*, 2H, $^3J_{H,H}$ = 7.3 Hz, C*H*$_2$), 1.71 − 1.61 (*m*, 4H, C*H*$_2$), 1.60 (*d*, 3H, $^3J_{H,H}$ = 7.4 Hz, HC-C*H*$_3$), 1.42 (*sext*, 2H, $^3J_{H,H}$ = 7.4 Hz, H$_3$C-C*H*$_2$), 1.37 − 1.23 (*m*, 14H, C*H*$_2$), 0.93 (*t*, 3H, $^3J_{H,H}$ = 7.4 Hz, H$_2$C-C*H*$_3$).

<u>^{13}C-NMR (CDCl$_3$, 100 MHz):</u> δ = 222.1 (*C*=S), 171.2 (*C*=O), 136.3 (N-CH-N), 123.6 (*C*H), 122.1 (*C*H), 119.8 (*q*, *J* = 321.2 Hz, *C*F$_3$), 65.9 (*C*H$_2$-O), 50.3 (N-*C*H$_2$), 48.1 (H$_3$C-*C*H), 36.9 (N-*C*H$_3$), 36.4 (S-*C*H$_2$), 30.0 (*C*H$_2$), 29.9, 29.3, 29.3, 29.1, 29.0, 28.8, 28.4, 26.1, 25.7, 22.0 (H$_3$C-*C*H$_2$), 16.9 (HC-*C*H$_3$), 13.6 (H$_2$C-*C*H$_3$).

<u>ESI-ToF-MS (direct injection, without addition of salt, THF 0.001 mg/mL) [*m/z*]:</u> (positive mode) [M]$^+$ C$_{23}$H$_{41}$N$_2$O$_2$S$_3^+$: simulated: 473.232 g/mol, measured: 473.230 g/mol. (negative mode) [NTf$_2$]$^-$ C$_2$F$_6$NO$_4$S$_2^-$: simulated: 279.918 g/mol, measured: 280.014 g/mol.

A previous synthesis strategy made use of a tertiary bromide, providing in the last step a mixture of 1-((11-(3-methylimidazolium)propyloxy)carbonyl)2-methyl-ethyl butyl carbonotrithioate

bis(trifluormethyl)sulfonimide (**43**) and 3-(11-(2-bromo-2-methyl-propionyloxy)propyl)-methyl-1-imidazolium bis(trifluoromethane)sulfonimide (**42**) in turn of insufficient conversion and purification:

Scheme 15. Synthetic route attempt to obtain CTA-IL (**43**).

N-Methylimidazole (50.4 mmol, 4.0 mL) and 3-chloro-propanol (55.4 mmol, 4.63 mL) were mixed in a one-neck flask and heated to 80 °C for 24 hours. Cooling to room temperature afforded the crude product, which was washed with diethyl ether (three times x 10.0 mL). Final drying at high vacuum provided 3-(11-hydroxypropyl)-1-methylimidazolium chloride (**41**) as a colorless oil in a yield of 90%.

<u>^{1}H-NMR (DMSO-d_6, 400 MHz):</u> δ = 9.31 (t, 1H, J = 1.6 Hz, N-C*H*-N), 7.80 (t, 1H, $^3J_{H,H}$ = 1.8 Hz, C*H*), 7.72 (t, 1H, $^3J_{H,H}$ = 1.8 Hz, C*H*), 4.92 (t, 2H, $^3J_{H,H}$ = 5.2 Hz, O*H*), 4.23 (t, 2H, $^3J_{H,H}$ = 7.0 Hz, N-C*H*$_2$), 3.84 (s, 3H, C*H*$_3$), 3.38 (q, 2H, $^3J_{H,H}$ = 5.6 Hz, C*H*$_2$-OH), 1.91 (quint, 2H, $^3J_{H,H}$ = 7.0 Hz, $^3J_{H,H}$ = 5.9 Hz, C*H*$_2$).

<u>^{13}C-NMR (DMSO-d_6, 100 MHz):</u> δ = 136.8 (N-*C*H-N), 123.5 (*C*H), 122.4 (*C*H), 56.8 (*C*H$_2$-OH), 46.1 (N-*C*H$_2$), 35.7 (*C*H$_3$), 32.4 (*C*H$_2$).

3-(11-Hydroxypropyl)-1-methylimidazolium chloride (**41**) (45.0 mmol, 15.0 g, 1.0 eq.) was dissolved in anhydrous DCM and 2-bromo-propionic acid bromide (135.0 mmol, 29.1 g, 3.0 eq.) was added in drops over a period of 30 minutes. The reaction was allowed to stir for 48 hours at room temperature. After evaporation of the solvent under reduced pressure the crude product was diluted with water (20.0 mL), followed by the addition of lithium bis(trifluoromethane)sulfonimide (49.5 mmol, 14.2 g, 1.1 eq.). The resulting suspension was extracted five times with DCM (each 20.0 mL). The combined organic layers were dried over magnesium sulfate and filtered. The solvent was removed under reduced pressure, providing 3-(11-(2-bromo-2-methyl-propionyloxy)propyl)-methyl-1-imidazolium bis(trifluoromethane)sulfonimide (**42**) as a colorless oil in a yield of 87%.

<u>^{1}H-NMR (C*D*Cl$_3$, 400 MHz):</u> δ = 8.75 (t, 1H, J = 1.6 Hz, N-C*H*-N), 7.39 (t, 1H, $^3J_{H,H}$ = 1.8 Hz, C*H*), 7.32 (t, 1H, $^3J_{H,H}$ = 1.8 Hz, C*H*), 4.33 (t, 2H, $^3J_{H,H}$ = 7.1 Hz, N-C*H*$_2$), 4.23 (t, 2H, $^3J_{H,H}$ = 5.8 Hz, O-C*H*$_2$), 3.94 (s, 3H, N-C*H*$_3$), 2.30 (quint, 2H, $^3J_{H,H}$ = 7.1 Hz, $^3J_{H,H}$ = 5.8 Hz, C*H*$_2$), 1.92 (s, 6H, C*H*$_3$).

<u>^{13}C-NMR (C*D*Cl$_3$, 100 MHz):</u> δ = 171.4 (*C*=O), 136.3 (N-*C*H-N), 123.8 (*C*H), 122.6 (*C*H), 119.8 (q, J = 321.2 Hz, *C*F$_3$), 61.8 (*C*H$_2$-O), 56.1 (*C*$_{quart.}$), 47.0 (N-*C*H$_2$), 36.4 (N-*C*H$_3$), 30.5 (*C*H$_3$), 29.0 (*C*H$_2$).

<u>ESI-ToF-MS (direct injection, without addition of salt, MeOH 0.001 mg/mL) [*m/z*]:</u> [M]$^+$ C$_{11}$H$_{18}$N$_2$O$_2$Br$^+$; simulated: 289.055 g/mol, measured: 289.047 g/mol.

Ethanethiol (1.4 mmol, 104 µL, 2.0 eq.) and triethylamine (1.4 mmol, 194 µL, 2.0 eq.) were dissolved in anhydrous THF (20.0 mL). Carbon disulfide (1.4 mmol, 84 µL, 2.0 eq.) dissolved in anhydrous THF

(5.0 mL) was slowly added to the stirred solution. The yellowish mixture was cooled to 0 °C and stirred for one hour. Subsequently, **42** (0.7 mmol, 400.0 mg, 1.0 eq.) dissolved in anhydrous THF (5.0 mL) was added dropwise to the ice-cooled solution, which was stirred over a period of 24 hours. The solvent was removed under reduced pressure, the resulting residue was diluted with DCM (20.0 mL) and washed three times with water (3 x 15.0 mL). After drying over sodium sulfate, the suspension was filtered and the solvent was removed under reduced pressure. Further purification by chromatography (SiO$_2$, DCM/MeOH 99:1, R$_f$ = 0.5 in DCM/MeOH 15:1) afforded 1-((11-(3-methylimidazolium)propyloxy)carbonyl)2-methyl-ethyl butyl carbonotrithioate bis(trifluormethyl)sulfonimide (**43**), including **42** as an impurity to an extent of 30%.

<u>^{1}H-NMR (CDCl$_3$, 400 MHz):</u> δ = 8.72 (s, 1H, N-C*H*-N), 7.34 (t, 1H, $^3J_{H,H}$ = 1.8 Hz, C*H*), 7.32 (t, 1H, $^3J_{H,H}$ = 1.8 Hz, C*H*), 4.24 (t, 2H, $^3J_{H,H}$ = 6.8 Hz, N-C*H$_2$*), 4.15 (t, 2H, $^3J_{H,H}$ = 5.7 Hz, O-C*H$_2$*), 3.94 (s, 3H, N-C*H$_3$*), 3.28 (q, $^3J_{H,H}$ = 7.4 Hz, 2H, S-C*H$_2$*), 2.22 (quint, 2H, $^3J_{H,H}$ = 6.8 Hz, $^3J_{H,H}$ = 5.7 Hz, C*H$_2$*), 1.69 (s, 6H, C*H$_3$*), 1.31 (t, 3H, $^3J_{H,H}$ = 7.4 Hz, C*H$_3$*).

<u>^{13}C-NMR (CDCl$_3$, 100 MHz):</u> δ = 222.5 (*C*=O), 172.8 (*C*=O), 136.3 (N-*C*H-N), 123.5 (*C*H), 122.6 (*C*H), 119.7 (q, J = 321.2 Hz, *C*F$_3$), 61.8 (*C*H$_2$-O), 56.0 (*C*$_{quart.}$), 47.9 (N-*C*H$_2$), 36.5 (N-*C*H$_3$), 31.4 (S-*C*H$_2$), 30.5 (*C*H$_2$), 25.2 (*C*H$_3$), 12.8 (*C*H$_3$).

<u>ESI-ToF-MS (direct injection, without addition of salt, MeOH 0.001 mg/mL) [*m/z*]:</u> [M]$^+$ C$_{14}$H$_{23}$N$_2$O$_2$S$_3$$^+$: simulated: 347.092 g/mol, measured: 347.085 g/mol.

4.3.1.2 Synthesis of CTA-COOH (44, 46)[343]
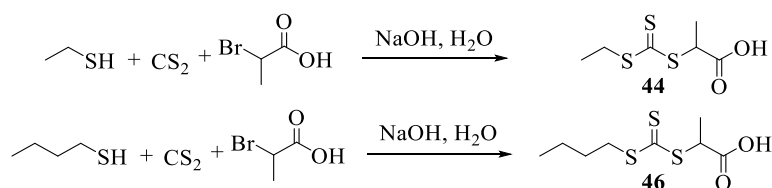
Scheme 16. Synthesis of test chain-transfer agents **44** and **46**.

The thiol component (20 mmol of either Et-SH = 1.4 mL or Bu-SH = 2.2 mL) was dissolved in water (3.0 mL). Sodium hydroxide (1.6 g, 50 wt%-solution) and acetone (1.0 mL) were added carefully to keep the temperature always < 30 °C. To the ice-cooled solution carbon disulfide (22.5 mmol, 1.35 mL) was added, keeping the temperature < 10 °C for 30 minutes. Subsequently, 2-bromo-propane-carboxylic acid (20.5 mmol, 1.8 mL) was added, followed by the addition of NaOH (1.6 g, 50 wt%-solution). After diluting the yellow-orange suspension with water (3.0 mL) the mixture was stirred for further 24 hours at room temperature. Hydrochloric acid (10 M, 3.0 mL) was dropped carefully to the ice-cooled solution. In case of ethyl-CTA (**44**) *n*-hexane (15.0 mL) was added to the suspension. The organic phase was washed three times with water (3 x 15.0 mL). The combined organic layers were dried over sodium sulfate, filtrated and the solvent was removed under reduced pressure, providing ethyl-CTA (**44**) in a yield of 78%.

<u>^{1}H-NMR (500 MHz, CDCl$_3$):</u> δ = 8.30 (s, 1H, COO*H*), 4.87 (q, $^3J_{H,H}$ = 7.4 Hz, 1H, C*H*-COOH), 3.38 (q, $^3J_{H,H}$ = 7.4 Hz, 2H, C*H$_2$*), 1.63 (d, $^3J_{H,H}$ = 7.4 Hz, 3H, C*H$_3$*), 1.36 (s, 3H, C*H$_3$*).

<u>^{13}C-NMR (126 MHz, CDCl$_3$):</u> δ = 221.6 (*C*=S), 176.7 (*C*=O), 47.4 (*C*HCH$_3$), 31.7 (*C*H$_2$), 16.6 (CH*C*H$_3$), 12.9 (*C*H$_3$).

In case of the butyl-CTA (**46**) the crude product was precipitated, filtered and washed three times with water (3 x 15.0 mL). Drying was accomplished in high vacuum to obtain butyl-CTA (**46**) in a yield of 88%.

<u>^{1}H-NMR (500 MHz, C*D*Cl$_3$):</u> δ = 9.20 (*s*, 1H, COO*H*), 4.87 (*q*, $^3J_{H,H}$ = 7.4 Hz, 1H, C*H*-COOH), 3.37 (*t*, $^3J_{H,H}$ = 7.4 Hz, 2H, C*H*$_2$-S), 1.69 (*p*, $^3J_{H,H}$ = 7.4 Hz, 2H, C*H*$_2$), 1.63 (*d*, $^3J_{H,H}$ = 7.4 Hz, 3H, HC-C*H*$_3$), 1.43 (*sep*, $^3J_{H,H}$ = 7.3 Hz, 2H, C*H*$_2$), 0.94 (*t*, $^3J_{H,H}$ = 7.3 Hz, 3H, H$_2$C-C*H*$_3$).

<u>^{13}C-NMR (126 MHz, C*D*Cl$_3$):</u> δ = 221.8 (*C*=S), 176.8 (*C*=O), 47.4 (*C*HCH$_3$), 37.1 (*C*H$_2$-S), 29.9 (*C*H$_2$), 22.0 (CH*C*H$_3$), 16.6 (*C*H$_2$), 13.6 (*C*H$_3$).

4.3.2 Synthesis of RAFT-polymers (PS (48, 49a-m), P-*n*BuA (50, 51a-j))[315-318]
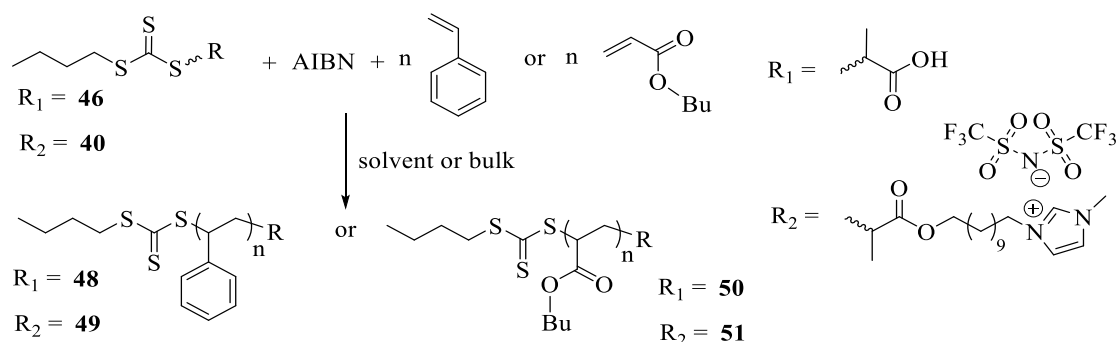
Scheme 17. RAFT synthesis of PS-COOH (**48**) and P-*n*BuA-COOH (**50**), applying CTA-COOH (**46**) or RAFT synthesis of PS-NHC (**49**) and P-*n*BuA-NHC (**51**), applying CTA-NHC (**40**).

Approach A – solution RAFT: General procedure for solution RAFT polymerizations of poly(styrene) (**48**, **49**) and poly(*n*-butyl acrylate) (**50**, **51**) using **46** or **40** as CTA: All RAFT polymerizations were carried out under dry and inert conditions using common Schlenk techniques. CTA **46** or **40** (4.0 – 10.0 eq.), AIBN (1.0 eq.) and the destabilized and freshly distilled monomers styrene (1000 – 6000 eq.) or *n*-butyl acrylate (1 000 – 6 000 eq.) were placed in a Schlenk tube and were dissolved in the anhydrous solvent (same amount as used as monomer-volume, see Table 22 for PS and Table 23 for P-*n*BuA). The suspension was subjected to several freeze-pump thaw cycles to get rid of oxygen. Subsequently, the reaction mixture was placed in a preheated oil bath to 80 °C in case of PS and to 65 – 80 °C in case of P-*n*BuA and stirred until the desired molecular weight was achieved (GPC control). Shock-freezing in liquid nitrogen terminated the reaction and the crude product was purified by diluting the reaction mixture with a small amount of toluene and precipitating three times in ice-cold MeOH in case of **48**, **49** or ice-cold MeOH/H$_2$O 2:1 mixture in case of **50**, **51**. The pure products were obtained after drying the sample in high vacuum for several hours.

Approach B – bulk RAFT: General procedure for RAFT polymerizations of poly(styrene) (**49**) and poly(*n*-butyl acrylate) (**51**) using **40** as chain transfer agent (CTA): All RAFT polymerizations were carried out as bulk polymerizations under dry and inert conditions using common Schlenk techniques. CTA **40** (1 equivalent), the destabilized and freshly distilled monomers styrene (100 – 500 eq.) or *n*-butyl acrylate (100 – 500 eq.) were placed in a Schlenk tube and subjected to several freeze-pump thaw cycles (see Table 22 for PS and Table 23 for P-*n*BuA). Subsequently, the reaction mixture was placed in a preheated oil bath to 120 °C and stirred until the desired molecular weight was achieved (GPC control). Shock-freezing in liquid nitrogen terminated the reaction and the crude product was purified by diluting the reaction mixture with a small amount of toluene and precipitating three times in ice-cold MeOH in case of **49** or ice-cold MeOH/H$_2$O 2:1 mixture in case of **51**. The pure products were obtained after drying the sample in high vacuum for several hours.

Table 22. Synthesis details of RAFT-polymerization of styrene (**48**, **49**).

PS	CTA	CTA:I:M [eq.]	n_{CTA} [mmol]	$n_{monomer}$ [mmol]	$M_{n(GPC)}$[a] [g/mol]	$M_{n(NMR)}$[b] [g/mol]	PDI	solvent	T [°C]	yield [%]
A)	**RAFT-polymerization conducted in solution**									
48	**46**	4:1:2400	0.16	96.0	3 000	4 200	1.23	toluene	80	6
49a	**40**	10:1:6000	0.20	119.7	10 900	20 400	1.24	toluene	80	13
49b	**40**	10:1:1000	1.20	119.7	4 000	4 500	1.16	MeCN	80	23
49c	**40**	10:1:2500	0.48	119.7	11 400	14 500	1.16	dioxane	80	32
B)	**RAFT-polymerization conducted in bulk in absence of AIBN**									
49d	**40**	10:500	1.75	87.4	5 900	6 000	1.07	/	120	70
49e	**40**	10:1000	0.88	87.4	11 500	11 100	1.17	/	120	67
49f	**40**	10:2500	0.35	87.4	25 300	26 000	1.15	/	120	68

a) GPC-measurements were performed in HPLC-grade DMF with the addition of LiNTf$_2$ (c = 10.0 mM) and molecular weight was determined by calibration with external PS-standards (M_P ~ 1 000 – 115 000 g/mol) and detection of refractive-index. b) Calculated by the ratio of initiator at δ = 3.28 ppm and repetitive unit at δ = 7.24 – 6.32 ppm.

<u>^{1}H-NMR of **48**</u> (C*D*Cl$_3$, 400 MHz): δ = 7.24 − 6.32 (*m*, Ar-*H* of phenyl-residue), 4.96 − 4.68 (*m*, 1H, H$_3$C-C*H*), 3.32 − 3.22 (*m*, 2H, S-C*H$_2$*), 2.44 − 1.18 (*m*, C*H$_2$*- + C*H*- of repetitive unit), 0.97 − 0.82 (*m*, 6H, C*H$_3$*).

<u>MALDI-ToF-MS of **48**</u> [DCTB, no addition of a salt] [m/z]: two potassium series of PS were found as [M+K]$^+$ for (C$_8$H$_8$)$_{47}$C$_8$H$_{14}$O$_2$S$_3$K$^+$; simulated 5171.933 g/mol, found 5171.477 g/mol, 2nd series was found as [M-H+2K]$^+$ for (C$_8$H$_8$)$_{47}$C$_8$H$_{13}$O$_2$S$_3$K$_2^+$; simulated 5209.889 g/mol, found 5209.511 g/mol.

<u>^{1}H-NMR of **49**</u> (THF-*d$_8$*, 400 MHz): δ = 8.85 (*s*, 1H, N-C*H*-N), 7.56 (*s*, 1H, C*H*), 7.52 (*s*, 1H, C*H*), 7.24 − 6.34 (*m*, Ar-*H* of phenyl-residue), 4.21 (*t*, 2H, $^3J_{H,H}$ = 7.4 Hz, O-C*H$_2$*), 3.92 (*s*, 3H, N-C*H$_3$*), 3.28 (*m*, 2H, S-C*H$_2$*), 2.26 − 1.22 (*m*, C*H$_2$*- + C*H*- of repetitive unit), 0.97 − 0.82 (*m*, 6H).

<u>MALDI-ToF-MS of **49**</u> [DCTB, no addition of a salt] [m/z]: a monovalent imidazolium telechelic PS series was found as [M]$^+$ for (C$_8$H$_8$)$_{29}$C$_{23}$H$_{41}$N$_2$O$_2$S$_3^+$; simulated 3493.054 g/mol, found 3493.135 g/mol.

Table 23. Synthesis details of RAFT-polymerization of *n*-butyl acrylate (**50**, **51**).

P-*n*BuA	CTA	CTA:I:M [eq.]	n_{CTA} [mmol]	$n_{monomer}$ [mmol]	$M_{n(GPC)}$[a] [g/mol]	$M_{n(NMR)}$[b] [g/mol]	PDI	solvent	T [°C]	yield [%]
A)	**RAFT-polymerization conducted in solution**									
50	**46**	10:1:1000	0.30	30.0	12 700	13 500	1.19	DMF	65	91
51a	**40**	10:1:6000	0.04	23.9	9 600	13 700	1.62	toluene	70	10
51b	**40**	10:1:1000	0.30	30.0	12 100	14 600	1.35	MeCN	80	41
51c	**40**	10:1:1000	0.30	30.0	11 200	15 300	1.48	dioxane	80	25
51d	**40**	10:1:500	0.84	42.1	13 400	13 900	1.21	DMF	65	80
51e	**40**	10:1:1000	0.70	70.2	21 800	23 800	1.23	DMF	65	66
51f	**40**	10:1:1000	0.30	30.0	25 600	24 400	1.30	DMF	65	93
B)	**RAFT-polymerization conducted in bulk in absence of AIBN**									
51g	**40**	10:1000	0.88	87.8	16 000	16 900	1.15	/	120	51
51h	**40**	10:250	3.51	87.8	2 300	2 100	1.13	/	120	42

a) GPC-measurements were performed in HPLC-grade DMF with the addition of LiNTf$_2$ (c = 10.0 mM) and molecular weight was determined by calibration with external PBMA-standards (M_P ~ 0.8 kg mol^{-1} – 111 kg mol^{-1}) and detection of refractive-

index. b) Calculated by the ratio of methylene-group of initiator at $\delta = 3.39$ ppm and repetitive unit at $\delta = 4.12 - 3.94$ ppm, of which the integral-value of 2 was subtracted, due to overlay with methylene-group of initiator-part.

<u>^{1}H-NMR of **50** (CDCl$_3$, 400 MHz):</u> $\delta = 4.88 - 4.76$ (*m*, 1H, H$_3$C-CH), 4.16 – 3.83 (*m*, CH_2 of repetitive unit), 3.34 (*t*, 2H, $^3J_{H,H} = 7.4$ Hz, S-CH_2), 2.39 – 2.21 (*m*, CH_2 of repetitive unit), 1.98 – 1.83 (*m*, CH of repetitive unit), 1.72 – 1.52 (*m*, CH_2 of repetitive unit), 1.50 – 1.30 (*m*, 2 CH_2 of CTA + CH_2 of repetitive unit), 1.08 (*t*, $^3J_{H,H} = 7.4$ Hz, CH_3 of CTA), 0.93 (*t*, $^3J_{H,H} = 7.3$ Hz, CH_3 of repetitive unit + HC-CH_3).

<u>MALDI-ToF-MS of **50** [DCTB, no addition of a salt] [m/z]:</u> two potassium series of P-*n*BuA were found as $[M+K]^+$ for $(C_7H_{12}O_2)_{96}C_8H_{14}O_2S_3K^+$; simulated 12 581.042 g/mol, found 12 580.744 g/mol, 2nd series was found as $[M-H+2K]^+$ for $(C_7H_{12}O_2)_{96}C_8H_{13}O_2S_3K_2^+$; simulated 12 618.997 g/mol, found 12 618.678 g/mol.

<u>^{1}H-NMR of **51** (CDCl$_3$, 400 MHz):</u> $\delta = 8.96$ (*s*, 1H, N-CH-N), 7.58 (*s*, 1H, CH), 7.54 (*s*, 1H, CH), 4.85 (*m*, 1H, H$_3$C-CH), 4.21 (*t*, 2H, $^3J_{H,H} = 7.5$ Hz, O-CH_2), 4.12 – 3.94 (*m*, CH_2 of repetitive unit), 3.93 (*s*, 3H, N-CH_3), 3.39 (*t*, 2H, $^3J_{H,H} = 7.4$ Hz, S-CH_2), 2.39 – 2.19 (*m*, CH_2 of repetitive unit), 1.99 – 1.81 (*m*, CH of repetitive unit), 1.70 – 1.53 (*m*, 9 CH_2 of CTA + CH_2 of repetitive unit), 1.50 – 1.24 (*m*, 2 CH_2 of CTA + CH_2 of repetitive unit), 1.10 (*m*, CH_3 of CTA), 0.95 (*m*, CH_3 of repetitive unit + HC-CH_3).

<u>MALDI-ToF-MS of **51** [DCTB, no addition of a salt] [m/z]:</u> a monovalent imidazolium telechelic P-*n*BuA series was found as $[M]^+$ for $(C_7H_{12}O_2)_{12}C_{23}H_{41}N_2O_2S_3^+$; simulated 2011.241 g/mol, found 2011.391 g/mol.

4.3.3 Synthesis of mechanocatalysts (52a-f)[48, 223, 302, 346-347]
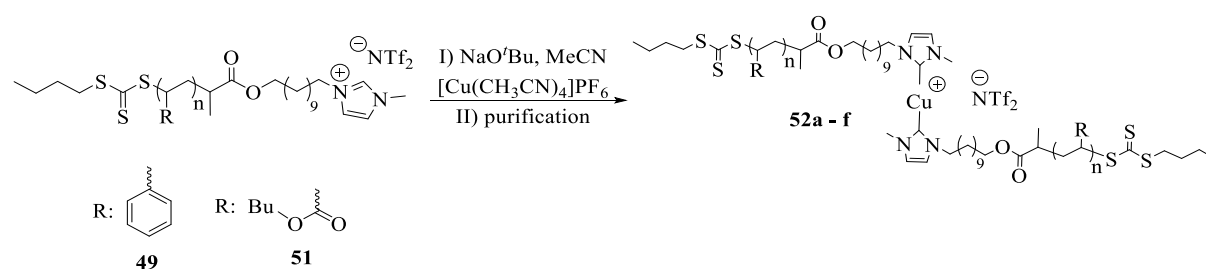
Scheme 18. Synthesis of mechanophoric Cu^I-catalysts based on PS and P-*n*BuA.

Poly(styrene): The desired amount of linear poly(styrene) (**49**, 1.0 eq., see Table 24) was transferred to a Schlenk tube, dissolved in anhydrous acetonitrile (10 mM) and subjected to five freeze-pump thaw cycles in order to get rid of oxygen. The components were transferred to the glovebox to ensure a water and an oxygen free atmosphere. NaO^{t}Bu (1.3 eq., dissolved in MeCN (20 mM)) was added to the reaction mixture, which was stirred at room temperature for 15 minutes, followed by the addition of tetrakis(acetonitrilo)copper(I)-hexafluorophosphate (0.5 eq., dissolved in MeCN (10 mM)). The suspension was allowed to stir for 24 hours. The solvent was removed under reduced pressure and the residue was purified by two different methods (approach A and B):

Approach A – preparative GPC: The samples were dissolved in DMF in a maximum concentration of 20 mg/mL (V = 300 µL) before subjecting to the device and per manual command separately collected in tubes, subsequently followed by the immediate evaporation of the solvent under reduced pressure. This procedure was repeated multiple times until the initial reaction mixture was entirely consumed, obtaining pure linear PS-Cu(I) bis(NHC) complexes (**52a-c**) as a light yellow solid in very low yields (4 – 7% = collection of all runs), caused by decomposition of the complexes into the monovalent precursor (according to GPC) during the purification process at harsh conditions (55 °C, > 10 bar). Verification by shift of NCHCHN resonances from $\delta = 7.56 - 7.52$ ppm (precursor) to $\delta = 6.25 - 6.22$

ppm was just accomplished in case of **52a**, while for **52b-c** amounts were too low to conduct NMR experiment. However, complete conversion for **52b-c** was assumed, due to monomodal distribution of doubled molecular weight in analytical GPC and presence of the NC*H*C*H*N resonance proof before preparative GPC was conducted.

Approach B – precipitation: The purification by precipitation of the crude mixture in acetonitrile to get rid of excess of NaO*t*Bu and [Cu(MeCN)$_4$]PF$_6$ afforded the mixtures **52d-f** (according to GPC and NMR measurements), consisting of the desired bis(NHC) complexes and NHC telechelic PS precursor (**36**) in moderate to high yields (45 – 71%) (see Table 25 for characterization data of **52a-f**).

Poly(*n*-butyl acrylate): In case of *n*-butyl acrylate **51** same procedure as for PS (approach A or B) was applied (for synthesis attempts see Table S4 in appendix 7.13), but side reactions were preventing the formation of P-*n*BuA bis(NHC) complexes. Similar to PS a doubling of molecular weight was detected via GPC control, but the missing shift of NC*H*C*H*N protons in ^{1}H-NMR spectra led to the assumption that the trithiocarbonate group was hydrolyzed in basic media, forming disulfide-bridged polymer chains. Further experimental spectra and synthesis attempts for both, PS-bis(NHC)- and P-*n*BuA-bis(NHC) complexes can be found in the appendix 7.13.

Table 24. Reaction conditions for PS-Cu(I) bis(NHC) complex (**52**) formation.

entry	precursor	$n_{(precursor)}$ [mmol][a]	$n_{(NaO^tBu)}$ [mmol]	$m_{(NaO^tBu)}$ [mg]	$n_{(Cu\text{-}salt)}$ [mmol]	$m_{(Cu\text{-}salt)}$ [mg]	purification	yield of **38** [%]
	synthesis of PS-mechanophores							
1	**49d**	0.080	0.104	10.0	0.040	14.9	**52a**: prep. GPC **52d**: precipitation	4 45
2	**49e**	0.045	0.059	5.6	0.023	8.8	**52b**: prep. GPC **52e**: precipitation	7 57
3	**49f**	0.019	0.025	2.4	0.0095	3.5	**52d**: prep GPC **52f**: precipitation	5 71

a) Determined by using molecular weight via ^{1}H-NMR measurement.

Table 25. Characterization data of PS based bis(NHC)-Cu(I)-mechanocatalysts (**52**).

comp.	precursor	precursor **49**			complex **52**		
		$M_{n(GPC)}$ [g/mol][a]	$M_{n(NMR)}$ [g/mol][b]	PDI	$M_{n(GPC)}$ [g/mol][a]	biscarbene content [%][c]	PDI
52a	**49d**	5 900	6 000	1.07	12 000	100	1.08
52b	**49e**	11 500	11 100	1.17	23 000	100	1.16
52c	**49f**	25 300	26 000	1.15	50 500	100	1.38
52d	**49d**	5 900	6 000	1.07	10 100	55	1.36
52e	**49e**	11 500	11 100	1.17	19 200	76	1.73
52f	**49f**	25 300	26 000	1.15	38 700	23	1.53

a) Determined via GPC (DMF + LiNTf$_2$) using PS standard calibration. b) Calculated by the ratio of initiator at $\delta = 3.28$ ppm and repetitive unit at $\delta = 7.24 – 6.32$ ppm. b) Determined via ^{1}H-NMR measurement and the ratio of NC*H*C*H*N resonances of precursor (**49**) located at $\delta = 7.56 – 7.52$ ppm and NC*H*C*H*N resonances, belonging to the biscarbene structure (**52**) at $\delta = 6.25 – 6.22$ ppm. The presumably apparent monocarbene structure was not taken into account, in turn of overlapping signals of suspected structure with multiplet at $\delta = 7.24 – 6.34$ ppm, belonging to the aromatic part of the repetitive unit.

^{1}H-NMR of **52** (tetrahydrofuran-*d$_8$*, 400 MHz): $\delta = 7.27 − 6.35$ (*m*, Ar-*H* of phenyl-residue), 6.25 (*d*, 2H, $^3J_{H,H} = 2.7$ Hz, NC*H*C*H*N), 6.23 (*d*, 2H, $^3J_{H,H} = 2.9$ Hz, NC*H*C*H*N), 3.98 (*t*, 4H, $^3J_{H,H} = 6.9$ Hz, O-C*H$_2$*), 3.95 − 3.82 (*m*, 4H, N-C*H$_2$*), 3.50 (*s*, 6H, N-C*H$_3$*), 2.39 − 1.08 (*m*, C*H$_2$*- + C*H*- of repetitive unit), 0.97 − 0.82 (*m*, 12H, C*H$_3$*).

MALDI-ToF-MS of **52**: While using different matrices, salts and ionization methods, no matching spectrum could be found.

4.3.4 CuAAC upon ultra-sonication of mechanocatalysts[284, 296, 302]
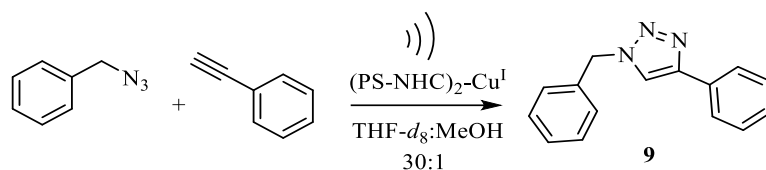
Scheme 19. Mechanochemically triggered „click"-reaction by ultra-sonication.

A headspace vial was evacuated and flushed with nitrogen for several times while transferring it to the glovebox. Benzyl azide (526 μmol, 70.0 mg, 1.0 eq.), phenylacetylene (526 μmol, 54 mg, 1.0 eq.) and the Cu(I)-mechanocatalyst (**52d-f**) were added to the headspace vial and dissolved in deuterated THF (1.0 mL). The three necked reaction-vessel equipped with the Sonics VCX 500 ultrasonic processor equipped with a long full wave solid probe (diameter 13 mm) and an internally threaded stainless steel adapter, a three-way-gas-tap and a rubber-septum was evacuated and flushed with argon for several times. After cooling the reaction vessel with an ice-bath to 0 °C the mixture, containing the "clicking" components, was added via syringe to the reaction-vessel. Subsequently, the mixture was diluted with a mixture of deuterated THF/MeOH 30:1 (6.0 mL) to finally adjust a concentration of 75 mM of benzyl azide and phenylacetylene and 0.75 mM of the Cu(I)-mechanophore (**52d-f**). The experiment was started by applying ultrasound (frequency: 20 kHz, max. amplitude: 30% of 125 μm, sonication intensity: 8.75 W/cm^2 which belongs to an energy of 21 kJ per sonication cycle) for 90 minutes (pulse sequence: 5 s on, followed by 10 s off) followed by 60 minutes without ultra-sonication. During the complete experiment the reaction system was permanently cooled with an external ice-bath to keep the temperature below 25 °C towards the experiment. Immediately after mixing (0th cycle) and after 450 minutes (3rd cycle), 750 minutes (5th cycle) and 1 500 minutes (10th cycle) aliquots were taken from the mixture (see Table 26) to monitor the "click" conversion via ^{1}H-NMR measurements. NMR experiments were conducted without further purification. As a control experiment a Schlenk flask was evacuated and flushed with argon for several times. Benzyl azide (75 μmol, 10.0 mg, 1.0 eq.), phenylacetylene (75 μmol, 7.7 mg, 1.0 eq.) and the Cu(I)-mechanocatalyst **52d-f** (0.01 eq.) were dissolved in a deuterated solvent:MeOH, 30:1 mixture (1.0 mL) and added to the Schlenk flask. As solvents either THF or DMF were used. The mixture was stirred at room temperature without ultra-sonication. Aliquots were taken after different periods of time and used for NMR-experiments without further purification (see Table 26).

Table 26. Conversions of phenylacetylene and benzyl azide in THF-d_8 or DMF-d_7 in presence of a Cu(I)- mechanocatalyst (**52**), applying ultra-sonication or not (control-experiments)[a].

entry	Cu(I)-catalyst	$M_{n(GPC)}$ [g/mol]	solvent	T [°C]	US	conversion [%][b]			
A	**control-experiments without US**					t [h]	1	2	18	24
1	**52d**	10 100	THF:MeOH	20	off	-	-	100	100
2	**52e**	19 200	THF:MeOH	20	off	-	-	100	100
3	**52f**	38 700	THF:MeOH	20	off	-	-	100	100
4	**52d**	10 100	DMF:MeOH	20	off	2	-	-	80
5	**52e**	19 200	DMF:MeOH	20	off	4	20	-	-
6	**52f**	38 700	DMF:MeOH	20	off	2	-	-	-
B	**mechanochemical activation with US**				US-cycles	0	3	5	10
					t [h]	0	7.5	12.5	25
7	**52d**	10 100	THF:MeOH	0	on	13	36	62	75

a) For all reactions an equimolar concentration (75 mM) of benzyl azide and phenylacetylene in the mentioned solvent mixture (30:1) was adjusted. Additionally, the concentration of Cu(I)-mechanophore (**52d-f**) was adjusted to 0.75 mM (0.01 equivalents). b) Conversion was calculated by determining the increasing triazole-resonance at δ = 8.10 ppm and the CH_2 resonance of the triazole product at δ = 5.58 ppm. Comparing them with the CH_2-resonance of benzyl azide at δ = 4.34 ppm afforded the conversion to different period of times, when the aliquots were taken and ^{1}H-NMR-experiments were conducted.

4.3.5 Synthesis and testing of an autonomous sensing approach applying mechanocatalysts

4.3.5.1 Incorporation of PS-mechanocatalysts into pTHF-matrix (pellets) (53a-d)[37, 48, 276]
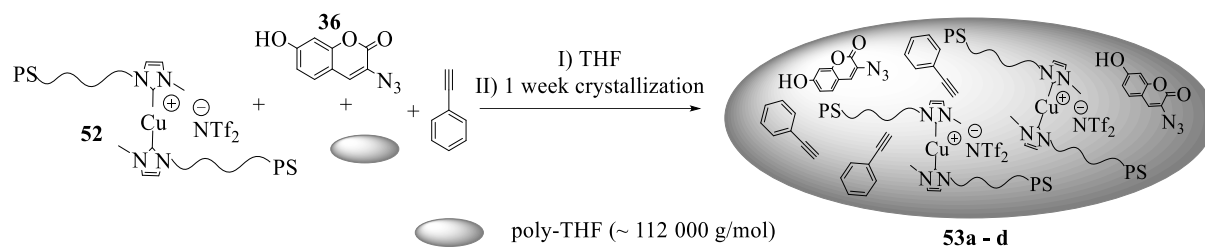
Scheme 20. Incorporation of (PS-NHC)$_2$-Cu^I-machenocatalysts (**52**) into pTHF matrix.

High molecular weight pTHF (~ 112 000 g/mol, 200.0 mg) and 3-azido-7-hydroxy-coumarin **36** (36 µmol, 7.3 mg, 1.0 eq.) were stored in a flask, followed by evacuation and flushing with nitrogen for several times. The flask was further transferred to the glovebox to ensure an oxygen free environment. Phenylacetylene (36 µmol, 4.0 µL, 1.0 eq.) and anhydrous THF (5.0 mL) were added via syringe and the mixture was stirred at room temperature for two hours in the dark. The flask was removed from the glovebox and the solvent was removed under reduced pressure at 25 °C. Followed by the addition of (PS-NHC)$_2$-Cu^I (**52a, 52d – f**) (0.006 – 0.033 eq., see Table 27) dissolved in anhydrous DMF. In the next step, the solvent was removed under reduced pressure and the system was evacuated and flushed with nitrogen. Subsequently, the flask was stored for one week in the glovebox in the dark for crystallization of pTHF matrix, providing the specimen (**53a-d**). Crystallinity of the specimen was determined by DSC-experiments before the first compression cycle was started (see Table 27).

Table 27. Experimental details and calculation of crystallinity of sensing pellets **53a-d**.

| entry | pellet | mechanocatalyst | | | | | T_M [°C] | ΔH_m [J/g] | degree of crystallinity [%]$^{c)}$ |
		No.	$M_{n(GPC)}$ [g/mol]$^{a)}$	m_{total} [mg]$^{b)}$	m_{pure} [mg]	n_{pure} [µmol]			
1[48]	**Ref.**	-	-	-	-	-	46.3	117.8	68
2	**53a**	**52a**	12 090 (100%)	14.4 (6.4 wt%)	14.4	1.2 (0.033 eq.)	39.8	103.0	60
3	**53b**	**52d**	12 090 (55%)	26.2 (11.0 wt%)	14.4	1.2 (0.033 eq.)	40.9	105.6	61
4	**53c**	**52e**	23 520 (76%)	36.8 (14.2 wt%)	28.0	1.2 (0.033 eq.)	38.4	81.1	47
5	**53d**	**52f**	49 090 (23%)	50.0 (19.2 wt%)	11.5	0.2 (0.006 eq.)	41.2	95.2	55

a) Values in brackets represent the amount of Cu(I) bis(NHC) complex according to ^{1}H-NMR. b) Values in brackets represent wt% of mechanocatalyst (or mixture) in pTHF pellet. c) For calculation 172 J/g was used as ΔH_m for 100% crystalline pTHF.[348]

4.3.5.2. Compression experiments for fluorescence sensing of a pTHF-matrix activated via mechanocatalysts[48]
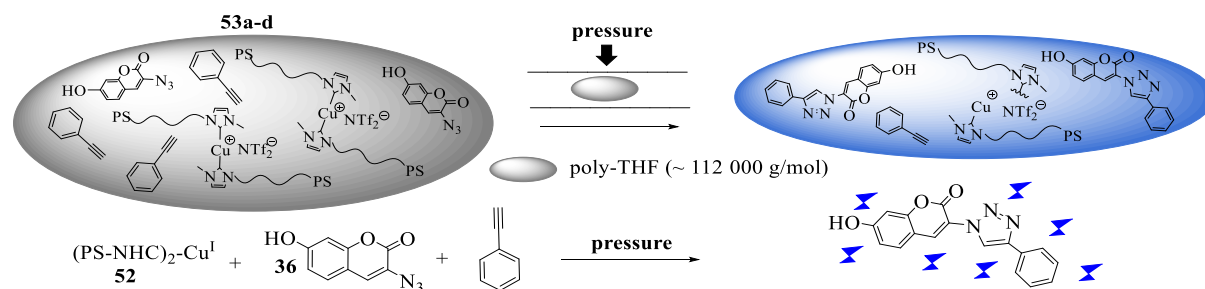
Scheme 21. Compression-fluorescence measurements of pTHF pellets **53a-d**.

The mechanophoric specimen (**53a-d**) were removed from the flask by a spatula and transferred to an IR-press, where they were transformed to a pellet by gently pressing with a spatula. In the next step, the fluorescence intensity of the not activated pellet was measured by fixing the sample in a special quartz glass holder (λ_{ex} = 360 nm, λ_{em} = 427 nm), followed by conduction of cyclic compression experiments: the samples (d = 13 mm) were subjected to an automatic hydraulic press and 10 tons pressure (corresponding to 0.74 GPa) were applied for 30 minutes, followed by 30 minutes of relaxation of the system. This procedure was repeated for 20 times, while the pellet was folded once with spatula each time before the next compressing cycle was started. Fluorescence intensity was measured at three different positions after 1st, 2nd, 3rd, 5th, 10th and 20th cycle (see Table 28). Calibration of the fluorescence spectrometer can be found in the appendix 7.15.

Table 28. Calculated "click"-conversions for each fluorescence-compression cycle for each pTHF pellet **41a-d**, containing the mechanocatalysts **38a, 38d-f**, coumarin azide **40** and phenylacetylene.

entry	pTHF pellet	mechanocatalyst			compression cycle	fluorescence intensity [a.u.][c]	"click"-conversion [%][d]
		No.	$M_{n(GPC)}$ [g/mol] [a]	m [mg] [b]			
1	**53a**	**52a**	12 000 (100 %)	14.4 (6.4 wt%)	0	50	3.9 ± 0.4
					1	128	11.7 ± 1.1
					2	139	12.8 ± 0.4
					3	169	15.9 ± 1.4
					5	183	17.3 ± 0.3
					10	224	21.6 ± 1.6
					20	227	21.8 ± 0.8
2	**53b**	**52d**	12 000 (55 %)	26.2 (11.0 wt%)	0	3	0.0 ± 0.0
					1	18	1.5 ± 0.3
					2	65	6.2 ± 0.6
					3	75	7.3 ± 0.4
					5	106	10.5 ± 0.6
					10	108	10.7 ± 1.2
					20	112	11.1 ± 1.1
3	**53c**	**52e**	23 000 (76 %)	36.8 (14.8 wt%)	0	10	0.0 ± 0.0
					1	17	0.7 ± 0.1
					2	30	2.0 ± 0.4
					3	74	6.5 ± 0.4
					5	95	8.6 ± 0.2
					10	130	12.1 ± 0.2
					20	170	16.2 ± 0.3
4	**53d**	**52f**	50 500 (23 %)	50.0 (19.2 wt%)	0	13	0.0 ± 0.0
					1	15	0.2 ± 0.2
					2	26	1.3 ± 0.4
					3	42	2.9 ± 0.6
					5	54	4.2 ± 0.2
					10	113	10.1 ± 0.5
					20	143	13.1 ± 1.2

a) Values in brackets represent the amount of Cu(I) bis(NHC) complex according to ^{1}H-NMR analysis. b) Values in brackets represent wt% of mechanocatalyst (or mixture) in pTHF pellet. c) Average value of multiple determined fluorescence spectra at three different positions of the sample after excitation at 382 nm and fluorescence emission at 432 nm. d) Calculated according to eq. 5 assuming a maximum concentration of fluorescence dye of $1.56 \cdot 10^{-4}$ mmol$_{dye}$/mg$_{sample}$.

5 Summary

The aim of this thesis was the development of an autonomous self-healing material, applicable at sub-ambient conditions. Therefore, crosslinking reagents were equipped with the newest "click" generation moiety – the picolyl azide, suiting the chelation-assisted CuAAC mechanism. The crosslinking efficiency in solution and in the melt state was determined and compared with results from the conventional CuAAC approach for the first time.

At first, *in situ* NMR solution experiments of picolyl azides **3** and **28**, reacting with phenylacetylene in presence of homogeneous Cu(I) catalysts were performed to probe the superior performance in "click" reactions compared to the standard CuAAC approach (see Figure 66a). The experiments were conducted in deuterated THF to find the ideal conditions for highly efficient and fast reaction-kinetics. CuBr in presence of DIPEA (0.1 eq.) was most suitable to gain fast acceleration in the chelation-assisted CuAAC of **3** by achieving quantitative conversion within five minutes. Confirmed by its polymeric counterpart **28**, providing similar conversions of > 99% within four minutes at lower concentrations of DIPEA (0.01 equivalents). Whereas control experiments, employing the conventional CuAAC (usage of benzyl azide and monovalent azido telechelic PIB), only achieved low conversions of < 10% within hours, emphasizing the tremendous difference in reaction acceleration of the CuAAC, caused by the nitrogen atom adjacent to the azide group.

In the next step, the beneficial acceleration behavior of picolyl azides in the chelation-assisted CuAAC was verified in crosslinking reactions in order to mimic the SH response. The picolyl azide moieties were successfully attached to star-shaped alcoholic-units, affording either low-molecular weight **18** or high-molecular weight PIB **34a** and **34b** (M_n ~ 6 000 g/mol) (see Figure 66b), verified by NMR- and IR-spectroscopy, ESI-ToF-MS and MALDI-ToF-MS. Further acceleration of the crosslinking rate included the deployment of homogeneous and heterogeneous catalysts. Thus, Cu(I)-nanoparticles were successfully implemented onto graphene-surfaces (**15**, **17**), proven by TEM and XRD. The Cu(I)-content on the carbon surface was in the range of 5 – 7wt%, confirmed via FAAS measurements.

Figure 66. a) Comparison of results from kinetic investigations of the chelation-assisted CuAAC and the conventional CuAAC by *in situ* NMR-measurements in solution. b) Crosslinking reactants **18**, **34a-b** suitable for the chelation-assisted CuAAC mechanism and heterogeneous Cu(I)-catalysts such as Cu-TRGO (**15**) and Cu-TREGO (**17**).

Subsequently, star-shaped azide **18** was converted with trivalent alkyne to undergo the network formation upon heating via DSC- experiments (see Figure 67a). The start of the ca-CuAAC reactions were observed at 4 °C (bis(NHC)$_2$-Cu(I)-catalyst + DBU), 20 °C (Cu(I)-TRGO) and 27 °C ([CuF(PPh$_3$)$_3$]), while peak T of the thermal Huisgen reaction (120 °C) was lowered to 38 °C (Cu(I)-TRGO) or 41 °C ([CuF(PPh$_3$)$_3$]). This verified the essential low temperature activity compared to the conventional CuAAC with homogeneous [CuBr/F(PPh$_3$)$_3$] or heterogeneous Cu-TRGO (**15**) or Cu-TREGO (**17**), beginning to crosslinking at 39 – 64 °C and having a peak T at 66 – 85 °C.

The high molecular weight concept was studied by subjecting star-shaped- picolyl azido telechelic PIBs (**34a**, **34b**) and alkyne telechelic PIB (**35**) to melt-rheology experiments (see Figure 67b). The molecular weight of both was limited to ~ 6 000 g/mol to maintain the required liquid flow-behavior. Contrary to the results in solution, where CuBr in presence of DIPEA turned out to accelerate the reaction the most, the air-stable catalyst [CuF(PPh$_3$)$_3$] conducted crosslinking most efficiently in the melt-state. Network formation of the ca-CuAAC crosslinking was more than 19 times faster compared to the conventional CuAAC (290 minutes), completing the process within 15 minutes at 20 °C. Lowering the temperature to sub-ambient conditions (10 °C) still achieved complete network-formation within 71 minutes. Activation of the crosslinking process was also accomplished at 5 °C, clearly pointing out the potential efficiency of the ca-CuAAC to provide self-healing systems at temperatures of less than 20 °C.
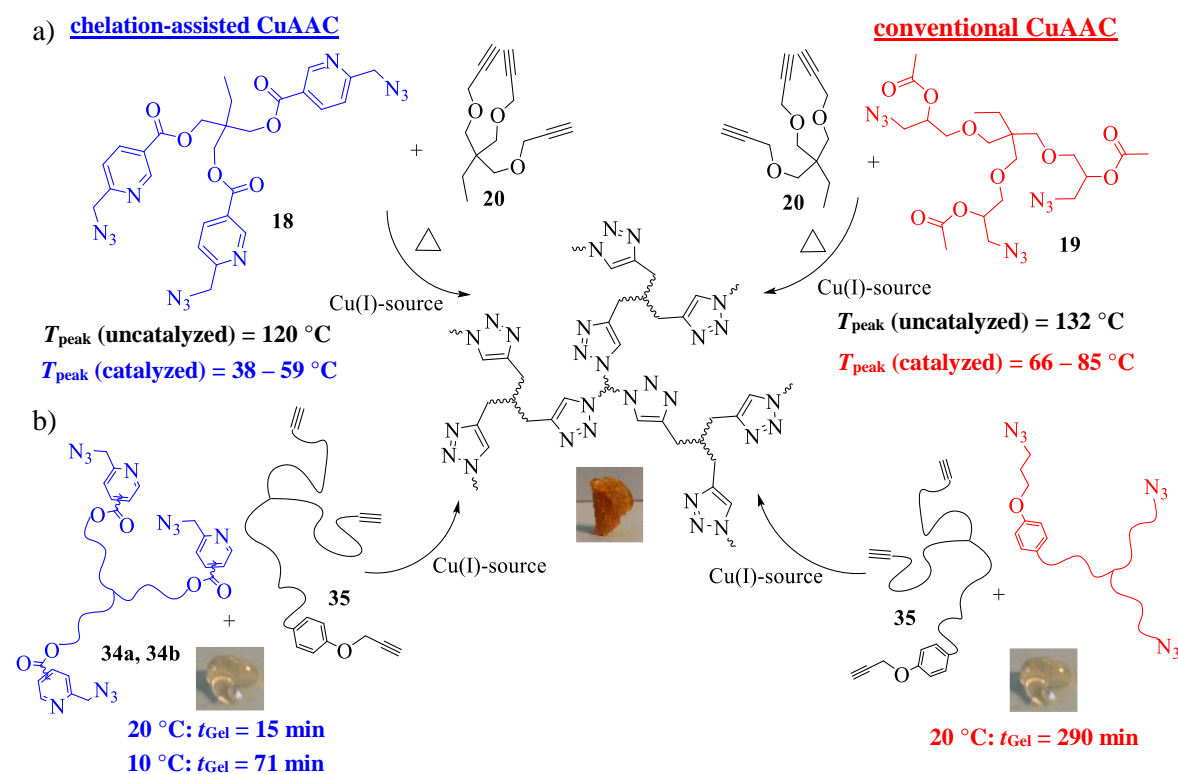
Figure 67. a) Comparison of the results from kinetic investigations of the chelation-assisted CuAAC and the conventional CuAAC by DSC-measurements. b) Comparison of the results from kinetic investigations of the chelation-assisted CuAAC and the conventional CuAAC by rheology-measurements of crosslinking star-shaped PIBs of a molecular weight of M_n ~ 6 000 g/mol.

Star-shaped picolyl azido telechelic PIB (**34b**), [CuBr(PPh$_3$)$_3$], coumarin azide (**36**) and a tridentate alkyne (**20**), encapsulated in UF-shell, were compounded to a scaffolding matrix in order to design the autonomous one-capsule based SH approach. Various matrices such as pure PDMS, blends of PDMS/PIB or pure PIB were used for the embedding procedure. The PIB-matrix of high molecular weight was best, since rejection of the PIB-components with PDMS prevented a sufficient embedding.

The star-shaped healing agent was enabled to undergo the fluorescent "click"-reaction with azido coumarin upon rupture of the capsules when notching the specimen with a razor blade. In turn, the increasing fluorescence intensity was indicative for the simultaneously occurring SH network-formation. In control experiments, missing either the Cu(I)-source or the damage impact, no increase of the fluorescence-intensity was detected as a consequence of the prevented "click"-reaction.

Efforts towards optimizing the activation efficiency of the mechanocatalysts have been made by tuning the molecular weight of the polymeric-NHC precursor handles. Therefore, a new CTA (**40**) was successfully designed, which allowed a simultaneous initiation of the RAFT-polymerization and the introduction of the NHC moiety at once (see Figure 68). NHC telechelic polymers, consisting of PS (**49a-m**) and P-*n*BuA (**51a-j**) of various molecular weights, ranging from 2 000 g/mol to 30 000 g/mol were synthesized, circumventing the common, but limited strategy of applying quaternization reactions to halo telechelic polymers. The established equilibrium between the dormant and the active species during RAFT polymerization, emerging from CTA (**40**), provided polymer chains of low PDI values (1.07 – 1.30). Analysis by GPC, NMR-spectroscopy, MALDI-ToF-MS and ESI-ToF-MS proved the complete attachment of the NHC-unit to each polymer-chain. Treatment of NHC telechelic PS with NaO^{t}Bu and [Cu(MeCN)$_4$]PF$_6$ afforded mixtures, consisting of the desired biscarbene-mechanophores and the unreacted precursor. Separation was accomplished either by preparative GPC, obtaining three pure PS-mechanophores of different molecular weights (**52a-c**) in an analytical scale or by precipitation in MeCN, leading to mixtures with a moderate purity (23 – 76% biscarbene content) and high yields. Presumably, the higher polarity of the P-*n*BuA backbone in combination with the trithiocarbonate group led to the formation of a side-product. The basic conditions during the mechanophore-synthesis hydrolyzed the trithiocarbonate group, forming disulfide-bridged polymers, which led to the observed doubling of the molecular weight in GPC analysis, while shift of the NC*HCH*N resonance in ^{1}H-NMR spectrum was missing. Hence, the autonomous sensing approach was limited to mechanophores, consisting of PS-backbones within this work.
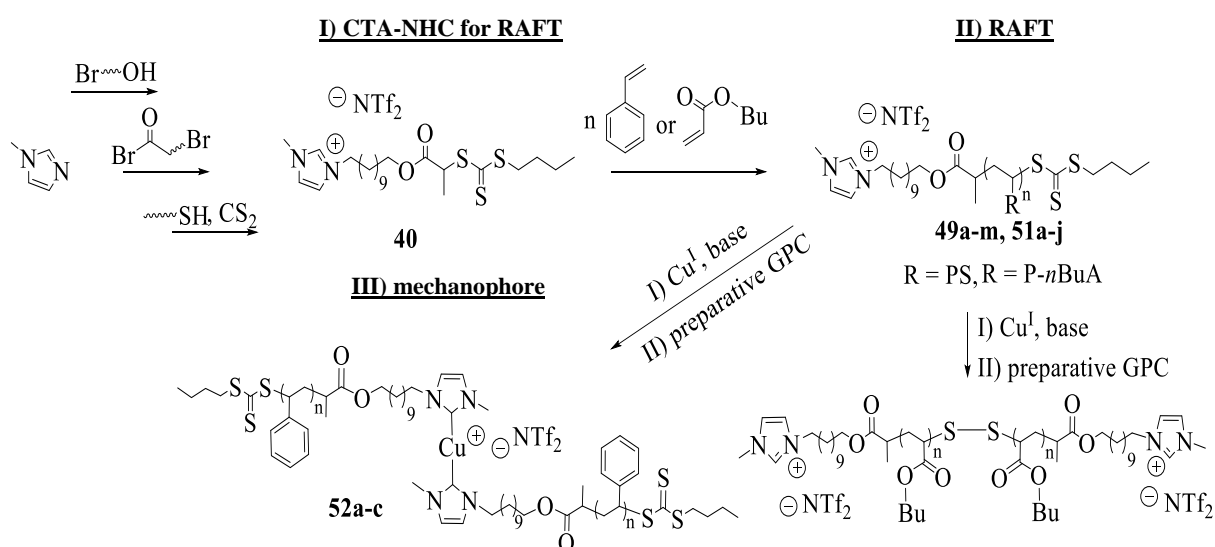
Figure 68. Synthetic route to I) obtain CTA-NHC (**40**) for II) RAFT of styrene to afford PS (**49**) and of *n*-butyl acrylate to afford P-*n*BuA (**51**) to build III) mechanophoric unit (**52**) in case of PS and disulfide-bridged P-*n*BuA.

In situ ^{1}H-NMR measurements in solution were performed to investigate the activation efficiency of PS-mechanophore mixtures (**52d-f**) (ratios of 76:24 up to 23:77 (mechanophore:PS-NHC)) in the CuAAC of phenylacetylene and benzyl azide. Upon ultra-sonication one of the NHC-shielding ligands should be cleaved, enabling the coordination of the alkyne-moiety to start the CuAAC, achieving a "click"-conversion of 75% after the 10th US-cycle. Control-experiments of the catalysts (**52d-f**) either in

deuterated THF or DMF without ultra-sonication showed similar to quantitative conversions within the same time, thus missing the required latency to be applied as mechanocatalysts in solution.

Finally, a capsule-free sensing approach within a solid host-material was accomplished by compounding the mechanocatalysts (**52a, 52d-f**), the non-fluorescent azido coumarin (**36**) and phenylacetylene into a high molecular weight pTHF (210 000 g/mol) (see Figure 69a). Compression-impact to pTHF-pellets (**53a-d**) induced the scission of the latent catalyst into the active Cu(I)-monocarbene species, initiating the formation of the highly fluorescent triazole-product (see Figure 69b). "Click" conversions increased with an increasing molecular weight of the polymer chains in turn of the more efficient transmittance of the compression impact, activating a larger quantity of the mechanocatalyst. For instance, the pellet (**53b**), containing the lowest molecular weight mechanocatalyst of 12 000 g/mol, provided a conversion of moderate 11%, while doubling the molecular weight to 23 500 g/mol led to 16% "click" conversion within the host-material (**53c**). Activation efficiency of the mechanocatalyst mixtures was exceeded, employing the pure mechanocatalyst of 12 000 g/mol to compression-fluorescence cycles, achieving the highest "click" conversion of 22%. Control experiments verified the mechanochemical activation, since neither the specimen missing a mechanocatalyst nor the ones (**53b-d**) missing compression impact showed an increase of fluorescence intensity.
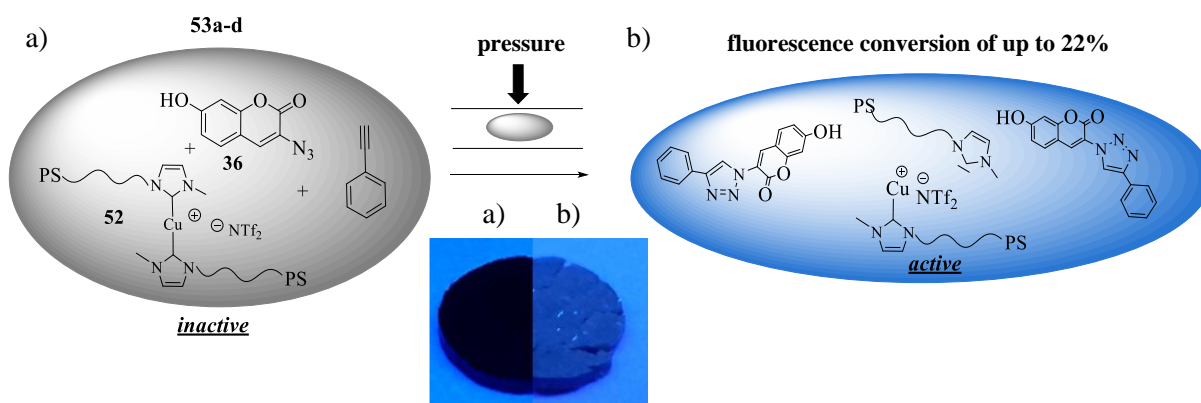
Figure 69. Fluorescence-compression cycles of sensing-materials (**53a–d**) revealed the mechanophoric activation of the catalyst (**52**), leading to „click" conversions of up to 22% within the pTHF-matrix, also visualized by the change of color of the pTHF pellets (**53a-d**) from a) black (initial state, before compression was applied) to b) blue appearance (λ_{em} = 432 nm) under UV-irradiation (λ_{ex} = 366 nm) after the 20th compression cycle.

In summary, appropriate reactants suiting the ca-CuAAC mechanism were successfully designed and tested upon crosslinking efficiency in solution (via DSC) and in the melt-state (via rheology) for the first time, proving the desired low temperature activity at ~ 5 °C for autonomous SH approaches. It was shown, that the homogeneous catalysts were better accelerating the "click"-reactions compared to the heterogeneous catalysts.

A new CTA was developed, allowing for the synthesis of high molecular weight (> 15 000 g/mol) NHC telechelic precursor polymers (PS, P-*n*BuA), which were subjected to subsequent mechanophore transformation. The high molecular weight Cu(I)-mechanocatalysts were activated upon compression impact, leading to a fluorescent "click" conversion of up to 22% within a scaffolding matrix (pTHF), proving the potential autonomous sensing behavior.

6 References

[1]   Kolb, H. C.; Finn, M. G.; Sharpless, K. B., Click Chemistry: Diverse Chemical Function from a Few Good Reactions. *Angewandte Chemie, International Edition* **2001,** *40* (11), 2004-2021.

[2]   Barner-Kowollik, C.; Du Prez, F. E.; Espeel, P.; Hawker, C. J.; Junkers, T.; Schlaad, H.; Van Camp, W., "Clicking" Polymers or Just Efficient Linking: What Is the Difference? *Angewandte Chemie International Edition* **2011,** *50* (1), 60-62.

[3]   Binder, W. H.; Sachsenhofer, R., "Click" Chemistry in Polymer and Materials Science. *Macromol. Rapid Commun.* **2007,** *28* (1), 15-54.

[4]   Binder, W. H.; Sachsenhofer, R., "Click"-Chemistry in Polymer and Material Science: An Update. *Macromol. Rapid Commun.* **2008,** *29*, 952-981.

[5]   Binder, W. H.; Kluger, C., Azide/alkyne-"click" reactions: applications in material science and organic synthesis. *Curr. Org. Chem.* **2006,** *10* (14), 1791-1815.

[6]   Döhler, D.; Michael, P.; Binder, W. H., CuAAC-Based Click Chemistry in Self-Healing Polymers. *Accounts of Chemical Research* **2017,** *50* (10), 2610-2620.

[7]   Meldal, M., Polymer "Clicking" by CuAAC Reactions. *Macromolecular Rapid Communications* **2008,** *29* (12-13), 1016-1051.

[8]   Meldal, M.; Tornøe, C. W., Cu-Catalyzed Azide−Alkyne Cycloaddition. *Chem. Rev.* **2008,** *108* (8), 2952-3015.

[9]   Schoffelen, S.; Meldal, M., Catalytic Click Reactions. In *Applied Homogeneous Catalysis with Organometallic Compounds*, (eds B. Cornils, W. A. Hermann, M. Beller and R. Paciello), Ed. **2017**.

[10]   Baskin, J. M.; Prescher, J. A.; Laughlin, S. T.; Agard, N. J.; Chang, P. V.; Miller, I. A.; Lo, A.; Codelli, J. A.; Bertozzi, C. R., Copper-free click chemistry for dynamic *in vivo* imaging. *Proceedings of the National Academy of Sciences* **2007,** *104* (43), 16793-16797.

[11]   Jewett, J. C.; Bertozzi, C. R., Cu-free click cycloaddition reactions in chemical biology. *Chemical Society Reviews* **2010,** *39* (4), 1272-1279.

[12]   Jewett, J. C.; Sletten, E. M.; Bertozzi, C. R., Rapid Cu-Free Click Chemistry with Readily Synthesized Biarylazacyclooctynones. *Journal of the American Chemical Society* **2010,** *132* (11), 3688-3690.

[13]   Debets, M. F.; van Berkel, S. S.; Dommerholt, J.; Dirks, A. J.; Rutjes, F. P. J. T.; van Delft, F. L., Bioconjugation with Strained Alkenes and Alkynes. *Accounts of Chemical Research* **2011,** *44* (9), 805-815.

[14]   Hoyle, C. E.; Lowe, A. B.; Bowman, C. N., Thiol-click chemistry: a multifaceted toolbox for small molecule and polymer synthesis. *Chemical Society Reviews* **2010,** *39* (4), 1355-1387.

[15]   Kade, M. J.; Burke, D. J.; Hawker, C. J., The power of thiol-ene chemistry. *Journal of Polymer Science Part A: Polymer Chemistry* **2010,** *48* (4), 743-750.

[16]   Lowe, A. B., Thiol–ene "click" reactions and recent applications in polymer and materials synthesis: a first update. *Polymer Chemistry* **2014,** *5* (17), 4820-4870.

[17]   Xu, J.; Tao, L.; Boyer, C.; Lowe, A. B.; Davis, T. P., Combining Thio−Bromo "Click" Chemistry and RAFT Polymerization: A Powerful Tool for Preparing Functionalized Multiblock and Hyperbranched Polymers. *Macromolecules* **2010,** *43* (1), 20-24.

[18]   Shao, H.; Crnogorac, M. M.; Kong, T.; Chen, S.-Y.; Williams, J. M.; Tack, J. M.; Gueriguian, V.; Cagle, E. N.; Carnevali, M.; Tumelty, D.; Paliard, X.; Miranda, L. P.; Bradburne, J. A.; Kochendoerfer, G. G., Site-Specific Polymer Attachment to a CCL-5 (RANTES) Analogue by Oxime Exchange. *Journal of the American Chemical Society* **2005,** *127* (5), 1350-1351.

[19] Heredia, K. L.; Tolstyka, Z. P.; Maynard, H. D., Aminooxy End-Functionalized Polymers Synthesized by ATRP for Chemoselective Conjugation to Proteins. *Macromolecules* **2007,** *40* (14), 4772-4779.

[20] Dag, A.; Durmaz, H.; Hizal, G.; Tunca, U., Preparation of 3-arm star polymers (A3) via Diels–Alder click reaction. *Journal of Polymer Science Part A: Polymer Chemistry* **2008,** *46* (1), 302-313.

[21] Sumerlin, B. S.; Vogt, A. P., Macromolecular Engineering through Click Chemistry and Other Efficient Transformations. *Macromolecules* **2010,** *43* (1), 1-13.

[22] Hizal, G.; Tunca, U.; Sanyal, A., Discrete macromolecular constructs via the Diels–Alder "Click" reaction. *Journal of Polymer Science Part A: Polymer Chemistry* **2011,** *49* (19), 4103-4120.

[23] Song, W.; Wang, Y.; Qu, J.; Lin, Q., Selective Functionalization of a Genetically Encoded Alkene-Containing Protein via "Photoclick Chemistry" in Bacterial Cells. *Journal of the American Chemical Society* **2008,** *130* (30), 9654-9655.

[24] Song, W.; Wang, Y.; Qu, J.; Madden, M. M.; Lin, Q., A Photoinducible 1,3-Dipolar Cycloaddition Reaction for Rapid, Selective Modification of Tetrazole-Containing Proteins. *Angewandte Chemie International Edition* **2008,** *47* (15), 2832-2835.

[25] Pounder, R. J.; Stanford, M. J.; Brooks, P.; Richards, S. P.; Dove, A. P., Metal free thiol–maleimide 'Click' reaction as a mild functionalisation strategy for degradable polymers. *Chemical Communications* **2008,** (41), 5158-5160.

[26] Stanford, M. J.; Dove, A. P., One-Pot Synthesis of α,ω-Chain End Functional, Stereoregular, Star-Shaped Poly(lactide). *Macromolecules* **2009,** *42* (1), 141-147.

[27] Klemm, E.; Stöckl, C., Synthesis of SH- and NCO-terminated thiocarbamate prepolymers. *Die Makromolekulare Chemie* **1991,** *192* (1), 153-158.

[28] Shin, J.; Matsushima, H.; Chan, J. W.; Hoyle, C. E., Segmented Polythiourethane Elastomers through Sequential Thiol−Ene and Thiol−Isocyanate Reactions. *Macromolecules* **2009,** *42* (9), 3294-3301.

[29] Singh, I.; Vyle, J. S.; Heaney, F., Fast, copper-free click chemistry: a convenient solid-phase approach to oligonucleotide conjugation. *Chemical Communications* **2009,** (22), 3276-3278.

[30] Singh, I.; Zarafshani, Z.; Lutz, J.-F.; Heaney, F., Metal-Free "Click" Chemistry: Efficient Polymer Modification via 1,3-Dipolar Cycloaddition of Nitrile Oxides and Alkynes. *Macromolecules* **2009,** *42* (15), 5411-5413.

[31] Inglis, A. J.; Barner-Kowollik, C., Ultra Rapid Approaches to Mild Macromolecular Conjugation. *Macromolecular Rapid Communications* **2010,** *31* (14), 1247-1266.

[32] Demko, Z. P.; Sharpless, K. B., A Click Chemistry Approach to Tetrazoles by Huisgen 1,3-Dipolar Cycloaddition: Synthesis of 5-Sulfonyl Tetrazoles from Azides and Sulfonyl Cyanides. *Angewandte Chemie International Edition* **2002,** *41* (12), 2110-2113.

[33] Wu, P.; Fokin, V. V., Catalytic Azide-Alkyne Cycloaddition: Reactivity and Applications. *Aldrichimica Acta* **2007,** *40* (1), 7-17.

[34] Binder, W. H.; Sachenshofer, R., "Click"-chemistry on supramolecular materials. In *Click Chemistry for Biotechnology and Materials Science*, Lahann, J., Ed. Wiley-Blackwell: **2009**; pp 119-175.

[35] Binder, W. H.; Zirbs, R., *"Click"-Chemistry in Macromolecular Synthesis*. John Wiley & Sons, Inc: **2009;** p DOI: 10.1002/0471440264.pst565.

[36] Hein, J. E.; Fokin, V. V., Copper-catalyzed azide–alkyne cycloaddition (CuAAC) and beyond: new reactivity of copper(I) acetylides. *Chemical Society Reviews* **2010,** *39* (4), 1302-1315.

[37] Le Droumaguet, C.; Wang, C.; Wang, Q., Fluorogenic click reaction. *Chemical Society Reviews* **2010,** *39* (4), 1233-1239.

[38] Qin, A.; Lam, J. W. Y.; Tang, B. Z., Click polymerization. *Chemical Society Reviews* **2010,** *39* (7), 2522-2544.

[39] Gragert, M.; Schunack, M.; Binder, W. H., Azide/Alkyne-"Click"-Reactions of Encapsulated Reagents: Toward Self-Healing Materials. *Macromol. Rapid Commun.* **2011,** *32* (5), 419-425.

[40] Döhler, D.; Michael, P.; Binder, W. H., Autocatalysis in the Room Temperature Copper(I)-Catalyzed Alkyne–Azide "Click" Cycloaddition of Multivalent Poly(acrylate)s and Poly(isobutylene)s. *Macromolecules* **2012,** *45* (8), 3335-3345.

[41] Hvilsted, S., Facile design of biomaterials by 'click' chemistry. *Polymer International* **2012,** *61* (4), 485-494.

[42] Schunack, M.; Gragert, M.; Döhler, D.; Michael, P.; Binder, W. H., Low-Temperature Cu(I)-Catalyzed "Click" Reactions for Self-Healing Polymers. *Macromol. Chem. Phys.* **2012,** *213* (2), 205-214.

[43] Uttamapinant, C.; Tangpeerachaikul, A.; Grecian, S.; Clarke, S.; Singh, U.; Slade, P.; Gee, K. R.; Ting, A. Y., Fast, Cell-Compatible Click Chemistry with Copper-Chelating Azides for Biomolecular Labeling. *Angewandte Chemie* **2012,** *124* (24), 5954-5958.

[44] Döhler, D.; Zare, P.; Binder, W. H., Hyperbranched polyisobutylenes for self-healing polymers. *Polym. Chem.* **2014,** *5* (3), 992-1000.

[45] Shaygan Nia, A.; Rana, S.; Döhler, D.; Noirfalise, X.; Belfiore, A.; Binder, W. H., Click chemistry promoted by graphene supported copper nanomaterials. *Chem. Commun.* **2014,** *50* (97), 15374-15377.

[46] Shoffelen, S.; Meldal, M., Alkyne-Azide Reactions. In *Modern Alkyne Chemistry*, eds. B. M. Trost and C. Li, Ed. **2014**.

[47] Vasiliu, S.; Kampe, B.; Theil, F.; Dietzek, B.; Döhler, D.; Michael, P.; Binder, W. H.; Popp, J., Insights into the Mechanism of Polymer Coating Self-Healing Using Raman Spectroscopy. *Appl. Spectrosc.* **2014,** *68* (5), 541-548.

[48] Michael, P.; Binder, W. H., A Mechanochemically Triggered "Click" Catalyst. *Angew. Chem., Int. Ed.* **2015,** *54* (47), 13918-13922.

[49] Shaygan Nia, A.; Rana, S.; Döhler, D.; Osim, W.; Binder, W. H., Nanocomposites via a direct graphene-promoted "click"-reaction. *Polymer* **2015,** *79*, 21-28.

[50] Shaygan Nia, A.; Rana, S.; Döhler, D.; Jirsa, F.; Meister, A.; Guadagno, L.; Koslowski, E.; Bron, M.; Binder, W. H., Carbon-Supported Copper Nanomaterials: Recyclable Catalysts for Huisgen [3+2] Cycloaddition Reactions. *Chem. Eur. J.* **2015,** *21* (30), 10763-10770.

[51] Döhler, D.; Rana, S.; Rupp, H.; Bergmann, H.; Behzadi, S.; Crespy, D.; Binder, W. H., Qualitative sensing of mechanical damage by a fluorogenic "click" reaction. *Chem. Commun.* **2016,** *52* (74), 11076-11079.

[52] Rana, S.; Döhler, D.; Nia, A. S.; Nasir, M.; Beiner, M.; Binder, W. H., "Click"-Triggered Self-Healing Graphene Nanocomposites. *Macromol. Rapid Commun.* **2016,** *37* (21), 1715-1722.

[53] Singh, M. S.; Chowdhury, S.; Koley, S., Advances of azide-alkyne cycloaddition-click chemistry over the recent decade. *Tetrahedron* **2016,** *72* (35), 5257-5283.

[54] Tornøe, C. W.; Meldal, M., *Dipolar cycloaddition reactions in peptide chemistry*. John Wiley & Sons, Ltd.: Chichester, United Kingdom: **2010**.

[55] Huisgen, R.; Szeimies, G.; Möbius, L., 1.3-Dipolare Cycloadditionen, XXXII. Kinetik der Additionen organischer Azide an CC-Mehrfachbindungen. *Chemische Berichte* **1967,** *100* (8), 2494-2507.

[56] Huisgen, R., *1,3-Dipolar Cycloaddition Chemistry*. WILEY: New York, **1984;** Vol. 1, p 1-176.

[57] Tornøe, C. W.; Meldal, M. In *Peptidotriazoles: copper(I)-catalyzed 1,3-dipolar cycloadditions on solid-phase*, American Peptide Society: ''Peptides, The wave of the Future'' in: *Proceedings of the Second International and the Seventeenth American Peptide Symposium*, M. Lebl, R. A. Houghten, Eds., San Diego **2001;** pp 263-264.

[58] Rostovtsev, V. V.; Green, L. G.; Fokin, V. V.; Sharpless, K. B., A Stepwise Huisgen Cycloaddition Process: Copper(I)-Catalyzed Regioselective "Ligation" of Azides and Terminal Alkynes. *Angewandte Chemie International Edition* **2002,** *41* (14), 2596-2599.

[59] Tornøe, C. W.; Christensen, C.; Meldal, M., Peptidotriazoles on Solid Phase: [1,2,3]-Triazoles by Regiospecific Copper(I)-Catalyzed 1,3-Dipolar Cycloadditions of Terminal Alkynes to Azides. *The Journal of Organic Chemistry* **2002,** *67* (9), 3057-3064.

[60] Vecchi, A.; Melai, B.; Marra, A.; Chiappe, C.; Dondoni, A., Microwave-Enhanced Ionothermal CuAAC for the Synthesis of Glycoclusters on a Calix[4]arene Platform. *The Journal of Organic Chemistry* **2008,** *73* (16), 6437-6440.

[61] Himo, F.; Lovell, T.; Hilgraf, R.; Rostovtsev, V. V.; Noodleman, L.; Sharpless, K. B.; Fokin, V. V., Copper(I)-Catalyzed Synthesis of Azoles. DFT Study Predicts Unprecedented Reactivity and Intermediates. *Journal of the American Chemical Society* **2005,** *127* (1), 210-216.

[62] Appukkuttan, P.; Dehaen, W.; Fokin, V. V.; Van der Eycken, E., A Microwave-Assisted Click Chemistry Synthesis of 1,4-Disubstituted 1,2,3-Triazoles via a Copper(I)-Catalyzed Three-Component Reaction. *Organic Letters* **2004,** *6* (23), 4223-4225.

[63] Golas, P. L.; Tsarevsky, N. V.; Sumerlin, B. S.; Matyjaszewski, K., Catalyst Performance in "Click" Coupling Reactions of Polymers Prepared by ATRP: Ligand and Metal Effects. *Macromolecules* **2006,** *39* (19), 6451-6457.

[64] Chowdhury, C.; Mandal, S. B.; Achari, B., Palladium–copper catalysed heteroannulation of acetylenic compounds: an expeditious synthesis of isoindoline fused with triazoles. *Tetrahedron Letters* **2005,** *46* (49), 8531-8534.

[65] Ding, S.; Jia, G.; Sun, J., Iridium-Catalyzed Intermolecular Azide–Alkyne Cycloaddition of Internal Thioalkynes under Mild Conditions. *Angewandte Chemie* **2014,** *126* (7), 1908-1911.

[66] Zhang, L.; Chen, X.; Xue, P.; Sun, H. H. Y.; Williams, I. D.; Sharpless, K. B.; Fokin, V. V.; Jia, G., Ruthenium-Catalyzed Cycloaddition of Alkynes and Organic Azides. *Journal of the American Chemical Society* **2005,** *127* (46), 15998-15999.

[67] Oppilliart, S.; Mousseau, G.; Zhang, L.; Jia, G.; Thuéry, P.; Rousseau, B.; Cintrat, J.-C., 1-Protected 5-amido 1,2,3-triazoles via ruthenium-catalyzed [3+2] cycloaddition of azides and ynamides. *Tetrahedron* **2007,** *63* (34), 8094-8098.

[68] Partyka, D. V.; Updegraff, J. B.; Zeller, M.; Hunter, A. D.; Gray, T. G., Carbon−Gold Bond Formation through [3 + 2] Cycloaddition Reactions of Gold(I) Azides and Terminal Alkynes. *Organometallics* **2007,** *26* (1), 183-186.

[69] Partyka, D. V.; Gao, L.; Teets, T. S.; Updegraff, J. B.; Deligonul, N.; Gray, T. G., Copper-Catalyzed Huisgen [3 + 2] Cycloaddition of Gold(I) Alkynyls with Benzyl Azide. Syntheses, Structures, and Optical Properties. *Organometallics* **2009,** *28* (21), 6171-6182.

[70] Heckler, J. E.; Deligonul, N.; Rheingold, A. L.; Gray, T. G., Gold(i) triazolyls: organometallic synthesis in air and aqueous media. *Chemical Communications* **2013,** *49* (53), 5990-5992.

[71] Stefani, H. A.; Silva, N. C. S.; Vasconcelos, S. N. S.; Manarin, F.; Souza, F. B., Functionalization of 5-telluro-1,2,3-triazoles: Te/Li exchange and Suzuki–Miyaura cross-coupling reaction. *Tetrahedron Letters* **2013,** *54* (22), 2809-2812.

[72] Golas, P. L.; Matyjaszewski, K., Marrying click chemistry with polymerization: expanding the scope of polymeric materials. *Chemical Society Reviews* **2010,** *39* (4), 1338-1354.

[73] Altintas, O.; Yankul, B.; Hizal, G.; Tunca, U., A3-type star polymers via click chemistry. *Journal of Polymer Science Part A: Polymer Chemistry* **2006,** *44* (21), 6458-6465.

[74] Whittaker, M. R.; Urbani, C. N.; Monteiro, M. J., Synthesis of 3-Miktoarm Stars and 1st Generation Mikto Dendritic Copolymers by "Living" Radical Polymerization and "Click" Chemistry. *Journal of the American Chemical Society* **2006,** *128* (35), 11360-11361.

[75] Binder, W. H.; Petraru, L.; Roth, T.; Groh, P. W.; Pálfi, V.; Keki, S.; Ivan, B., Magnetic and Temperature-Sensitive Release Gels from Supramolecular Polymers. *Advanced Functional Materials* **2007,** *17* (8), 1317-1326.

[76] Vogt, A. P.; Sumerlin, B. S., An Efficient Route to Macromonomers via ATRP and Click Chemistry. *Macromolecules* **2006,** *39* (16), 5286-5292.

[77] Ergin, M.; Kiskan, B.; Gacal, B.; Yagci, Y., Thermally Curable Polystyrene via Click Chemistry. *Macromolecules* **2007,** *40* (13), 4724-4727.

[78] Jung, J.-H.; Lim, Y.-G.; Lee, K.-H.; Koo, B. T., Synthesis of glycidyl triazolyl polymers using click chemistry. *Tetrahedron Letters* **2007,** *48* (37), 6442-6448.

[79] Zeng, Q.; Li, Z. a.; Li, Z.; Ye, C.; Qin, J.; Tang, B. Z., Convenient Attachment of Highly Polar Azo Chromophore Moieties to Disubstituted Polyacetylene through Polymer Reactions by Using "Click" Chemistry. *Macromolecules* **2007,** *40* (16), 5634-5637.

[80] Ornelas, C.; Aranzaes, J. R.; Cloutet, E.; Alves, S.; Astruc, D., Click Assembly of 1,2,3-Triazole-Linked Dendrimers, Including Ferrocenyl Dendrimers, Which Sense Both Oxo Anions and Metal Cations. *Angewandte Chemie International Edition* **2007,** *46* (6), 872-877.

[81] Voit, B., The potential of cycloaddition reactions in the synthesis of dendritic polymers. *New Journal of Chemistry* **2007,** *31* (7), 1139-1151.

[82] Rodionov, V. O.; Fokin, V. V.; Finn, M. G., Mechanism of the Ligand-Free Cu^I-Catalyzed Azide–Alkyne Cycloaddition Reaction. *Angewandte Chemie International Edition* **2005,** *44* (15), 2210-2215.

[83] Bock, V. D.; Hiemstra, H.; van Maarseveen, J. H., Cu^I-Catalyzed Alkyne–Azide "Click" Cycloadditions from a Mechanistic and Synthetic Perspective. *European Journal of Organic Chemistry* **2006,** *2006* (1), 51-68.

[84] Worrell, B. T.; Malik, J. A.; Fokin, V. V., Direct Evidence of a Dinuclear Copper Intermediate in Cu(I)-Catalyzed Azide-Alkyne Cycloadditions. *Science* **2013,** *340* (6131), 457-460.

[85] Himo, F.; Lovell, T.; Hilgraf, R.; Rostovtsev, V. V.; Noodleman, L.; Sharpless, K. B.; Fokin, V. V., Copper(I)-Catalyzed Synthesis of Azoles. DFT Study Predicts Unprecedented Reactivity and Intermediates. *Journal of the American Chemical Society* **2004,** *127* (1), 210-216.

[86] Tron, G. C.; Pirali, T.; Billington, R. A.; Canonico, P. L.; Sorba, G.; Genazzani, A. A., Click chemistry reactions in medicinal chemistry: Applications of the 1,3-dipolar cycloaddition between azides and alkynes. *Medicinal Research Reviews* **2008,** *28* (2), 278-308.

[87] Thirumurugan, P.; Matosiuk, D.; Jozwiak, K., Click Chemistry for Drug Development and Diverse Chemical−Biology Applications. *Chemical Reviews* **2013,** *113* (7), 4905-4979.

[88] Yang, M.; Li, J.; Chen, P. R., Transition metal-mediated bioorthogonal protein chemistry in living cells. *Chemical Society Reviews* **2014,** *43* (18), 6511-6526.

[89] Roice, M.; Johannsen, I.; Meldal, M., High Capacity Poly(ethylene glycol) Based Amino Polymers for Peptide and Organic Synthesis. *QSAR & Combinatorial Science* **2004,** *23* (8), 662-673.

[90] Holland-Nell, K.; Meldal, M., Maintaining Biological Activity by Using Triazoles as Disufide Bond Mimetics. *Angewandte Chemie International Edition* **2011,** *50* (22), 5204-5206.

[91] Johnson, R. P.; John, J. V.; Kim, I., Recent developments in polymer–*block*–polypeptide and protein–polymer bioconjugate hybrid materials. *European Polymer Journal* **2013,** *49* (10), 2925-2948.

[92] Fu, R.; Fu, G.-D., Polymeric nanomaterials from combined click chemistry and controlled radical polymerization. *Polymer Chemistry* **2011,** *2* (3), 465-475.

[93] Glaser, C., Beiträge zur Kenntniss des Acetenylbenzols. *Berichte der deutschen chemischen Gesellschaft* **1869,** *2* (1), 422-424.

[94] Chodkiewicz, W.; Cadiot, P., New synthesis of symmetrical and asymmetrical conjugates polyacetylenes. *C. R. Hebd. Seances Acad. Sci.* **1955,** *241*, 1055-1057.

[95] Siemsen, P.; Livingston, R. C.; Diederich, F., Acetylenic Coupling: A Powerful Tool in Molecular Construction. *Angewandte Chemie International Edition* **2000,** *39* (15), 2632-2657.

[96] Angell, Y.; Burgess, K., Base Dependence in Copper-Catalyzed Huisgen Reactions: Efficient Formation of Bistriazoles. *Angewandte Chemie International Edition* **2007,** *46* (20), 3649-3651.

[97] Staudinger, H.; Meyer, J., Über neue organische Phosphorverbindungen III. Phosphinmethylenderivate und Phosphinimine. *Helvetica Chimica Acta* **1919,** *2* (1), 635-646.

[98] Steinborn, D., *Grundlagen der metallorganischen Komplexkatalyse*. Teubner: Wiesbaden, Germany: **2007**.

[99] Kuijpers, B. H. M.; Groothuys, S.; Keereweer, A. R.; Quaedflieg, P. J. L. M.; Blaauw, R. H.; van Delft, F. L.; Rutjes, F. P. J. T., Expedient Synthesis of Triazole-Linked Glycosyl Amino Acids and Peptides. *Organic Letters* **2004,** *6* (18), 3123-3126.

[100] Link, A. J.; Tirrell, D. A., Cell Surface Labeling of Escherichia coli via Copper(I)-Catalyzed [3+2] Cycloaddition. *Journal of the American Chemical Society* **2003,** *125* (37), 11164-11165.

[101] Speers, A. E.; Adam, G. C.; Cravatt, B. F., Activity-Based Protein Profiling in Vivo Using a Copper(I)-Catalyzed Azide-Alkyne [3 + 2] Cycloaddition. *Journal of the American Chemical Society* **2003,** *125* (16), 4686-4687.

[102] Meunier, S.; Strable, E.; Finn, M. G., Crosslinking of and Coupling to Viral Capsid Proteins by Tyrosine Oxidation. *Chemistry & Biology* **2004,** *11* (3), 319-326.

[103] Beatty, K. E.; Liu, J. C.; Xie, F.; Dieterich, D. C.; Schuman, E. M.; Wang, Q.; Tirrell, D. A., Fluorescence Visualization of Newly Synthesized Proteins in Mammalian Cells. *Angewandte Chemie International Edition* **2006,** *45* (44), 7364-7367.

[104] Wollack, J. W.; Silverman, J. M.; Petzold, C. J.; Mougous, J. D.; Distefano, M. D., A Minimalist Substrate for Enzymatic Peptide and Protein Conjugation. *ChemBioChem* **2009,** *10* (18), 2934-2943.

[105] Ingale, S. A.; Pujari, S. S.; Sirivolu, V. R.; Ding, P.; Xiong, H.; Mei, H.; Seela, F., 7-Deazapurine and 8-Aza-7-deazapurine Nucleoside and Oligonucleotide Pyrene "Click"

Conjugates: Synthesis, Nucleobase Controlled Fluorescence Quenching, and Duplex Stability. *The Journal of Organic Chemistry* **2012,** *77* (1), 188-199.

[106] Ingale, S. A.; Seela, F., Stepwise Click Functionalization of DNA through a Bifunctional Azide with a Chelating and a Nonchelating Azido Group. *The Journal of Organic Chemistry* **2013,** *78* (7), 3394-3399.

[107] Wang, Q.; Chan, T. R.; Hilgraf, R.; Fokin, V. V.; Sharpless, K. B.; Finn, M. G., Bioconjugation by Copper(I)-Catalyzed Azide-Alkyne [3 + 2] Cycloaddition. *Journal of the American Chemical Society* **2003,** *125* (11), 3192-3193.

[108] Reddy, K. R.; Rajgopal, K.; Kantam, M. L., Copper(II)-Promoted Regioselective Synthesis of 1,4-Disubstituted 1,2,3-Triazoles in Water. *Synlett* **2006,** *2006* (06), 957-959.

[109] Brotherton, W. S.; Michaels, H. A.; Simmons, J. T.; Clark, R. J.; Dalal, N. S.; Zhu, L., Apparent Copper(II)-Accelerated Azide–Alkyne Cycloaddition. *Organic Letters* **2009,** *11* (21), 4954-4957.

[110] Tasdelen, M. A.; Yagci, Y., Light-induced copper(I)-catalyzed click chemistry. *Tetrahedron Letters* **2010,** *51* (52), 6945-6947.

[111] Adzima, B. J.; Tao, Y.; Kloxin, C. J.; DeForest, C. A.; Anseth, K. S.; Bowman, C. N., Spatial and temporal control of the alkyne–azide cycloaddition by photoinitiated Cu(II) reduction. *Nature Chemistry* **2011,** *3*, 256.

[112] Berg, R.; Straub, J.; Schreiner, E.; Mader, S.; Rominger, F.; Straub, B. F., Highly Active Dinuclear Copper Catalysts for Homogeneous Azide–Alkyne Cycloadditions. *Advanced Synthesis & Catalysis* **2012,** *354* (18), 3445-3450.

[113] Wang, W.; Wu, J.; Xia, C.; Li, F., Reusable ammonium salt-tagged NHC-Cu(I) complexes: preparation and catalytic application in the three component click reaction. *Green Chemistry* **2011,** *13* (12), 3440-3445.

[114] Gaulier, C.; Hospital, A.; Legeret, B.; Delmas, A. F.; Aucagne, V.; Cisnetti, F.; Gautier, A., A water soluble Cu^I-NHC for CuAAC ligation of unprotected peptides under open air conditions. *Chemical Communications* **2012,** *48* (33), 4005-4007.

[115] Han, X.; Weng, Z.; Young, D. J.; Jin, G.-X.; Andy Hor, T. S., Stoichiometric sensitivity and structural diversity in click-active copper(I) N,S-heterocyclic carbene complexes. *Dalton Transactions* **2014,** *43* (3), 1305-1312.

[116] Bergbreiter, D. E.; Hamilton, P. N.; Koshti, N. M., Self-Separating Homogeneous Copper (I) Catalysts. *Journal of the American Chemical Society* **2007,** *129* (35), 10666-10667.

[117] Deraedt, C.; Pinaud, N.; Astruc, D., Recyclable Catalytic Dendrimer Nanoreactor for Part-Per-Million Cu^I Catalysis of "Click" Chemistry in Water. *Journal of the American Chemical Society* **2014,** *136* (34), 12092-12098.

[118] Brewer, G. J., Risks of Copper and Iron Toxicity during Aging in Humans. *Chemical Research in Toxicology* **2010,** *23* (2), 319-326.

[119] Ning, X.; Guo, J.; Wolfert, M. A.; Boons, G. J., Visualizing Metabolically Labeled Glycoconjugates of Living Cells by Copper-Free and Fast Huisgen Cycloadditions. *Angewandte Chemie International Edition* **2008,** *47* (12), 2253-2255.

[120] Presolski, S. I.; Hong, V.; Cho, S.-H.; Finn, M. G., Tailored Ligand Acceleration of the Cu-Catalyzed Azide–Alkyne Cycloaddition Reaction: Practical and Mechanistic Implications. *Journal of the American Chemical Society* **2010,** *132* (41), 14570-14576.

[121] Chen, H.; Ni, B.-B.; Gao, F.; Ma, Y., Pressure-accelerated copper-free cycloaddition of azide and alkyne groups pre-organized in the crystalline state at room temperature. *Green Chemistry* **2012,** *14* (10), 2703-2705.

[122] Schüth, F., Heterogene Katalyse. Schlüsseltechnologie der chemischen Industrie. *Chemie in unserer Zeit* **2006,** *40* (2), 92-103.

[123] Chassaing, S.; Beneteau, V.; Pale, P., When CuAAC 'Click Chemistry' goes heterogeneous. *Catalysis Science & Technology* **2016,** *6* (4), 923-957.

[124] Girard, C.; Önen, E.; Aufort, M.; Beauvière, S.; Samson, E.; Herscovici, J., Reusable Polymer-Supported Catalyst for the [3+2] Huisgen Cycloaddition in Automation Protocols. *Organic Letters* **2006,** *8* (8), 1689-1692.

[125] Sirion, U.; Jin Bae, Y.; Se Lee, B.; Chi, D. Y., Ionic Polymer Supported Copper(I): A Reusable Catalyst for Huisgen's 1,3-Dipolar Cycloaddition. *Synlett* **2008,** 2326-2330.

[126] Chavan, P. V.; Pandit, K. S.; Desai, U. V.; Kulkarni, M. A.; Wadgaonkar, P. P., Cellulose supported cuprous iodide nanoparticles (Cell-CuI NPs): a new heterogeneous and recyclable catalyst for the one pot synthesis of 1,4-disubstituted - 1,2,3-triazoles in water. *RSC Advances* **2014,** *4* (79), 42137-42146.

[127] Lipshutz, B. H.; Taft, B. R., Heterogeneous Copper-in-Charcoal-Catalyzed Click Chemistry. *Angewandte Chemie International Edition* **2006,** *45* (48), 8235-8238.

[128] Sharghi, H.; Beyzavi, M. H.; Safavi, A.; Doroodmand, M. M.; Khalifeh, R., Immobilization of Porphyrinatocopper Nanoparticles onto Activated Multi-Walled Carbon Nanotubes and a Study of its Catalytic Activity as an Efficient Heterogeneous Catalyst for a Click Approach to the Three-Component Synthesis of 1,2,3-Triazoles in Water. *Advanced Synthesis & Catalysis* **2009,** *351* (14-15), 2391-2410.

[129] Li, P.; Wang, L.; Zhang, Y., SiO_2-NHC-Cu(I): an efficient and reusable catalyst for [3+2] cycloaddition of organic azides and terminal alkynes under solvent-free reaction conditions at room temperature. *Tetrahedron* **2008,** *64* (48), 10825-10830.

[130] Mukherjee, N.; Ahammed, S.; Bhadra, S.; Ranu, B. C., Solvent-free one-pot synthesis of 1,2,3-triazole derivatives by the 'Click' reaction of alkyl halides or aryl boronic acids, sodium azide and terminal alkynes over a Cu/Al_2O_3 surface under ball-milling. *Green Chemistry* **2013,** *15* (2), 389-397.

[131] Yamaguchi, K.; Oishi, T.; Katayama, T.; Mizuno, N., A Supported Copper Hydroxide on Titanium Oxide as an Efficient Reusable Heterogeneous Catalyst for 1,3-Dipolar Cycloaddition of Organic Azides to Terminal Alkynes. *Chemistry – A European Journal* **2009,** *15* (40), 10464-10472.

[132] Roy, S.; Chatterjee, T.; Pramanik, M.; Roy, A. S.; Bhaumik, A.; Islam, S. M., Cu(II)-anchored functionalized mesoporous SBA-15: An efficient and recyclable catalyst for the one-pot Click reaction in water. *Journal of Molecular Catalysis A: Chemical* **2014,** *386*, 78-85.

[133] Chassaing, S.; Sido, A. S. S.; Alix, A.; Kumarraja, M.; Pale, P.; Sommer, J., "Click Chemistry" in Zeolites: Copper(I) Zeolites as New Heterogeneous and Ligand-Free Catalysts for the Huisgen [3+2] Cycloaddition. *Chemistry – A European Journal* **2008,** *14* (22), 6713-6721.

[134] Li, P.; Regati, S.; Huang, H.; Arman, H. D.; Zhao, J. C. G.; Chen, B., A metal-organic framework as a highly efficient and reusable catalyst for the solvent-free 1,3-dipolar cycloaddition of organic azides to alkynes. *Inorganic Chemistry Frontiers* **2015,** *2* (1), 42-46.

[135] Prasad, A. N.; Thirupathi, B.; Raju, G.; Srinivas, R.; Reddy, B. M., One pot 'click' reaction: Cu^{II}–hydrotalcite catalyzed tandem synthesis of ß-hydroxy triazoles *via* regioselective opening of epoxide followed by [3+2] cycloaddition. *Catalysis Science & Technology* **2012,** *2* (6), 1264-1268.

[136] Jlalia, I.; Elamari, H.; Meganem, F.; Herscovici, J.; Girard, C., Copper(I)-doped Wyoming's montmorillonite for the synthesis of disubstituted 1,2,3-triazoles. *Tetrahedron Letters* **2008,** *49* (48), 6756-6758.

[137] Kamata, K.; Nakagawa, Y.; Yamaguchi, K.; Mizuno, N., 1,3-Dipolar Cycloaddition of Organic Azides to Alkynes by a Dicopper-Substituted Silicotungstate. *Journal of the American Chemical Society* **2008,** *130* (46), 15304-15310.

[138] Anil Kumar, B. S. P.; Harsha Vardhan Reddy, K.; Madhav, B.; Ramesh, K.; Nageswar, Y. V. D., Magnetically separable $CuFe_2O_4$ nano particles catalyzed multicomponent synthesis of 1,4-disubstituted 1,2,3-triazoles in tap water using 'click chemistry'. *Tetrahedron Letters* **2012,** *53* (34), 4595-4599.

[139] Masuyama, Y.; Yoshikawa, K.; Suzuki, N.; Hara, K.; Fukuoka, A., Hydroxyapatite-supported copper(II)-catalyzed azide–alkyne [3+2] cycloaddition with neither reducing agents nor bases in water. *Tetrahedron Letters* **2011,** *52* (51), 6916-6918.

[140] Huang, L.; Liu, W.; Wu, J.; Fu, Y.; Wang, K.; Huo, C.; Du, Z., Nano-copper catalyzed three-component reaction to construct 1,4-substituted 1,2,3-triazoles. *Tetrahedron Letters* **2014,** *55* (14), 2312-2316.

[141] Tienan, J.; Mei, Y.; Menggenbateer; Taketoshi, M.; Ming, B.; Yoshinori, Y., Nanoporous Copper Metal Catalyst in Click Chemistry: Nanoporosity-Dependent Activity without Supports and Bases. *Advanced Synthesis & Catalysis* **2011,** *353* (17), 3095-3100.

[142] Cook, T. L.; Walker, J. A.; Mack, J., Scratching the catalytic surface of mechanochemistry: a multi-component CuAAC reaction using a copper reaction vial. *Green Chemistry* **2013,** *15* (3), 617-619.

[143] Kun, K. A.; Kunin, R., The pore structure of macroreticular ion exchange resins. *Journal of Polymer Science Part C: Polymer Symposia* **1967,** *16* (3), 1457-1469.

[144] Jlalia, I.; Beauvineau, C.; Beauvière, S.; Önen, E.; Aufort, M.; Beauvineau, A.; Khaba, E.; Herscovici, J.; Meganem, F.; Girard, C., Automated Synthesis of a 96 Product-Sized Library of Triazole Derivatives Using a Solid Phase Supported Copper Catalyst. *Molecules* **2010,** *15* (5), 3087.

[145] Albadi, J.; Keshavarz, M., Polymer-Supported Azide and Copper(I): Green Reusable Reagent and Catalyst for Click Cyclization. *Synthetic Communications* **2013,** *43* (15), 2019-2030.

[146] Valentin, R.; Bonelli, B.; Garrone, E.; Di Renzo, F.; Quignard, F., Accessibility of the Functional Groups of Chitosan Aerogel Probed by FT-IR-Monitored Deuteration. *Biomacromolecules* **2007,** *8* (11), 3646-3650.

[147] Chtchigrovsky, M.; Primo, A.; Gonzalez, P.; Molvinger, K.; Robitzer, M.; Quignard, F.; Taran, F., Functionalized Chitosan as a Green, Recyclable, Biopolymer-Supported Catalyst for the [3+2] Huisgen Cycloaddition. *Angewandte Chemie International Edition* **2009,** *48* (32), 5916-5920.

[148] Martina, K.; Leonhardt, S. E. S.; Ondruschka, B.; Curini, M.; Binello, A.; Cravotto, G., In situ cross-linked chitosan Cu(I) or Pd(II) complexes as a versatile, eco-friendly recyclable solid catalyst. *Journal of Molecular Catalysis A: Chemical* **2011,** *334* (1), 60-64.

[149] Baig, R. B. N.; Varma, R. S., Copper on chitosan: a recyclable heterogeneous catalyst for azide-alkyne cycloaddition reactions in water. *Green Chemistry* **2013,** *15* (7), 1839-1843.

[150] Rajender Reddy, K.; Rajgopal, K.; Lakshmi Kantam, M., Copper-alginates: a biopolymer supported Cu(II) catalyst for 1,3-dipolar cycloaddition of alkynes with azides and oxidative coupling of 2-naphthols and phenols in water. *Catalysis Letters* **2007,** *114* (1), 36-40.

[151] Besson, M.; Gallezot, P.; Perrard, A.; Pinel, C., Active carbons as catalysts for liquid phase reactions. *Catalysis Today* **2005,** *102-103*, 160-165.

[152] Shaygan Nia, A.; Binder, W. H., Graphene as initiator/catalyst in polymerization chemistry. *Progress in Polymer Science* **2017,** *67*, 48-76.

[153] Fuchs, M.; Goessler, W.; Pilger, C.; Kappe, C. O., Mechanistic Insights into Copper(I)-Catalyzed Azide-Alkyne Cycloadditions using Continuous Flow Conditions. *Advanced Synthesis & Catalysis* **2010,** *352* (2-3), 323-328.

[154] Sharghi, H.; Ebrahimpourmoghaddam, S.; Doroodmand, M. M.; Purkhosrow, A., Synthesis of Vasorelaxaing 1,4-Disubstituted 1,2,3-Triazoles Catalyzed by a 4′-Phenyl-2,2′:6′,2″-Terpyridine Copper(II) Complex Immobilized on Activated Multiwalled Carbon Nanotubes. *Asian Journal of Organic Chemistry* **2012,** *1* (4), 377-388.

[155] Rao, C. N. R.; Govindaraj, A., Carbon Nanotubes from Organometallic Precursors. *Accounts of Chemical Research* **2002,** *35* (12), 998-1007.

[156] Sarkar, S.; Moser, M. L.; Tian, X.; Zhang, X.; Al-Hadeethi, Y. F.; Haddon, R. C., Metals on Graphene and Carbon Nanotube Surfaces: From Mobile Atoms to Atomtronics to Bulk Metals to Clusters and Catalysts. *Chemistry of Materials* **2014,** *26* (1), 184-195.

[157] Zhang, J.; Cheng, Y.; Lu, S.; Jia, L.; Shen, P. K.; Jiang, S. P., Significant promotion effect of carbon nanotubes on the electrocatalytic activity of supported Pd NPs for ethanol oxidation reaction of fuel cells: the role of inner tubes. *Chemical Communications* **2014,** *50* (89), 13732-13734.

[158] Dreyer, D. R.; Ruoff, R. S.; Bielawski, C. W., From Conception to Realization: An Historial Account of Graphene and Some Perspectives for Its Future. *Angewandte Chemie International Edition* **2010,** *49* (49), 9336-9344.

[159] Eigler, S.; Hirsch, A., Chemistry with Graphene and Graphene Oxide—Challenges for Synthetic Chemists. *Angewandte Chemie International Edition* **2014,** *53* (30), 7720-7738.

[160] Machado, B. F.; Serp, P., Graphene-based materials for catalysis. *Catalysis Science & Technology* **2012,** *2* (1), 54-75.

[161] Su, C.; Loh, K. P., Carbocatalysts: Graphene Oxide and Its Derivatives. *Accounts of Chemical Research* **2013,** *46* (10), 2275-2285.

[162] Fan, X.; Zhang, G.; Zhang, F., Multiple roles of graphene in heterogeneous catalysis. *Chemical Society Reviews* **2015,** *44* (10), 3023-3035.

[163] Li, Y.; Wang, H.; Xie, L.; Liang, Y.; Hong, G.; Dai, H., MoS$_2$ Nanoparticles Grown on Graphene: An Advanced Catalyst for the Hydrogen Evolution Reaction. *Journal of the American Chemical Society* **2011,** *133* (19), 7296-7299.

[164] Hummers, W. S.; Offeman, R. E., Preparation of Graphitic Oxide. *Journal of the American Chemical Society* **1958,** *80* (6), 1339-1339.

[165] Naeimi, H.; Nejadshafiee, V., Efficient one-pot click synthesis of ß-hydroxy-1,2,3-triazoles catalyzed by copper(I)@phosphorated SiO$_2$ *via* multicomponent reaction in aqueous media. *New Journal of Chemistry* **2014,** *38* (11), 5429-5435.

[166] Cravotto, G.; Fokin, V. V.; Garella, D.; Binello, A.; Boffa, L.; Barge, A., Ultrasound-Promoted Copper-Catalyzed Azide–Alkyne Cycloaddition. *Journal of Combinatorial Chemistry* **2010,** *12* (1), 13-15.

[167] Alonso, F.; Moglie, Y.; Radivoy, G., Copper Nanoparticles in Click Chemistry. *Accounts of Chemical Research* **2015,** *48* (9), 2516-2528.

[168] Tienan, J.; Mei, Y.; Yoshinori, Y., Click Chemistry of Alkyne–Azide Cycloaddition using Nanostructured Copper Catalysts. *ChemCatChem* **2012,** *4* (9), 1217-1229.

[169] Kupracz, L.; Hartwig, J.; Wegner, J.; Ceylan, S.; Kirschning, A., Multistep flow synthesis of vinyl azides and their use in the copper-catalyzed Huisgen-type cycloaddition under inductive-heating conditions. *Beilstein Journal of Organic Chemistry* **2011,** *7*, 1441-1448.

[170] Ceylan, S.; Klande, T.; Vogt, C.; Friese, C.; Kirschning, A., Chemical Synthesis with Inductively Heated Copper Flow Reactors. *Synlett* **2010,** *2010* (13), 2009-2013.

[171] Ötvös, S. B.; Georgiádes, Á.; Mándity, I. M.; Kiss, L.; Fülöp, F., Efficient continuous-flow synthesis of novel 1,2,3-triazole-substituted ß-aminocyclohexanecarboxylic acid derivatives with gram-scale production. *Beilstein Journal of Organic Chemistry* **2013,** *9*, 1508-1516.

[172] Bogdan, A. R.; Sach, N. W., The Use of Copper Flow Reactor Technology for the Continuous Synthesis of 1,4-Disubstituted 1,2,3-Triazoles. *Advanced Synthesis & Catalysis* **2009,** *351* (6), 849-854.

[173] Berg, R.; Straub, B. F., Advancements in the mechanistic understanding of the copper-catalyzed azide–alkyne cycloaddition. *Beilstein Journal of Organic Chemistry* **2013,** *9*, 2715-2750.

[174] Rodionov, V. O.; Presolski, S. I.; Díaz Díaz, D.; Fokin, V. V.; Finn, M. G., Ligand-Accelerated Cu-Catalyzed Azide–Alkyne Cycloaddition: A Mechanistic Report. *Journal of the American Chemical Society* **2007,** *129* (42), 12705-12712.

[175] Rodionov, V. O.; Presolski, S. I.; Gardinier, S.; Lim, Y.-H.; Finn, M. G., Benzimidazole and Related Ligands for Cu-Catalyzed Azide-Alkyne Cycloaddition. *Journal of the American Chemical Society* **2007,** *129* (42), 12696-12704.

[176] Bratsch, S. G., Standard Electrode Potentials and Temperature Coefficients in Water at 298.15 K. *Journal of Physical and Chemical Reference Data* **1989,** *18* (1), 1-21.

[177] Moen, A.; Nicholson, D. G., Reduction of copper(II) with subsequent disproportionation of copper(I) during the hydrothermal syntheses of microporous silicoaluminium phosphates sapo-5 and -11. *Journal of the Chemical Society, Faraday Transactions* **1995,** *91* (19), 3529-3535.

[178] Greenwood, N. N.; Earnshaw, A., *Chemistry of the Elements*. Pergamon Press: Oxford, **1993**.

[179] Lee, J. D., *Concise Inorganic Chemistry*. Chapman and Hall: London, **1991**.

[180] Ahrland, S.; Nilsson, K.; Tagesson, B., Thermodynamics of the Copper(I) Halide and Thiocyanate Complex Formation in Acetonitrile. *Acta Chemica Scandinavica* **1983,** *37A*, 193-201.

[181] Gupta, A. K., 666. Electrochemical measurements in pyridine. Part I. The system Cu–Cu+–Cu++. *Journal of the Chemical Society (Resumed)* **1952,** (0), 3473-3479.

[182] Ciavatta, L.; Ferri, D.; Palombari, R., On the equilibrium $Cu2+ + Cu(s) \rightleftarrows 2Cu+$. *Journal of Inorganic and Nuclear Chemistry* **1980,** *42* (4), 593-598.

[183] Chan, T. R.; Hilgraf, R.; Sharpless, K. B.; Fokin, V. V., Polytriazoles as Copper(I)-Stabilizing Ligands in Catalysis. *Organic Letters* **2004,** *6* (17), 2853-2855.

[184] Teyssot, M. L.; Nauton, L.; Canet, J. L.; Cisnetti, F.; Chevry, A.; Gautier, A., Aromatic Nitrogen Donors for Efficient Copper(I)–NHC CuAAC under Reductant-Free Conditions. *European Journal of Organic Chemistry* **2010,** *2010* (18), 3507-03515.

[185] Bevilacqua, V.; King, M.; Chaumontet, M.; Nothisen, M.; Gabillet, S.; Buisson, D.; Puente, C.; Wagner, A.; Taran, F., Copper-Chelating Azides for Efficient Click Conjugation Reactions in Complex Media. *Angewandte Chemie International Edition* **2014,** *53* (23), 5872-5876.

[186] Wu, Y.-M.; Deng, J.; Fang, X.; Chen, Q.-Y., Regioselective synthesis of fluoroalkylated [1,2,3]-triazoles by Huisgen cycloaddition. *Journal of Fluorine Chemistry* **2004,** *125* (10), 1415-1423.

[187] Yan, Z.-Y.; Zhao, Y.-B.; Fan, M.-J.; Liu, W.-M.; Liang, Y.-M., General synthesis of (1-substituted-1H-1,2,3-triazol-4-ylmethyl)-dialkylamines via a copper(I)-catalyzed three-component reaction in water. *Tetrahedron* **2005,** *61* (39), 9331-9337.

[188] Teruaki, H.; Mariko, U.; Munenori, N.; Tomohisa, F.; Shuichi, H.; Kazuo, S.; Seiji, S., Click Chemistry on Curdlan: A Regioselective and Quantitative Approach to Develop Artificial β-1,3-Glucans with Various Functional Appendages. *Chemistry Letters* **2006,** *35* (1), 82-83.

[189] Kalesh, K. A.; Liu, K.; Yao, S. Q., Rapid synthesis of Abelson tyrosine kinase inhibitors using click chemistry. *Organic & Biomolecular Chemistry* **2009,** *7* (24), 5129-5136.

[190] Hong, V.; Presolski, S. I.; Ma, C.; Finn, M. G., Analysis and Optimization of Copper-Catalyzed Azide–Alkyne Cycloaddition for Bioconjugation. *Angewandte Chemie International Edition* **2009,** *48* (52), 9879-9883.

[191] Hong, V.; Steinmetz, N. F.; Manchester, M.; Finn, M. G., Labeling Live Cells by Copper-Catalyzed Alkyne-Azide Click Chemistry. *Bioconjugate Chemistry* **2010,** *21* (10), 1912-1916.

[192] Besanceney-Webler, C.; Jiang, H.; Zheng, T.; Feng, L.; Soriano del Amo, D.; Wang, W.; Klivansky, L. M.; Marlow, F. L.; Liu, Y.; Wu, P., Increasing the Efficacy of Bioorthogonal Click Reactions for Bioconjugation: A Comparative Study. *Angewandte Chemie* **2011,** *123* (35), 8201-8206.

[193] Rudolf, G. C.; Sieber, S. A., Copper-Assisted Click Reactions for Activity-Based Proteomics: Fine-Tuned Ligands and Refined Conditions Extend the Scope of Application. *ChemBioChem* **2013,** *14* (18), 2447-2455.

[194] Yang, M.; Jalloh, A. S.; Wei, W.; Zhao, J.; Wu, P.; Chen, P. R., Biocompatible click chemistry enabled compartment-specific pH measurement inside E. coli. *Nature Communications* **2014,** *5*, 4981.

[195] Lewis, W. G.; Magallon, F. G.; Fokin, V. V.; Finn, M. G., Discovery and Characterization of Catalysts for Azide–Alkyne Cycloaddition by Fluorescence Quenching. *Journal of the American Chemical Society* **2004,** *126* (30), 9152-9153.

[196] Zhu, Z.; Chen, H.; Li, S.; Yang, X.; Bittner, E.; Cai, C., Tripodal amine ligands for accelerating Cu-catalyzed azide-alkyne cycloaddition: efficiency and stability against oxidation and dissociation. *Catalysis Science & Technology* **2017,** *7* (12), 2474-2485.

[197] Gonda, Z.; Novak, Z., Highly active copper-catalysts for azide-alkyne cycloaddition. *Dalton Transactions* **2010,** *39* (3), 726-729.

[198] Pérez-Balderas, F.; Ortega-Muñoz, M.; Morales-Sanfrutos, J.; Hernández-Mateo, F.; Calvo-Flores, F. G.; Calvo-Asín, J. A.; Isac-García, J.; Santoyo-González, F., Multivalent Neoglycoconjugates by Regiospecific Cycloaddition of Alkynes and Azides Using Organic-Soluble Copper Catalysts. *Organic Letters* **2003,** *5* (11), 1951-1954.

[199] Campbell-Verduyn, L. S.; Mirfeizi, L.; Dierckx, R. A.; Elsinga, P. H.; Feringa, B. L., Phosphoramidite accelerated copper(I)-catalyzed [3 + 2] cycloadditions of azides and alkynes. *Chemical Communications* **2009,** (16), 2139-2141.

[200] Tanaka, K.; Kageyama, C.; Fukase, K., Acceleration of Cu(I)-mediated Huisgen 1,3-dipolar cycloaddition by histidine derivatives. *Tetrahedron Letters* **2007,** *48* (37), 6475-6479.

[201] Kennedy, D. C.; McKay, C. S.; Legault, M. C. B.; Danielson, D. C.; Blake, J. A.; Pegoraro, A. F.; Stolow, A.; Mester, Z.; Pezacki, J. P., Cellular Consequences of Copper Complexes Used To Catalyze Bioorthogonal Click Reactions. *Journal of the American Chemical Society* **2011,** *133* (44), 17993-18001.

[202] Aucagne, V.; Berná, J.; Crowley, J. D.; Goldup, S. M.; Hänni, K. D.; Leigh, D. A.; Lusby, P. J.; Ronaldson, V. E.; Slawin, A. M. Z.; Viterisi, A.; Walker, D. B., Catalytic "Active-Metal" Template Synthesis of [2]Rotaxanes, [3]Rotaxanes, and Molecular Shuttles, and Some Observations on the Mechanism of the Cu(I)-Catalyzed Azide–

Alkyne 1,3-Cycloaddition. *Journal of the American Chemical Society* **2007,** *129* (39), 11950-11963.

[203] Gerard, B.; Ryan, J.; Beeler, A. B.; Porco, J. A., Synthesis of 1,4,5-trisubstituted-1,2,3-triazoles by copper-catalyzed cycloaddition-coupling of azides and terminal alkynes. *Tetrahedron* **2006,** *62* (26), 6405-6411.

[204] Wang, F.; Fu, H.; Jiang, Y.; Zhao, Y., Quick and highly efficient copper-catalyzed cycloaddition of aliphatic and aryl azides with terminal alkynes "on water". *Green Chemistry* **2008,** *10* (4), 452-456.

[205] Gupta, S. S.; Kuzelka, J.; Singh, P.; Lewis, W. G.; Manchester, M.; Finn, M. G., Accelerated Bioorthogonal Conjugation: A Practical Method for the Ligation of Diverse Functional Molecules to a Polyvalent Virus Scaffold. *Bioconjugate Chemistry* **2005,** *16* (6), 1572-1579.

[206] Soriano del Amo, D.; Wang, W.; Jiang, H.; Besanceney-Webler, C.; Yan, A. C.; Levy, M.; Liu, Y.; Marlow, F. L.; Wu, P., Biocompatible Copper(I) Catalysts for in Vivo Imaging of Glycans. *Journal of the American Chemical Society* **2010,** *132* (47), 16893-16899.

[207] Wei, W.; Senglian, H.; Andrew, T.; Hao, J.; Rebecca, T.; Yi, L.; Xing, C.; Peng, W., Sulfated Ligands for the Copper(I)-Catalyzed Azide–Alkyne Cycloaddition. *Chemistry – An Asian Journal* **2011,** *6* (10), 2796-2802.

[208] Fabbrizzi, P.; Cicchi, S.; Brandi, A.; Sperotto, E.; van Koten, G., An Efficient (2-Aminoarenethiolato)copper(I) Complex for the Copper-Catalysed Huisgen Reaction (CuAAC). *European Journal of Organic Chemistry* **2009,** *2009* (31), 5423-5430.

[209] Marion, N.; Díez-González, S.; Nolan, S. P., N-Heterocyclic Carbenes as Organocatalysts. *Angewandte Chemie International Edition* **2007,** *46* (17), 2988-3000.

[210] Bantreil, X.; Broggi, J.; Nolan, S. P., N-Heterocyclic carbene containing complexes in catalysis. *Annual Reports Section "B" (Organic Chemistry)* **2009,** *105* (0), 232-263.

[211] Lazreg, F.; Nahra, F.; Cazin, C. S. J., Copper–NHC complexes in catalysis. *Coordination Chemistry Reviews* **2015,** *293-294*, 48-79.

[212] Díez-González, S.; Correa, A.; Cavallo, L.; Nolan, S. P., (NHC)Copper(I)-Catalyzed [3+2] Cycloaddition of Azides and Mono- or Disubstituted Alkynes. *Chemistry – A European Journal* **2006,** *12* (29), 7558-7564.

[213] Díez-González, S.; Stevens, E. D.; Nolan, S. P., A [(NHC)CuCl] complex as a latent Click catalyst. *Chemical Communications* **2008,** (39), 4747-4749.

[214] Li, P.; Wang, L.; Zhang, Y., SiO2–NHC–Cu(I): an efficient and reusable catalyst for [3+2] cycloaddition of organic azides and terminal alkynes under solvent-free reaction conditions at room temperature. *Tetrahedron* **2008,** *64* (48), 10825-10830.

[215] Teyssot, M.-L.; Chevry, A.; Traïkia, M.; El-Ghozzi, M.; Avignant, D.; Gautier, A., Improved Copper(I)–NHC Catalytic Efficiency on Huisgen Reaction by Addition of Aromatic Nitrogen Donors. *Chemistry – A European Journal* **2009,** *15* (26), 6322-6326.

[216] Díez-González, S.; Escudero-Adán, E. C.; Benet-Buchholz, J.; Stevens, E. D.; Slawin, A. M. Z.; Nolan, S. P., [(NHC)CuX] complexes: Synthesis, characterization and catalytic activities in reduction reactions and Click Chemistry. On the advantage of using well-defined catalytic systems. *Dalton Transactions* **2010,** *39* (32), 7595-7606.

[217] Collinson, J.-M.; Wilton-Ely, J. D. E. T.; Díez-González, S., Reusable and highly active supported copper(i)–NHC catalysts for Click chemistry. *Chemical Communications* **2013,** *49* (97), 11358-11360.

[218] Díez-González, S.; Nolan, S. P., [(NHC)2Cu]X Complexes as Efficient Catalysts for Azide–Alkyne Click Chemistry at Low Catalyst Loadings. *Angewandte Chemie International Edition* **2008,** *47* (46), 8881-8884.

[219] Lazreg, F.; Slawin, A. M. Z.; Cazin, C. S. J., Heteroleptic Bis(N-heterocyclic carbene)Copper(I) Complexes: Highly Efficient Systems for the [3+2] Cycloaddition of Azides and Alkynes. *Organometallics* **2012,** *31* (22), 7969-7975.

[220] Hohloch, S.; Sarkar, B.; Nauton, L.; Cisnetti, F.; Gautier, A., Are Cu(I)-mesoionic NHC carbenes associated with nitrogen additives the best Cu-carbene catalysts for the azide–alkyne click reaction in solution? A case study. *Tetrahedron Letters* **2013,** *54* (14), 1808-1812.

[221] Hohloch, S.; Scheiffele, D.; Sarkar, B., Activating Azides and Alkynes for the Click Reaction with [Cu(aNHC)2I] or [Cu(aNHC)2]+ (aNHC = Triazole-Derived Abnormal Carbenes): Structural Characterization and Catalytic Properties. *European Journal of Inorganic Chemistry* **2013,** *2013* (22-23), 3956-3965.

[222] Sau, S. C.; Roy, S. R.; Sen, T. K.; Mullangi, D.; Mandal, S. K., An Abnormal N-Heterocyclic Carbene–Copper(I) Complex in Click Chemistry. *Advanced Synthesis & Catalysis* **2013,** *355* (14-15), 2982-2991.

[223] Díez-González, S.; Stevens, E. D.; Scott, N. M.; Petersen, J. L.; Nolan, S. P., Synthesis and Characterization of [Cu(NHC)2]X Complexes: Catalytic and Mechanistic Studies of Hydrosilylation Reactions. *Chemistry – A European Journal* **2008,** *14* (1), 158-168.

[224] Díez-González, S.; Marion, N.; Nolan, S. P., N-Heterocyclic Carbenes in Late Transition Metal Catalysis. *Chemical Reviews* **2009,** *109* (8), 3612-3676.

[225] Ko, S. K.; Jang, H. J.; Kim, E.; Park, S. B., Concise and diversity-oriented synthesis of novel scaffolds embedded with privileged benzopyran motif. *Chemical Communications* **2006,** (28), 2962-2964.

[226] Ritschel, J.; Sasse, F.; Maier, M. E., Synthesis of a Benzolactone Collection using Click Chemistry. *European Journal of Organic Chemistry* **2007,** *2007* (1), 78-87.

[227] Kuang, G.-C.; Michaels, H. A.; Simmons, J. T.; Clark, R. J.; Zhu, L., Chelation-Assisted, Copper(II)-Acetate-Accelerated Azide-Alkyne Cycloaddition. *The Journal of Organic Chemistry* **2010,** *75* (19), 6540-6548.

[228] Uttamapinant, C.; Sanchez, M. I.; Liu, D. S.; Yao, J. Z.; Ting, A. Y., Site-specific protein labeling using PRIME and chelation-assisted click chemistry. *Nat. Protocols* **2013,** *8* (8), 1620-1634.

[229] Binder, W. H., *Self-Healing Polymers. From Principles to Applications.* Wiley-VCH Verlag GmbH & Co. KGaA: Weinheim, **2013**; p 425 pages.

[230] Hillewaere, X. K. D.; Du Prez, F. E., Fifteen chemistries for autonomous external self-healing polymers and composites. *Progress in Polymer Science* **2015,** *49-50*, 121-153.

[231] Döhler, D.; Michael, P.; Neumann, S.; Binder, W. H., Biomimetische Materialien: Selbstheilende Polymere. *Chemie in unserer Zeit* **2016,** *50* (2), 90-101.

[232] Díaz, D. D.; Punna, S.; Holzer, P.; McPherson, A. K.; Sharpless, K. B.; Fokin, V. V.; Finn, M. G., Click chemistry in materials synthesis. 1. Adhesive polymers from copper-catalyzed azide-alkyne cycloaddition. *Journal of Polymer Science Part A: Polymer Chemistry* **2004,** *42* (17), 4392-4403.

[233] Liu, Y.; Díaz, D. D.; Accurso, A. A.; Sharpless, K. B.; Fokin, V. V.; Finn, M. G., Click chemistry in materials synthesis. III. Metal-adhesive polymers from Cu(I)-catalyzed azide–alkyne cycloaddition. *Journal of Polymer Science Part A: Polymer Chemistry* **2007,** *45* (22), 5182-5189.

[234] Sheng, X.; Mauldin, T. C.; Kessler, M. R., Kinetics of bulk azide/alkyne "click" polymerization. *Journal of Polymer Science Part A: Polymer Chemistry* **2010,** *48* (18), 4093-4102.

[235] Sheng, X.; Rock, D. M.; Mauldin, T. C.; Kessler, M. R., Evaluation of different catalyst systems for bulk polymerization through "click" chemistry. *Polymer* **2011,** *52* (20), 4435-4441.

[236] Kargarfard, N.; Diedrich, N.; Rupp, H.; Döhler, D.; Binder, W., Improving Kinetics of "Click-Crosslinking" for Self-Healing Nanocomposites by Graphene-Supported Cu-Nanoparticles. *Polymers* **2018**, *10* (1), 17.

[237] Shaygan Nia, A.; Enders, C.; Binder, W. H., Hydrogen-Bonded Perylene/Terthiophene-Materials: Synthesis and Spectroscopic Properties. *Tetrahedron* **2012**, *68* (2), 722-729

[238] Parvez, K.; Wu, Z.-S.; Li, R.; Liu, X.; Graf, R.; Feng, X.; Müllen, K., Exfoliation of Graphite into Graphene in Aqueous Solutions of Inorganic Salts. *Journal of the American Chemical Society* **2014**, *136* (16), 6083-6091.

[239] Binder, W. H.; Stojanovic, A.; Shaygan Nia, A.; Osim, W.; Rana, S., Proof of successful surface modification of nanofillers with metal catalysts via EDX and FE-SEM measurements. *Jahresbericht 2013 Nanotechnikum Weinberg, Interdisziplinäres Zentrum für Materialwissenschaften* **2014**, 67-68.

[240] Rana, S.; Döhler, D.; Nia, A. S.; Nasir, M.; Wilton, O.; Beiner, M.; Binder, W. H., "Click"-Triggered Self-Healing Graphene Nanocomposites. *Macromol. Rapid Commun.* **2016**, *37* (21), 1715-1722.

[241] Yang, S.; Lohe, M. R.; Müllen, K.; Feng, X., New-Generation Graphene from Electrochemical Approaches: Production and Applications. *Advanced Materials* **2016**, *28* (29), 6213-6221.

[242] Michael, P.; Biewend, M.; Binder, W. H., Mechanochemical Activation of Fluorogenic CuAAC "Click" Reactions for Stress-Sensing Applications. *Macromolecular Rapid Communications* **2018**, *0* (0), 1800376.

[243] White, S. R.; Sottos, N. R.; Geubelle, P. H.; Moore, J. S.; Kessler, M. R.; Sriram, S. R.; Brown, E. N.; Viswanathan, S., Autonomic healing of polymer composites. *Nature* **2001**, *409*, 794.

[244] Yang, Y.; Ding, X.; Urban, M. W., Chemical and physical aspects of self-healing materials. *Progress in Polymer Science* **2015**, *49-50*, 34-59.

[245] Blaiszik, B. J.; Sottos, N. R.; White, S. R., Nanocapsules for self-healing materials. *Composites Science and Technology* **2008**, *68* (3), 978-986.

[246] Zhu, D. Y.; Rong, M. Z.; Zhang, M. Q., Self-healing polymeric materials based on microencapsulated healing agents: From design to preparation. *Progress in Polymer Science* **2015**, *49-50*, 175-220.

[247] Rule, J. D.; Sottos, N. R.; White, S. R., Effect of microcapsule size on the performance of self-healing polymers. *Polymer* **2007**, *48* (12), 3520-3529.

[248] Lv, Z.; Chen, H.; Yuan, H., Quantitative solution on dosage of repair-agent for healing of 3D simplified cracks in materials: short capsule model. *Materials and Structures* **2011**, *44* (5), 987-995.

[249] Lv, Z.; Chen, H., Analytical models for determining the dosage of capsules embedded in self-healing materials. *Computational Materials Science* **2013**, *68*, 81-89.

[250] Wilson, G. O.; Porter, K. A.; Weissman, H.; White, S. R.; Sottos, N. R.; Moore, J. S., Stability of Second Generation Grubbs' Alkylidenes to Primary Amines: Formation of Novel Ruthenium-Amine Complexes. *Advanced Synthesis & Catalysis* **2009**, *351* (11-12), 1817-1825.

[251] Jones, A. S.; Rule, J. D.; Moore, J. S.; White, S. R.; Sottos, N. R., Catalyst Morphology and Dissolution Kinetics of Self-Healing Polymers. *Chemistry of Materials* **2006**, *18* (5), 1312-1317.

[252] Ye, X. J.; Zhang, J.-L.; Zhu, Y.; Rong, M. Z.; Zhang, M. Q.; Song, Y. X.; Zhang, H.-X., Ultrafast Self-Healing of Polymer toward Strength Restoration. *ACS Applied Materials & Interfaces* **2014**, *6* (5), 3661-3670.

[253] Bekas, D. G.; Tsirka, K.; Baltzis, D.; Paipetis, A. S., Self-healing materials: A review of advances in materials, evaluation, characterization and monitoring techniques. *Composites Part B: Engineering* **2016,** *87*, 92-119.

[254] Brown, E. N.; Sottos, N. R.; White, S. R., Fracture testing of a self-healing polymer composite. *Experimental Mechanics* **2002,** *42* (4), 372-379.

[255] Brown, E. N.; White, S. R.; Sottos, N. R., Microcapsule induced toughening in a self-healing polymer composite. *Journal of Materials Science* **2004,** *39* (5), 1703-1710.

[256] Hillewaere, X. K. D.; Teixeira, R. F. A.; Nguyen, L. T. T.; Ramos, J. A.; Rahier, H.; Du Prez, F. E., Autonomous Self-Healing of Epoxy Thermosets with Thiol-Isocyanate Chemistry. *Advanced Functional Materials* **2014,** *24* (35), 5575-5583.

[257] Pratama, P. A.; Sharifi, M.; Peterson, A. M.; Palmese, G. R., Room Temperature Self-Healing Thermoset Based on the Diels−Alder Reaction. *ACS Applied Materials & Interfaces* **2013,** *5* (23), 12425-12431.

[258] Cho, S. H.; Andersson, H. M.; White, S. R.; Sottos, N. R.; Braun, P. V., Polydimethylsiloxane-Based Self-Healing Materials. *Advanced Materials* **2006,** *18* (8), 997-1000.

[259] Keller, M. W.; White, S. R.; Sottos, N. R., A Self-Healing Poly(Dimethyl Siloxane) Elastomer. *Advanced Functional Materials* **2007,** *17* (14), 2399-2404.

[260] Jin, H.; Mangun, C. L.; Stradley, D. S.; Moore, J. S.; Sottos, N. R.; White, S. R., Self-healing thermoset using encapsulated epoxy-amine healing chemistry. *Polymer* **2012,** *53* (2), 581-587.

[261] Jin, H.; Mangun, C. L.; Griffin, A. S.; Moore, J. S.; Sottos, N. R.; White, S. R., Thermally Stable Autonomic Healing in Epoxy using a Dual-Microcapsule System. *Advanced Materials* **2014,** *26* (2), 282-287.

[262] Yuan, Y. C.; Rong, M. Z.; Zhang, M. Q.; Chen, J.; Yang, G. C.; Li, X. M., Self-Healing Polymeric Materials Using Epoxy/Mercaptan as the Healant. *Macromolecules* **2008,** *41* (14), 5197-5202.

[263] Patrick, J. F.; Sottos, N. R.; White, S. R., Microvascular based self-healing polymeric foam. *Polymer* **2012,** *53* (19), 4231-4240.

[264] Fifo, O.; Ryan, K.; Basu, B., Glass fibre polyester composite within vivovascular channel for use in self-healing. *Smart materials and structures* **2014,** *23* (9), 095017/1-8.

[265] White, S. R.; Moore, J. S.; Sottos, N. R.; Krull, B. P.; Santa Cruz, W. A.; Gergely, R. C. R., Restoration of Large Damage Volumes in Polymers. *Science* **2014,** *344* (6184), 620-623.

[266] Caruso, M. M.; Delafuente, D. A.; Ho, V.; Sottos, N. R.; Moore, J. S.; White, S. R., Solvent-Promoted Self-Healing Epoxy Materials. *Macromolecules* **2007,** *40* (25), 8830-8832.

[267] Caruso, M. M.; Blaiszik, B. J.; White, S. R.; Sottos, N. R.; Moore, J. S., Full Recovery of Fracture Toughness Using a Nontoxic Solvent-Based Self-Healing System. *Advanced Functional Materials* **2008,** *18* (13), 1898-1904.

[268] Li, W.; Shang, T.; Yang, W.; Yang, H.; Lin, S.; Jia, X.; Cai, Q.; Yang, X., Effectively Exerting the Reinforcement of Dopamine Reduced Graphene Oxide on Epoxy-Based Composites via Strengthened Interfacial Bonding. *ACS Applied Materials & Interfaces* **2016,** *8* (20), 13037-13050.

[269] Xu, C.; Wang, X.; Zhu, J., Graphene−Metal Particle Nanocomposites. *The Journal of Physical Chemistry C* **2008,** *112* (50), 19841-19845.

[270] Raimondo, M.; De Nicola, F.; Volponi, R.; Binder, W.; Michael, P.; Russo, S.; Guadagno, L., Self-repairing CFRPs targeted towards structural aerospace applications. *International Journal of Structural Integrity* **2016,** *7* (5), 656-670.

[271] Li, J.; Nagamani, C.; Moore, J. S., Polymer Mechanochemistry: From Destructive to Productive. *Accounts of Chemical Research* **2015,** *48* (8), 2181-2190.

[272] Caruso, M. M.; Davis, D. A.; Shen, Q.; Odom, S. A.; Sottos, N. R.; White, S. R.; Moore, J. S., Mechanically-Induced Chemical Changes in Polymeric Materials. *Chemical Reviews* **2009,** *109* (11), 5755-5798.

[273] Lenhardt, J. M.; Black Ramirez, A. L.; Lee, B.; Kouznetsova, T. B.; Craig, S. L., Mechanistic Insights into the Sonochemical Activation of Multimechanophore Cyclopropanated Polybutadiene Polymers. *Macromolecules* **2015,** *48* (18), 6396-6403.

[274] Price, G. J.; Smith, P. F., Ultrasonic degradation of polymer solutions: 2. The effect of temperature, ultrasound intensity and dissolved gases on polystyrene in toluene. *Polymer* **1993,** *34* (19), 4111-4117.

[275] Zhang, H.; Chen, Y.; Lin, Y.; Fang, X.; Xu, Y.; Ruan, Y.; Weng, W., Spiropyran as a Mechanochromic Probe in Dual Cross-Linked Elastomers. *Macromolecules* **2014,** *47* (19), 6783-6790.

[276] Jakobs, R. T. M.; Ma, S.; Sijbesma, R. P., Mechanocatalytic Polymerization and Cross-Linking in a Polymeric Matrix. *ACS Macro Letters* **2013,** *2* (7), 613-616.

[277] Potisek, S. L.; Davis, D. A.; Sottos, N. R.; White, S. R.; Moore, J. S., Mechanophore-Linked Addition Polymers. *Journal of the American Chemical Society* **2007,** *129* (45), 13808-13809.

[278] Kingsbury, C. M.; May, P. A.; Davis, D. A.; White, S. R.; Moore, J. S.; Sottos, N. R., Shear activation of mechanophore-crosslinked polymers. *Journal of Materials Chemistry* **2011,** *21* (23), 8381-8388.

[279] Davis, D. A.; Hamilton, A.; Yang, J.; Cremar, L. D.; Van Gough, D.; Potisek, S. L.; Ong, M. T.; Braun, P. V.; Martínez, T. J.; White, S. R.; Moore, J. S.; Sottos, N. R., Force-induced activation of covalent bonds in mechanoresponsive polymeric materials. *Nature* **2009,** *459*, 68.

[280] Beyer, M. K., The mechanical strength of a covalent bond calculated by density functional theory. *The Journal of Chemical Physics* **2000,** *112* (17), 7307-7312.

[281] Hickenboth, C. R.; Moore, J. S.; White, S. R.; Sottos, N. R.; Baudry, J.; Wilson, S. R., Biasing reaction pathways with mechanical force. *Nature* **2007,** *446*, 423.

[282] Ong, M. T.; Leiding, J.; Tao, H.; Virshup, A. M.; Martínez, T. J., First Principles Dynamics and Minimum Energy Pathways for Mechanochemical Ring Opening of Cyclobutene. *Journal of the American Chemical Society* **2009,** *131* (18), 6377-6379.

[283] Groote, R.; Szyja, B. M.; Pidko, E. A.; Hensen, E. J. M.; Sijbesma, R. P., Unfolding and Mechanochemical Scission of Supramolecular Polymers Containing a Metal–Ligand Coordination Bond. *Macromolecules* **2011,** *44* (23), 9187-9195.

[284] Groote, R.; van Haandel, L.; Sijbesma, R. P., The effect of molecular weight and catalyst concentration on catalytic activity in mechanochemically activated transesterification using silver(I)-N-heterocyclic carbene latent catalysts. *Journal of Polymer Science Part A: Polymer Chemistry* **2012,** *50* (23), 4929-4935.

[285] Groote, R.; Jakobs, R. T. M.; Sijbesma, R. P., Mechanocatalysis: forcing latent catalysts into action. *Polymer Chemistry* **2013,** *4* (18), 4846-4859.

[286] Akbulatov, S.; Boulatov, R., Experimental Polymer Mechanochemistry and its Interpretational Frameworks. *ChemPhysChem* **2017,** *18* (11), 1422-1450.

[287] Brantley, J. N.; Wiggins, K. M.; Bielawski, C. W., Polymer mechanochemistry: the design and study of mechanophores. *Polymer International* **2013,** *62* (1), 2-12.

[288] Huan, Z.; Fei, G.; Xiaodong, C.; Yanqun, L.; Yuanze, X.; Wengui, W.; Roman, B., Mechanochromism and Mechanical-Force-Triggered Cross-Linking from a Single Reactive Moiety Incorporated into Polymer Chains. *Angewandte Chemie International Edition* **2016,** *55* (9), 3040-3044.

[289] Kean, Z. S.; Gossweiler, G. R.; Kouznetsova, T. B.; Hewage, G. B.; Craig, S. L., A coumarin dimer probe of mechanochemical scission efficiency in the sonochemical activation of chain-centered mechanophore polymers. *Chemical Communications* **2015,** *51* (44), 9157-9160.

[290] Song, Y.-K.; Lee, K.-H.; Hong, W.-S.; Cho, S.-Y.; Yu, H.-C.; Chung, C.-M., Fluorescence sensing of microcracks based on cycloreversion of a dimeric anthracene moiety. *Journal of Materials Chemistry* **2012,** *22* (4), 1380-1386.

[291] Clough, J. M.; Sijbesma, R. P., Dioxetane Scission Products Unchanged by Mechanical Force. *ChemPhysChem* **2014,** *15* (16), 3565-3571.

[292] Díez-González, S.; Nolan, S. P., Stereoelectronic parameters associated with N-heterocyclic carbene (NHC) ligands: A quest for understanding. *Coordination Chemistry Reviews* **2007,** *251* (5), 874-883.

[293] Arduengo, A. J.; Harlow, R. L.; Kline, M., A stable crystalline carbene. *Journal of the American Chemical Society* **1991,** *113* (1), 361-363.

[294] Hopkinson, M. N.; Richter, C.; Schedler, M.; Glorius, F., An overview of N-heterocyclic carbenes. *Nature* **2014,** *510*, 485.

[295] Hu, X.; Castro-Rodriguez, I.; Olsen, K.; Meyer, K., Group 11 Metal Complexes of N-Heterocyclic Carbene Ligands: Nature of the Metal−Carbene Bond. *Organometallics* **2004,** *23* (4), 755-764.

[296] Karthikeyan, S.; Potisek, S. L.; Piermattei, A.; Sijbesma, R. P., Highly Efficient Mechanochemical Scission of Silver-Carbene Coordination Polymers. *Journal of the American Chemical Society* **2008,** *130* (45), 14968-14969.

[297] Rooze, J.; Groote, R.; Jakobs, R. T. M.; Sijbesma, R. P.; van Iersel, M. M.; Rebrov, E. V.; Schouten, J. C.; Keurentjes, J. T. F., Mechanism of Ultrasound Scission of a Silver–Carbene Coordination Polymer. *The Journal of Physical Chemistry B* **2011,** *115* (38), 11038-11043.

[298] Piermattei, A.; Karthikeyan, S.; Sijbesma, R. P., Activating catalysts with mechanical force. *Nature Chemistry* **2009,** *1*, 133.

[299] Jakobs, R. T. M.; Sijbesma, R. P., Mechanical Activation of a Latent Olefin Metathesis Catalyst and Persistence of its Active Species in ROMP. *Organometallics* **2012,** *31* (6), 2476-2481.

[300] Groote, R.; Jakobs, R. T. M.; Sijbesma, R. P., Performance of Mechanochemically Activated Catalysts Is Enhanced by Suppression of the Thermal Effects of Ultrasound. *ACS Macro Letters* **2012,** *1* (8), 1012-1015.

[301] Clough, J. M.; Balan, A.; van Daal, T. L. J.; Sijbesma, R. P., Probing Force with Mechanobase-Induced Chemiluminescence. *Angewandte Chemie International Edition* **2016,** *55* (4), 1445-1449.

[302] Michael, P.; Sheidaee Mehr, S. K.; Binder, W. H., Synthesis and characterization of polymer linked copper(I) bis(N-heterocyclic carbene) mechanocatalysts. *Journal of Polymer Science Part A: Polymer Chemistry* **2017,** *55* (23), 3893-3907.

[303] Beiermann, B. A.; Kramer, S. L. B.; Moore, J. S.; White, S. R.; Sottos, N. R., Role of Mechanophore Orientation in Mechanochemical Reactions. *ACS Macro Letters* **2012,** *1* (1), 163-166.

[304] Nandivada, H.; Jiang, X.; Lahann, J., Click Chemistry: Versatility and Control in the Hands of Materials Scientists. *Advanced Materials (Weinheim, Germany)* **2007,** *19* (17), 2197-2208.

[305] Neises, B.; Steglich, W., Simple Method for the Esterification of Carboxylic Acids. *Angewandte Chemie International Edition in English* **1978,** *17* (7), 522-524.

[306] Pappuru, S.; Chakraborty, D.; Ramkumar, V., Nb and Ta benzotriazole or benzoxazole phenoxide complexes as catalysts for the ring-opening polymerization of glycidol to

synthesize hyperbranched polyglycerols. *Dalton Transactions* **2017,** *46* (47), 16640-16654.

[307] Jardine, F. H.; Rule, L.; Vohra, A. G., The chemistry of copper(I) complexes. Part I. Halogeno-complexes. *Journal of the Chemical Society A: Inorganic, Physical, Theoretical* **1970,** (0), 238-240.

[308] Ampudia, J.; Larrauri, E.; Gil, E. M.; Rodríguez, M.; León, L. M., Thermal scanning rheometric analysis of curing kinetic of an epoxy resin. I. An anhydride as curing agent. *J. Appl. Polym. Sci.* **1999,** *71* (8), 1239-1245.

[309] Barton, J. M.; Greenfield, D. C. L.; Hodd, K. A., Some effects of structure on the cure of glycidylether epoxy resins. *Polymer* **1992,** *33* (6), 1177-1186.

[310] Müller, M.; Seidel, U.; Stadler, R., Influence of hydrogen bonding on the viscoelastic properties of thermoreversible networks: analysis of the local complex dynamics. *Polymer* **1995,** *36* (16), 3143-3150.

[311] Feldman, K. E.; Kade, M. J.; Meijer, E. W.; Hawker, C. J.; Kramer, E. J., Model Transient Networks from Strongly Hydrogen-Bonded Polymers. *Macromolecules* **2009,** *42* (22), 9072-9081.

[312] Chiefari, J.; Chong, Y. K.; Ercole, F.; Krstina, J.; Jeffery, J.; Le, T. P. T.; Mayadunne, R. T. A.; Meijs, G. F.; Moad, C. L.; Moad, G.; Rizzardo, E.; Thang, S. H., Living Free-Radical Polymerization by Reversible Addition−Fragmentation Chain Transfer: The RAFT Process. *Macromolecules* **1998,** *31* (16), 5559-5562.

[313] Flory, P. J., The Mechanism of Vinyl Polymerization. *Journal of the American Chemical Society* **1937,** *59* (2), 241-253.

[314] Mayo, F. R., Chain Transfer in the Polymerization of Styrene. VIII. Chain Transfer with Bromobenzene and Mechanism of Thermal Initiation. *Journal of the American Chemical Society* **1953,** *75* (24), 6133-6141.

[315] Chen, Y.; Chen, G.; Stenzel, M. H., Synthesis and Lectin Recognition of Glyco Star Polymers Prepared by "Clicking" Thiocarbohydrates onto a Reactive Scaffold. *Macromolecules* **2010,** *43* (19), 8109-8114.

[316] Döhler, D.; Kaiser, J.; Binder, W. H., Supramolecular H-bonded three-arm star polymers by efficient combination of RAFT polymerization and thio-bromo "click" reaction. *Polymer* **2017,** *122* (Supplement C), 148-158.

[317] Tao, L.; Kaddis, C. S.; Loo, R. R. O.; Grover, G. N.; Loo, J. A.; Maynard, H. D., Synthesis of Maleimide-End-Functionalized Star Polymers and Multimeric Protein−Polymer Conjugates. *Macromolecules* **2009,** *42* (21), 8028-8033.

[318] Srinivasan, S.; Lee, M. W.; Grady, M. C.; Soroush, M.; Rappe, A. M., Self-Initiation Mechanism in Spontaneous Thermal Polymerization of Ethyl and n-Butyl Acrylate: A Theoretical Study. *The Journal of Physical Chemistry A* **2010,** *114* (30), 7975-7983.

[319] Dröge, T.; Glorius, F., Das Maß aller Ringe – N-heterocyclische Carbene. *Angewandte Chemie* **2010,** *122* (39), 7094-7107.

[320] Dröge, T.; Glorius, F., The Measure of All Rings—N-Heterocyclic Carbenes. *Angewandte Chemie International Edition* **2010,** *49* (39), 6940-6952.

[321] Fèvre, M.; Pinaud, J.; Gnanou, Y.; Vignolle, J.; Taton, D., N-Heterocyclic carbenes (NHCs) as organocatalysts and structural components in metal-free polymer synthesis. *Chemical Society Reviews* **2013,** *42* (5), 2142-2172.

[322] Clayden, J.; Greeves, N.; Warren, S.; Wothers, P., Organic Chemistry. Oxford University Press: Oxford, 2006.

[323] Fraser, R. R.; Mansour, T. S.; Savard, S., Acidity measurements on pyridines in tetrahydrofuran using lithiated silylamines. *The Journal of Organic Chemistry* **1985,** *50* (17), 3232-3234.

[324] Vijayalakshmi, S. P.; Madras, G., Effect of initial molecular weight and solvents on the ultrasonic degradation of poly(ethylene oxide). *Polymer Degradation and Stability* **2005,** *90* (1), 116-122.

[325] Wiggins, K. M.; Brantley, J. N.; Bielawski, C. W., Methods for activating and characterizing mechanically responsive polymers. *Chemical Society Reviews* **2013,** *42* (17), 7130-7147.

[326] Ito, M.; Koyakumaru, K.-i.; Ohta, T.; Takaya, H., A Simple and Convenient Synthesis of Alkyl Azides under Mild Conditions. *Synthesis* **1995,** *1995* (04), 376-378.

[327] kantheti, S.; Sarath, P. S.; Narayan, R.; Raju, K. V. S. N., Synthesis and characterization of triazole rich polyether polyols using click chemistry for highly branched polyurethanes. *Reactive and Functional Polymers* **2013,** *73* (12), 1597-1605.

[328] Storey, R. F.; Lee, Y., Sulfonation of tert-alkyl chlorides: Application to the tert-chloride-terminated polyisobutylene system. *Journal of Polymer Science Part A: Polymer Chemistry* **1991,** *29* (3), 317-325.

[329] Storey, R. F.; Lee, Y., Living Carbocationic Polymerization of Isobutylene Using Blocked Dicumyl Chloride or Tricumyl Chloride/TiCl$_4$/Pyridine Initiating System. *Journal of Macromolecular Science, Part A* **1992,** *29* (11), 1017-1030.

[330] Gyor, M.; Wang, H.-C.; Faust, R., Living Carbocationic Polymerization of Isobutylene with Blocked Bifunctional Initiators in the Presence of Di-tert-butylpyridine as a Proton Trap. *Journal of Macromolecular Science, Part A* **1992,** *29* (8), 639-653.

[331] Mishra, M.; Wang, B.; Kennedy, J., Living carbocationic polymerization. *Polymer Bulletin (Berlin)* **1987,** *17* (4), 307-314.

[332] Binder, W. H.; Kunz, M. J.; Kluger, C.; Hayn, G.; Saf, R., Synthesis and Analysis of Telechelic Polyisobutylenes for Hydrogen-Bonded Supramolecular Pseudo-Block Copolymers. *Macromolecules* **2004,** *37* (5), 1749-1759.

[333] Morgan, D. L.; Martinez-Castro, N.; Storey, R. F., End-Quenching of TiCl$_4$-Catalyzed Quasiliving Polyisobutylene with Alkoxybenzenes for Direct Chain End Functionalization. *Macromolecules* **2010,** *43* (21), 8724-8740.

[334] Iván, B.; Kennedy, J. P., Living carbocationic polymerization. XXX. One-pot synthesis of allyl-terminated linear and tri-arm star polyisobutylenes, and epoxy- and hydroxy-telechelics therefrom. *Journal of Polymer Science Part A: Polymer Chemistry* **1990,** *28* (1), 89-104.

[335] Schulz, M.; Tanner, S.; Barqawi, H.; Binder, W. H., Macrocyclization of polymers via ring-closing metathesis and azide/alkyne-"click"-reactions: An approach to cyclic polyisobutylenes. *Journal of Polymer Science Part A: Polymer Chemistry* **2010,** *48* (3), 671-680.

[336] Brown, E. N.; Kessler, M. R.; Sottos, N. R.; White, S. R., *In situ* poly(urea-formaldehyde) microencapsulation of dicyclopentadiene. *J. Microencapsulation* **2003,** *20* (6), 719 - 730.

[337] Banert, K.; Wutke, J.; Rüffer, T.; Lang, H., Reactions of Unsaturated Azides; Part 22: The Alkyne Azide Click Chemistry as a Synthetic Tool for the Generation of Cage-Like Triazole Compounds. *Synthesis* **2008,** *2008* (16), 2603-2609.

[338] Hull, K. G.; Visnick, M.; Tautz, W.; Sheffron, A., Synthesis of Ro 25-8210 via an enantioselective oxazaborolidine-catalyzed reduction. *Tetrahedron* **1997,** *53* (37), 12405-12414.

[339] Wang, X.-B.; Dacres, J. E.; Yang, X.; Broadus, K. M.; Lis, L.; Wang, L.-S.; Kass, S. R., Photodetachment of Zwitterions: Probing Intramolecular Coulomb Repulsion and Attraction in the Gas Phase Using Pyridinium Dicarboxylate Anions. *Journal of the American Chemical Society* **2002,** *125* (1), 296-304.

[340] Neumann, S.; Döhler, D.; Ströhl, D.; Binder, W. H., Chelation-assisted CuAAC in star-shaped polymers enables fast self-healing at low temperatures. *Polym. Chem.* **2016,** *7* (13), 2342-2351.

[341] Morgan, D. L.; Storey, R. F., End-Quenching of Quasi-Living Isobutylene Polymerizations with Alkoxybenzene Compounds. *Macromolecules* **2009,** *42* (18), 6844-6847.

[342] Sivakumar, K.; Xie, F.; Cash, B. M.; Long, S.; Barnhill, H. N.; Wang, Q., A Fluorogenic 1,3-Dipolar Cycloaddition Reaction of 3-Azidocoumarins and Acetylenes. *Organic Letters* **2004,** *6* (24), 4603-4606.

[343] Ferguson, C. J.; Hughes, R. J.; Nguyen, D.; Pham, B. T. T.; Gilbert, R. G.; Serelis, A. K.; Such, C. H.; Hawkett, B. S., Ab Initio Emulsion Polymerization by RAFT-Controlled Self-Assembly. *Macromolecules* **2005,** *38* (6), 2191-2204.

[344] Alcalde, E.; Dinarès, I.; Ibáñez, A.; Mesquida, N., A Simple Halide-to-Anion Exchange Method for Heteroaromatic Salts and Ionic Liquids. *Molecules* **2012,** *17* (4), 4007.

[345] Dervaux, B.; Meyer, F.; Raquez, J.-M.; Olivier, A.; Du Prez, F. E.; Dubois, P., Imidazolium End-Functionalized ATRP Polymers as Directing Agents for CNT Dispersion and Confinement. *Macromolecular Chemistry and Physics* **2012,** *213* (12), 1259-1265.

[346] Benhamou, L.; Vujkovic, N.; César, V.; Gornitzka, H.; Lugan, N.; Lavigne, G., Facile Derivatization of a "Chemo-active" NHC Incorporating an Enolate Backbone and Relevant Tuning of Its Electronic Properties. *Organometallics* **2010,** *29* (11), 2616-2630.

[347] Lazreg, F.; Cordes, D. B.; Slawin, A. M. Z.; Cazin, C. S. J., Synthesis of Homoleptic and Heteroleptic Bis-N-heterocylic Carbene Group 11 Complexes. *Organometallics* **2015,** *34* (2), 419-425.

[348] Yoshida, S.; Suga, H.; Seki, S., Thermodynamic Studies of Solid Polyethers. III. Poly(tetrahydrofuran), $-[-(CH_2)_4O-]_n-$. *Polymer Journal* **1973,** *5*, 25-32.

[349] Biewend, M.; Neumann, S.; Michael, P.; Binder, W. H., Synthesis of polymer-linked copper(I) bis(*N*-heterocyclic carbene) complexes of linear and chain extended architecture. *Polym. Chem.* **2019**, *10* (9), 1078-1088.

7 Appendix

7.1. Characterization of picolyl azides (1-7)
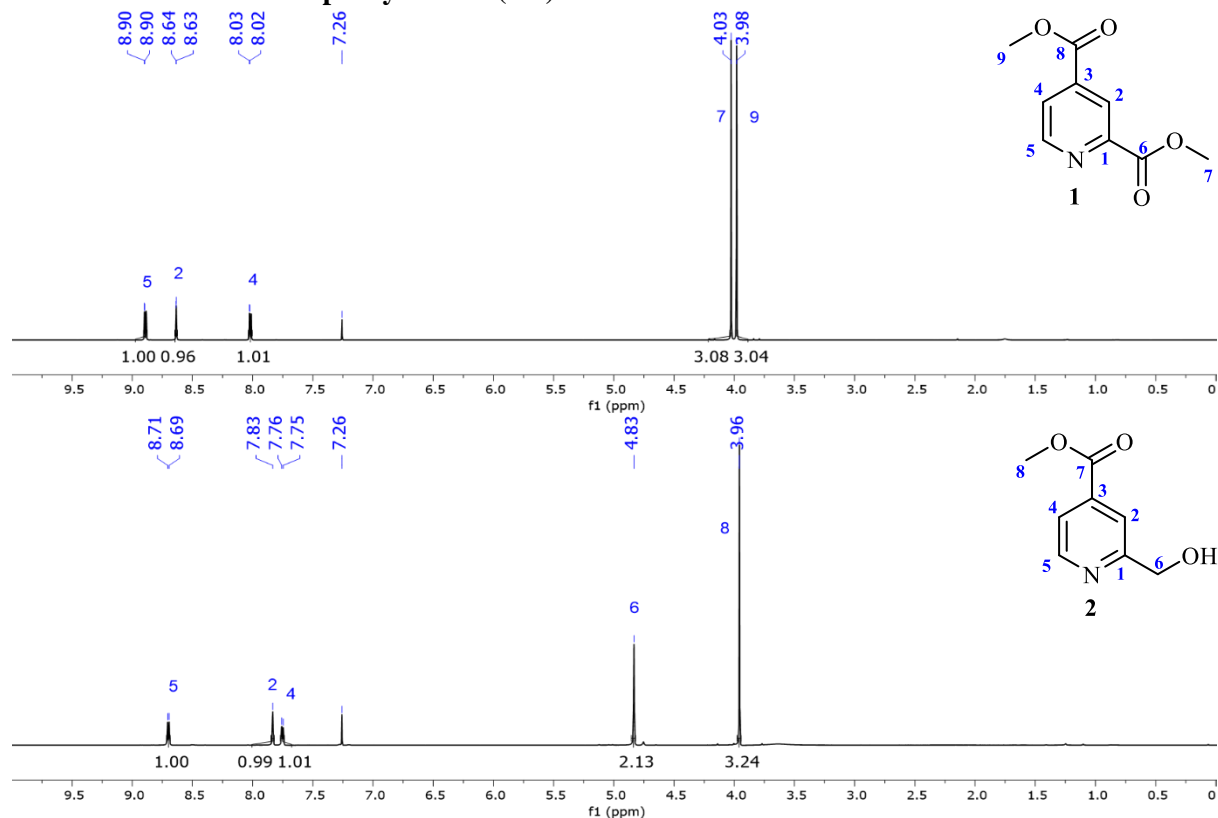
Figure S 1. ^{1}H-NMR spectra in CDCl$_3$ of 2,4-pyridinedicarboxylic acid dimethyl ester (**1**) (top) and 2-(6-hydroxymethyl)-pyridine-4-carboxylic acid methyl ester (**2**) (bottom).
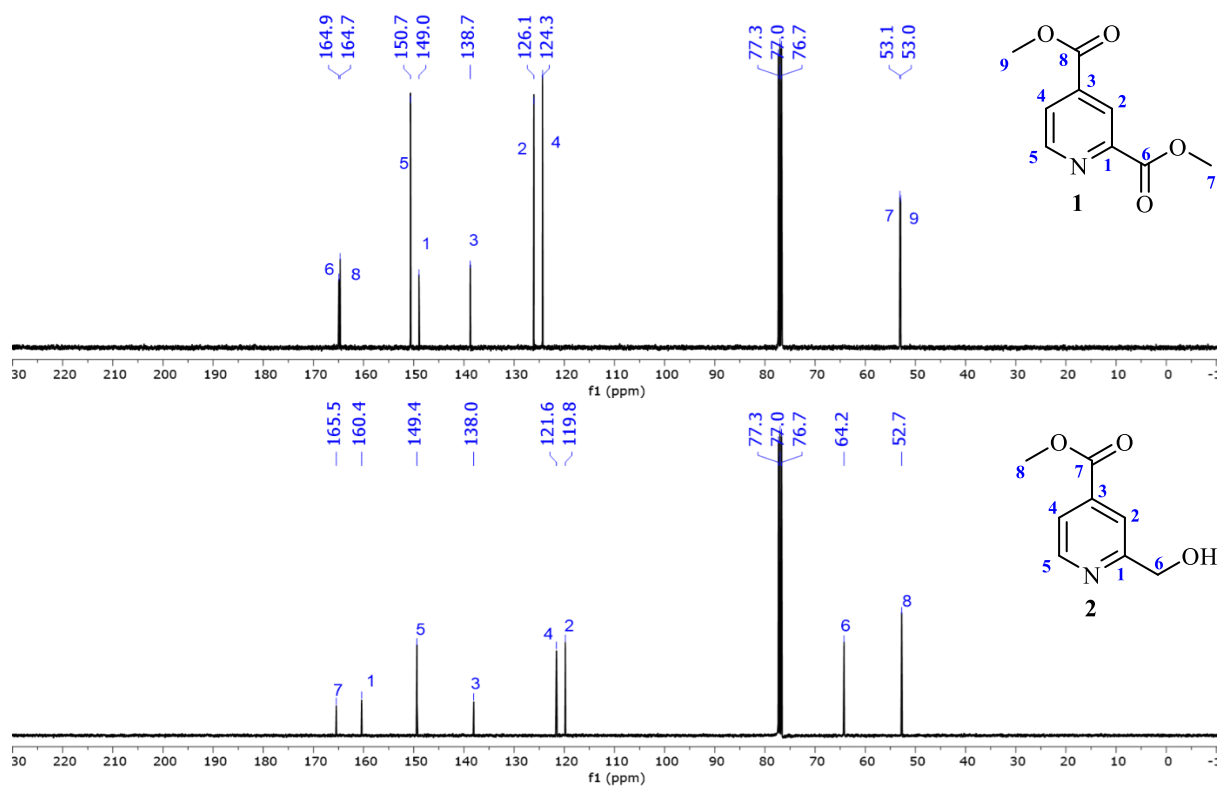
Figure S 2. ^{13}C-NMR spectra in CDCl$_3$ of 2,4-pyridinedicarboxylic acid dimethyl ester (**1**) (top) and 2-(6-hydroxymethyl)-pyridine-4-carboxylic acid methyl ester (**2**) (bottom).
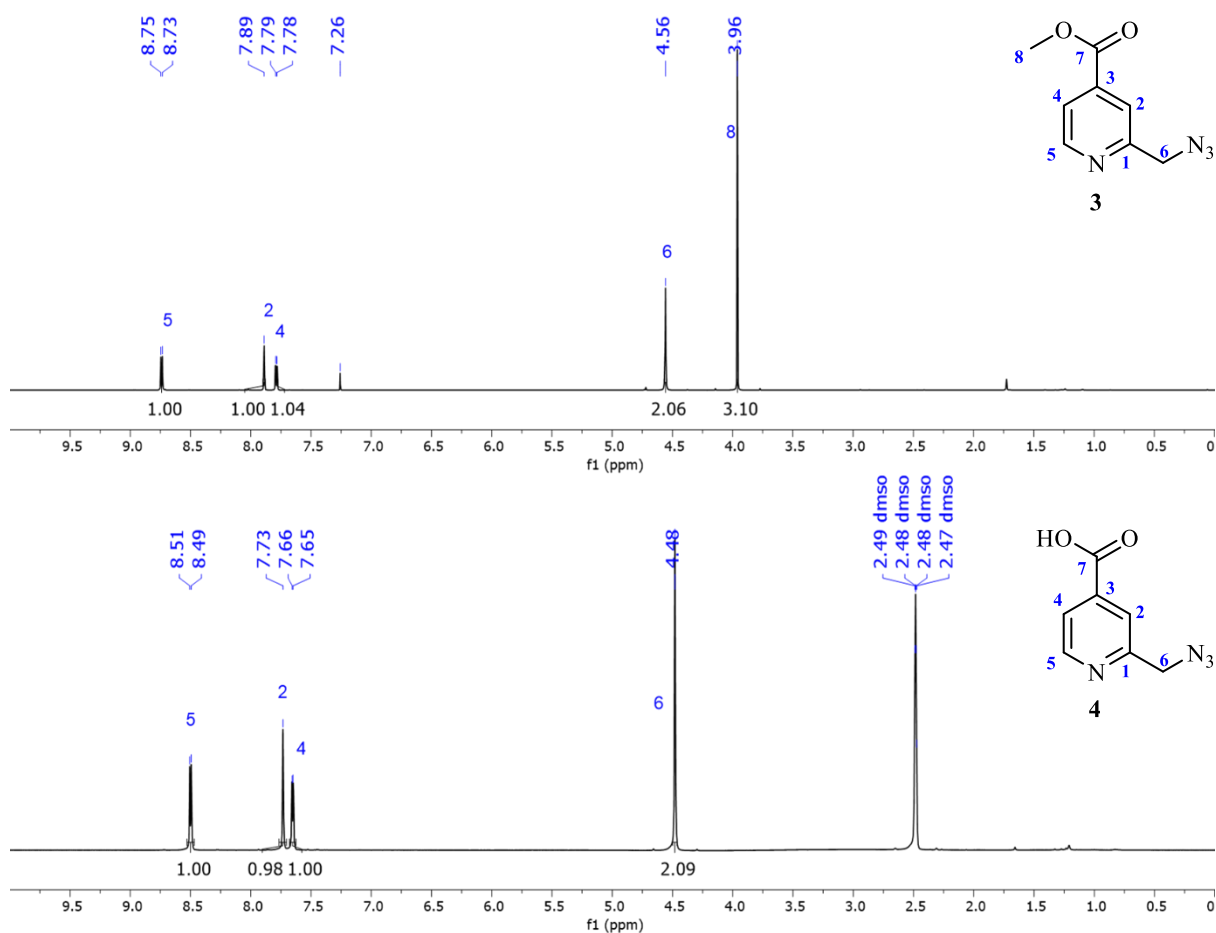
Figure S 3. ^{1}H-NMR spectra of 2-(6-azidomethyl)-pyridine-4-carboxylic acid methyl ester (**3**) in CDCl$_3$ (top) and 2-(6-azidomethyl)-pyridine-4-carboxylic acid (**4**) in DMSO-d_6 (bottom).
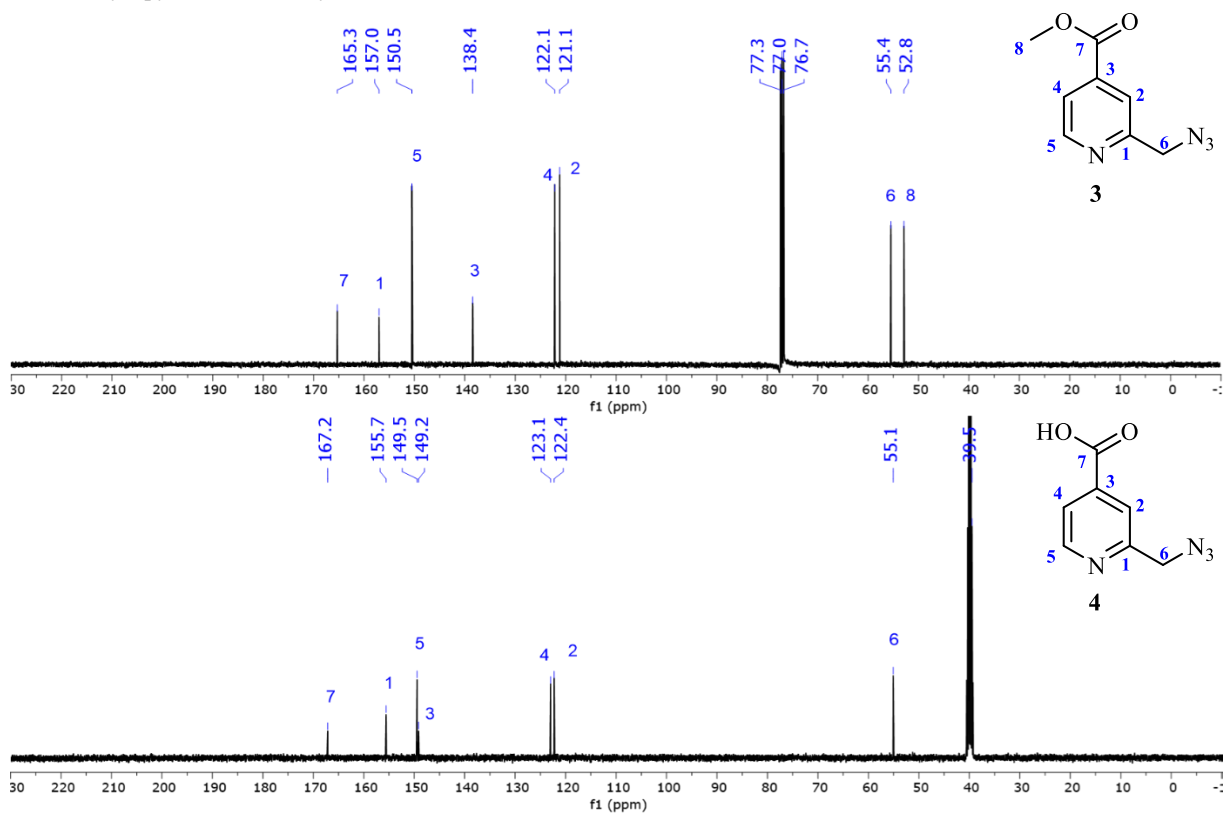
Figure S 4. ^{13}C-NMR spectra of 2-(6-azidomethyl)-pyridine-4-carboxylic acid methyl ester (**3**) in CDCl$_3$ (top) and 2-(6-azidomethyl)-pyridine-4-carboxylic acid (**4**) in DMSO-d_6 (bottom).

138
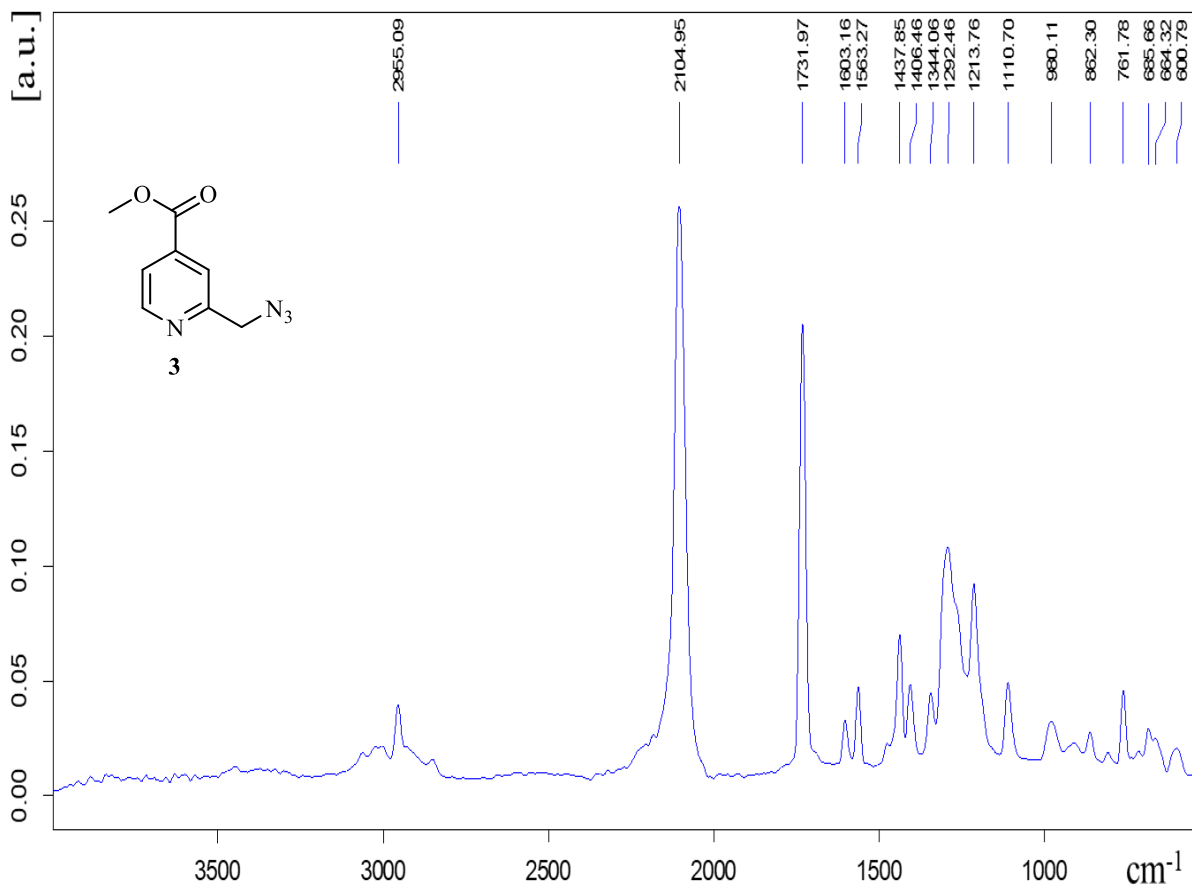
Figure S 5. IR spectrum of 2-(6-azidomethyl)-pyridine-4-carboxylic acid methyl ester (**3**).
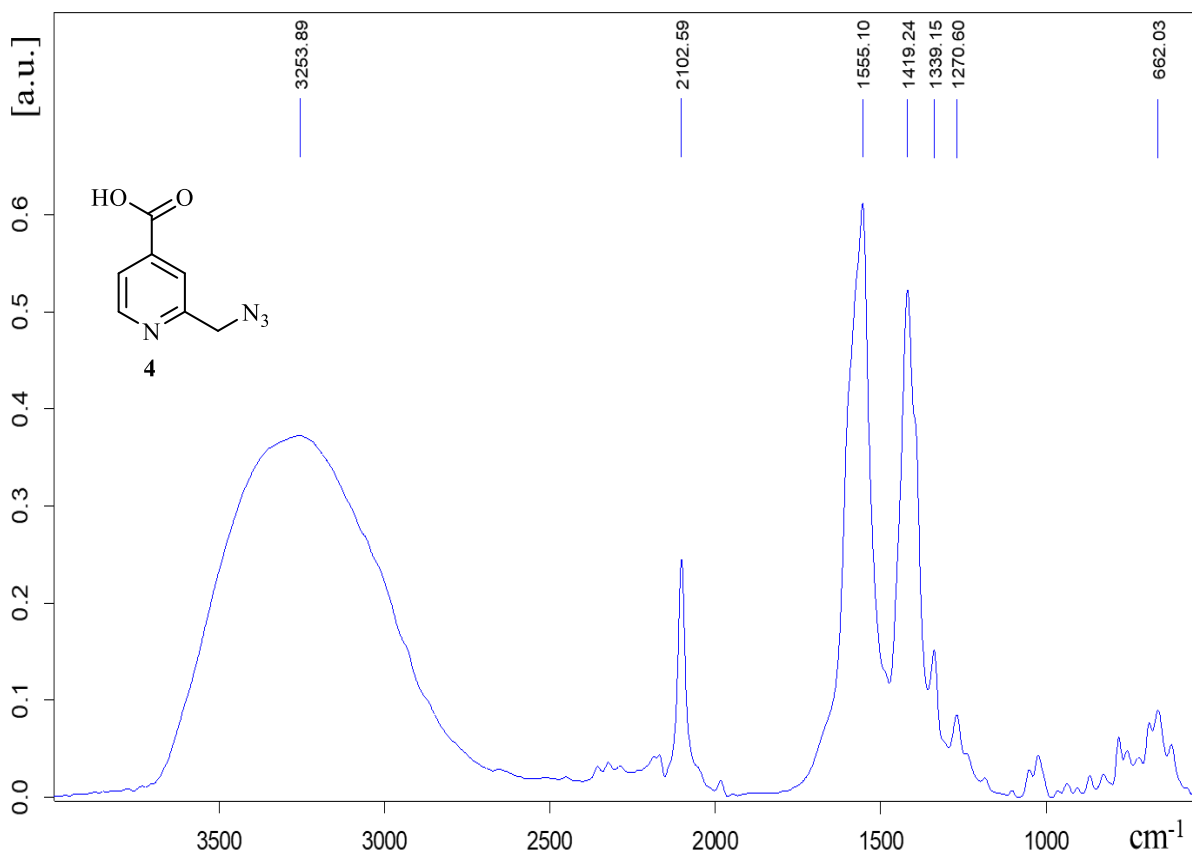
Figure S 6. IR spectrum of 2-(6-azidomethyl)-pyridine-4-carboxylic acid (**4**).
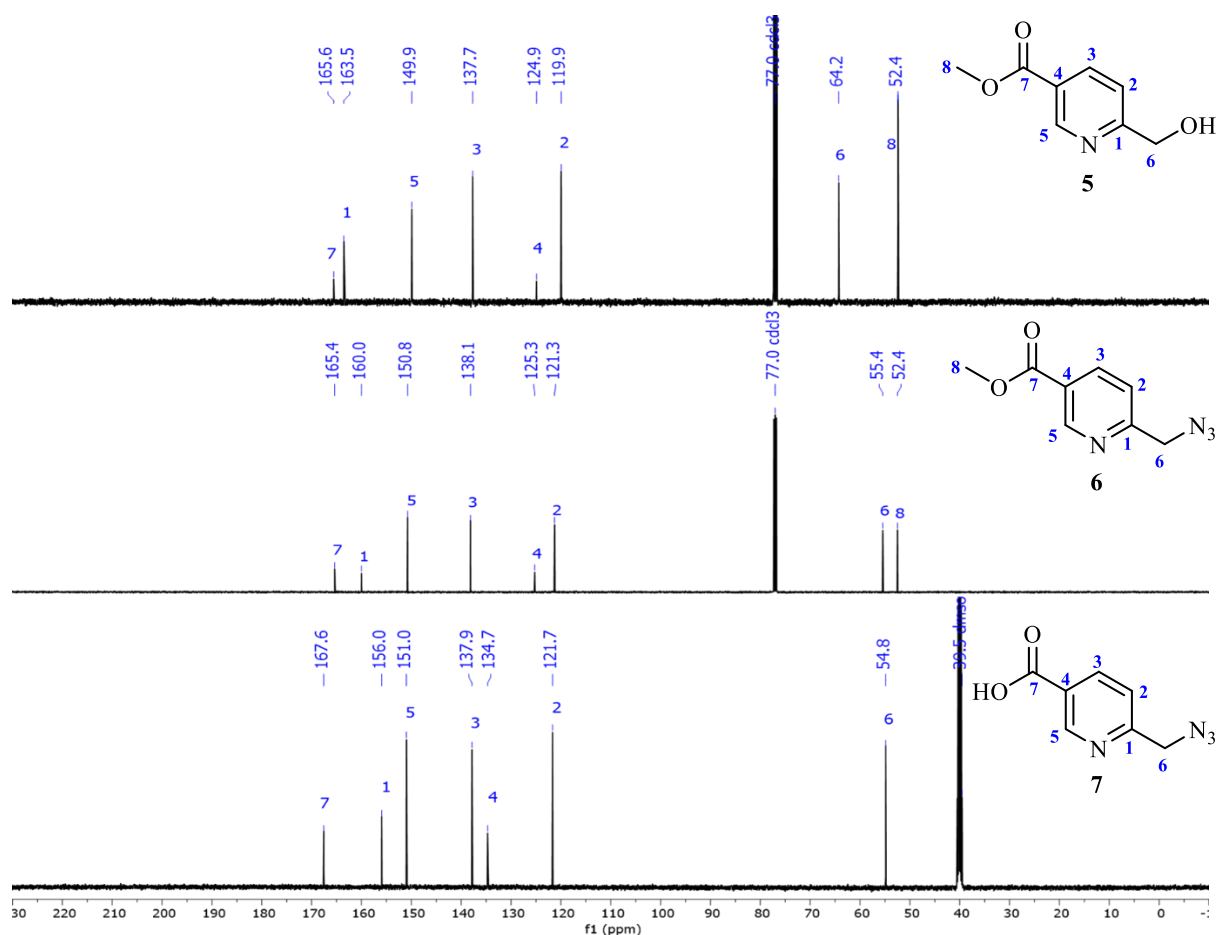
Figure S 7. ^{13}C-NMR spectra in C*D*Cl$_3$ of 2-(6-hydroxymethyl)-pyridine-5-carboxylic acid methyl ester (**5**) (top), 2-(6-azidomethyl)-pyridine-5-carboxylic acid methyl ester (**6**) (middle) and 2-(6-azidomethyl)-pyridine-5-carboxylic acid (**7**) in DMSO-*d$_6$* (bottom).
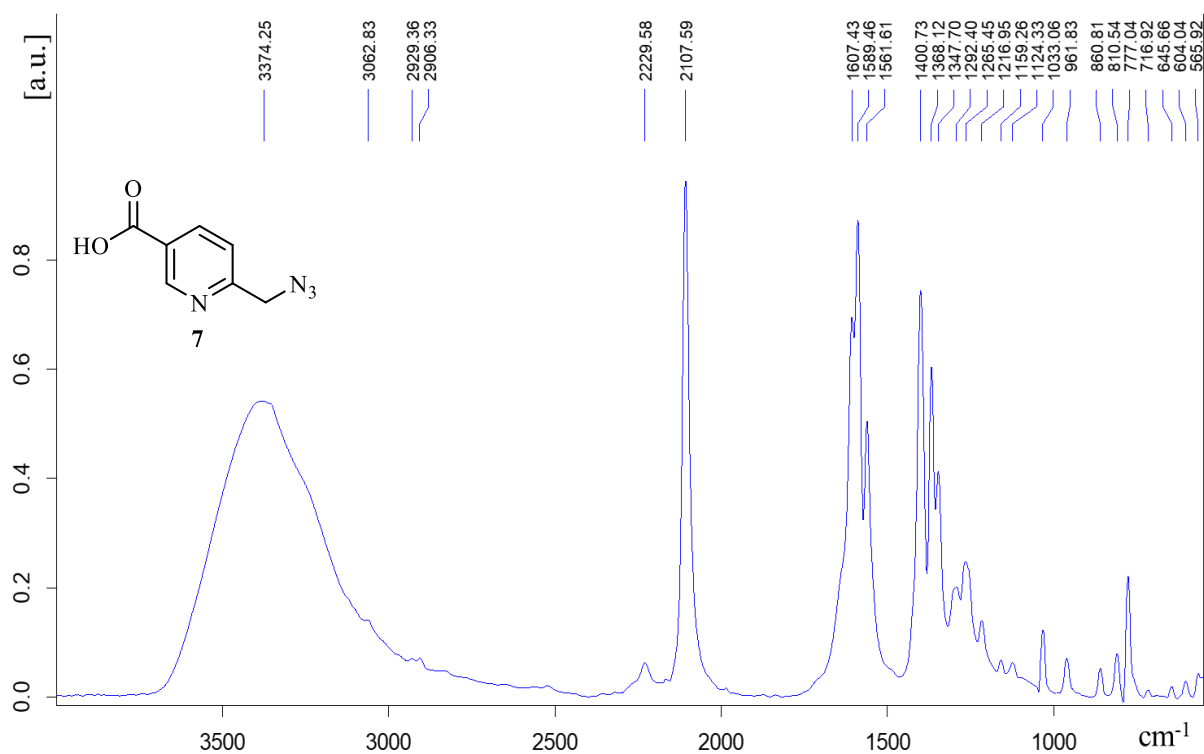
Figure S 8. IR spectrum of 2-(6-azidomethyl)-pyridine-5-carboxylic acid (**7**).

7.2. *In-situ* NMR of the ca-CuAAC applying picolyl azides.
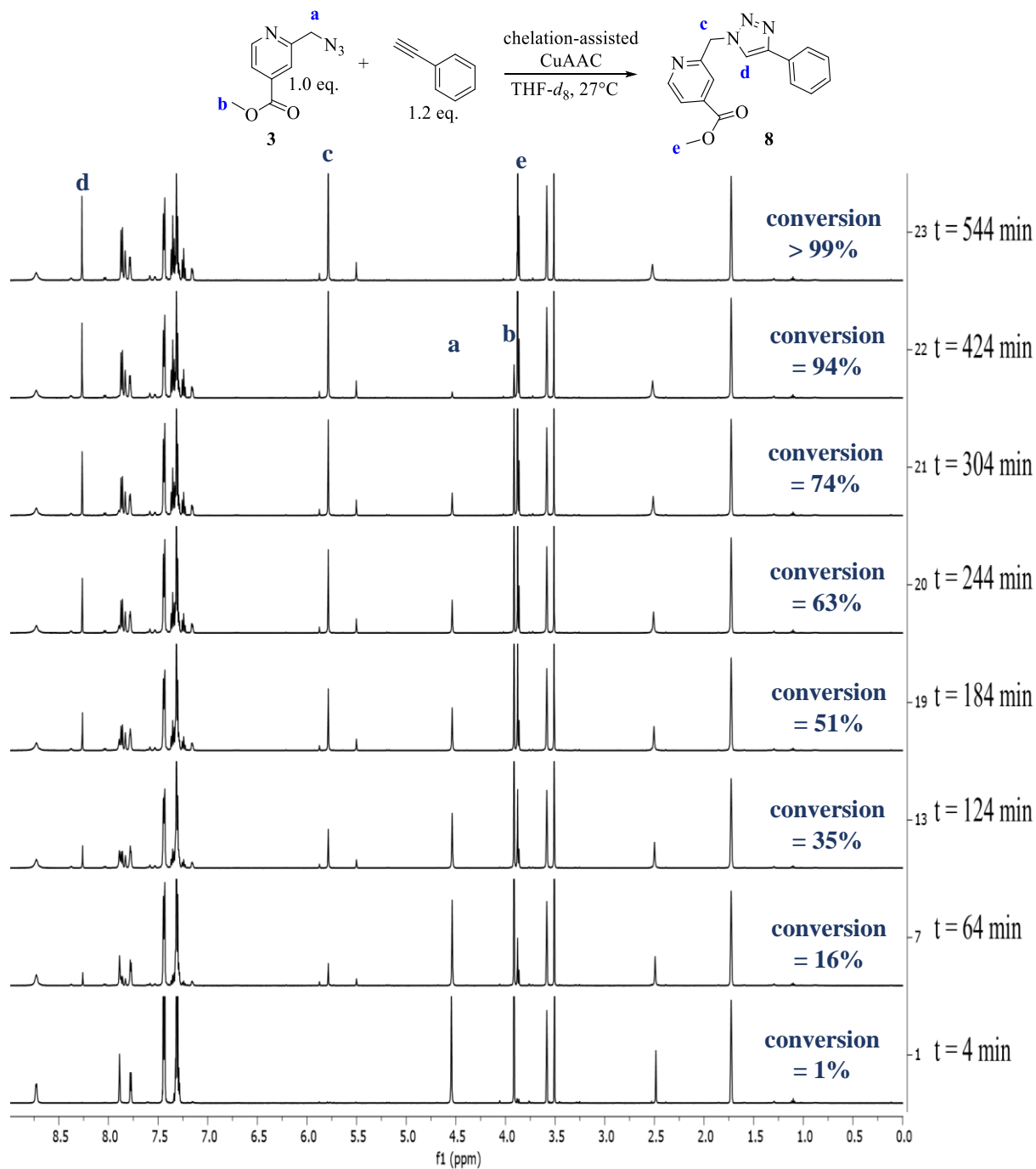
Figure S 9. *In situ* NMR measurement of the chelation-assisted CuAAC of picolyl azide (**3**) and phenylacetylene conducted in THF-d_8 in presence of CuBr (0.1 eq.) (Table 3A, entry 3).
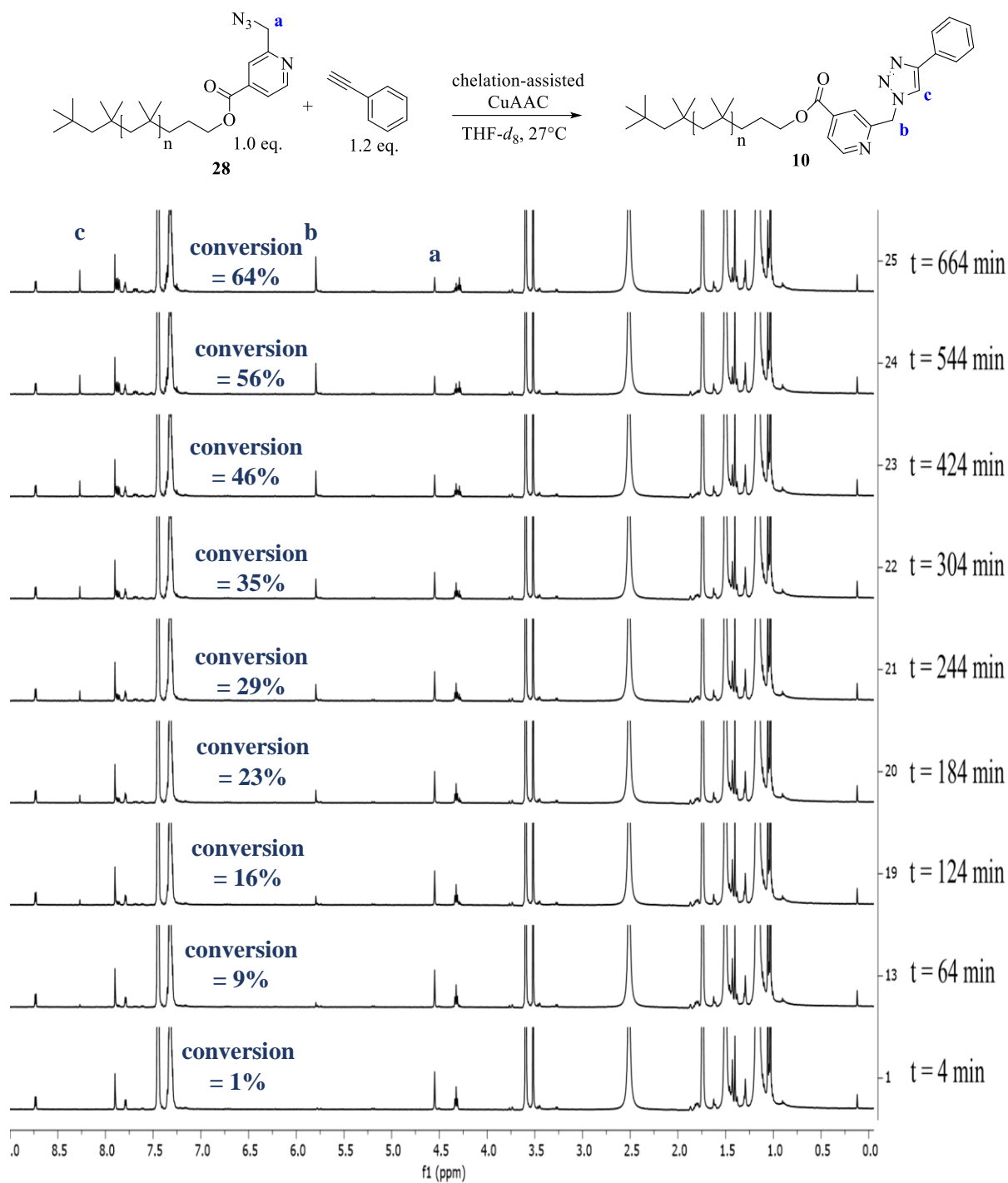
Figure S 10. *In situ* NMR measurement of the chelation-assisted CuAAC of picolyl azido telechelic PIB (**28**) and phenylacetylene conducted in THF-*d8* in presence of [CuF(PPh3)3] (0.1 eq.) (Table 3A, entry 11).
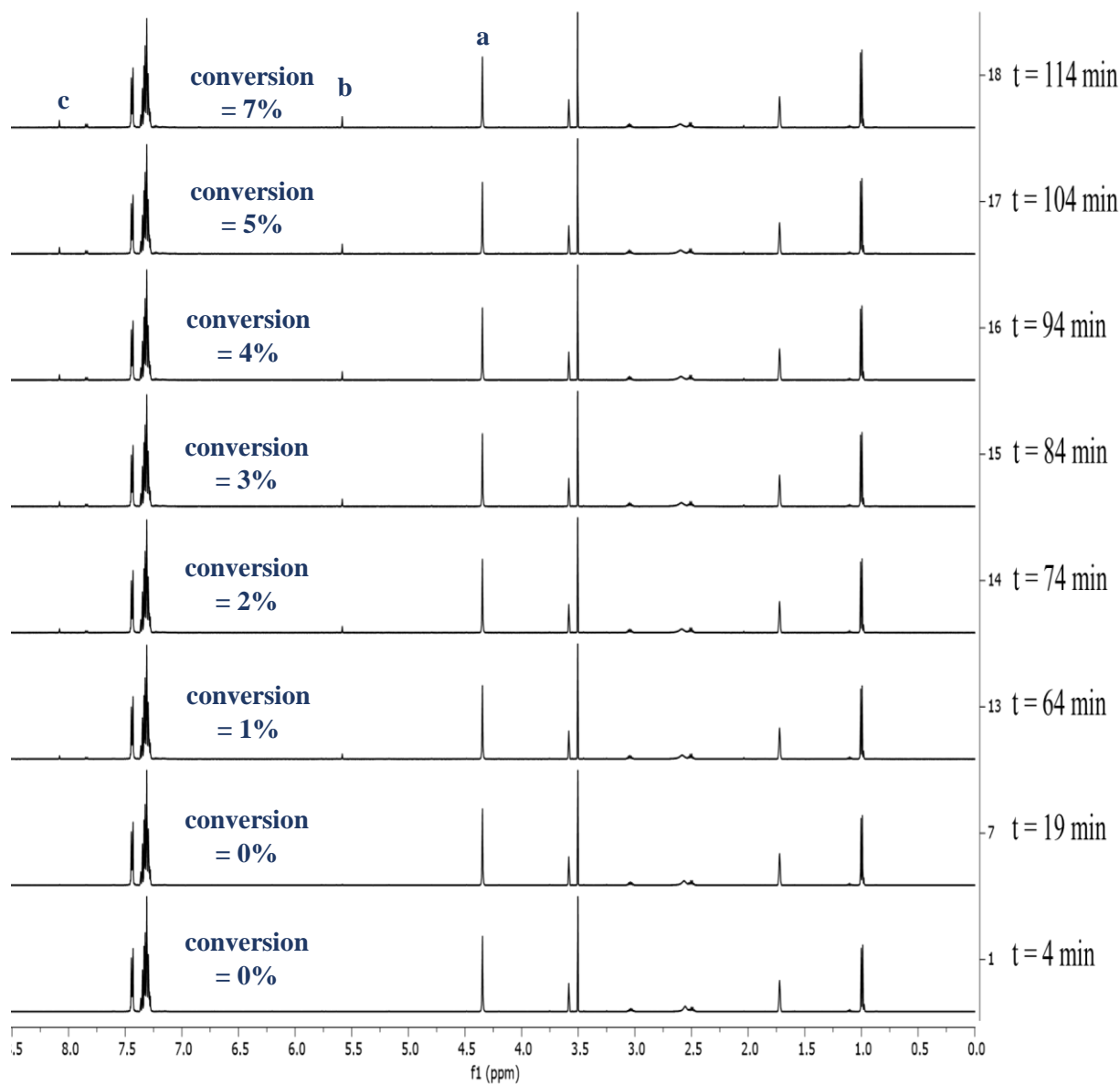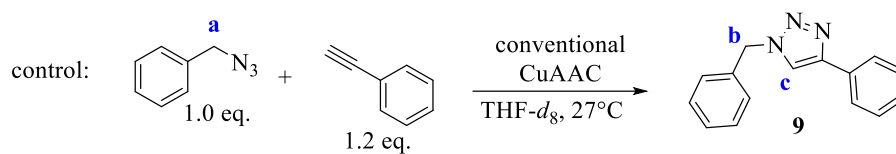
Figure S 11. *In situ* NMR measurement of control and the conventional CuAAC of benzyl azide and phenylacetylene conducted in THF-*d₈* in presence of CuBr (0.1 eq.) and DIPEA (0.01 eq.) (Table 3B, entry 14).

7.3. Characterization of graphene based catalysts (15, 17)
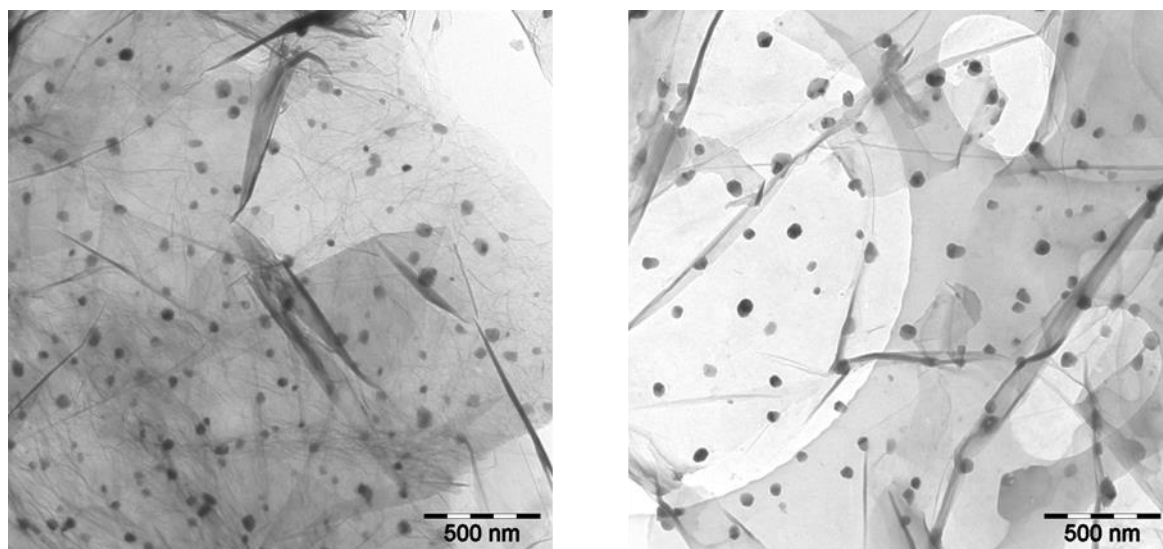
Figure S12. TEM-image of Cu-TRGO (**15**) (left) and Cu-TREGO (**17**) (right).

7.4. Characterization of crosslinking picolyl azide (18)
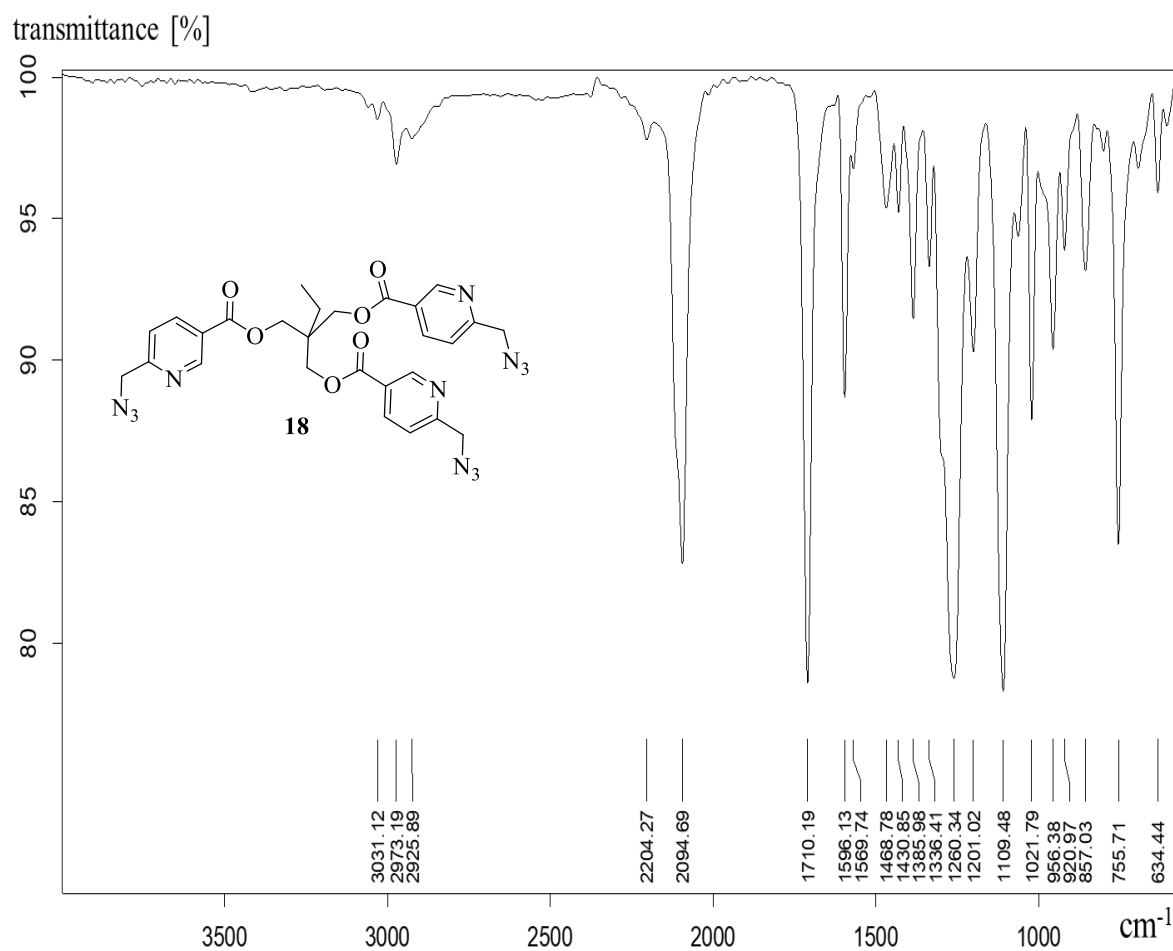
Figure S 13. IR spectrum of trimethylolpropane-tris-(pyridine-2-(6-azidomethyl)-5-carboxylat) (**18**).
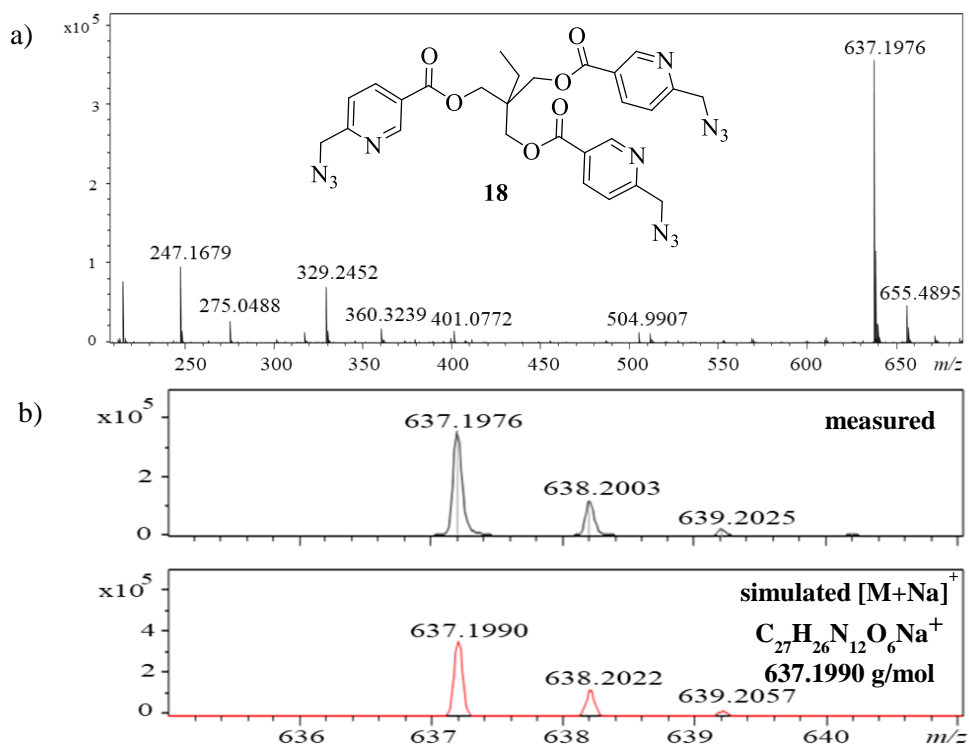
Figure S 14. a) Full ESI-ToF-MS of trimethylolpropane-tris-(pyridine-2-(6-azidomethyl)-5-carboxylat) (**18**), showing main peak at 637.1976 g/mol. b) Measured peak (top) and its simulated isotopic pattern (bottom), belonging to the displayed structure.

7.5. DSC of multivalent components (solution crosslinking)
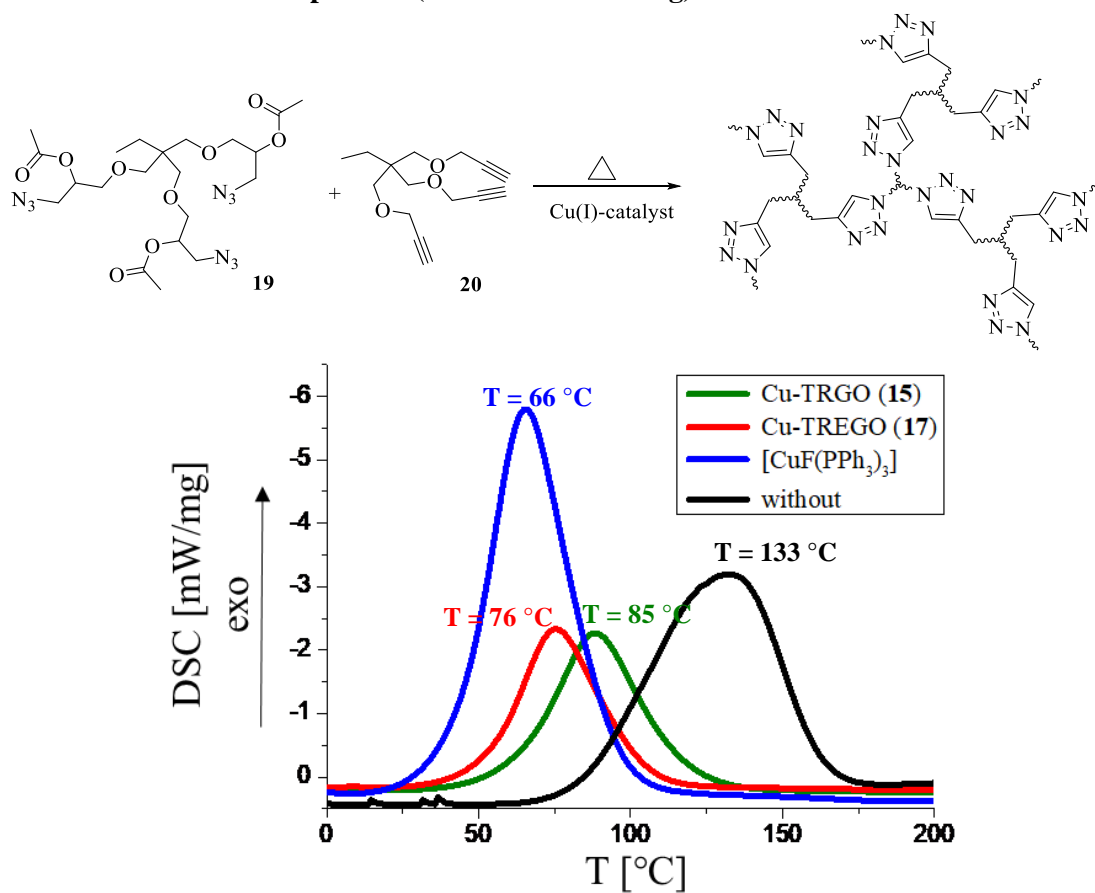
Figure S 15. DSC investigations of the CuAAC "click" reaction of **19** and **20** applying different Cu(I)-catalysts.
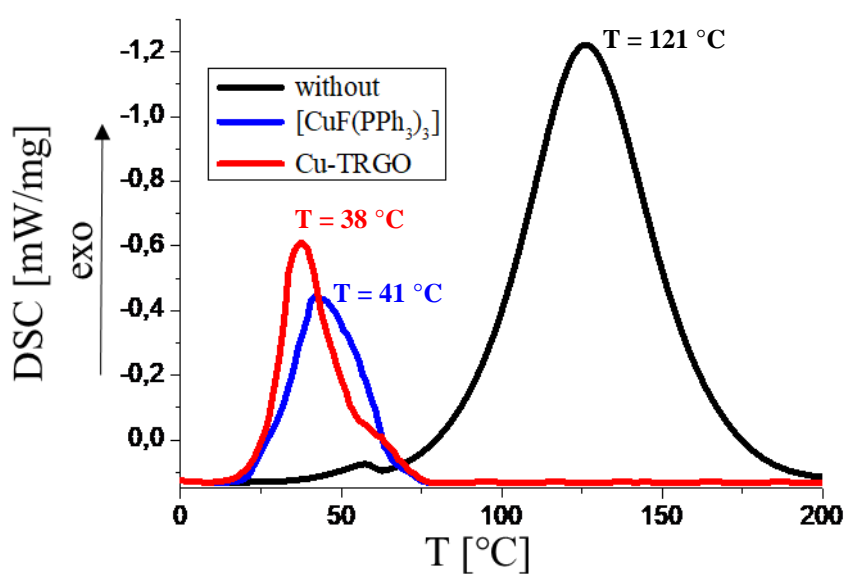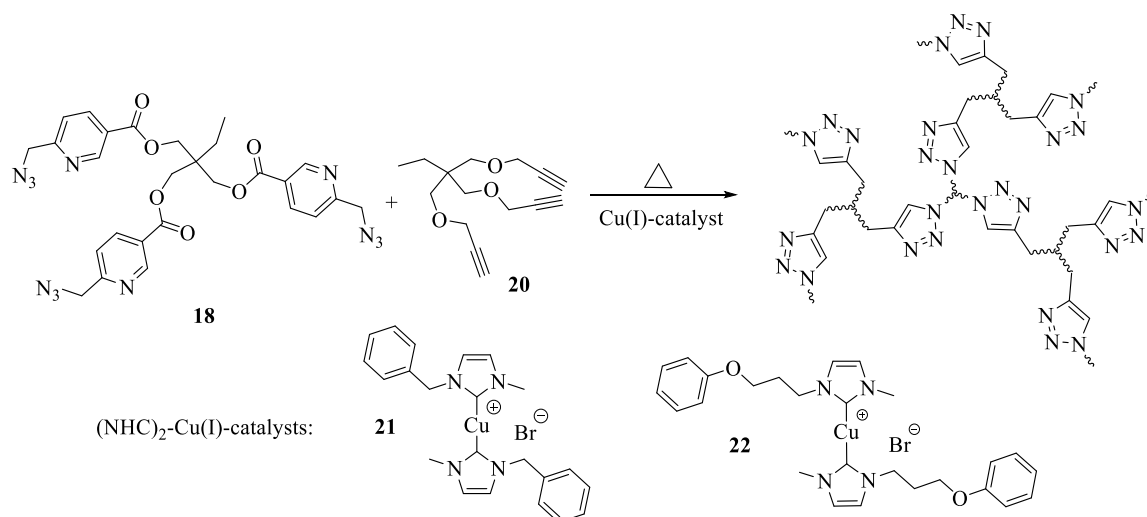
Figure S 16. DSC investigations of the chelation-assisted CuAAC "click" reaction of **18** and **20**, applying different Cu(I)-catalysts.
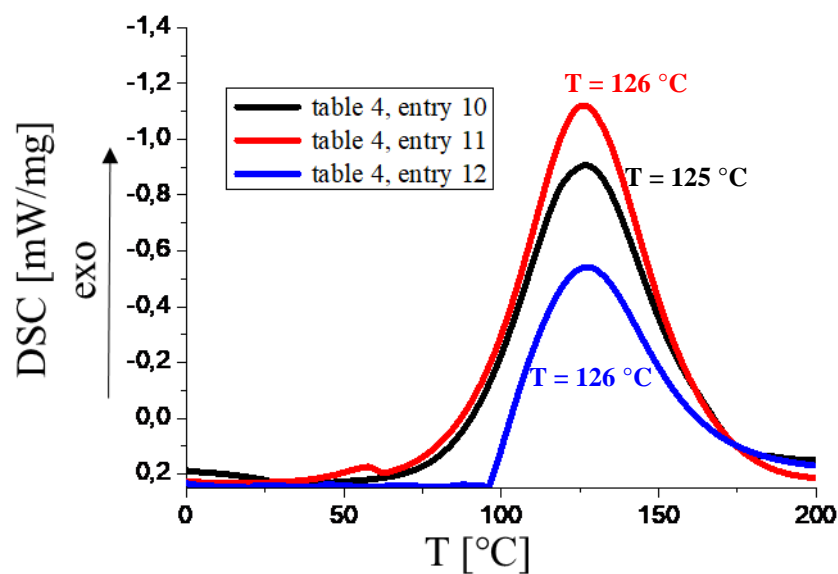
Figure S 17. DSC investigations of the chelation-assisted CuAAC "click" reaction of **18** and **20**, applying different (NHC)₂-Cu(I)-catalysts (**21** and **22**), showing no thermal activation.
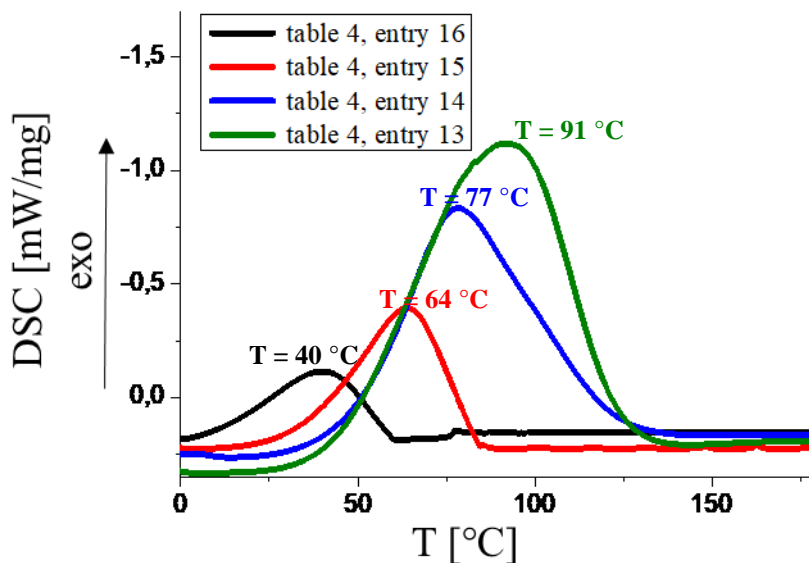
Figure S 18. DSC investigations of the chelation-assisted CuAAC "click" reaction of **18** and **20**, applying different (NHC)₂-Cu(I)-catalysts **21** in presence of entry 13; DBN; entry 14: DBU; or **22** in presence of entry 15: DBN; entry 16: DBU.

7.6. Characterization of picolyl azido telechelic PIBs
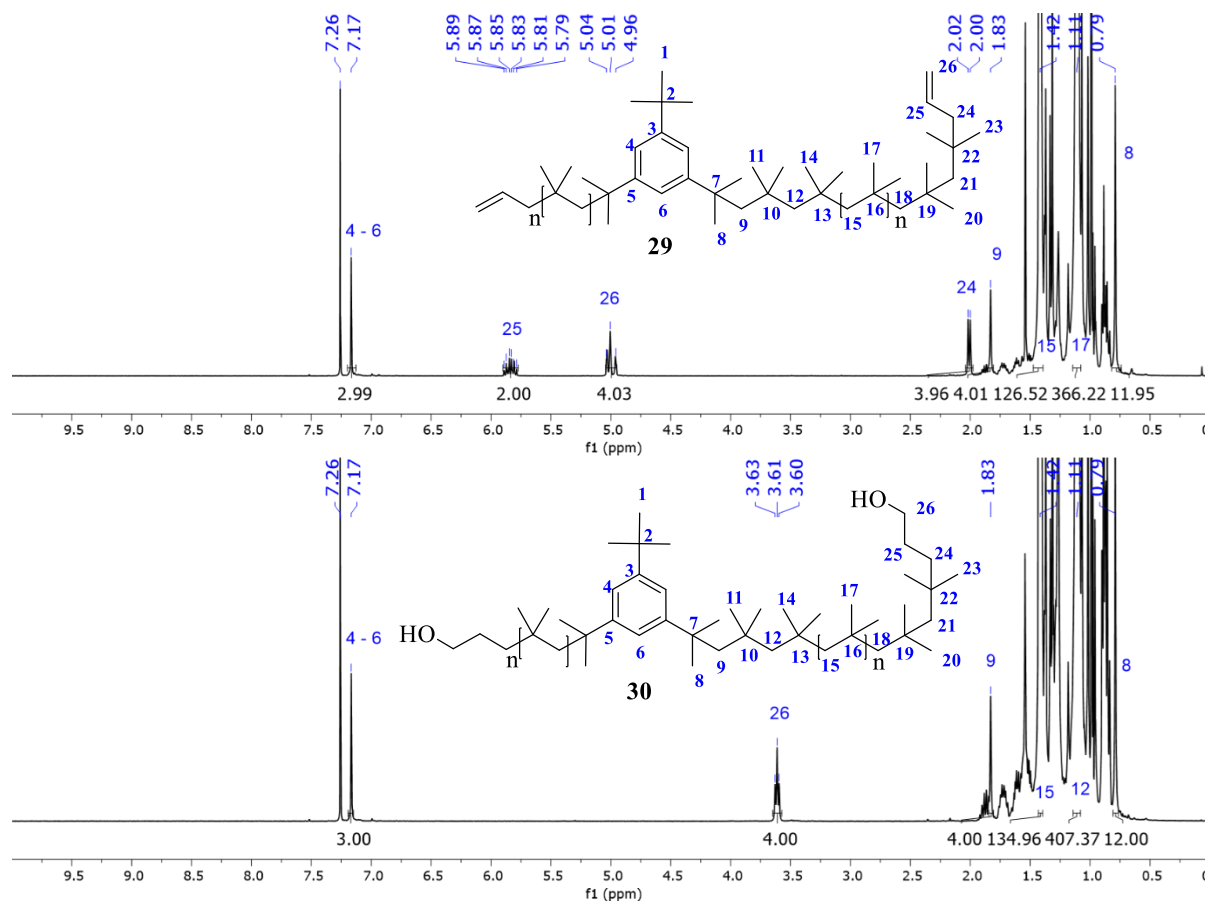
Figure S 19. ¹H-NMR spectra in C*D*Cl₃ of bivalent allyl telechelic PIB (**29**) (top) and bivalent hydroxy telechelic PIB (**30**).
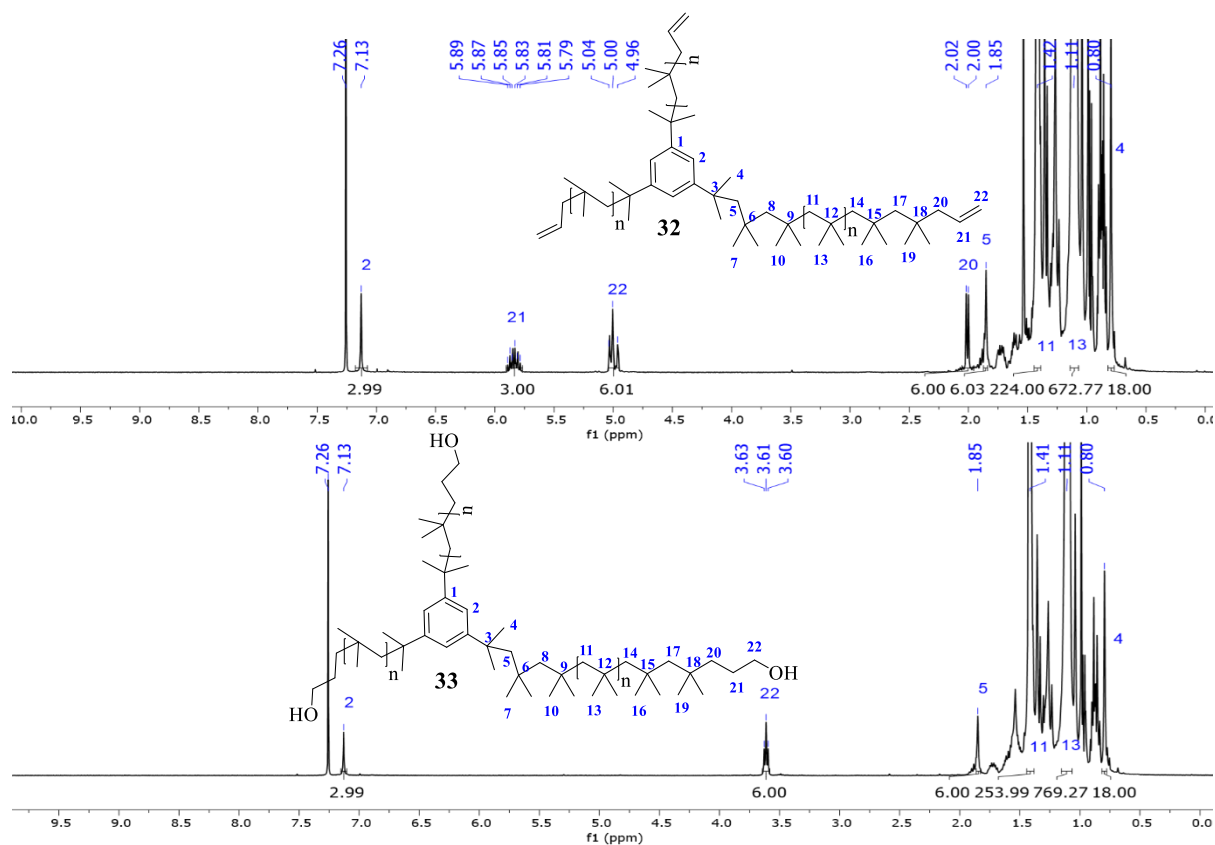
Figure S 20. ^{1}H-NMR spectra in C*D*Cl$_3$ of trivalent allyl telechelic PIB (**32**) (top) and trivalent hydroxy telechelic PIB (**33**).
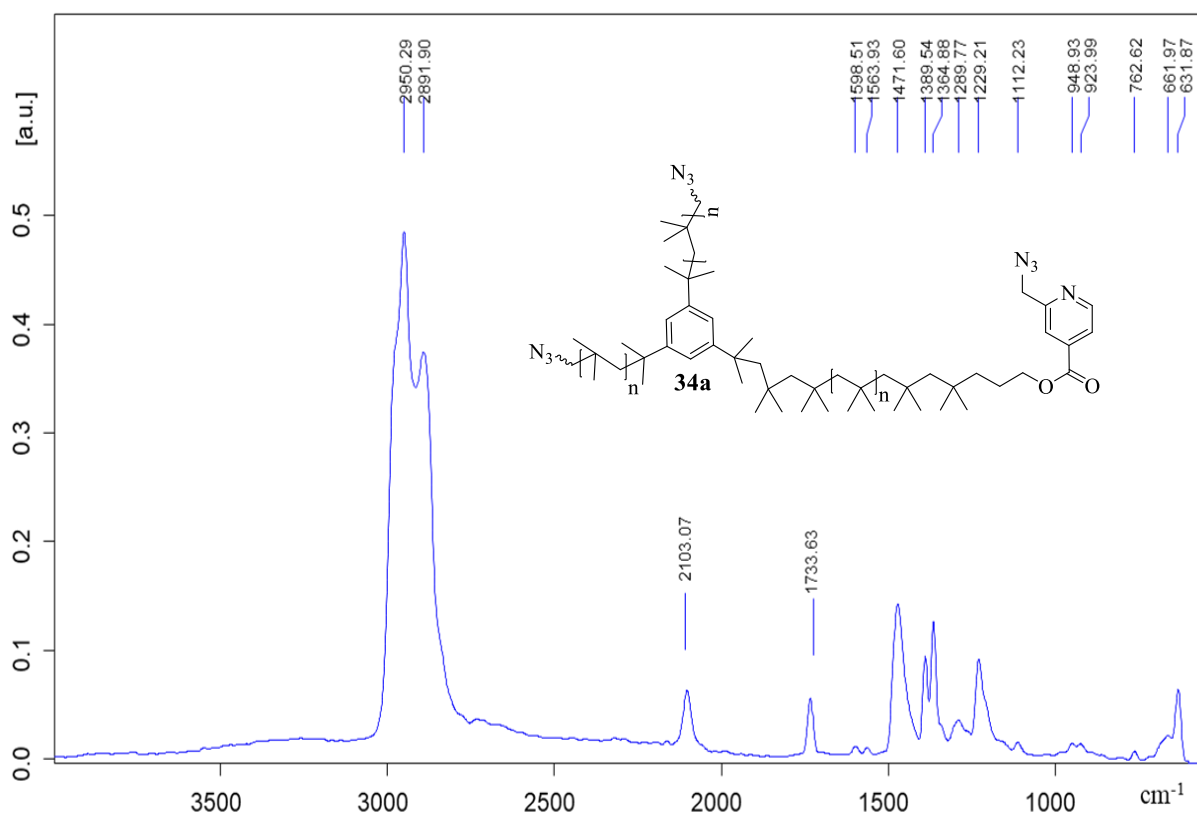
Figure S 21. IR spectrum of trivalent picolyl azido telechelic PIB (**34a**).
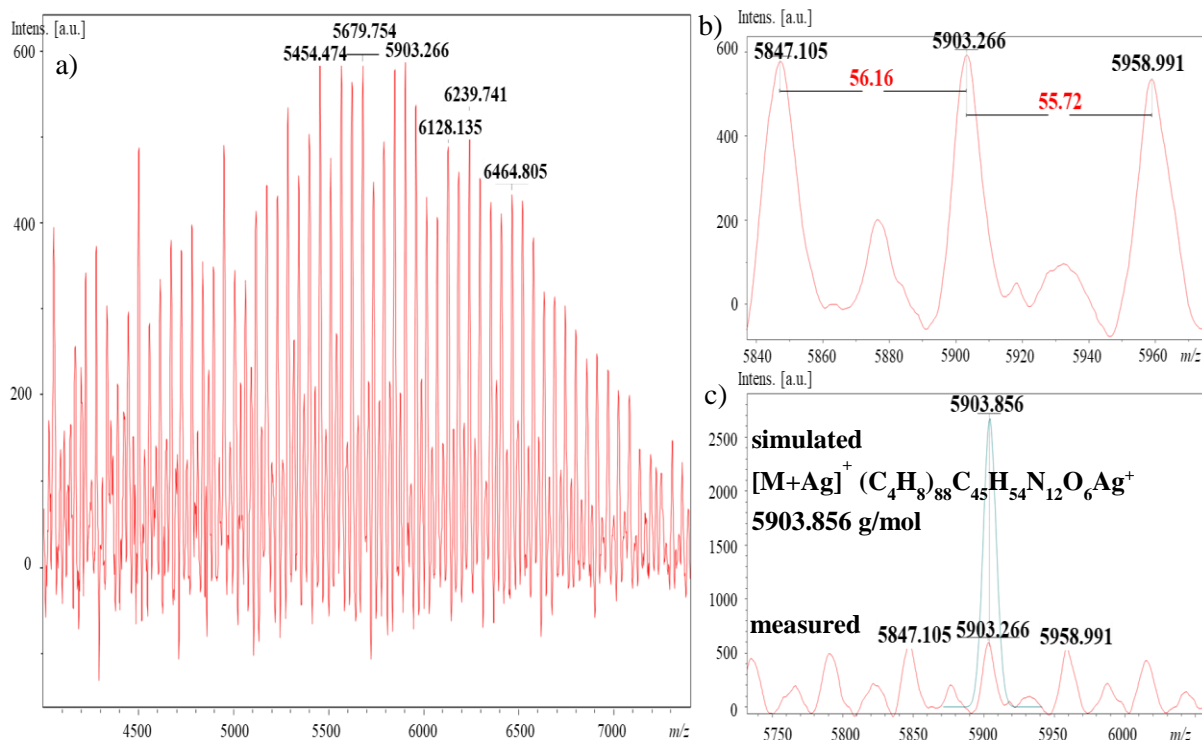
Figure S 22. MALDI-ToF-MS of trivalent picolyl azido telechelic PIB (**34a**). a) Full spectrum of **34a**, showing two series. b) Superimposed area of spectrum of **34a**, showing a distance between peaks of main series of 56 g/mol, belonging to the repetitive unit of isobutylene. c) Measured peaks (red) and their simulated isotopic pattern (green), belonging to the displayed structure.

7.7. Rheology of star-shaped PIBs suiting the chelation-assisted CuAAC mechanism

For determination of k' the following formula was used (**e4**)[40]:

$$\ln(\eta) = k' \cdot t + \ln(\eta_0) \tag{e4}$$

Plotting of ln (η) vs. $k' \cdot t$ led to determination of the apparent rate constant k' by linear fit of the slope, while η is the real part of the viscosity (see Figure S 23).
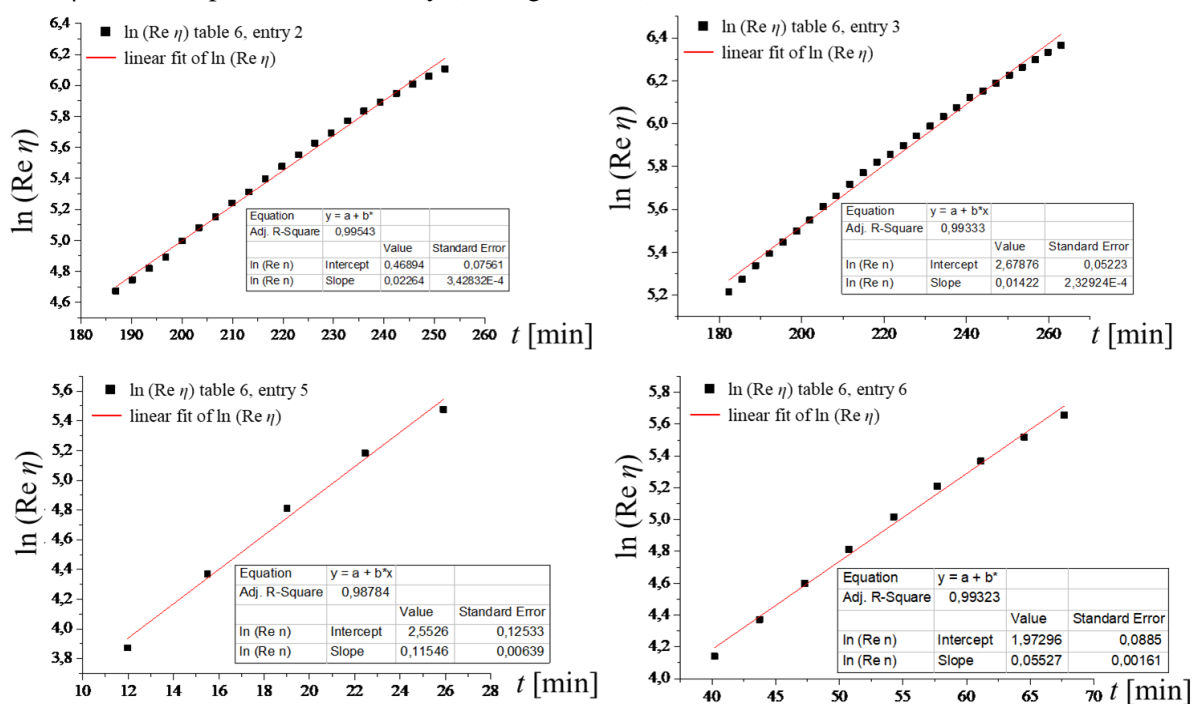
Figure S 23. Determination of the apparent rate constant k' by plotting of ln (Re η) vs. $k' \cdot t$ and linear fit of the slope.
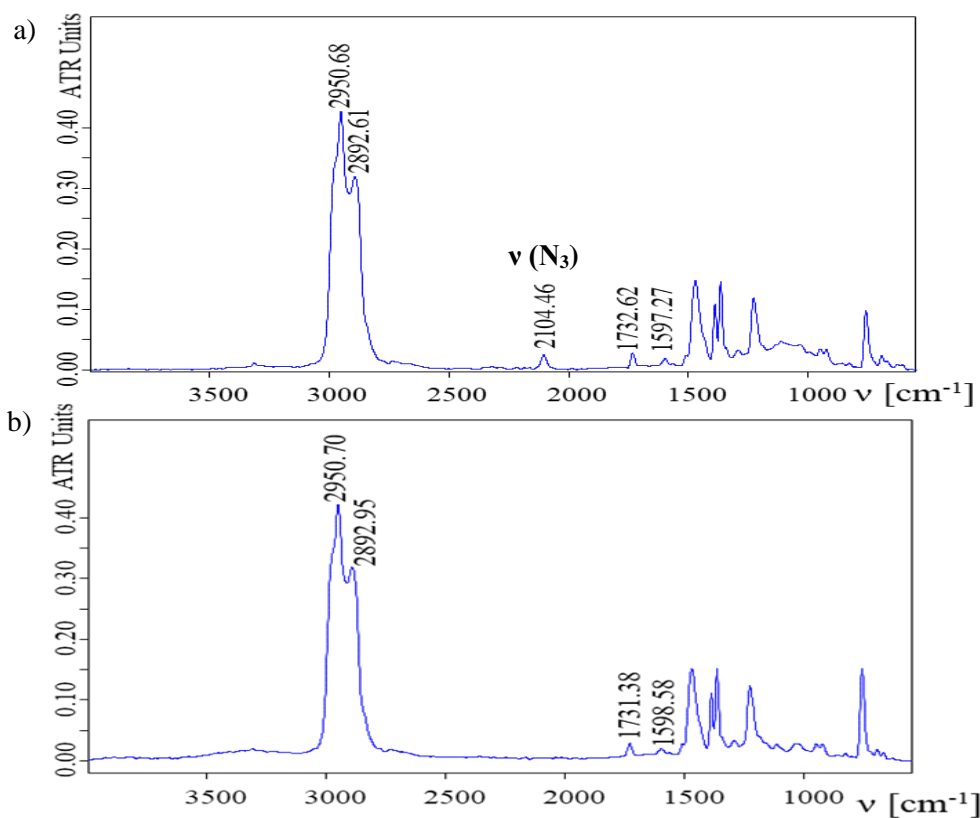
Figure S 24. IR spectra of the crosslinked networks of **34a/b** + **35**; a) see Table 6, entry 1; b) see Table 6, entry 6 (also all other).

7.8. Characterization of coumarin azide (36)
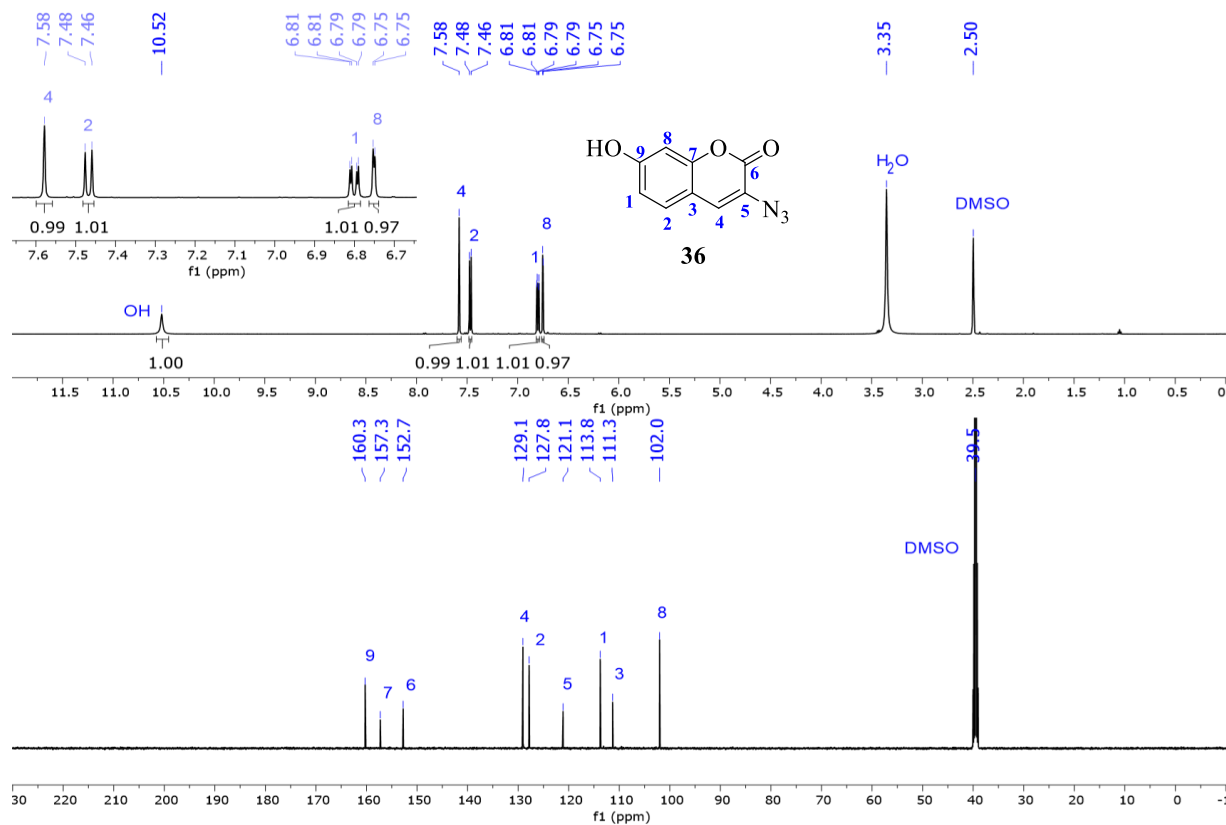
Figure S 25. ¹H-NMR spectrum in DMSO-*d₆* of 3-azido-7-hydroxy-coumarin (**36**) and superimposed area (top). ¹³C-NMR spectrum of 3-azido-7-hydroxy-coumarin (**36**) in DMSO-*d₆* (bottom).
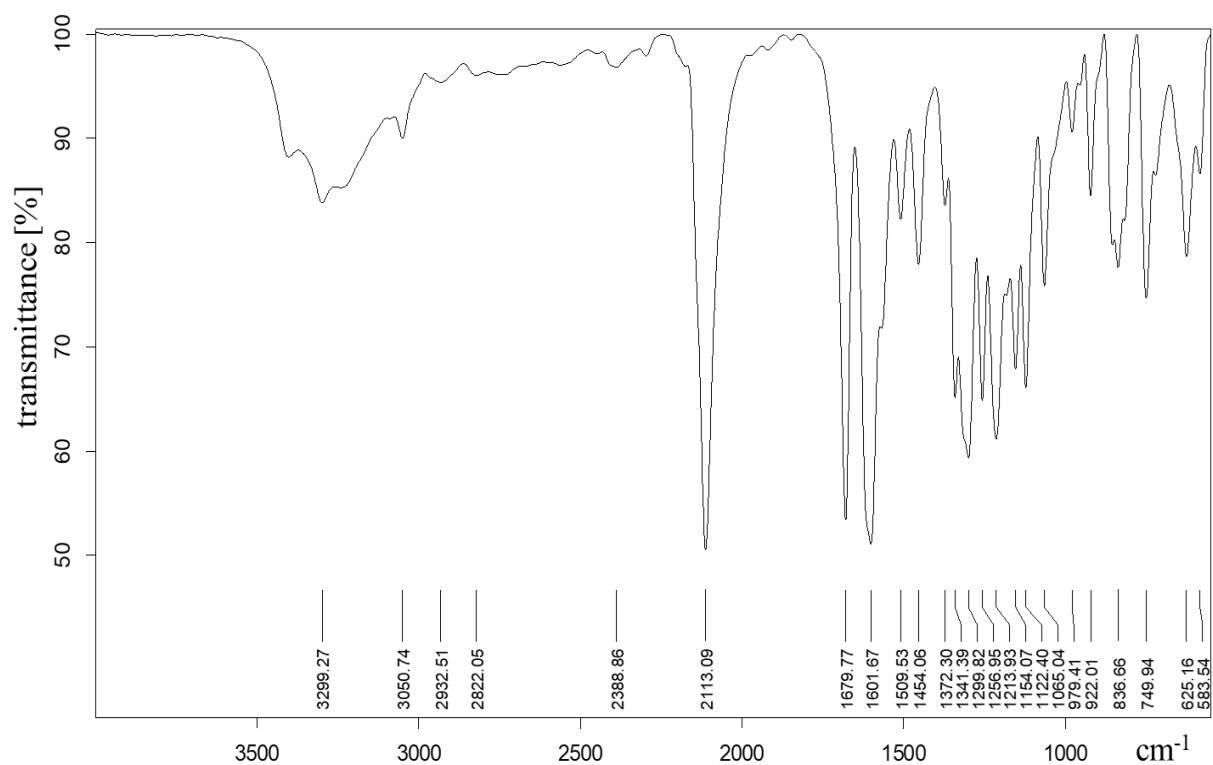
Figure S 26. IR spectrum of 3-azido-7-hydroxy-coumarin (**36**).
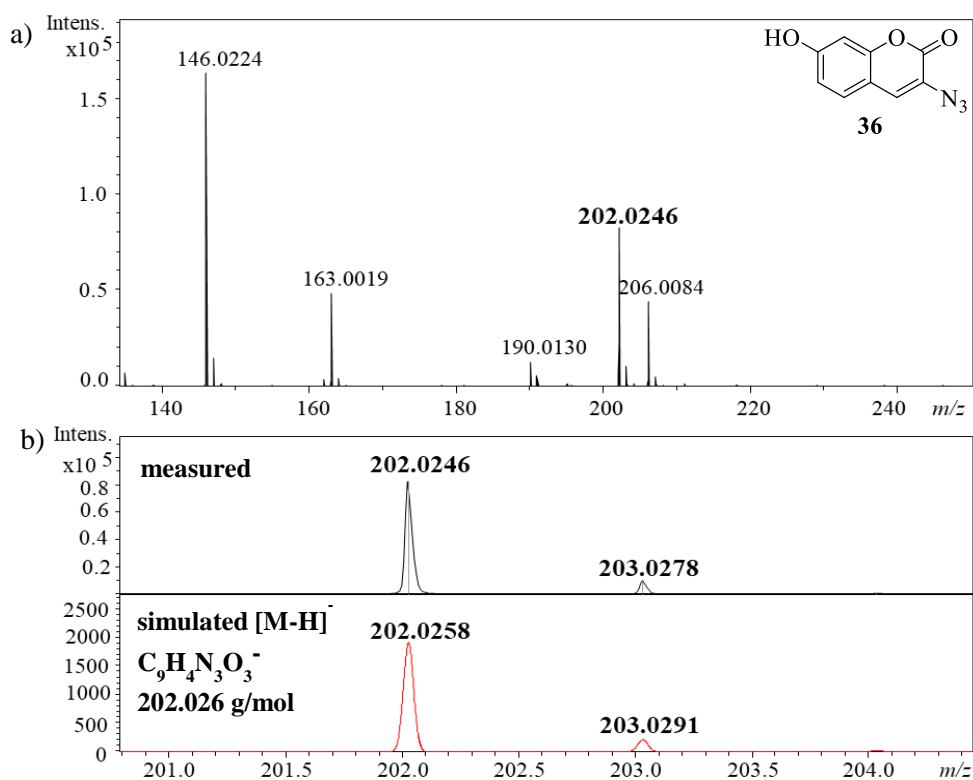
Figure S 27. a) ESI-ToF-MS of **36** (negative mode); b) superimposed area, showing measured peak (top) and its simulated isotopic pattern (bottom), belonging to the displayed structure.

7.9. Synthesis and test of the autonomous SH approach (PIB-matrix)
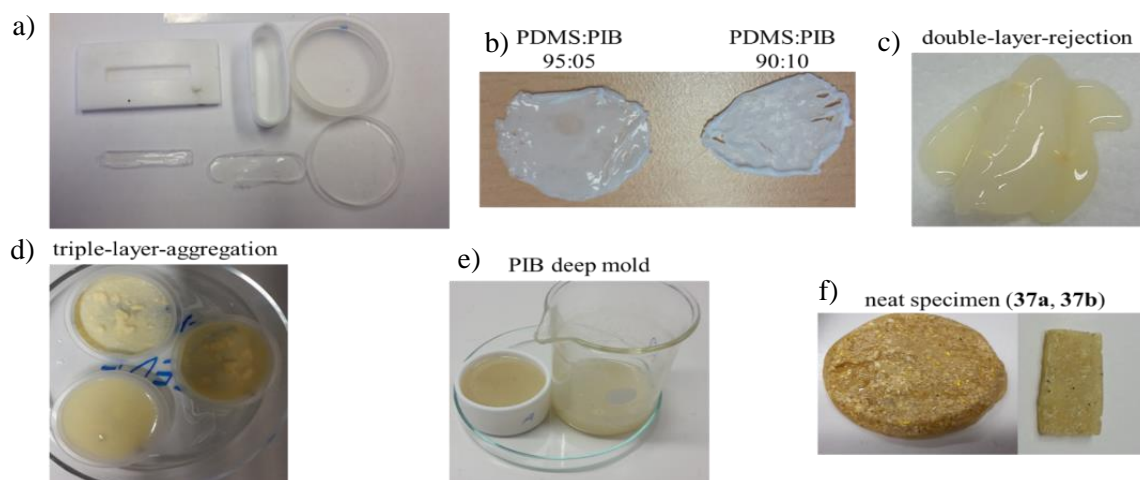
Figure S 28. Photographs of attempts to embed SH components to surrounding matrices. a) Molds applied (from left to right): stretched mold, deep stretched mold, deep round mold; b) see Table 20, entry 10 (left) and entry 8 (right); c) see Table 20, entry 5 (1st layer was cured before the 2nd layer, containing the capsules filled with alkyne moiety, dissolved in *n*-hexane was added); d) see Table 20, entry 6; e) beaker (right) used for synthesis and mixing of components with dissolved matrix, round deep mold (left) used for drying of specimen; f) neat specimen (**37a-b**) obtained after drying (left) and the sliced piece of approximate dimension: 5 mm x 13 mm x 0.8 mm (right) applied to the subsequent SH-scratch-fluorescent measurement.

7.10. Characterization of chain-transfer agents (CTAs) (40, 43, 44, 46)
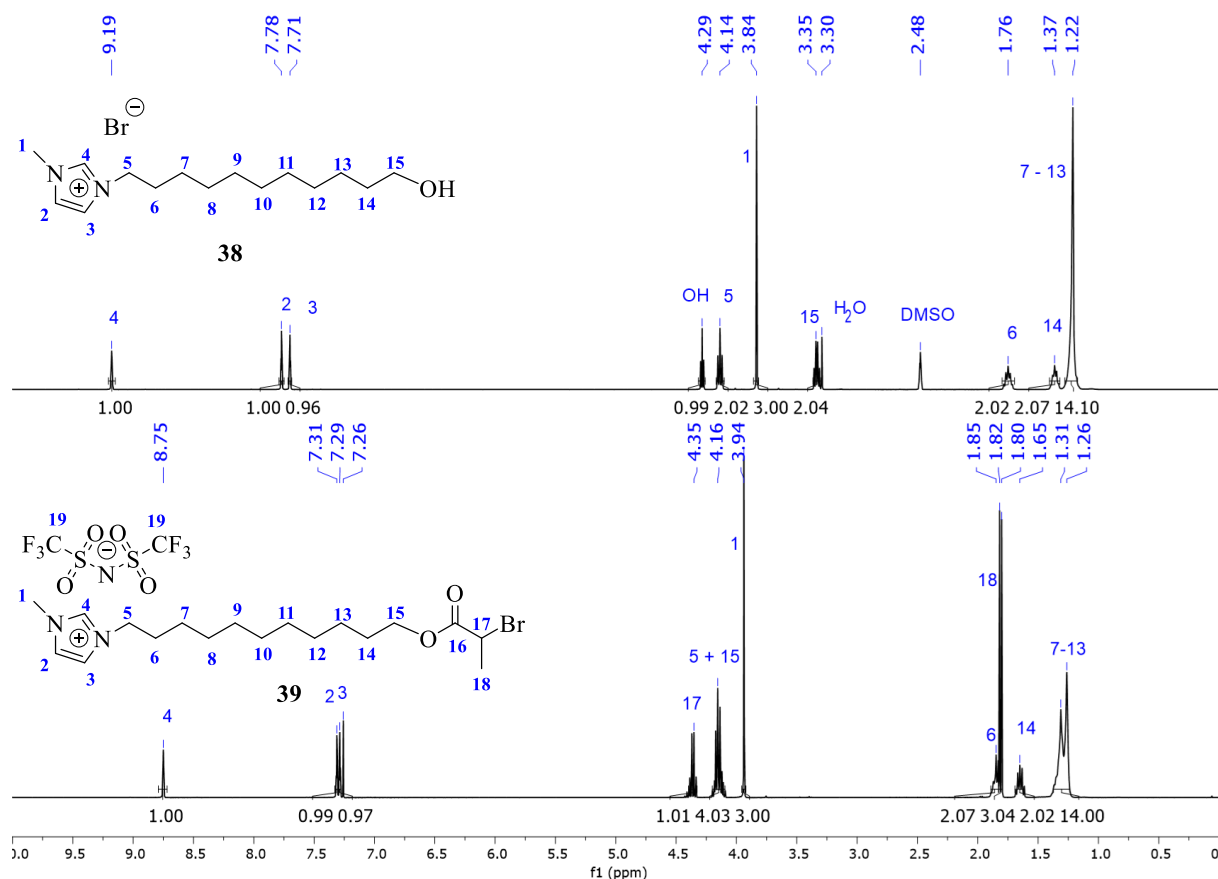
Figure S 29. ¹H-NMR spectra of 3-(11-hydroxyundecyl)-1-methylimidazolium bromide (**38**) in DMSO-*d₆* (top); 3-(11-(2-brompropionyloxy)undecyl)-methyl-1-imidazolium bis(trifluoro-methane)sulfonimide (**39**) in C*D*Cl₃ (bottom).
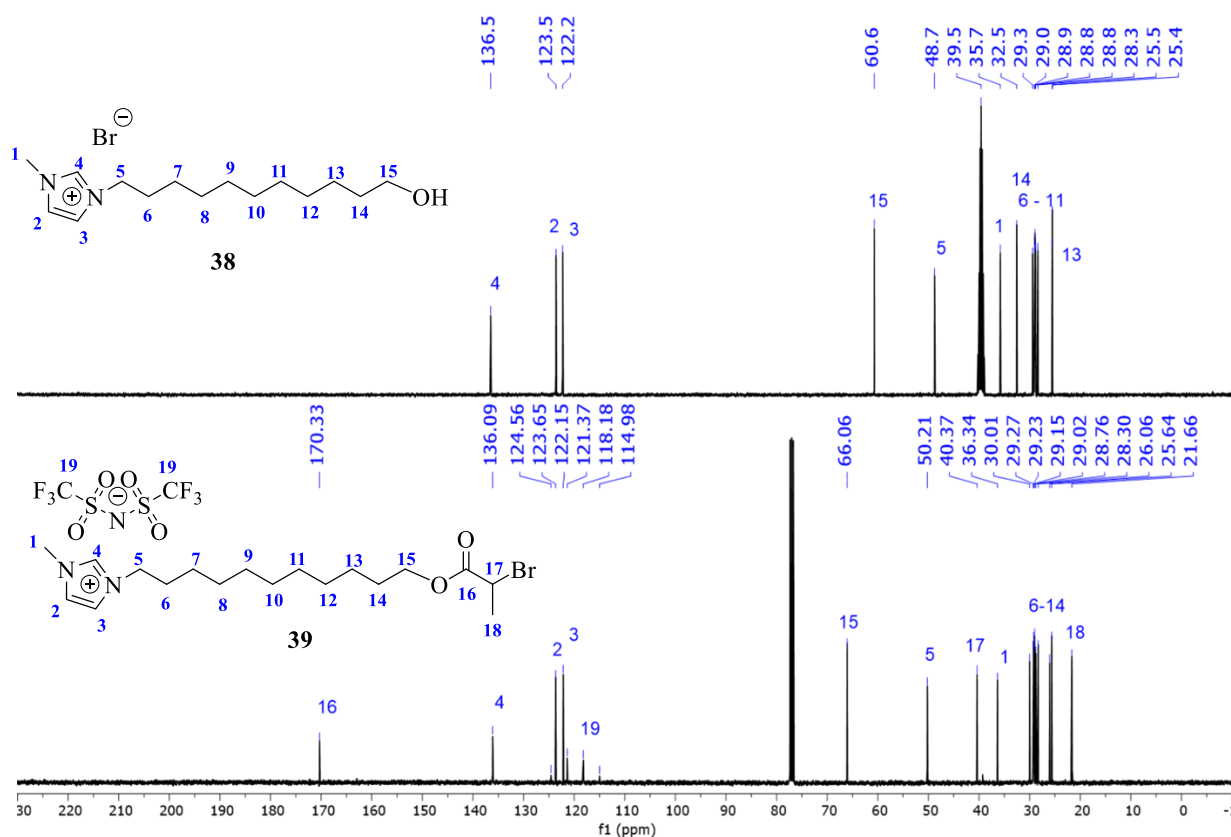
Figure S 30. ¹³C-NMR spectra of 3-(11-hydroxyundecyl)-1-methylimidazolium bromide (**38**) in DMSO-d_6 (top); 3-(11-(2-brompropionyloxy)undecyl)-methyl-1-imidazolium bis(trifluoro-methane)sulfonimide (**39**) in C*D*Cl₃ (bottom).
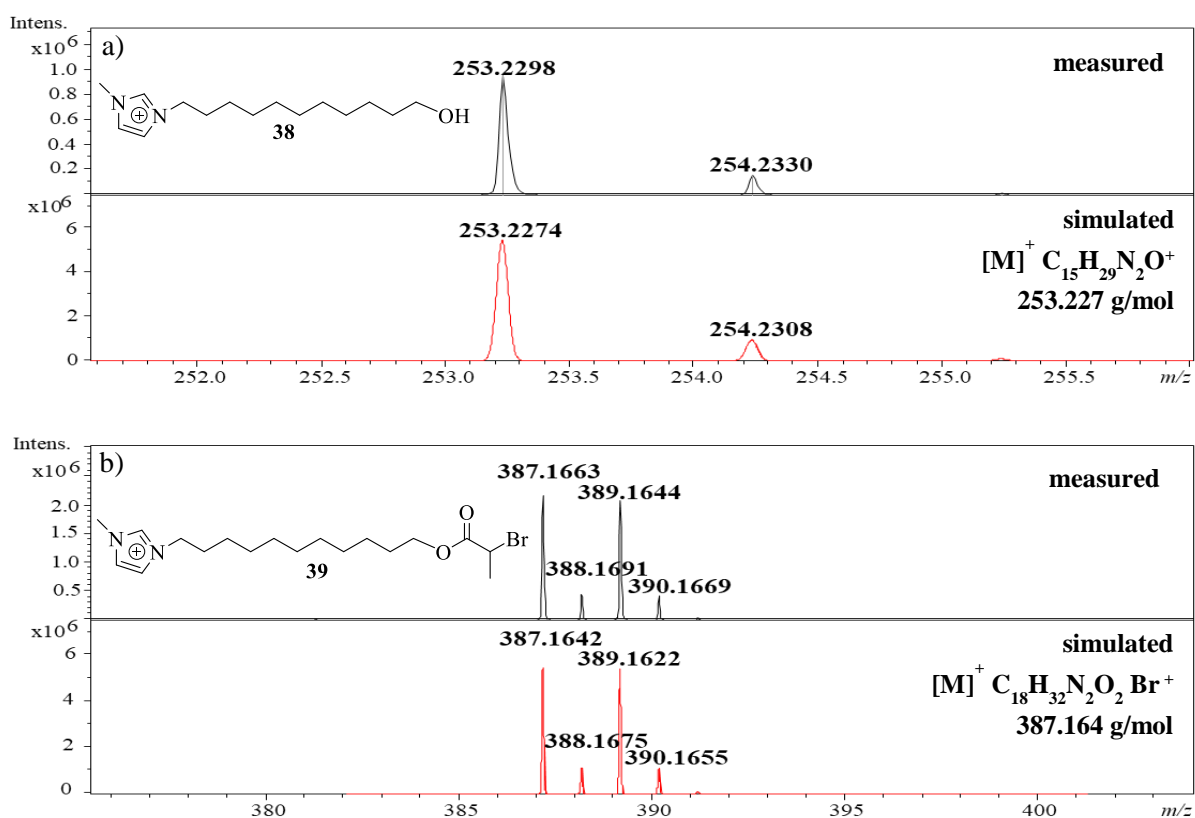
Figure S 31. a) Superimposed ESI-ToF-MS of **38**, showing measured peak (top) and its simulated isotopic pattern (bottom), belonging to the displayed structure. b) Superimposed ESI-ToF-MS of **39**, showing measured peak (top) and its simulated isotopic pattern (bottom), belonging to the displayed structure.
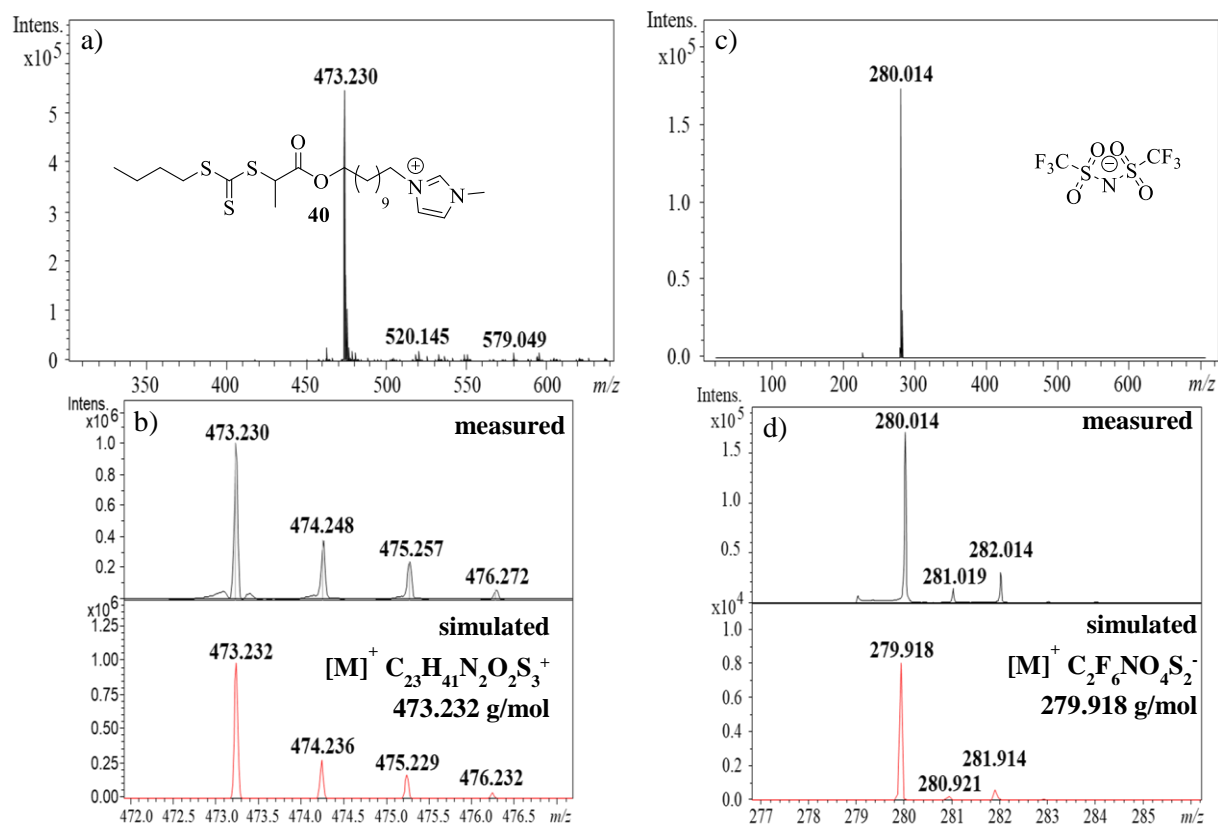
Figure S 32. a) Full ESI-ToF-MS of **40** (positive mode). b) Superimposed area, showing measured peak (top) and its simulated isotopic pattern (bottom), belonging to the displayed structure. c) Full ESI-ToF-MS of **40** (negative mode); d) superimposed area, showing the measured peak (top) and its simulated isotopic pattern (bottom), belonging to the displayed structure.
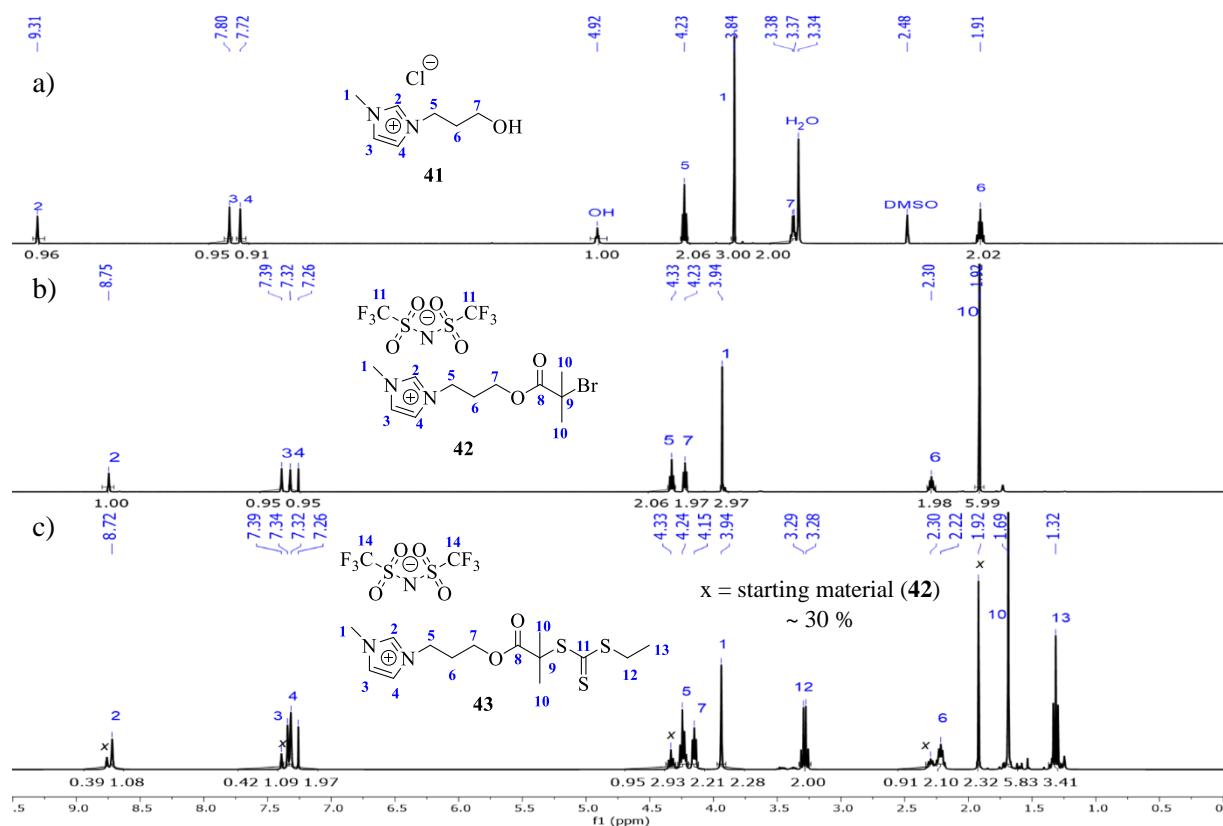
Figure S 33. ^{1}H-NMR spectra of a) 3-methylimidazole-propanol (**41**) in DMSO-d_6; b) 3-methylimidazole-propanoic acid-2'bromo-2'-methyl-propanylester (**42**) in CDCl$_3$; c) CTA-NHC (**43**) in CDCl$_3$.
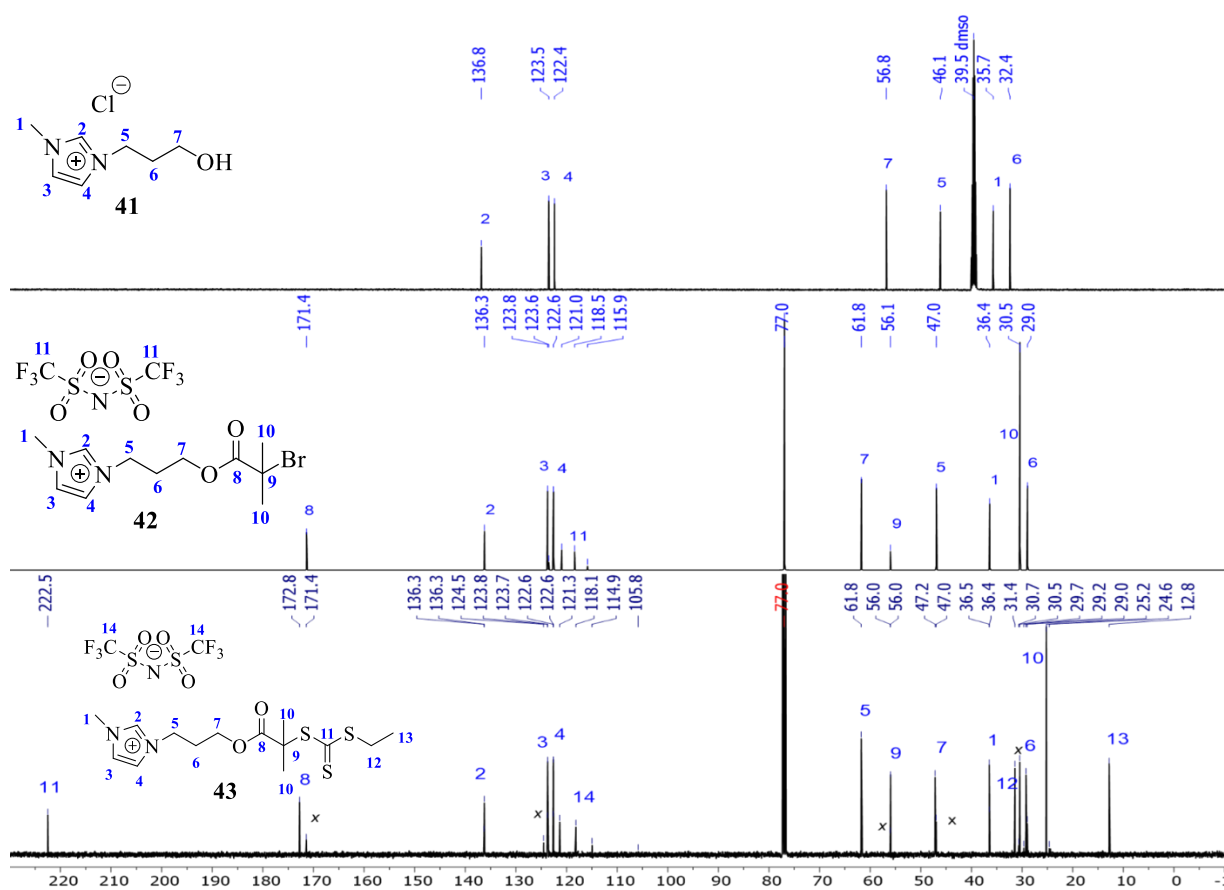
Figure S 34. ^{13}C-NMR spectra of 3-methylimidazole-propanol (**41**) (top) in DMSO-d_6; 3-methylimidazole-propanoic acid-2'bromo-2'-methyl-propanylester (**42**) (middle) in C*D*Cl$_3$; c) CTA-NHC (**43**) (bottom) in C*D*Cl$_3$.
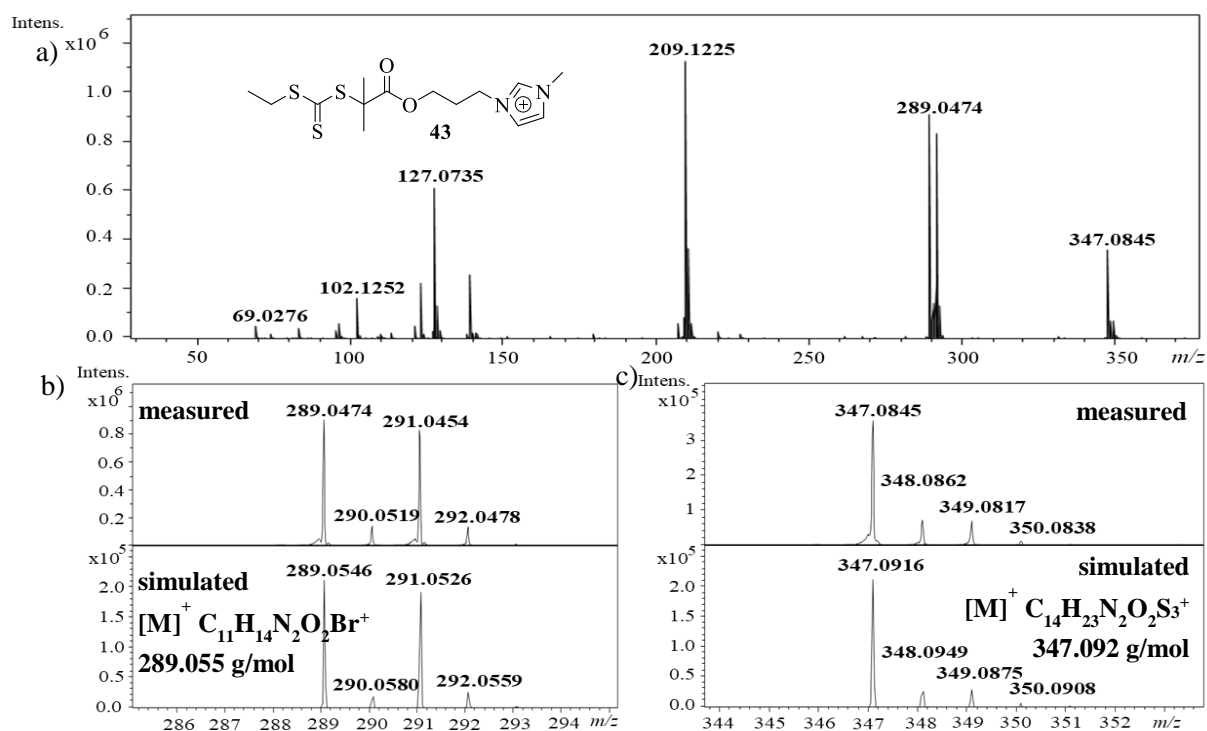
Figure S 35. a) Full ESI-ToF-MS of **43**; b) superimposed area, showing measured peak (top) and its simulated isotopic pattern (bottom), belonging to the displayed structure (precursor **42**); c) superimposed area, showing measured peak (top) and its simulated isotopic pattern (bottom), belonging to the displayed structure of the product (**43**).
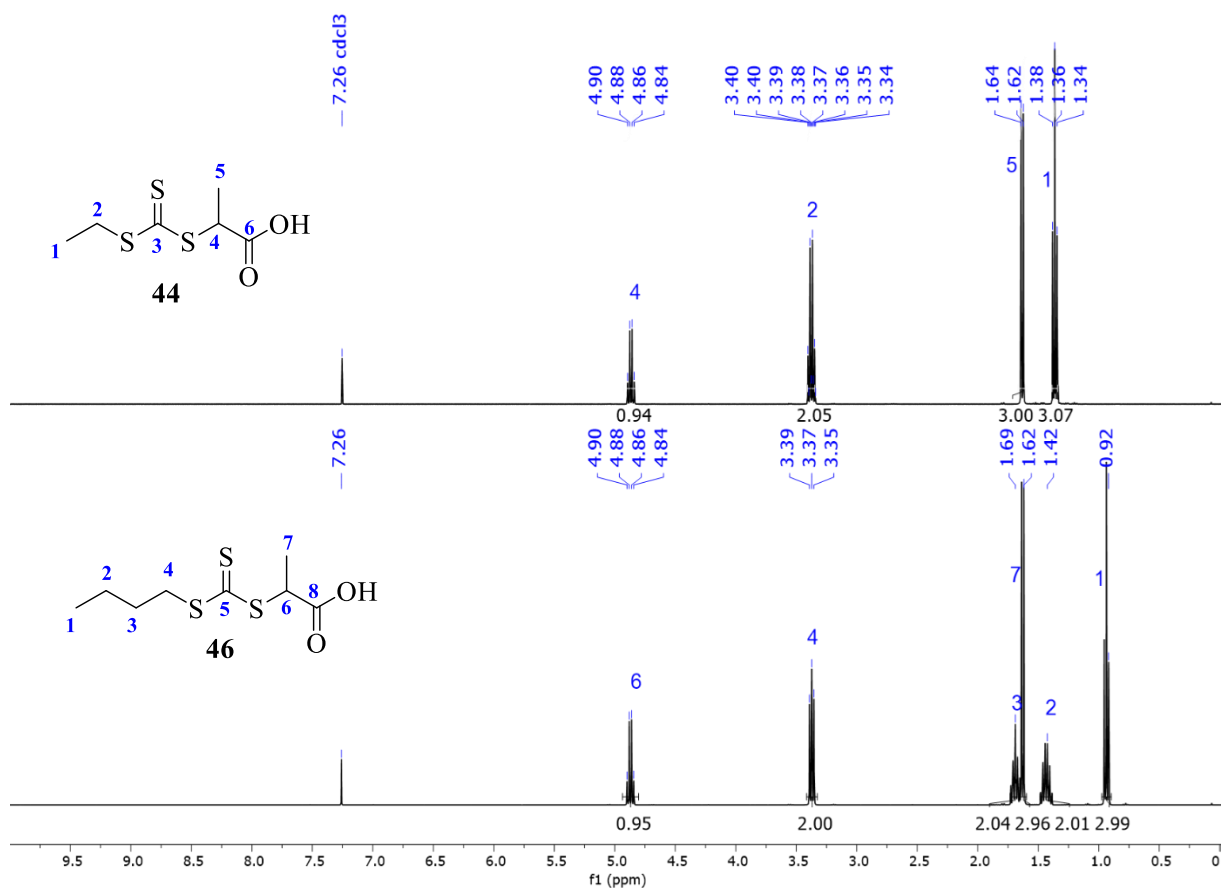
Figure S 36. ^{1}H-NMR spectra in C*D*Cl$_3$ of ethyl CTA-COOH (**44**) (top); butyl CTA-COOH (**46**) (bottom).
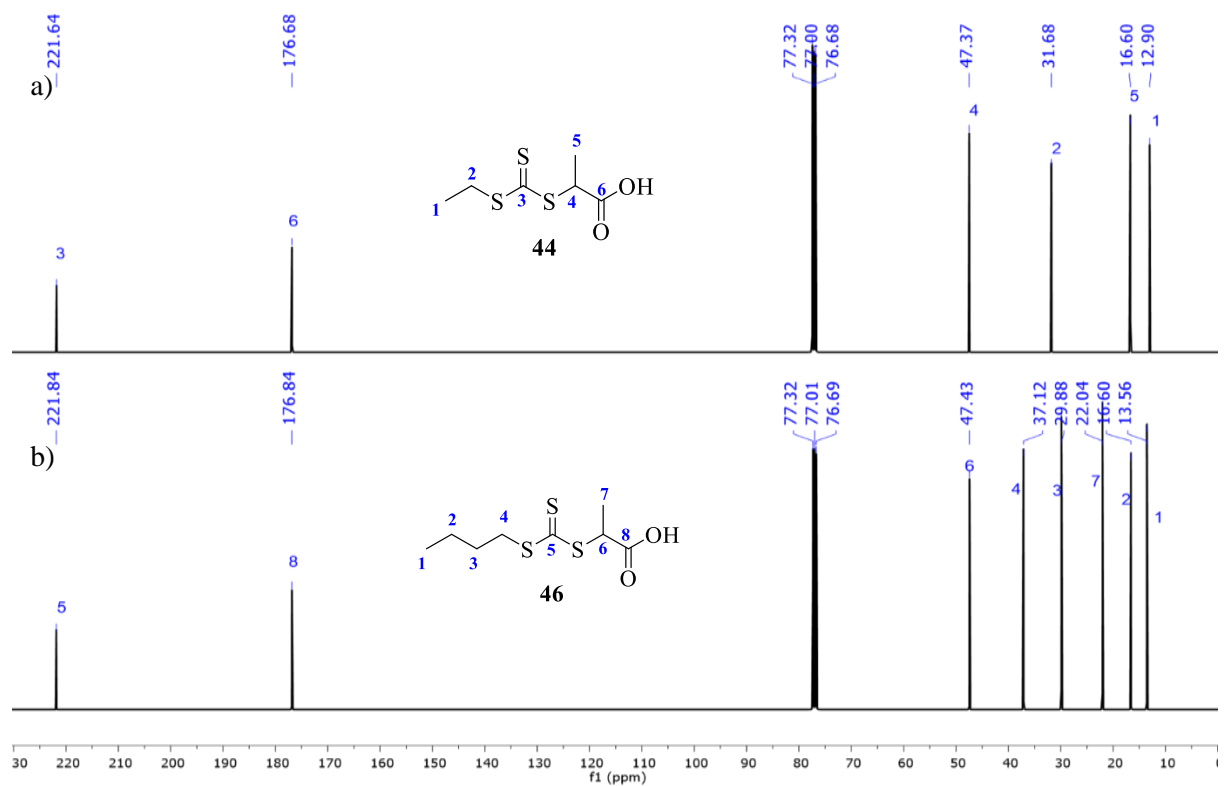
Figure S 37. ^{13}C-NMR spectra in C*D*Cl$_3$ of a) CTA-COOH (**44**); b) CTA-COOH (**46**).

7.11. Characterization of RAFT-PS (48, 49a-m)
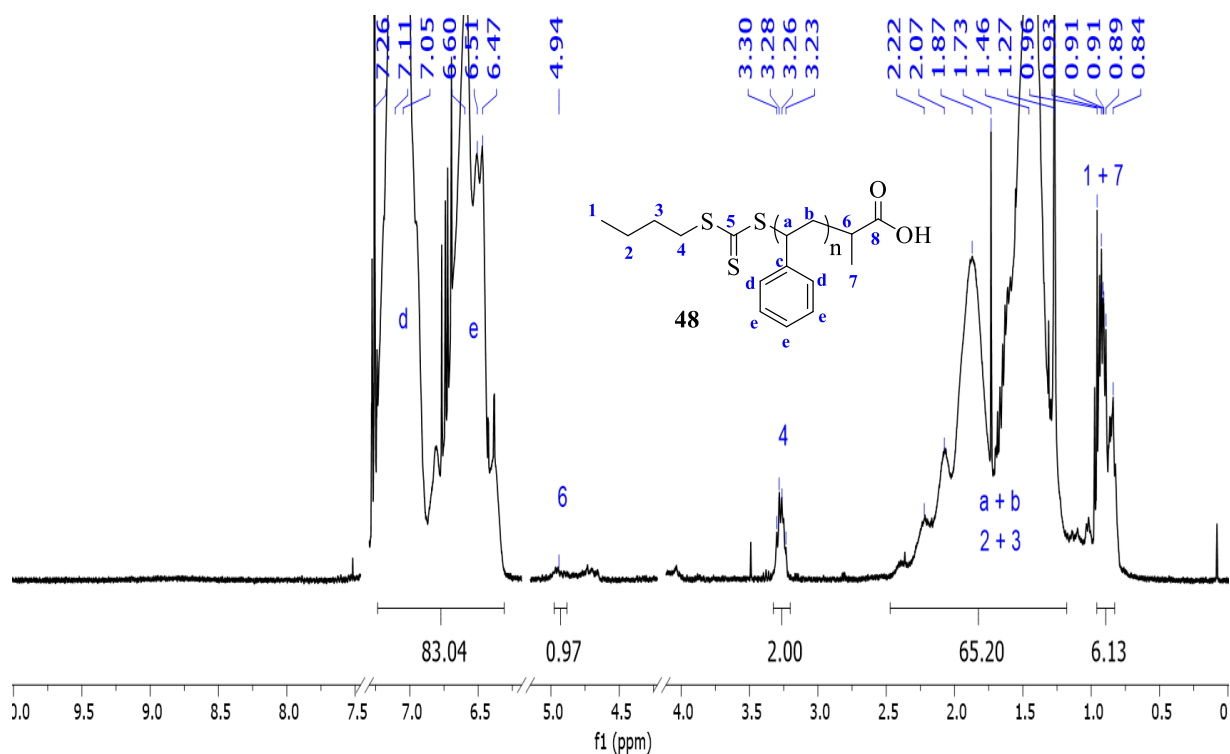
Figure S 38. ^{1}H-NMR spectrum of control RAFT polymerization, providing PS-COOH (**48**) ($M_{n(NMR)}$ = 4 200 g/mol, PDI = 1.23) in C*D*Cl₃. Polymer remained unpurified from residual styrene monomer (signals were cut out).
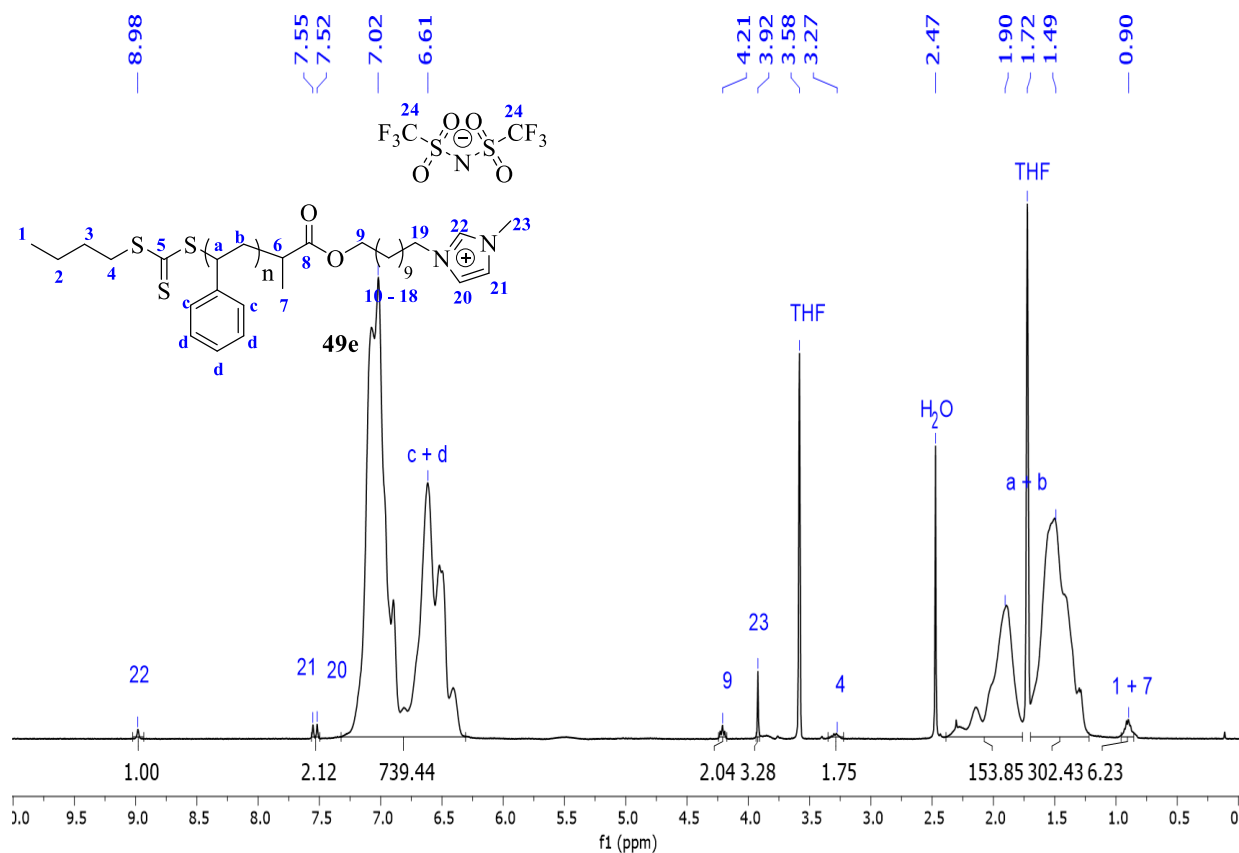
Figure S 39. ^{1}H-NMR spectrum of **49e** ($M_{n(NMR)}$ = 11 100 g/mol, PDI = 1.17) in THF-*d₈*.
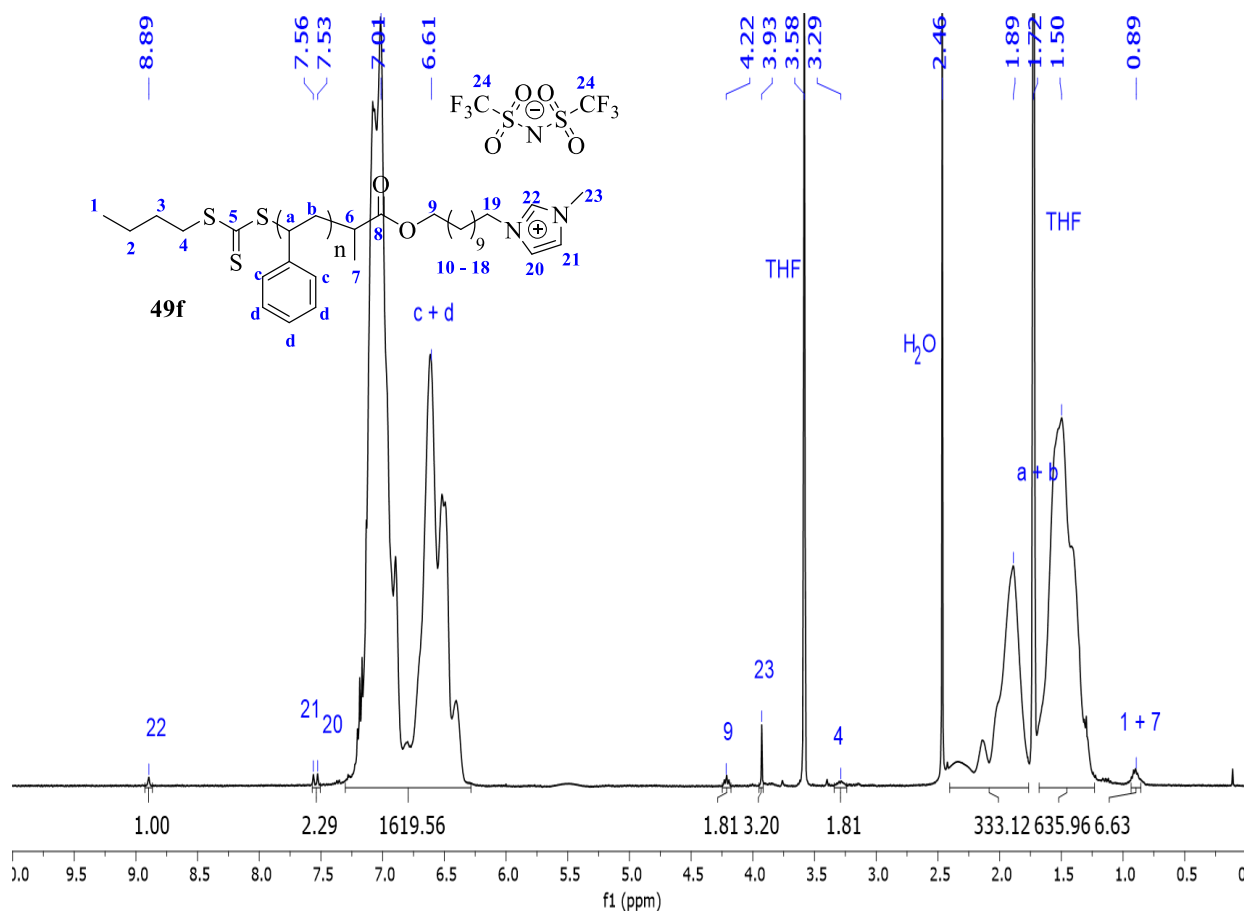
Figure S 40. ^{1}H-NMR spectrum of **49f** ($M_{n(NMR)}$ = 26 000 g/mol, PDI = 1.15) in THF-d_8.
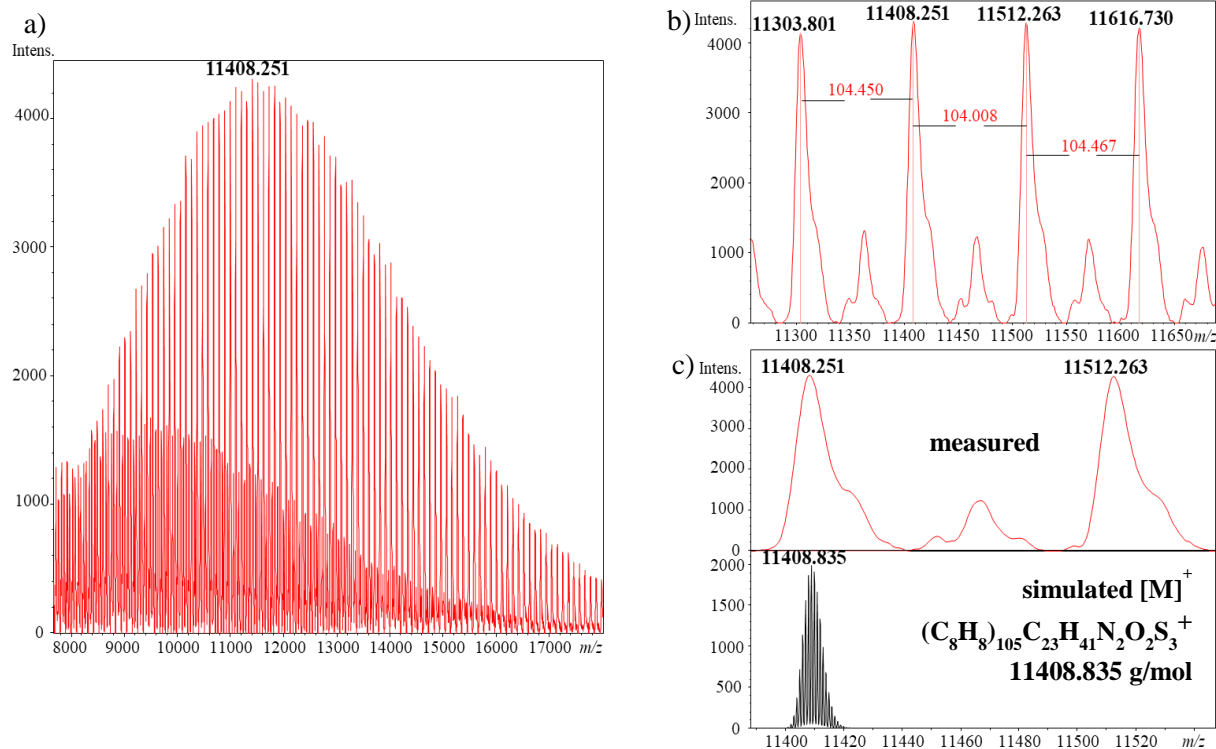
Figure S 41. MALDI-ToF-MS of PS-NHC (**49e**). a) Full spectrum of **49e**, showing two series. b) Superimposed area of spectrum of **49e**, showing distance between peaks of both series of 104 g/mol, belonging to the repetitive unit of styrene. c) Measured peak (top) and its simulated isotopic pattern (bottom), belonging to the displayed structure.

Table S1. Synthesis details of the remaining RAFT-polymerization of styrene.

PS	CTA	CTA:I:M [eq.]	n_{CTA} [mmol]	$n_{monomer}$ [mmol]	$M_{n(GPC)}$[a] [g/mol]	$M_{n(NMR)}$[b] [g/mol]	PDI	solvent	T [°C]	yield [%]
A)	**RAFT-polymerization conducted in solution**									
49g	**40**	4:1:2400	0.16	96.0	13 200	21 900	1.31	toluene	80	14
49h	**40**	10:1:1000	0.29	28.8	5 100	5 000	1.17	dioxane	80	27
49i	**40**	10:1:5000	0.30	149.8	10 400	12 100	1.17	dioxane	80	13
B)	**RAFT-polymerization conducted in bulk in absence of AIBN**									
49j	**40**	10:5000	0.25	124.8	41 800	62 900	1.23	/	120	73

a) GPC-measurements were performed in HPLC-grade DMF with the addition of LiNTf$_2$ (c = 10.0 mM) and molecular weight was determined by calibration with external PS-standards (M_P ~ 1 000 – 115 000 g/mol) and detection of refractive-index. b) Calculated by the ratio of the initiator signal at δ = 3.28 ppm and the signal of the repetitive unit at δ = 7.24 – 6.32 ppm.

Table S2. Synthesis details of kinetic (growing of molecular weight by time) measurements of RAFT polymerization of PS.

PS	CTA	CTA:I:M [eq.]	n_{CTA} [mmol]	$n_{monomer}$ [mmol]	t [h]: $M_{n(GPC)}$[a] [g/mol]	PDI	solvent	T [°C]	yield [%][b]
A)	**RAFT-polymerization conducted in solution**								
49k	**40**	10:1:6000	0.04	24.0	1: 5 960	1.30	toluene	80	5
					2: 9 000	1.30			
					3: 12 280	1.25			
					4: 13 930	1.24			
					5: 14 440	1.24			
49l	**40**	10:1:2000	0.30	60.0	1: 2 690	1.12	dioxane	80	15
					2: 3 590	1.13			
					3: 5 040	1.10			
					4: 5 910	1.11			
					5: 6 480	1.11			
					6: 7 010	1.11			
B)	**RAFT-polymerization conducted in bulk in absence of AIBN**								
49m	**40**	10:1000	0.60	60.0	1: 1 720	1.13	/	120	71
					2: 2 660	1.12			
					3: 3 380	1.11			
					4: 4 160	1.10			
					5: 4 910	1.09			
					6: 5 390	1.10			

a) GPC-measurements were performed in HPLC-grade DMF with the addition of LiNTf$_2$ (c = 10.0 mM) and molecular weight was determined by calibration with external PS-standards (M_P ~ 1 000 – 115 000 g/mol) and detection of the refractive-index. b) Isolated yield of all collected fractions.
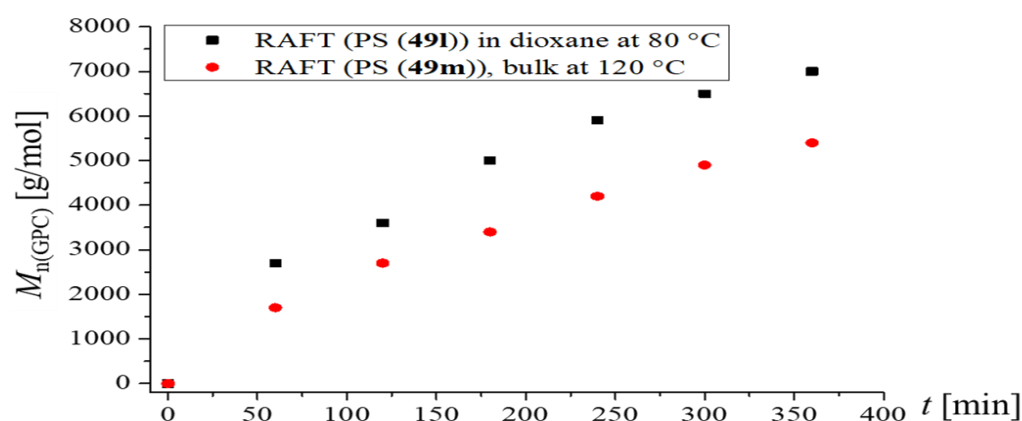
Figure S 42. Linear chain growth of molecular weight during RAFT of styrene employing CTA **40** either in dioxane or in bulk.

7.12. Characterization of RAFT-P-*n*BuA (50, 51a-j)
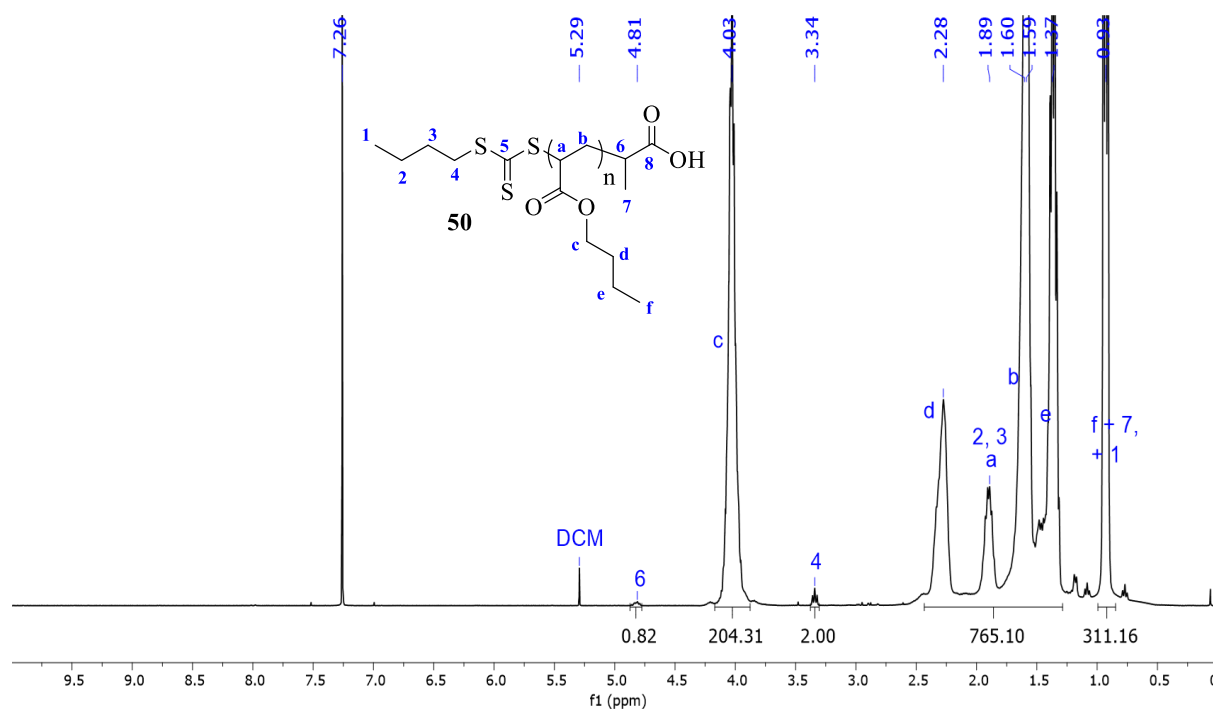
Figure S 43. ^{1}H-NMR spectrum in C*D*Cl$_3$ of control RAFT polymerization, providing P-*n*BuA-COOH (**50**) ($M_{n(NMR)}$ = 13 500 g/mol, PDI = 1.19).
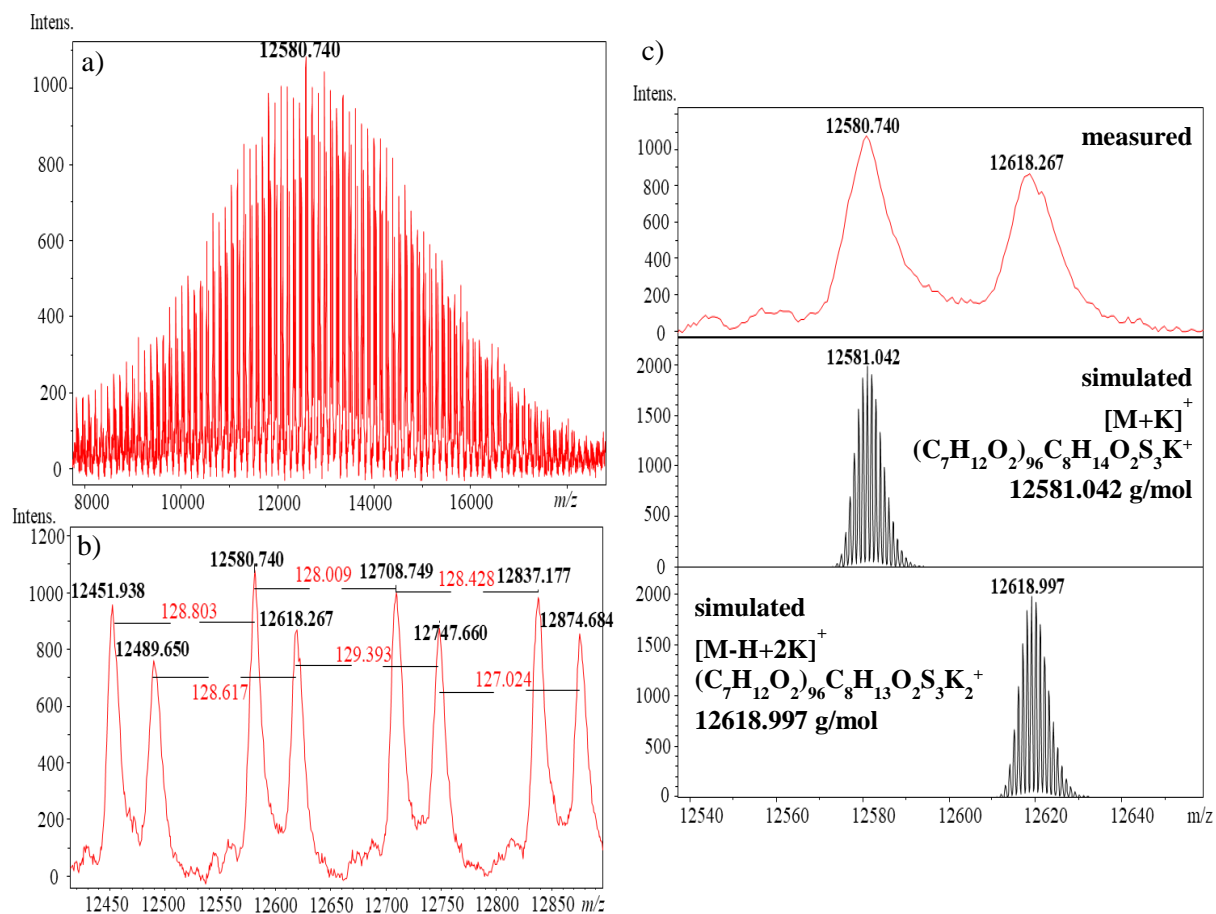
Figure S 44. MALDI-ToF-MS of P-*n*BuA-COOH (**50**); a) full spectrum of **50**, showing two series; b) Superimposed area of spectrum of **50**, showing distance between peaks of both series of 128 g/mol, belonging to the repetitive unit of *n*-butyl acrylate. c) Measured peaks and their simulated isotopic pattern, belonging to the displayed structures.

Figure S 45. ^{1}H-NMR spectrum of **51d** ($M_{n(NMR)}$ = 13 900 g/mol, PDI = 1.21) in THF-d_8.

Figure S 46. ^{1}H-NMR spectrum of **51e** ($M_{n(NMR)}$ = 23 800 g/mol, PDI = 1.23) in THF-d_8.
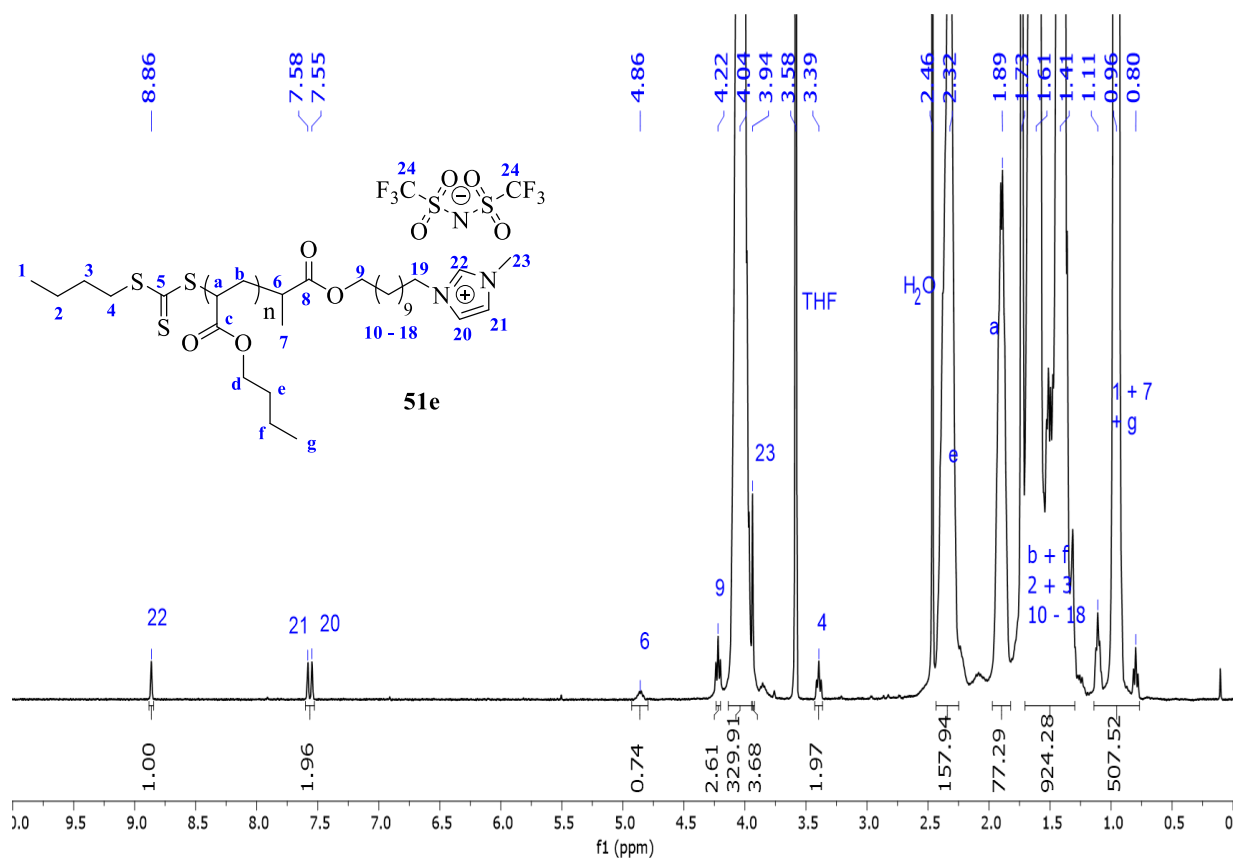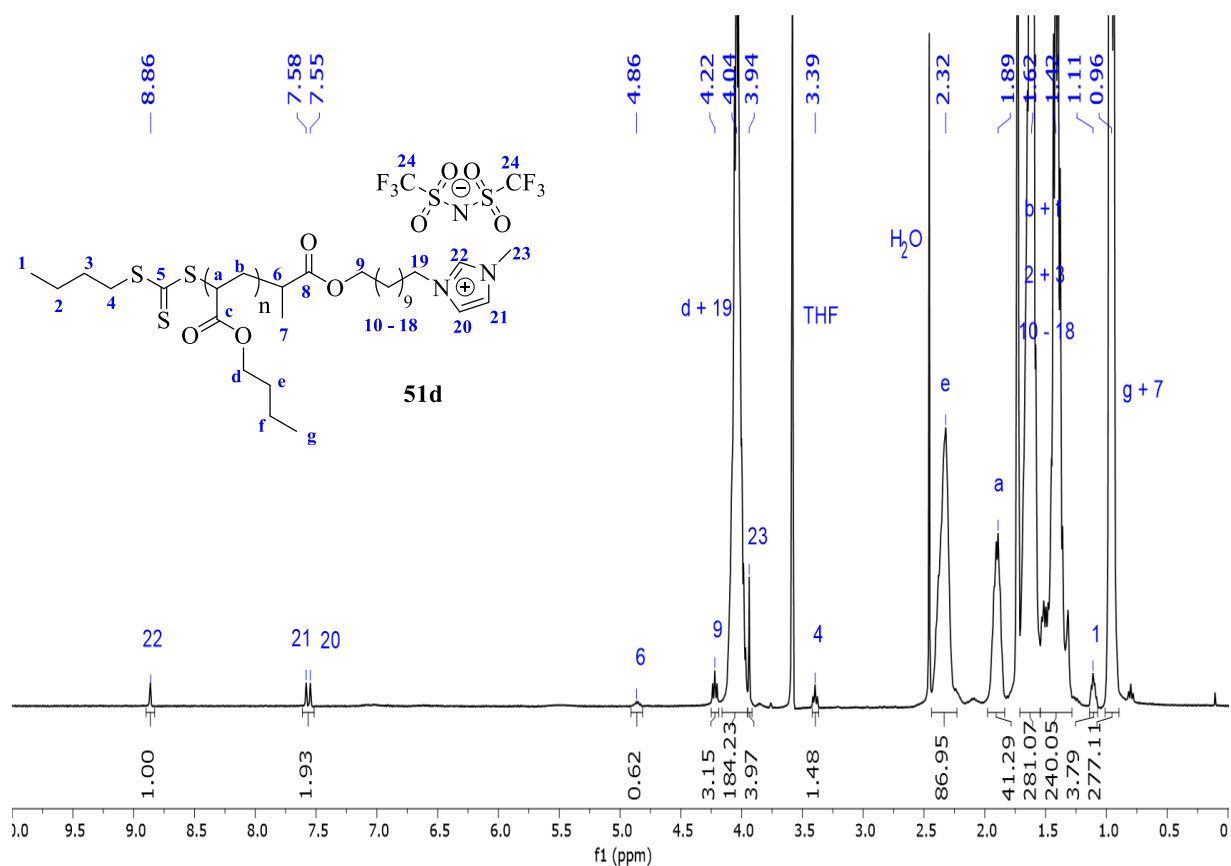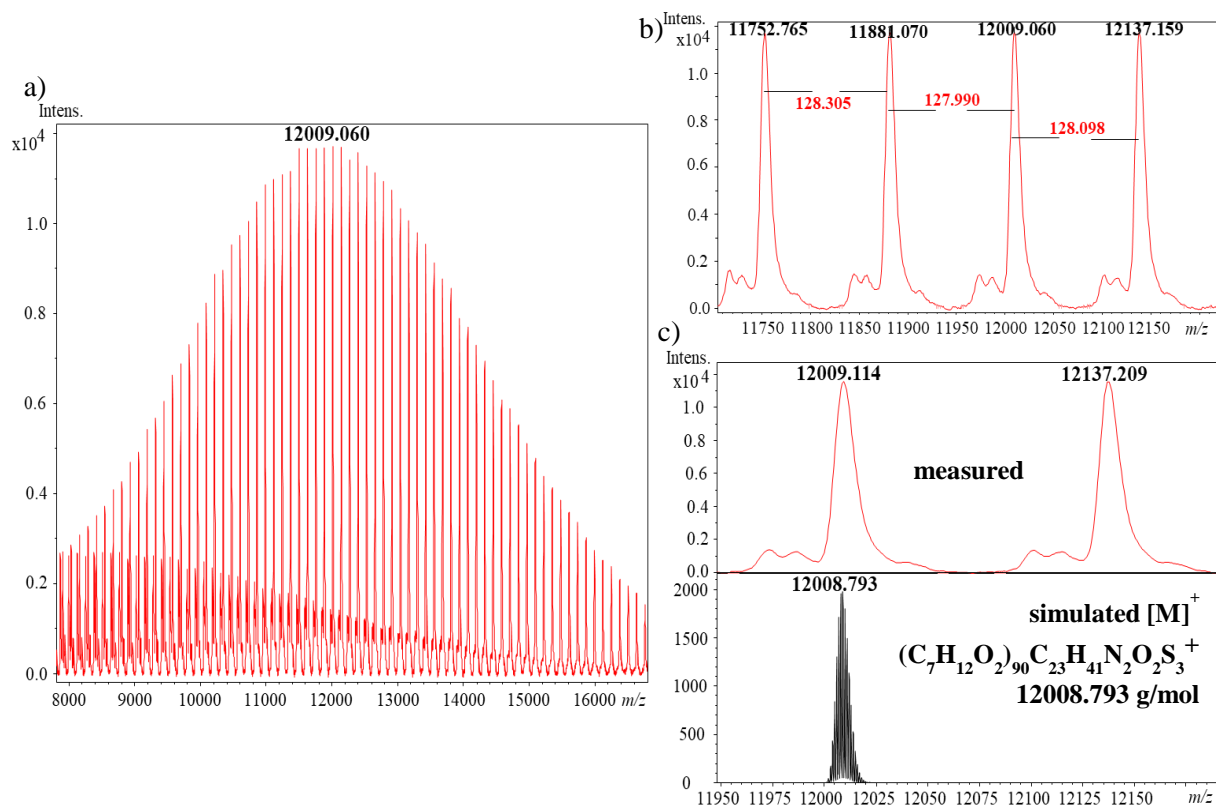
Figure S 47. MALDI-ToF-MS of P-*n*BuA-NHC (**51d**); a) full spectrum of **51d**, showing two series; b) Superimposed area of spectrum of **51d**, showing distance between peaks of 128 g/mol, belonging to the repetitive unit of *n*-butyl acrylate. c) Measured peak (top) and its simulated isotopic pattern (bottom), belonging to the displayed structure.
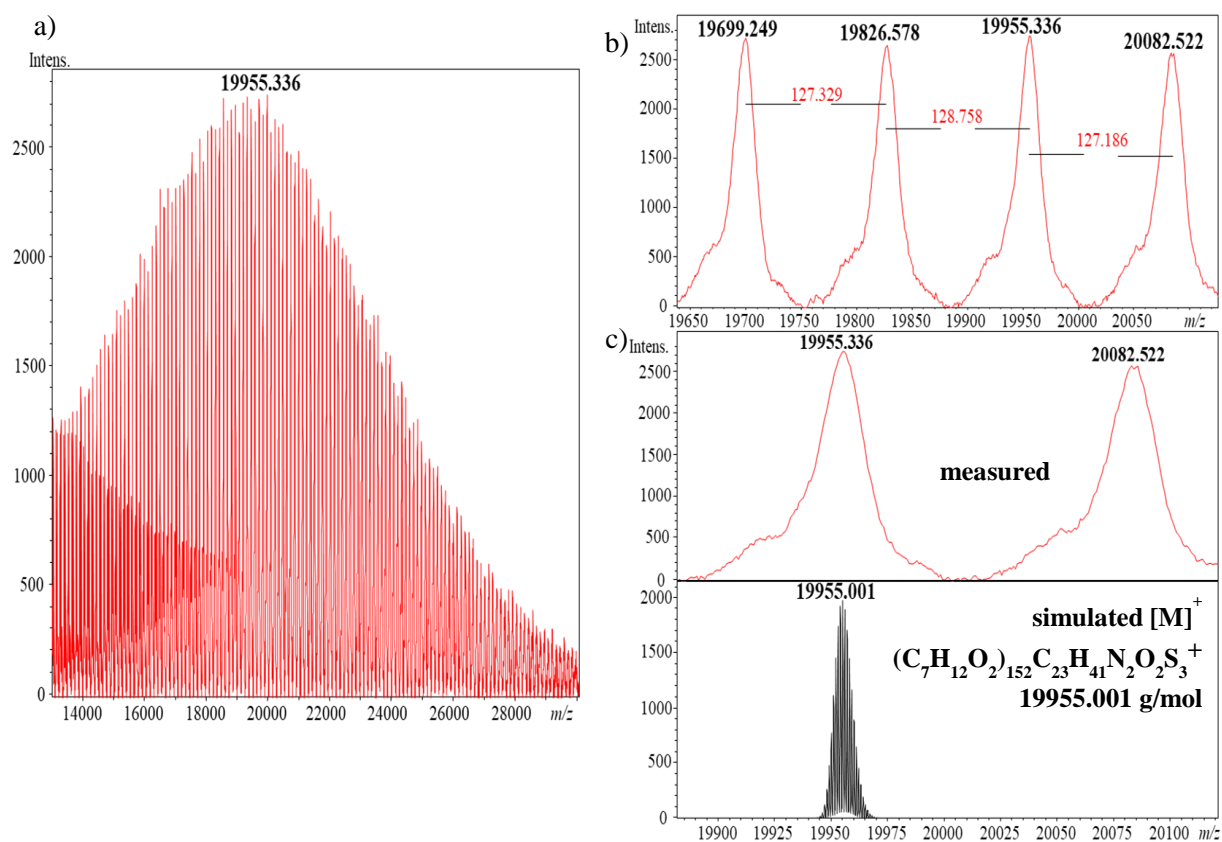
Figure S 48. MALDI-ToF-MS of P-*n*BuA-NHC (**51e**); a) full spectrum of **51e**, showing two series; b) Superimposed area of spectrum of **51e**, showing distance between peaks of 128 g/mol, belonging to the repetitive unit of *n*-butyl acrylate. c) Measured peak (top) and its simulated isotopic pattern (bottom), belonging to the displayed structure.

Table S3. Synthesis details of the remaining RAFT-polymerization of *n*-butyl acrylate.

P-*n*BuA	CTA	CTA:I:M [eq.]	n_{CTA} [mmol]	$n_{monomer}$ [mmol]	$M_{n(GPC)}$[a) [g/mol]	$M_{n(NMR)}$[b) [g/mol]	PDI	solvent	T [°C]	yield [%]
A)	**RAFT-polymerization conducted in solution**									
51i	**40**	10:1:2000	0.21	42.1	37 200	50 400	1.31	DMF	65	60
B)	**RAFT-polymerization conducted in bulk in absence of AIBN**									
51j	**40**	10:500	1.76	87.8	2 300	2 100	1.15	/	120	18

a) GPC-measurements were performed in HPLC-grade DMF with the addition of LiNTf$_2$ (c = 10.0 mM) and molecular weight was determined by calibration with external PBMA-standards (M_P ~ 0.8 kg/mol – 111 kg/mol) and detection of refractive-index. b) Calculated by the ratio of integrals of the methylene-group of the initiator at δ = 3.39 ppm and the repetitive unit at δ = 4.12 – 3.94 ppm, of which the integral-value of 2 was subtracted, due to overlay with methylene-group of initiator-part.

7.13. Characterization of polymeric mechanocatalysts
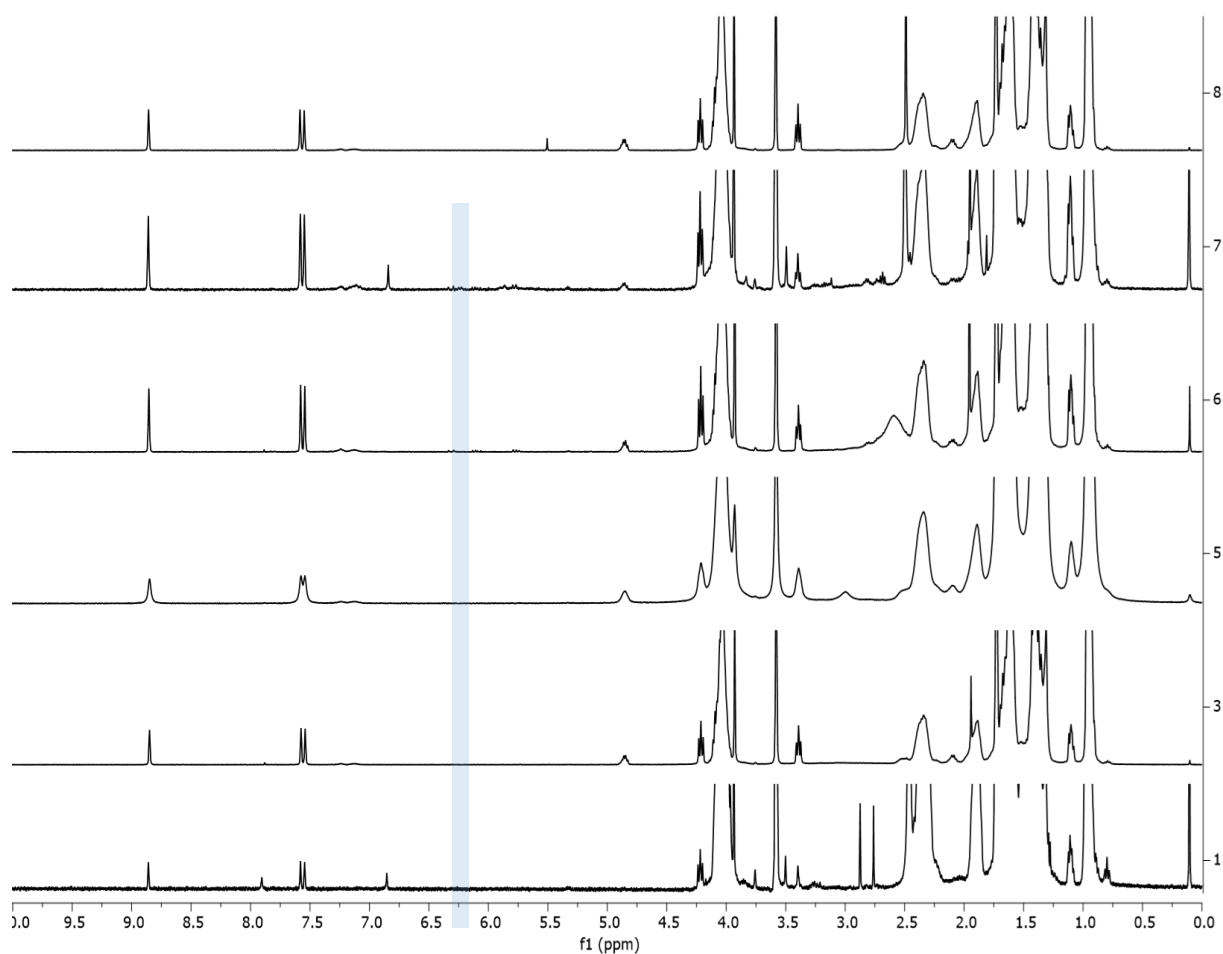
Figure S 49. Stacked ^{1}H-NMR spectra of attempted P-*n*BuA mechanophore synthesis; (8) pure P-*n*BuA-NHC (**51h**) for better comparison; (7) see Table S 4B, entry 7; (6) see Table S 4B, entry 8; (5) see Table S 4B, entry 9; (3) see Table S 4B, entry 12; (1) see Table S 4B, entry 14; All of them missed the biscarbene proof by shift of NC*H*C*H*N resonance from δ = 7.58 – 7.54 ppm to approximately δ = 6.25 – 6.22 ppm (area highlighted by light blue transparent marker).
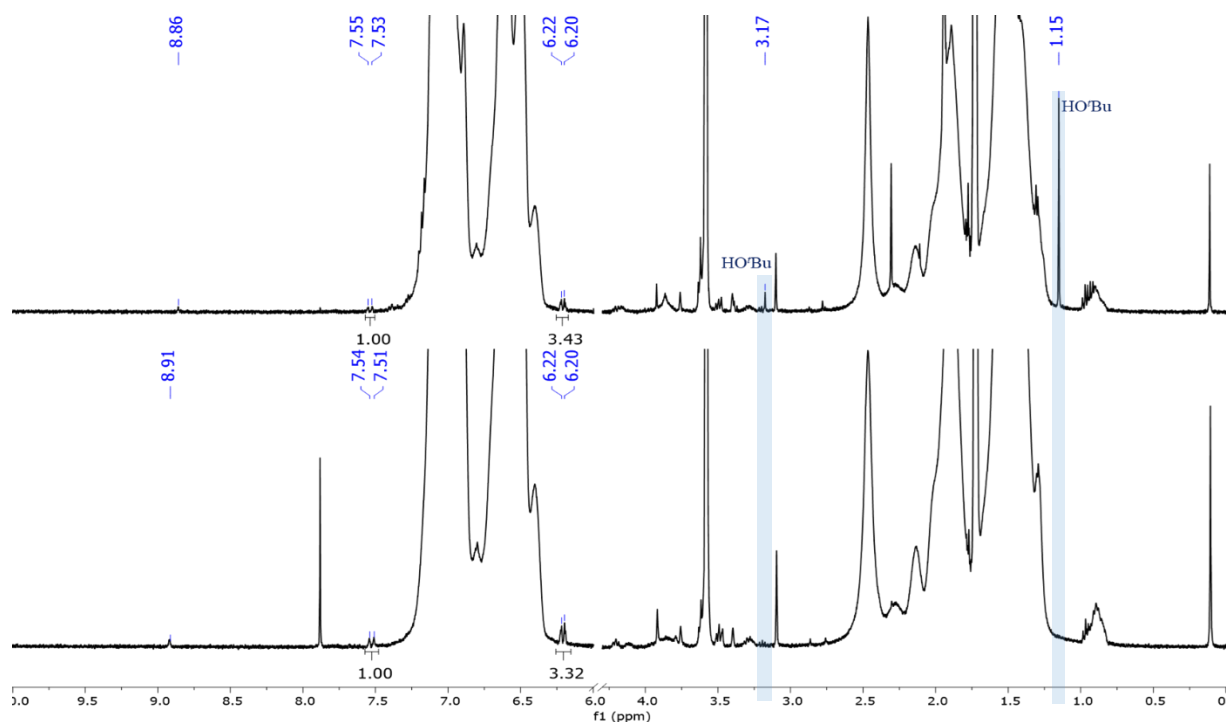
Figure S 50. Stacked ^{1}H-NMR spectra of aliquot taken from the reaction of PS-NHC with NaO^{t}Bu and [Cu(MeCN)$_4$]PF$_6$ in order to synthesize the bis(NHC)-mechanophore (top) and after purification by precipitation of the crude mixture in MeCN to remove excess of the base (HO^{t}Bu) (area highlighted by light blue transparent marker) and the catalyst [Cu(MeCN)$_4$]PF$_6$. Ratio of integrals of the biscarbene at $\delta = 6.25 – 6.20$ ppm and the precursor at $\delta = 7.60 – 7.48$ ppm remained the same.
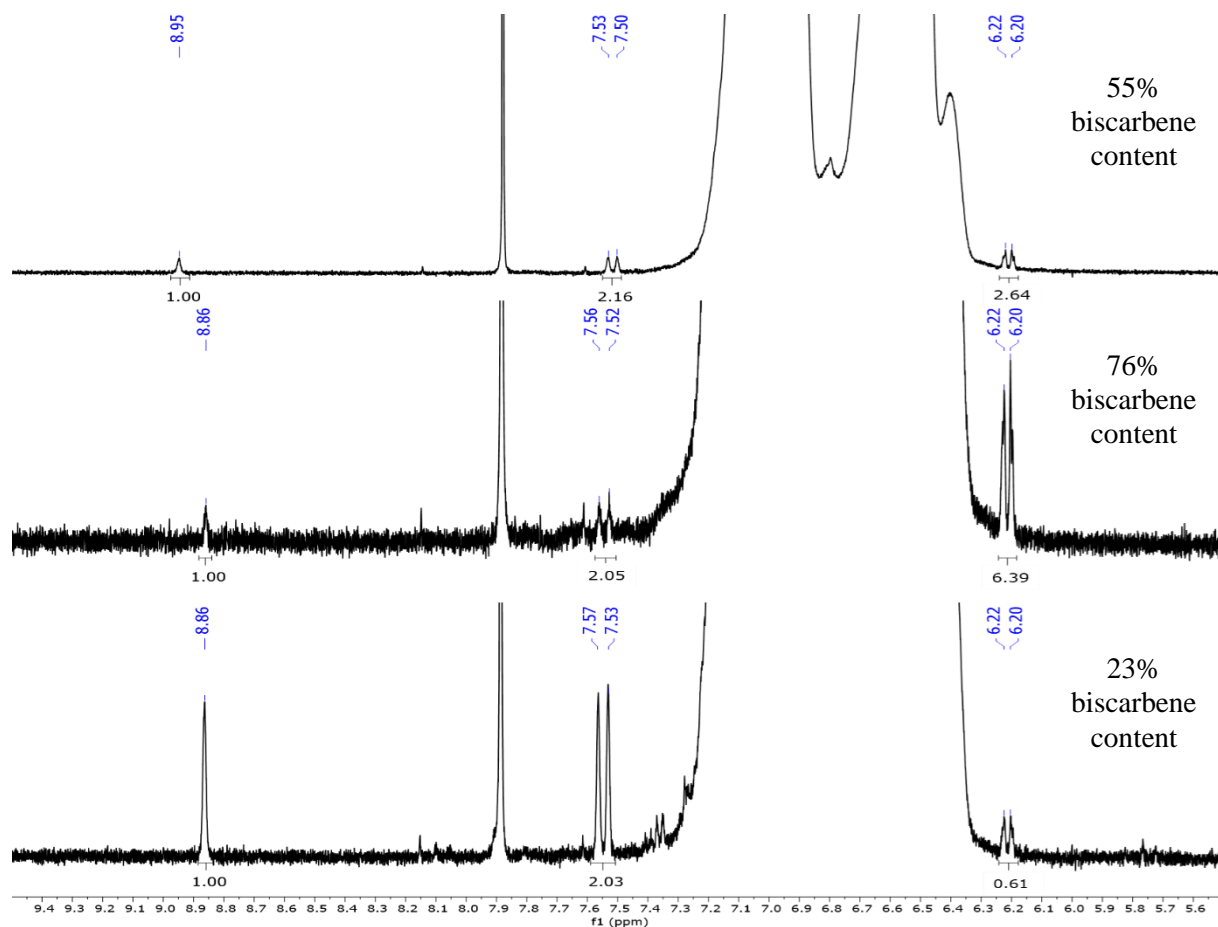
Figure S 51. ^{1}H-NMR spectra of the mechanophore mixtures (**52d**) (top); (**52e**) (middle); (**52f**) (bottom) in THF-d_8, showing the ratio of integrals, belonging to the biscarbene moiety at $\delta = 6.25 – 6.20$ ppm and the precursor at $\delta = 7.60 – 7.48$ ppm. Purification was accomplished by precipitation of the crude reaction mixture in MeCN (compare with Figure S 50).

Table S4. Different reaction conditions applied for synthesis of PS-mechanophores (A) and P-nBuA-mechanophores (B).

entry	precursor	$n_{(precursor)}$ [mmol][a]	$n_{(NaO^tBu)}$ [mmol]	$m_{(NaO^tBu)}$ [mg]	$n_{(Cu-salt)}$ [mmol]	$m_{(Cu-salt)}$ [mg]	solvent/purification	biscarbene formation?[b]
A)	**synthesis fails for PS-mechanophores at 20 °C**							
1	**49e**	0.080	0.104 (1.3 eq.)	10.0	0.040 (0.5 eq.)	14.9	THF/precipitation (MeOH)	no
2	**49e**	0.080	0.104 (1.3 eq.)	10.0	0.040 (0.5 eq.)	14.9	toluene/precipitation (MeOH)	no
3	**49d-f**	0.080	0.104 (1.3 eq.)	10.0	0.040 (0.5 eq.)	14.9	MeCN/column (neutral Al$_2$O$_3$ or diatomaceous earth)	no
4	**49d-f**	0.080	0.104 (1.3 eq.)	10.0	0.040 (0.5 eq.)	14.9	MeCN + toluene[c]/ precipitation (MeCN)	no
5	**49d-f**	0.080	0.184 (2.3 eq.)	17.7	0.040 (0.5 eq.)	14.9	MeCN /column (silica)	no
6	**49d-f**	0.080	0.184 (2.3 eq.)	17.7	0.040 (0.5 eq.)	14.9	MeCN + THF[c]/ precipitation (MeCN)	no
B)	**synthesis fails for P-nBuA-mechanophores at -40 – +20 °C**							
7	**51h**	0.080	0.104 (1.3 eq.)	10.0	0.040 (0.5 eq.)	14.9	MeCN (+20 °C)/precipitation (MeOH:H$_2$O, 2:1)	no
8	**51h**	0.080	0.104 (1.3 eq.)	10.0	0.040 (0.5 eq.)	14.9	THF (+20 °C)/precipitation (MeOH:H$_2$O, 2:1)	no
9	**51h**	0.080	KHMDS 0.104 (1.3 eq.)	KHMDS 20.8	0.040 (0.5 eq.)	14.9	MeCN (+20 °C)/precipitation (MeOH:H$_2$O, 2:1)	no
10	**51h**	0.080	0.104 (1.3 eq.)	10.0	0.040 (0.5 eq.)	14.9	MeCN (-40 °C)/without workup	no
11	**51h**	0.080	0.08 (1.0 eq.)	7.7	0.040 (0.5 eq.)	14.9	MeCN (-40 °C)/without workup	no
12	**51h**	0.080	0.07 (0.9 eq.)	6.9	0.040 (0.5 eq.)	14.9	MeCN (-40 °C)/without workup	no
12	**51h**	0.080	0.04 (0.5 eq.)	5.0	0.040 (0.5 eq.)	14.9	MeCN (-40 °C)/without workup	no
13	**51d**	0.080	0.104 (1.3 eq.)	10.0	0.040 (0.5 eq.)	14.9	MeCN:THF, 1:1 (+20 °C)/without workup	no
14	**51d**	0.080	0.184 (2.3 eq.)	17.7	0.040 (0.5 eq.)	14.9	MeCN (+20 °C)/without workup	no

a) Determined by using the calculated molecular weight via ^{1}H-NMR measurement. b) Resonance shift of NC*HCH*N in ^{1}H-NMR spectra measured in THF-d_8 from δ = 7.56 – 7.52 ppm (precursor) to δ = 6.25 – 6.23 ppm (bis-carbene-structure) for PS and from δ = 7.58 – 7.54 ppm (precursor) for P-nBuA to ca. δ = 6.3x – 6.1x ppm (resonance location for P-nBuA-biscarbene structure is unknown, but should be similar to PS). c) A few µL of a second mentioned solvent were added to get a clear solution by dissolving of the remaining solid in the suspension.

7.14. Ultra-sonication experiments of mechanocatalysts (52d-f)
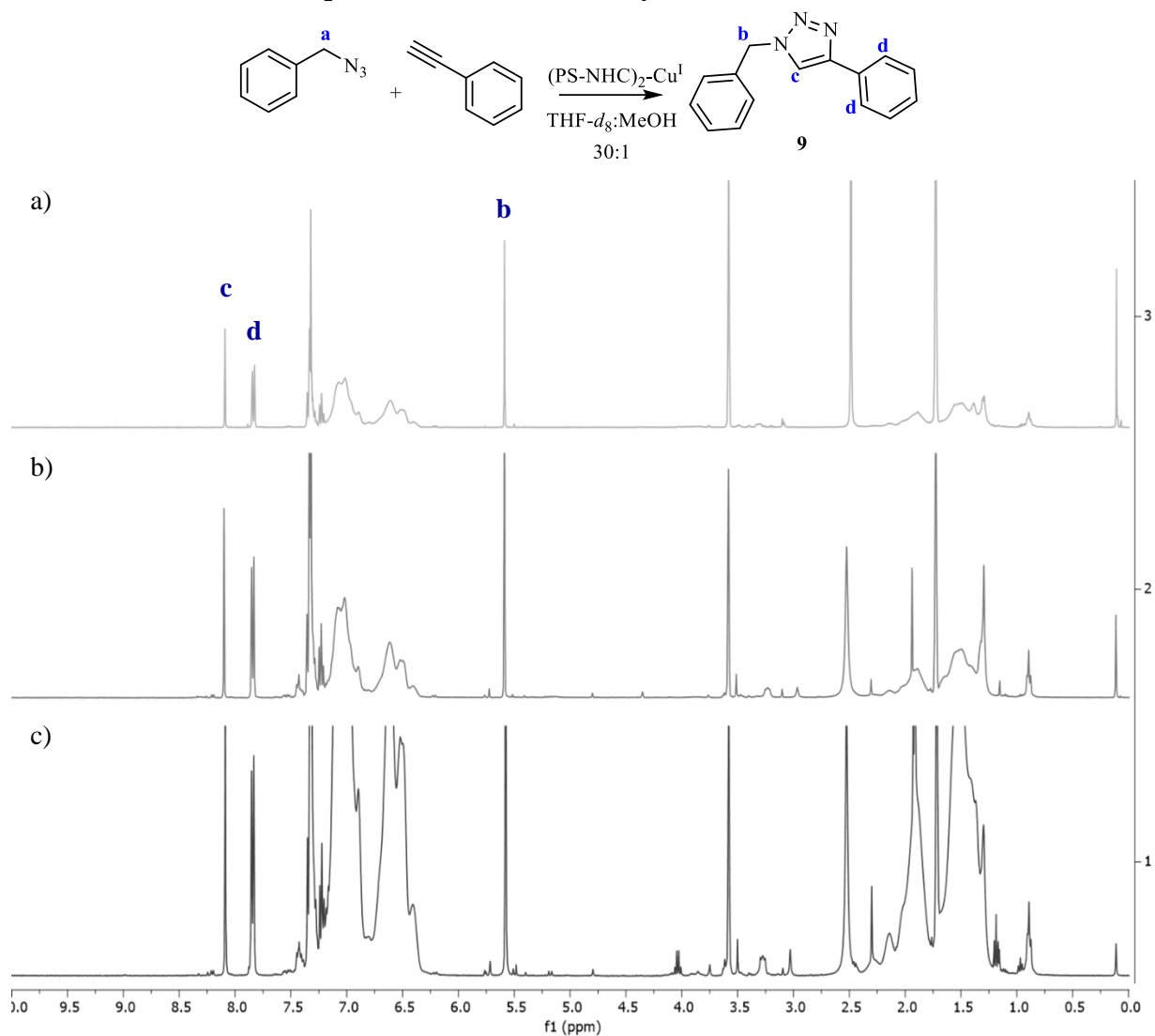
Figure S 52. Stacked ^{1}H-NMR spectra of the control experiment (without US), showing complete conversion of phenylacetylene and benzyl azide (equimolar ratio, $c = 75$ mM, 1.0 eq.) at RT after 18 hours of stirring in a THF-d_8:MeOH, 30:1 mixture, applying the mechanocatalyst ($c = 0.75$ mM, 0.01 eq.): a) **52d**; b) **52e**; c) **52f**.
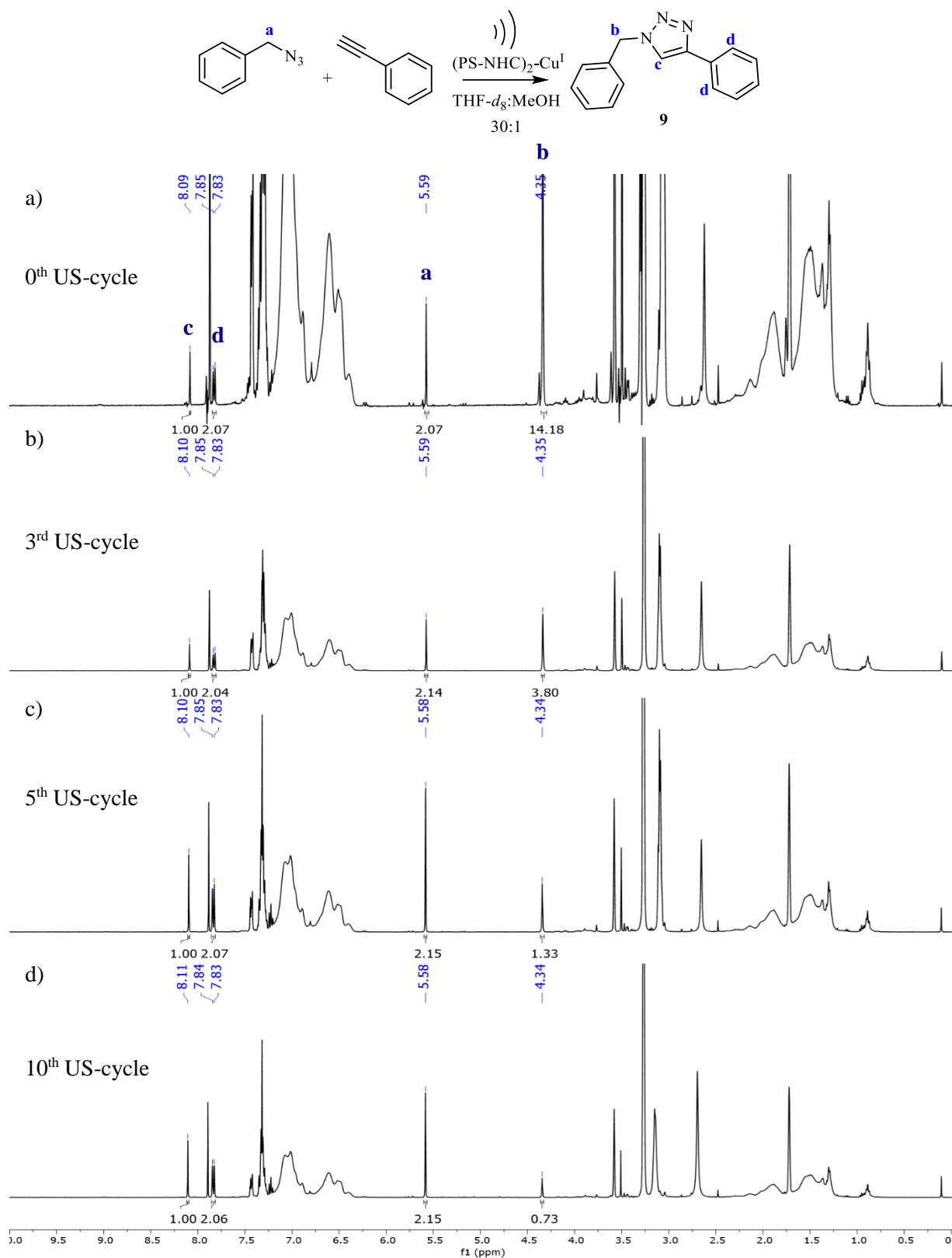
Figure S 53. Stacked ^{1}H-NMR spectra of US experiment, showing conversion (calculated by comparing integral ratio of signals at δ = 5.59 ppm (product) and at δ = 4.34 ppm (educt)) of phenylacetylene and benzyl azide (equimolar ratio, c = 75 mM, 1.0 eq.), applying the mechanocatalyst **52d** (c = 0.75 mM, 0.01 eq.) and US in THF-d_8:MeOH, 30:1; a) 13% conversion (0th Cycle); b) 36% conversion (3rd cycle); c) 64% conversion (5th cycle); d) 75% conversion (10th cycle).

7.15. Detection of fluorogenic sensing within pTHF-pellets (53a-d) triggered by compression experiments (activated via mechanocatalysts)
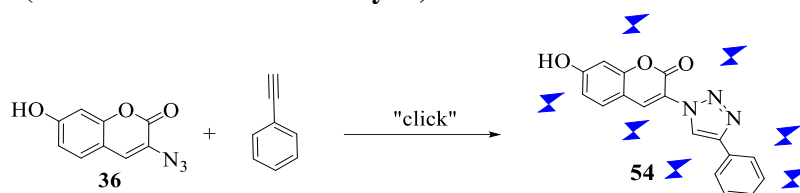
The calibration of the fluorescence spectrometer was done, embedding the "clicked" fluorogenic dye **54** in different concentrations in a high molecular weight PTHF matrix (see Table S5). Fluorescence quenching effects based on the chromaticity of the dye were neglected, adjusting an overall concentration of the coumarin based dyes (**36** + **54**) constant at $1.6 \cdot 10^{-4}$ mmol/mg. The experimentally used concentrations ($c(\mathbf{54}) = 0$, $1.5 \cdot 10^{-6}$, $2.9 \cdot 10^{-6}$, $7.7 \cdot 10^{-6}$, $1.6 \cdot 10^{-5}$, $3.2 \cdot 10^{-5}$, $6.4 \cdot 10^{-5}$ as well as $1.6 \cdot 10^{-4}$ $\text{mmol}_{(\mathbf{54})}/\text{mg}_{(\text{sample})}$) of **54** were adjusted, dissolving the pTHF matrix (200 mg, $M_n = 112\,000$ g/mol), the corresponding amounts of **54** and the non-fluorescent dye **36** in dry THF. After the solution becomes homogenous, the solvent was removed under reduced pressure and the sample was brought roughly into a cylindrical form (diameter ~ 13 mm) using spatula and tweezer and was allowed to crystallize for one week into dark. After crystallization the samples were compressed using an automatic hydraulic press together with a 13 mm pellet compression tool, applying 10 tons pressure (corresponding to 0.74 GPa). The fluorescence intensity was measured at 427 nm after excitation at 360 nm and the obtained fluorescence was fitted versus the concentration to yield equation 5 (**e5**).[349]

$$I_{\text{Fluorescence}} = 6.01 \cdot 10^6 \, (\pm \, 2.94 \cdot 10^5) \, c_{(H)} + 1.12 \cdot 10^1 \, (\pm \, 1.86 \cdot 10^1) \qquad \textbf{(e5)}$$

Table S5. Detailed data for the calibration of the fluorescence intensity versus the concentration of the 7-hydroxy-3-(4-phenyl-1H-[1,2,3]triazole-1-yl)-coumarin (**54**) in a pTHF matrix.

	$c_{(\mathbf{54})}$ [$\text{mmol}_{(\mathbf{54})}/\text{mg}_{\text{sample}}$]	$n_{(\mathbf{54})}$ [mmol]	$m_{(\mathbf{54})}$ [mg]	$n_{(\mathbf{36})}$ [mmol]	$m_{(\mathbf{36})}$ [mg]	$I_{\text{fluorescence}}$ (427 nm) sample1 [a.u.]	$I_{\text{fluorescence}}$ (427 nm) sample2 [a.u.]	$I_{\text{fluorescence}}$ (427 nm) sample3 [a.u.]	$I_{\text{fluorescence}}$ (427 nm) average [a.u.]
1	**0**	**0**	0	$3.4 \cdot 10^{-2}$	6.98	17	17	17	17
2	$1.5 \cdot 10^{-6}$	$3.0 \cdot 10^{-4}$	0.10	$3.4 \cdot 10^{-2}$	6.91	23	24	25	24
3	$2.9 \cdot 10^{-6}$	$6.0 \cdot 10^{-4}$	0.20	$3.4 \cdot 10^{-2}$	6.85	25	26	26	26
4	$7.7 \cdot 10^{-6}$	$1.6 \cdot 10^{-3}$	0.50	$3.2 \cdot 10^{-2}$	6.65	44	49	49	47
5	$1.6 \cdot 10^{-5}$	$3.2 \cdot 10^{-3}$	1.00	$3.1 \cdot 10^{-2}$	6.31	74	78	88	80
6	$3.2 \cdot 10^{-5}$	$6.6 \cdot 10^{-3}$	2.02	$2.8 \cdot 10^{-2}$	5.63	160	170	182	170
7	$6.4 \cdot 10^{-5}$	$1.3 \cdot 10^{-2}$	4.08	$2.1 \cdot 10^{-2}$	4.26	477	483	510	490
8	$1.6 \cdot 10^{-4}$	$3.4 \cdot 10^{-2}$	10.50	0	0	939	973	989	967
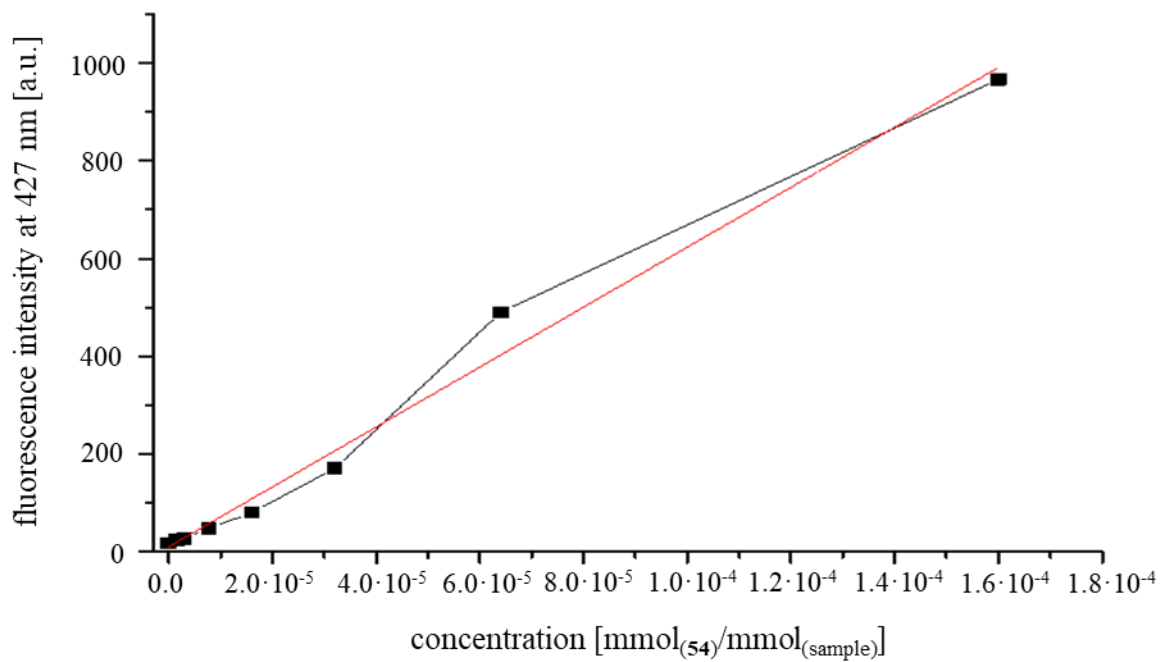
Figure S 54. Calibration plot of the fluorescence intensity versus the concentration of the "clicked" dye (**54**) in the polymer matrix.

Steve Neumann (M. Sc.)

Tel.: 0176/81116211

E-Mail: steve.neumann@chemie.uni-halle.de

Persönliche Daten

Geburtsdaten:	22.11.1988
Geburtsort:	Berlin
Nationalität:	deutsch
Familienstand:	ledig
Anschrift:	Lange Straße 11, 06110 Halle (Saale)

Schulausbildung/Studium

seit 10/2013   **Promotionsstudium** am Institut für Chemie / Technische und **Makromolekulare Chemie**, Martin-Luther-Universität Halle-Wittenberg unter der Leitung von Prof. Dr. Wolfgang Binder, Thema der Dissertation: *„Homogeneous and heterogeneous CuAAC-systems for self-healing and stress-sensing applications"*

10/2011 – 09/2013   **Master-Studium** an der Martin-Luther-Universität Halle-Wittenberg mit Schwerpunkt **Makromolekularer Chemie**; Thema der Masterarbeit: *„Synthese und Charakterisierung von selbstheilenden Polymeren mit intern Kupfer-chelatierenden Funktionalitäten"* (Abschluss: 1,8)

10/2008 – 09/2011   **Bachelor-Studium** an der Martin-Luther-Universität Halle-Wittenberg mit Schwerpunkt **Organischer Chemie**; Thema der Bachelorarbeit: *„Synthese von antineoplastischen Zimtsäurederivaten der Oleanolsäure"* (Abschluss: 2,4)

08/2001 – 07/2008   Oberstufenausbildung/ Abschluss: Abitur (Note 2,3)
Primo-Levi-Schule (Gymnasium), Berlin-Pankow

1995 – 2001   Unterstufenausbildung
Georg-Zacharias-Grundschule, Berlin-Pankow

Besondere Kenntnisse

- ❖ Deutsch (Muttersprache), Englisch (fließend in Wort und Schrift), Französisch (Grundkenntnisse)
- ❖ umfassende Sachkunde nach § 5 Abs. 2 der Chemikalien-Verbotsordnung
- ❖ Pharmazeutische Regelwerke (AMG, AMWHV) und internationale GMP-Anforderungen (EU-GMP, 21-CFR 211, ICH-Guidelines)
- ❖ QM-Systeme, KVP, Personalschulung
- ❖ Projekt-/Konfliktmanagement
- ❖ MS-Office, Windows Betriebssysteme
- ❖ Wissenschaftliche Software / Datenbanken (Endnote, Scifinder, Reaxys, Origin, Mestre-C, Chemdraw, flexAnalysis, OmniSec)
- ❖ Analytische Methoden (NMR, GPC, DSC, MALDI-ToF-MS, DMA, Rheologie)

Publikationen

- ❖ D. Döhler, P. Michael, **S. Neumann** und W. H. Binder; Biomimetische Materialien Selbstheilende Polymere, *Chem. Unserer Zeit* **2015**, *50*, 90-101.

- ❖ **S. Neumann**, D. Döhler, D. Ströhl and W. H. Binder; Chelation-assisted CuAAC in star-shaped polymers enables fast self-healing at low temperatures, *Polym. Chem.* **2016**, 7, 2342 – 2351.

- ❖ M. Biewend, **S. Neumann**, P. Michael and W. H. Binder; Synthesis of Polymer-Linked Copper(I) Bis(*N*-Heterocyclic Carbene) Complexes of Different Architecture, *Polym. Chem.* **2018**, manuscript in preparation.

Präsentationen auf Konferenzen

- ❖ **Steve Neumann**, Wolfgang H. Binder, International Conference of Self-Healing Materials (ICSHM), *Chelation-assisted CuAAC of star-shaped polymers enables fast crosslinking at low temperatures*, Juni 16-20, **2015**, Durham, NC, USA, Vortrag.

- ❖ **Steve Neumann**, Wolfgang H. Binder, Makro 2016, *Fast crosslinking of star-shaped polymers visualized by a fluorogenic „click"-reaction*, September 11-13, **2016**, Halle, Deutschland, Poster-Präsentation.

Halle (Saale),

_____
Steve Neumann

9 Eigenständigkeitserklärung

Hiermit erkläre ich an Eides statt, dass ich die vorliegende Arbeit selbstständig und ohne fremde Hilfe verfasst habe. Andere als die angegebenen Quellen und Hilfsmittel wurden nicht benutzt und die den benutzten Werken wörtlich oder inhaltlich entnommenen Stellen wurden als solche kenntlich gemacht.

Außerdem erkläre ich, dass ich die vorliegende Dissertation an keiner anderen wissenschaftlichen Einrichtung zur Erlangung eines akademischen Grades eingereicht zu haben.

Halle (Saale), den   _____

                                                                                                  Steve Neumann